Engineering Geological Characterisation and Slope Stability Assessment of Whitehall Quarry, Waikato.

A Thesis

submitted in partial fulfilment of the requirements of the degree

of

Master of Science in Engineering Geology

at the

University of Canterbury

by

Daniel Rodney Strang

UNIVERSITY OF CANTERBURY

2010

Frontispiece

“Over 4,000 tonnes of aggregate goes into every 1 km of a two lane road”

Abstract

Whitehall Quarry is located 4 km east of Karapiro, near Cambridge within the Waikato District. Current quarrying operations produce between 150,000 and 300,000 tonnes of aggregate for use in the surrounding region. This study is an investigation into the engineering geological model for the quarry and pit slope stability assessment. Pit slope stability is an integral aspect of quarrying and open-pit mining since slopes should be as steep as possible to minimise waste material which needs to be removed, yet shallow enough to minimise potential hazards to personnel and equipment below pit slopes. This study also assesses the stability of complex wedge located within the north western corner of the quarry. Initial estimates approximate a wedge mass volume of 500,000 m^3; failure was triggered during the late 80's due a stripping programme at the head of the mass.

Field and laboratory investigations were carried out to identify and quantify engineering geological parameters. Photogrammetric and conventional scanline analytical techniques identified two domains within the quarry divided by the Main Quarry Shear Zone (MQSZ). Discontinuity orientations are the key differences between the two domains. Bedding planes appear to have slightly different orientations and each domain has very different joint sets identified.

Point load, shear box, ring shear testing approximated intact rock strength, shear strength and fault gouge behaviour properties. The main geological units at the quarry are greywacke sandstone interbedded with argillaceous mudstone. Uniaxial compressive strength estimates approximated the intact rock strength for sandstone to be between 30 and 230 MPa depending on weathering grade, while the strength of mudstone was approximated at 5 MPa. Residual shear strength was carried out to estimate the approximate effective angle of internal friction for both a smooth UW-SW sandstone joint and a mudstone bedding plane, these being 37^o and 34^o respectively. Laboratory testing on fault gouge indicated an approximate angle of internal friction of 13^o and the presence of kaolinte and montmorillonite was identified.

Pit slope stability analysis utilised the Markland test for identification of potential failures within slopes. Wedge failures are the most common potential failure type, then planar failures along bedding planes. Potential failures are most likely to be less than 10 m^3 due to the high fracture frequency and low persistence of common joint sets. However, larger failures in the order of 100 m^3 are possible along fault and bedding planes where persistence is typically greater than 20 m.

Kinematic analysis of the Northern Wedge Failure estimated a mean factor of safety of 0.97. Currently the wedge is assessed as marginally unstable. Electronic distance measurement over 11 months recorded an approximate mean wedge velocity of 19 mm/month. Sensitivity analysis identified pore water pressure as a key parameter. De-watering the wedge via a series of inclined drainage holes appears to be the best mitigation method. However, the mine and monitor approach is also acceptable but with anticipated risk to personnel and equipment. Monitoring instrumentation such as a wireline and crack-meters should be implemented.

Table of Contents

List of Figures

List of Tables

List of Map Sheets

1.0 Introduction

1.1 Background

Pit slope stability is an important aspect of any mining or quarrying operation. However there is a fundamental difference between slopes designed for permanent civil engineering ventures and those for quarries. Generally in civil engineering projects slope failures are unacceptable and are likely to have major consequences. In quarrying, there is much greater flexibility when considering the stability of working pit slopes. Both the slope orientation and sequence of excavation can be adjusted to take into account slope instability, and while instability is undesirable most failures can be tolerated. Access to the area by personnel and equipment can be restricted, exposure of the working slope to failure is usually for a limited time, and the consequences for failure at a quarry are much easier to control (Chapple, 1998).

Successful quarrying requires stringent pit slope design to maximise profits. Pit slopes must be designed as steep as possible while maintaining adequate safety, therefore maximising the volume of material to be excavated from the face itself and lower pit levels (Bell, 1987). However, the design of pit slopes is not only controlled by economic factors but geological features as well. It is the assessment of geological controls and maintaining a safe amount of risk that determines the stability of open pit excavations.

Whitehall Quarry is located 4 km east of Karapiro, near Cambridge within the Waikato district. The quarry exhibits large volumes of high grade greywacke aggregate suitable for road construction and consists of two main excavation pits, Pit 1 and Pit 2. Pit 1 was the original excavation pit that was abandoned due to a significant complex wedge failure that was creeping into the working pit. The failure was triggered about November 1988 immediately following a very wet period, which occurred after a major overburden stripping programme in April-June 1988 (Hancock Consultants Ltd, 1989). The wedge failure now exhibits several metres of displacement and remains a constant threat to pit operations. Pit 2 is the current operating pit and produces between 150,000 and 300,000 tonnes of aggregate to the surrounding region. Pit 2 has also had stability issues in the past, the western wall has experienced complex translational and wedge failures in the order of approximately 50 to 120 m^3.

Instability in the past has highlighted the need for greater assessment of pit slopes to prevent failures from 'diluting' high grade aggregate with low grade and overburden material, which could have some major economic consequences. By gaining greater understanding the modes failure within the two pits it is possible to increase profits through pit slope design and increase the overall safety of personnel and equipment within the excavation site.

1.2 Thesis Aim

The aim of this thesis is to develop an engineering geological model for Whitehall Quarry, devised from field and laboratory investigations focussing on the following:

- Rock and soil parameters
- Hydrogeology
- Discontinuities

The engineering geological model will be utilised in assessing the stability of pit slopes within the quarry and the instability of the Northern Wedge Failure within Pit 1. The end result will be a concise set of recommendations for better quarrying practices and future quarry management.

1.3 Study Area

1.3.1 Site Location

Whitehall Quarry is located on Whitehall Road, 4 km to the north of Karapiro and 8 km east of Cambridge at approximately 90 m above sea-level within the Waikato district, New Zealand. The field area covers 2.0 km^2 of land and encompasses the two main excavation pits as well as the processing plant, waste dumps, surrounding bush and farm land (Figure 1-1).

The quarry is situated within a topographic low of moderate relief ranges. The eastern edge of the quarry is bound by Karapiro Stream, whereas the western edge is relatively steep topography. The overall long axis of the quarry is orientated approximately north-south. Quarry expansion has resulted in major face development on the northwest, north and northeast sides of the pit (Figure 1-1). The current operating pit floor lies at approximately 50 masl.

Figure 1-1: Location of Whitehall Quarry (Google Earth, 2010).

1.3.2 Quarry History

Whitehall Quarry has been operating for more than 60 years. It was initially established by the landowner of the neighbouring Scholes property to provide material for farming operations, but was then expanded by Scholes Bros Ltd in the 1940's to provide aggregate resources for the construction of the Karapiro Hydro Dam on the Waikato River. Construction of the dam began in 1940, and was finally completed in 1947 after many delays due to World War Two.

In 1973 the plant and equipment was purchased by Whitehall Quarries Ltd, a subsidiary company of Earthmovers Waikato Ltd. This company was later purchased by Firth Aggregates in March 1987, and in 1988 Winstone Aggregates took over management of Whitehall Quarry. Excavation within Pit 1 ceased in approximately 1996, and it was allowed to flood. Excavation then focussed on developing Pit 2 (Figure 1-1).

Until 2005 Karapiro Stream flowed through the western edge of the quarry floor. In May 2005 Winstone Aggregates undertook a major earthworks project to divert the stream around the quarry along the eastern edge. The project was designed by Tonkin and Taylor Ltd and entailed the development of several benches on the existing eastern bank; a channel was cut at the base, with a spillway installed to cope with large flood events. The diversion was completed in December 2005, which allowed quarrying to continue to greater depths and access to high grade material on the eastern edge where the stream previously flowed (Tonkin & Taylor Ltd, 2004).

The quarry has experienced multiple large slope failures ranging from 10's to 100's of thousand cubic metres in volume. The largest is a significant complex wedge failure. Wedge movement began after a stripping programme on the head of the mass was completed in 1989, allowing water to infiltrate the wedge raising pore pressure resulting in wedge failure (Hancock Consultants Ltd, 1989). Extensive investigation was carried out on the failure by Mr John Ashby and Hancock Consultants Ltd. A wireline was installed in 1989 and monitored for at least 2 years, Ashby then concluded that catastrophic failure was imminent on the basis of approximated wedge strain versus the anticipated failure strain. At the present, the wedge seems to be stable and showing little sign of continued movement.

1.3.3 Current Activities

Whitehall Quarry currently produces between 150,000 and 300,000 tonnes of aggregate product to be distributed throughout the Waikato, Bay of Plenty, East Coast and Auckland (M. Harris, personal communication, December 15, 2009). Whitehall produces 'premium' aggregates which are used in manufacturing (concrete, asphaltic concrete, etc), road surfacing, and structural base courses (Winstone Aggregates, 2010).

The transformation of rock from the ground into aggregate products requires firstly the removal of any vegetation, then the stripping of overburden (soils and low quality material) overlying the rock resource. Once the rock resource is exposed explosives are used to loosen the rock rather than break it. Currently Pit 2 is the only operational pit at Whitehall due to the slope instability in Pit 1 (Figure 1-2).

Figure 1-2: Aerial view of Whitehall Quarry (Precision Aerial Surveys, 2007).

The fragmented rock is excavated from the quarry face or floor and loaded to dump trucks to be hauled, sometimes directly to stockpile storage for sale, or more commonly from the pit to the processing plant. At the processing plant an array of jaw, gyratory and impact crushers followed by various washing systems and screening units transform the raw material into a range of quarry products. These products vary from very tightly specified crushed, screened and graded rock for use in roading and building construction, to a selection of lower quality material, which is used for general non-specified works. Figure 1-3 shows a generalised flow chart of aggregate production. Overburden or rock that is of little or no value is dumped in the waste dumps on site, for example rock with high argillite (mudstone) content will not be processed but dumped.

Products are removed from the processing plant at various points, depending on the desired characteristics, and transported by truck, loader or conveyor to the stockpiles ready for sale. Road trucks are weighed at the weighbridge immediately after entering the site via the main gateway. They then drive to the appropriate stockpiles, where they are loaded, before returning to the weighbridge and the main entrance to transport the products off site.

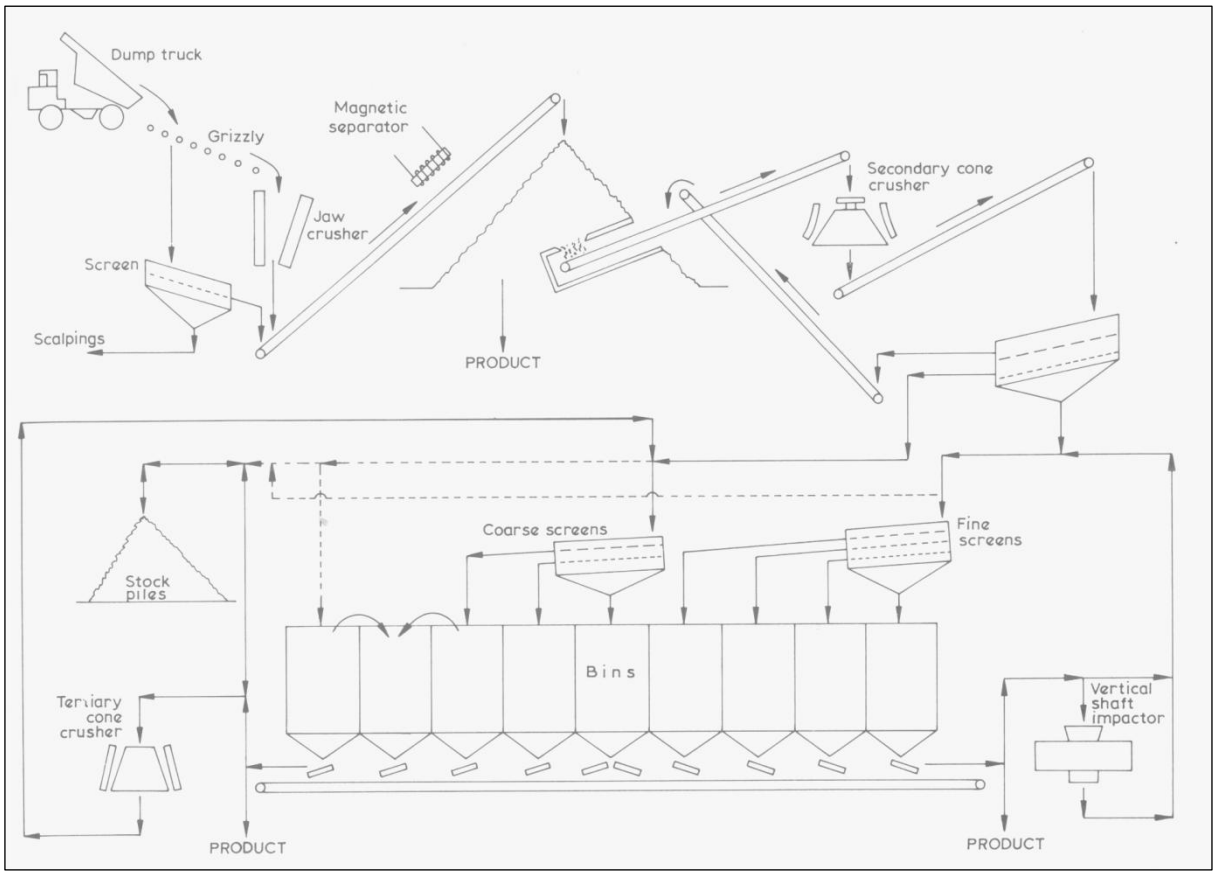

Figure 1-3: A generalised flow chart showing the production of crushed aggregate from raw rock material into premium grade aggregates (Smith & Collis, 1993).

1.3.4 Rainfall Data

Whitehall Quarry, and the nearby township of Cambridge, is situated within the greater Waikato region. An electronic weather station 10 km from the quarry records daily rainfall and monthly averages from previous years. The average total rainfall for the area is 1090 mm/yr (Appendix B1). Rainfall is typically in the order of 10 to 20 mm/day during the drier summer months, while 40 to 80 mm/day is not uncommon during the wetter winter months. Sub-tropical storms are not uncommon as well during the summer causing flooding of the quarry and surrounding low areas. High periods of rainfall can have an adverse effect on quarry slope stability.

Monthly rainfall totals for the Whitehall region are recorded and presented in Figure 1-4.

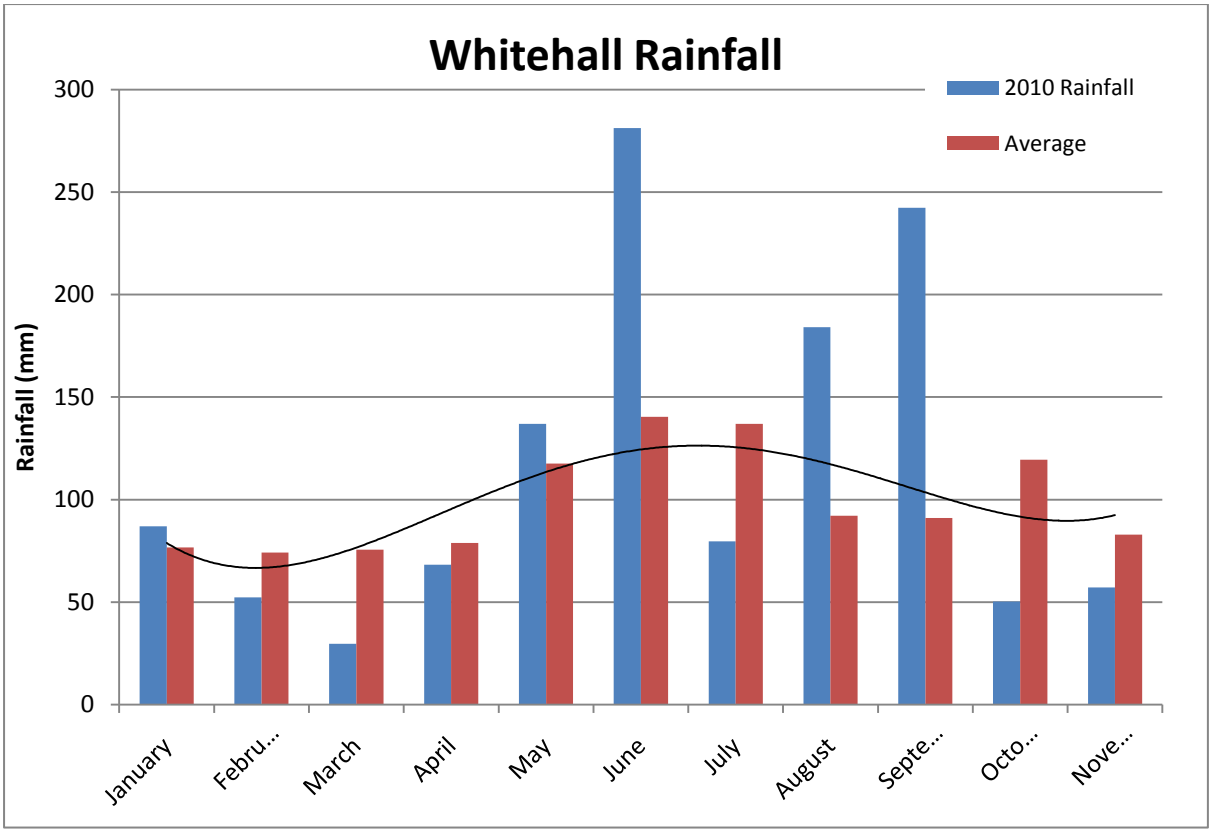

Figure 1-4: Monthly rainfall for the Whitehall area.

The months of May, June and July represent the wettest period during the year with higher rainfall and lower evapotranspiration, while January, February and March are typically the driest. The year 2010 was a wetter than average year, with approximately 1270 mm of

rainfall recorded. This is some 200 mm higher than average, therefore there is a possibility of identifying a greater number of instability features within the quarry during 2010.

1.4 Geological Setting

1.4.1 Regional Geology

The predominant basement rock of the Waikato region in the North Island of New Zealand belongs to the Waipapa superterrane. These basement rocks broadly consist of fine to coarse-grained, bedded felsarenites, more commonly known as greywacke sandstone, and argillaceous mudstones (Saeed, 2000) (Figure 1-5).

Whitehall Quarry is situated within the Morrinsville facies (Late Jurassic to Early Cretaceous), of the Manaia Hill Group of the Waipapa Composite terrane (Black, 1996). The Manaia Hill group is characterised by lithic volcanic greywacke and sub-greywacke type sedimentary rocks, which were derived from an eroding landmass comprising an assemblage of calc-alkaline volcanic and plutonic rocks, with minor sedimentary rocks (Wandres, 2002). Later burial has altered the sediments to the quartz-prehnite zone of the prehnite-pumpellyite metagreywacke facies (Kear, 1970). Kear (1970) described the group as variously indurated and sparsely fossiliferous, giving a considerable thickness of monotonous rock (Figure 1-5). Locally, bedding within the rock mass is dipping at approximately 60 degrees and striking about east-west (Healy, et al. 1964).

Ongatiti ignimbrite which forms prominent steep faces within the Whitehall landscape is located to the immediate east of the quarry. The ignimbrite was erupted from the Mangakino Volcanic Centre approximately 1.2 Ma. The volume of erupted material is believed to be in the order of 300 km^3 (Stanley, 1994).

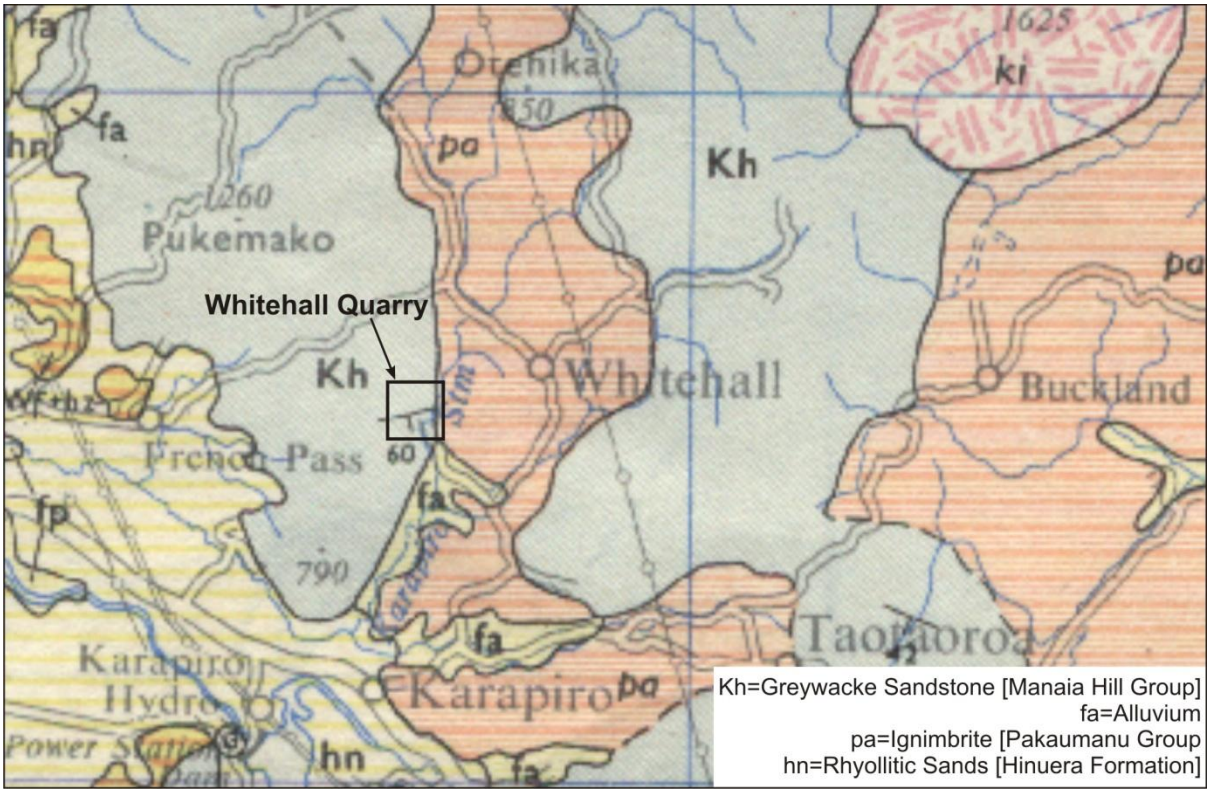

Figure 1-5: Simplistic map showing regional geology (Kear, 1970).

1.4.2 Quarry Geology

Tonkin & Taylor Ltd (2004) described the quarry rock mass as indurated, strong, massive to moderately thick bedded greywacke sandstone. Also noted within the sandstone sequence were thin to moderately thin interbeds of argillaceous mudstone. Bedding plane defects are common within freshly exposed faces and exhibit moderate to steep dips to the southwest.

The structure of the rock is variably deformed by faults and well developed joint sets. Joints are pervasive throughout the rock mass and have a wide range of orientations. Most joints are of limited persistence and individually do not significantly influence slope conditions. Although joint sets with more persistence have caused localised instability on steeply cut interim faces, these are typically moderately or steeply dipping to the southeast and southwest (Tonkin & Taylor Ltd, 2008).

Tonkin & Taylor Ltd (2008) noted many major (greater than 30 m) and minor (less than 30 m) faults within Whitehall Quarry. Some surfaces within the fault zone exhibit well developed stepped striations indicating a normal sense of movement for at least the last phase of movement (Figure 1-6).

Figure 1-6: Fibre growths on fault planes indicating normal sense of movement.

1.5 Previous Work

The majority of previous work relevant to this project is contained within proprietary documents held at the quarry site or at the Winstone Aggregates office in Auckland. It must be noted that no real geotechnical work had been carried out by Winstone staff prior to the commencement of this thesis, with the majority of work having been undertaken by private consulting firms or students for research projects.

The main relevant works carried out by private firms and students are as follows:

- Tonkin & Taylor Ltd: -Karapiro Stream diversion reports; these reports were based on the geotechnical assessment of the eastern pit wall, design of the stream realignment, and interim stability review of overburden cut above stream diversion. Realignment and design reports were completed in 2004, while the stability review was completed in 2007.
- Hancock Consultants Ltd: -Engineering geology assessment of a major slope failure at Whitehall quarry. This extensive report was entirely concerned with the complex wedge failure in the north-western wall of Pit 1. This report was completed in 1989.

- Ashby Consultants Ltd: -Slope stability assessment, wireline monitoring and risk assessment. This assessment came as a series of reports summarising the overall movement of the north-western wedge in Pit 1, its associated risks to quarry operation and impending wedge failure. This series of reports began in 1989 with the final report on the wedge failure in 1992. Another report on a complex translational failure in the western wall of Pit 2 was carried out in great detail (Asbhy, 1991). This report outlined probable failure mechanisms, monitoring results and remedial recommendations, and was completed in 2001.
- Mr J. Hetherington: - Thesis titled 'Quantitative study of the weathering of the Manaia Hill greywacke at Whitehall Quarry'. This thesis focused on the effects varying degrees of weathering has on the strength of greywacke sandstone at Whitehall Quarry. Testing included point load, Schmidt hammer, uniaxial compressive strength and porosity-density, completed in 1989 at the Department of Earth Sciences Waikato University.

1.6 Thesis Objectives

The principal objectives of this thesis are:

1. To carry out geotechnical testing to determine relevant geotechnical and engineering geological parameters for the Whitehall Quarry. Strength testing of rock and fault gouge samples to give quantitative data which may be used for stability analyses.
2. To assess of structural domains within Whitehall Quarry. The orientations of geological features within the rock mass are one of the most important features in the assessment of pit slope stability. By calculating mean orientations for different structural features it is possible to predict failure types kinematically.
3. To analyse the stability of the complex wedge failure within the northern wall of Pit 1, and to provide geotechnical input data to assist in the design of possible remedial measures. Detailed field and laboratory investigations were undertaken to accurately assess the failure model; therefore the most effective remedial measures can be assessed.
4. To provide recommendations to increase safety and possibly productivity for future quarrying practices derived from the preceding detailed investigations and analysis.

1.7 Thesis Organisation

Following this introductory chapter, Chapter 2 outlines and discusses the engineering geological and geotechnical field and laboratory investigative programmes. Testing procedures, field practices and obtained results are discussed and validity assessed. Chapter 3 develops the engineering geology model for the quarry via analysis of the geotechnical parameters and aspects identified in the preceding chapter and data obtained from defect orientation analysis. Chapter 4 comprises various kinematic slope stability models of the various domains interpreted from the geotechnical database of wall defect orientations obtained from photogrammetric and conventional scanline analytical methods. Chapter 5 looks at the north-western complex wedge failure in Pit 1 as a case study using geotechnical and engineering geological data obtained in Chapters 2 to 4. Finally, Chapter 6 summarises and concludes on the aspects covered by this thesis.

2.0 Engineering Geological and Geotechnical Investigations

2.1 Introduction

The principal aims of this engineering geological investigation have been to provide geotechnical input data for the development of a engineering geological model of Whitehall Quarry (Chapter 3).

The investigative procedures implemented in this study follow the methodology developed by Bell and Pettinga (1983), and focuses on data acquisition for maintenance, operation and remedial work within the quarry.

The principal engineering geological and geotechnical aspects of this thesis are:

1. Engineering geological mapping of the quarry, surrounding areas and selected features.
2. Laboratory testing of intact rock and fault 'gouge' material collected during the field studies stage of the investigation. Geotechnical data gathered by independent sources may also be added to the database. This data may be used for the strength characterisation of these materials and to assist in interpretations of pit slope stability.
3. Desktop investigations involving the assessment of structural data of the quarry structural domains, analysis of kinematic slope stability of selected slopes and the development of pit design and recommendations.

2.2 Field Investigation Programme

2.2.1 Engineering Geological Mapping

Engineering geological mapping of Whitehall Quarry and the surrounding area was undertaken in December 2009 (Map Sheet 1). Mapping primarily focussed on rock mass characterisation, pit slope stability, and the northern wedge failure (Chapter 5). Mapping aimed at identifying key geomorphic features such as tension cracks and scarps that related to current rock mass instability, and structural data was recorded and compared to data gathered via photogrammetric (Section 2.2.2).

a) Identified Geological Units

The following units were identified during field mapping investigations:

Greywacke Sandstone

Greywacke sandstone was identified within the quarry with varying degrees of weathering. The extent of this material is presented in Map Sheet 1.

Highly weathered (HW) to residually weathered (RW) greywacke sandstone, also known as overburden, was encountered in the surrounding upper slopes of the quarry. This unit typically appears at varying elevations due to topography, but is generally approximately 20 to 30 m thick. Overburden typically comprises the sandy silts on the surface as well as the HW to RW sandstone. This unit is generally characterised by yellowish brown clayey and silty sands with varying proportions of greywacke sandstone gravel and by very weak, highly fractured, residually to highly weathered sandstone and siltstone.

Moderately weathered (MW) to highly weathered (HW) greywacke sandstone, also known as brown rock, was encountered in the surrounding slopes of the quarry below the overburden unit. This unit typically appears to follow topography, therefore exists at varying elevations, but generally has an approximate thickness of 15 to 30 m throughout the quarry.

Unweathered (UW) to slightly weathered (SW) greywacke sandstone, also known as blue rock is present within the base of both pits of the quarry. This unit occurs at maximum elevations of approximately 110 m RL but typically below 60 m RL. It comprises bluish grey, slightly weathered to unweathered, strong to extremely strong sandstone with localised bands argillaceous mudstone. Some very rare lithic conglomerate beds exist within the sequence. The rock mass is typically jointed (but less fractured than the overlying brown rock) with minor iron-rich limonite staining on some defect surfaces and unaltered joint surfaces. Within major joint sets quartz and feldspar veins are evident. Some areas within the quarry exhibit prehnite-pumpellyite zones of metagreywacke facies.

Argillaceous Mudstone

Argillaceous mudstone is interbedded within the greywacke sandstone with varying degrees and has the quarrying term of argillite. Mudstone content within the quarry varies however, there exists a zone of high mudstone content in the southern section of Pit 2 (Map Sheet 1). Typical mudstone comprises dark brown or dark blackish grey, varying weathering

grade, extremely fractured, moderately strong to very weak argillaceous mudstone. The rock structure is characterised by thin beds (typically 5 to 25 mm thick) interbedded with greywacke sandstone. Quartz and feldspar veins are evident along with pyrite on some defect surfaces.

Alluvial Sandy Silt

Sandy silt is the capping material overlaying the interbedded sandstone and mudstone. The sandy silt is alluvial based deposit with a varying degree of thickness. It is typically described as a yellowish brown, soft to stiff, massive, fine sandy silt with some clay.

Rhyolitic Alluvium

The rhyolitic alluvium exists within a paleo-channel within the eastern edge of the quarry. This channel was the original Karapiro Stream path before it was diverted in 2004. The material is described as light orangish brown with mottled brownish black lenses, pumaceous, coarse sandy gravel with some silt. The channel deposit is approximately 3 to 4 m thick and 3 to 4 m wide. Location of this material is presented in Map Sheet 1.

b) Structural Data Collection

Photogrammetric and scanline analytical methods were implemented in this project to gather structural data. Photogrammetry is explained in Section 2.2.2. Scanline analysis was carried out to gather information on structural features identified in rock slopes.

The current pit slope performance was also analysed during the mapping stage. This focussed on the following key features:

- Bench face angle
- Crest break back
- Rill accumulation

Analysis of these features would aid in estimating the future performance of the quarry pit slopes.

Detailed face maps were also carried out on selected sections of the quarry. This was mostly done via analysis of photographs as well as field observations (Map Sheets 4 to 8).

The main structural features controlling failure and instability indentified in the field were compared with those determined by slope stability analysis (Chapter 4). Selected fault gouge and intact rock samples were also collected during mapping for later strength determination.

2.2.2 Photogrammetry

a) Introduction

Photogrammetric methods were used to gather discontinuity data particularly orientation data of structural features within the quarry. This method was applied rather than conventional face mapping method due to the restricted access to pit slopes, high risk of rock fall at the base of slopes, and limiting disruption to quarrying operations.

Photogrammetry is the science of combining a series of 2D digital photographs with surveyed ground control points (GCP's) to create a 3D model of the rock face. Each 3D model consists of rectified digital photographs integrated with a cloud of several hundred thousand x-y-z points, with estimated positional errors typically on the order of millimetres to centimetres (Hanberg, et al. 2006). Discontinuity orientations are determined by fitting planes to user-selected surfaces or their traces, and the fitted planes can be added to the 3D model to facilitate visualisation of the outcrop-scale structural geology.

Five significant slope sections were selected within the quarry of which 3D models would be generated. Each section covered a specific portion of the quarry slopes. Surveying in GCP's, with a Trimble 5600-series total station, and photography, using a Canon 5D Mark II SLR camera, was carried out in January 2010. Images were then processed and analysed for geotechnical mapping purposes.

Appendix B2 presents images of digitised 3D models, GCP survey data and exterior model orientation and accuracy data.

b) Results

Five three-dimensional models were generated from multiple images and varying resolutions. A summary of each 3D model generated is shown in Table 2-1. After the models were generated they were analysed for features such as bedding planes, joints and faults. A summary of the number of features identified and measured is presented in Table 2-2. The number of features identified within the model relate to the number pole

orientations recorded per section, therefore the greater number of features the greater number of orientation measurements.

Table 2-1: Summary of 3D model generation.

Section	Approximate Coverage Area m^2	Number of Images	Model Size (MB)	Estimated Overall Accuracy (cm)	3D Model Processing Time (minutes)
A	26,000	30	359.8	2.9	8.2
B	21,400	18	243.9	2.4	5.5
C	1,400	12	70.4	1.6	2.3
D	2,500	30	215.22	1.1	7.8
E	2,700	6	61.5	1.7	2.1

Table 2-2: Summary of structural features identified and measured in each 3D model.

3D Model	Structural Feature		
	Bedding	Joint	Fault
A	17	711	10
B	40	148	7
C	6	100	2
D	14	613	0
E	8	144	2
Total	85	1716	21

c) Discussion

This method of orientation measurement and data collection is relatively new for projects at this scale, and has been drastically refined by ADAM Technology Ltd to produce increasingly accurate three dimensional models. In this investigation, the 5 models generated varied in quality. The two large models A and B required extra care and time during processing to produce models where accurate measurements could be recorded. The resulting quality of all models is to a standard where structural data is deemed to be reliable. However, to ensure the quality of data gathered via photogrammetric methods it must be calibrated with data collected via conventional scanline analysis.

Section A was analysed by both methods. Data gathered via each method was examined for relative similarities. Similarities between the data sets suggest reliability between data gathered by photogrammetric methods and that of hand measured defect data via conventional scanline analysis. A comparison of data is presented in Figure 2-1.

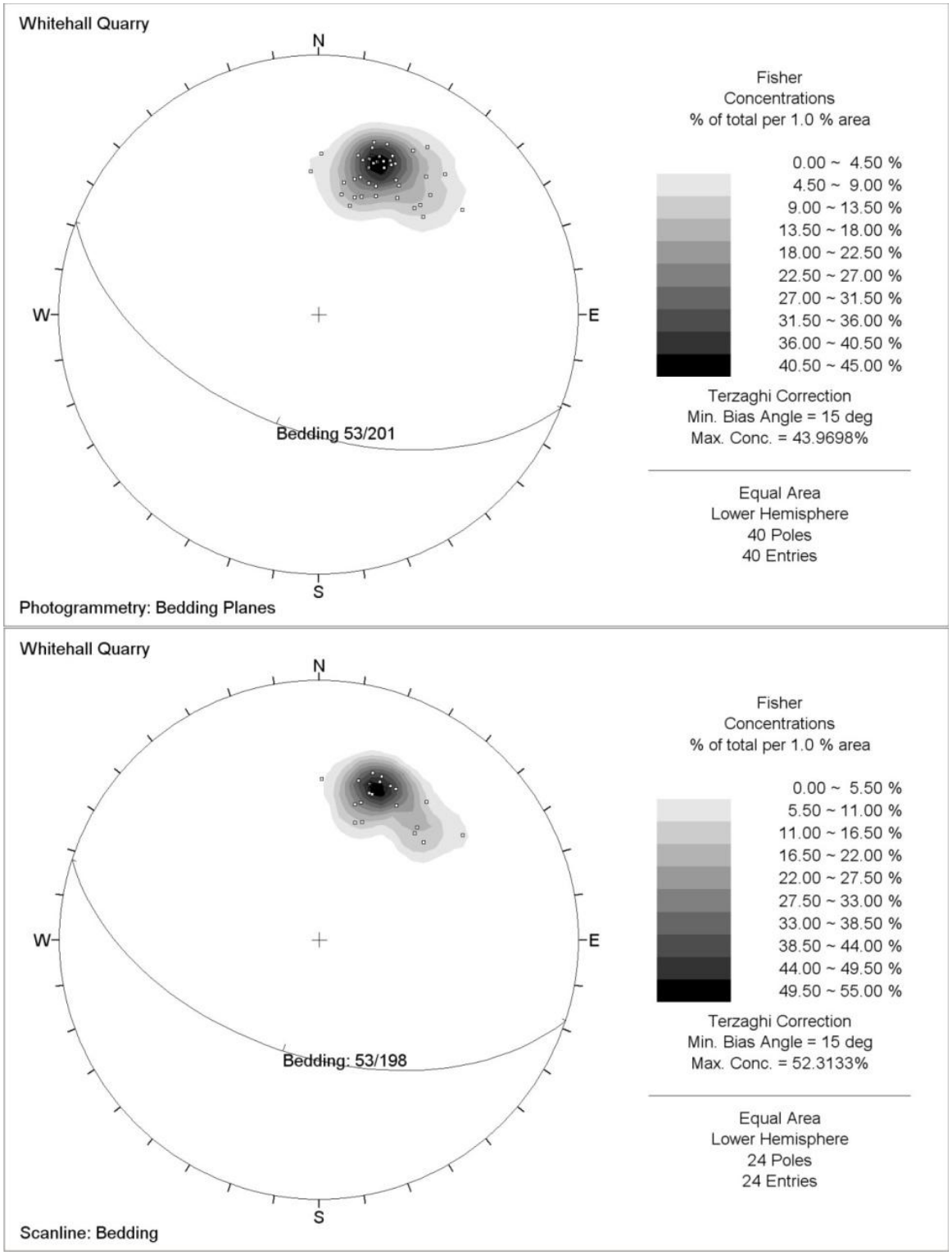

Figure 2-1: Stereoplots showing comparative data for both photogrammetric and scanline analysis of the same rock slope within the quarry.

The comparison of data collected via each method shows strong similarities. The key aspect is the inferred average dip and dip direction of the bedding plane. The dip value for both data sets is 53 degrees, while there is only a three degree difference in dip direction. This shows that data collected via photogrammetric methods is similar to established scanline

analysis thus ensuring in the reliability of data collected via photogrammetric methods throughout the quarry in this investigation.

It can be concluded that photogrammetry provides a safe, accurate and fast alternative to conventional scanline analysis. However, a notable drawback is the fact that there is a reduction in personally being able to analyse the face for key features, such as:

- Joint roughness coefficient (JRC)
- Discontinuity waviness
- Discontinuity spacing and terminations
- Defect infill type and strength

As a result of using photogrammetry, supplementary fieldwork was carried out on rock slopes where it was safely possible with the aim of measuring the features listed above and carry out a more in depth assessment of the rock slopes.

A universal standard has yet to be developed for photogrammetric methods. There appears a degree of bias in selecting and sampling different discontinuities within the rock slope. That is, discontinuities that have a strike sub-parallel to the face are more likely to be selected due to their increased clarity compared to discontinuities that strike sub-perpendicular to the face. The analysis in this study aimed at reducing this effect by identifying and examining sub-perpendicular discontinuities.

Orientation data obtained from photogrammetry for each section is presented and analysed for structural domains in Chapter 3.

The amount of time spent on selecting the discontinuities in each model far outweighed the time that would have been spent on conventional scanline analytical methods. However, time must be spent understanding the operation, abilities and implications within the process which can be time consuming.

2.2.3 Schmidt Hammer Field Testing

a) Introduction

The strength of the rock forming the walls of discontinuities will influence the shear strength of rough surfaces (Wyllie & Mah, 2004). Therefore, it is adequate to estimate the uniaxial compressive (UCS) strength from the Schmidt hammer field test (Hoek & Bray,

1981). The Schmidt hammer, developed in the late 1940's as an index apparatus for non-destructive testing of concrete in situ, has been used in rock mechanics practice since the early 1960's, mainly for estimating the uniaxial compressive strength of insitu rock material out in the field (Aydin & Basu, 2005).

The Schmidt hammer returns a rebound number for the tested sample which is then converted to UCS using the approximated density of the material tested. Testing was carried out during the field investigation stage of this study in accordance with the ISRM suggested methods (1978). Details of the test method and calculations are presented in Appendix B4.

The Schmidt hammer test was applied to slightly weathered (SW) to highly weathered (HW) greywacke sandstone, slightly weathered argillaceous mudstone and slightly weathered ignimbrite (located in cliffs to the east of the pit). An average of 40 rebound values were recorded per rock type tested.

b) Results

Results obtained from testing are summarised in Table 2-3, the conversion chart sourced from Hoek and Bray (1981) is presented in Appendix B4. The approximate densities used in the conversion of Schmidt hardness to UCS for the UW and SW greywacke sandstone was evaluated via porosity-density tests. Approximate unit weights for other lithologies were determined by the AusIMM Field Geologists' Manual (2001).

Table 2-3: Summary of Schmidt hammer insitu rock strength testing.

Lithology	Average Schmidt Hardness	Approximate Unit Weight (kN/m^3)	Corresponding UCS (MPa)	Strength Classification[1]
UW Sandstone	62	26	230	Very Strong
SW Sandstone	54	25	150	Very Strong
MW Sandstone	29	25	55	Strong
HW Sandstone	15	25	30	Strong
SW Mudstone	24	22	37	Strong
SW Ignimbrite	37	23	57	Strong

[1] Terms from Bell and Pettinga 1983

c) Discussion

The results obtained for greywacke sandstone are as expected with classifications of very strong to strong being similar to results obtained by Hetherington (1989). However, the classification of strong for the mudstone material appears to be too high, the expected classification is moderately weak. This highlights the issues with UCS estimation from Schmidt hardness particularly in the case of weak rocks; use of the same specimen for both tests can be very misleading, as hammering will induce microcracks inside the specimen and lowering its estimated UCS. This seems to be the case for the HW sandstone and SW mudstone sample.

The selection of surfaces for applying the hammer carries a considerable amount of bias. The Schmidt hammer will not return a result is the surface crumbles or breaks on hammering; therefore surfaces that appeared weak and exhibited small fracture frequency were avoided. This is likely to produce unrepresentative UCS values.

The UCS values for intact rock strength are to be correlated with point load values obtained from laboratory investigations. It is likely that results for argillaceous mudstone will be ignored in slope stability analysis due to the significantly high variability in testing of weak material.

2.3 Laboratory Testing

2.3.1 Introduction

In order to develop an engineering geological model for Whitehall Quarry it is paramount to provide as much information on the materials within the quarry as possible. This section aims at evaluating the various parameters of the materials identified during field investigations (Map Sheet 1).

The materials identified via field investigations were:

- Greywacke sandstone
- Argillaceous mudstone
- Fault gouge (Main Quarry Shear Zone and sliding plane of the Northern Wedge Failure)

Laboratory tests to be carried out on the sandstone and mudstone materials are:

- Point load index, to approximate the intact rock strength
- Shear box, to approximate the shear strengths of key defects

Laboratory tests to be carried out on fault gouge are:

- Direct shear, to approximate shear strength
- Atterberg Limits, to approximate soil behaviour with varying moisture content
- X-ray diffraction analysis, to identify clay mineralogy

2.3.2 Sample Collection

Samples were collected from the quarry in January 2010 to be tested in the laboratory at the University of Canterbury. The initial aim was to collect as many samples of each rock, soil and weathering type as possible. However, this was not possible for materials that were highly weathered. Highly weathered materials were significantly weaker than slightly or unweathered materials, thus too weak to collect a sample.

Samples that were to undergo point load testing were collected from various locations around the quarry. This was to allow the identification of variations in intact rock strength. Sandstone and mudstone discontinuities to have the shear strength approximated were selected as the most typically discontinuity type for that material. The sandstone joint sample was a smooth (joint roughness coefficient of 3) joint surface the typical type of sandstone joint within the quarry. The mudstone bedding plane was selected because it was the only mudstone sample to survive collection and transport. Fault gouge samples were collected from significant faults, namely the Main Quarry Shear Zone and a sliding plane of the Northern Wedge Failure. The locations of each sample collected are presented in Figure 2-2.

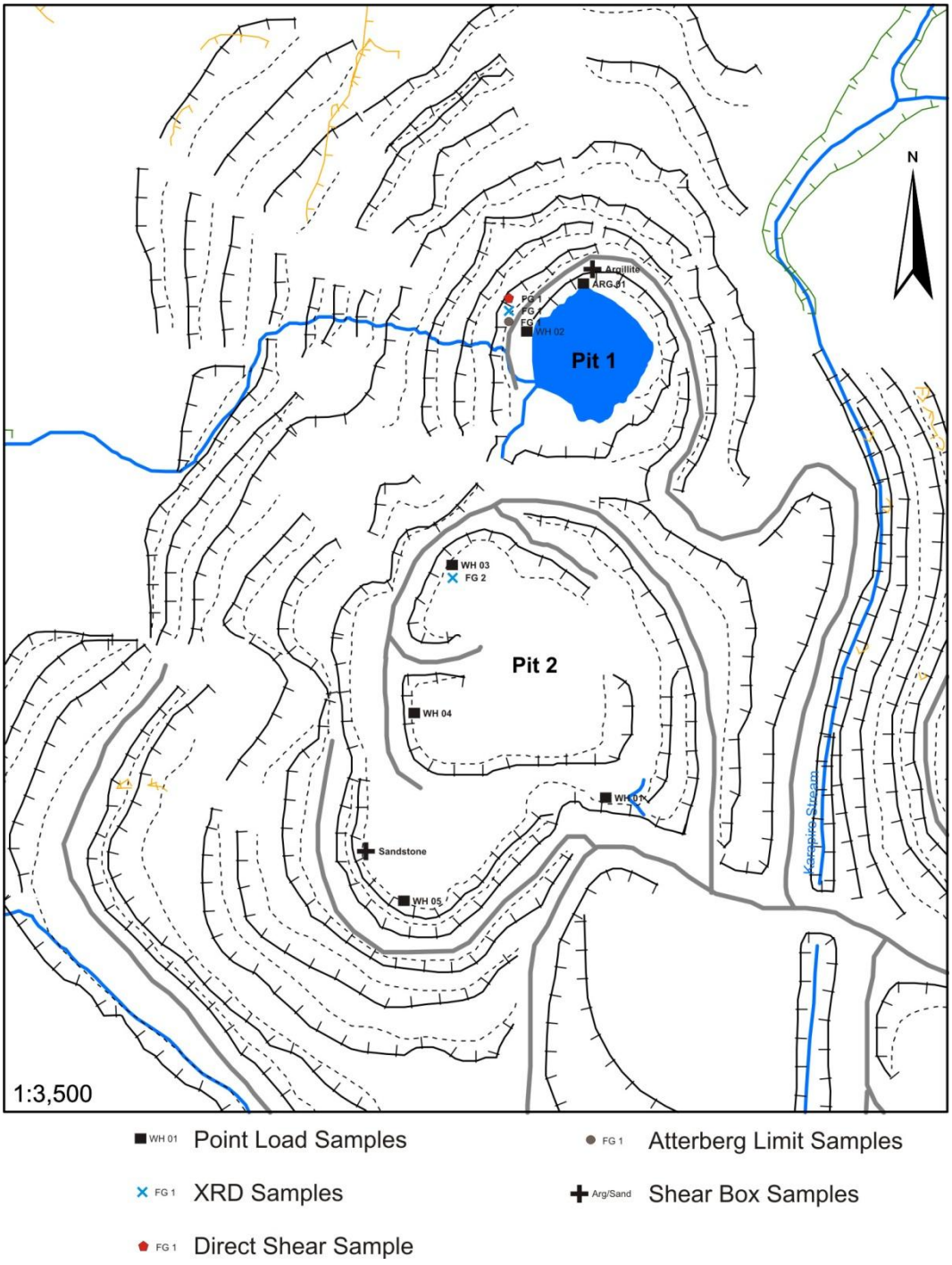

Figure 2-2: Map showing the locations where samples were collected.

On collection, all samples were wrapped in plastic film and stored out of direct sunlight to maintain the original or pit moisture conditions.

2.3.3 Point Load Testing

a) Introduction

Point load testing was undertaken on rock samples collected from the quarry to ascertain peak strengths providing intact rock strength data for the engineering geological model. Initially developed by Broch and Franklin (1975) the point load test is a technique which allows a rapid estimation of rock strength from either irregular lumps or drill core samples in the field or laboratory. Point load testing was undertaken in accordance with the ISRM suggested methods (1985) and details of the test method, calculations and selected photographs are presented in Appendix C2.

The point load strength index, I_s in MPa, is calculated as the ratio of the failure load to the square of the platen separation at failure. The size of the sample has an effect on the strength, and values are therefore calibrated back to a standardised platen separation of 50 mm referred to as $I_{s(50)}$ (Brook, 1985). Point load testing has the distinct advantage over uniaxial compressive strength (UCS) testing in that smaller samples may be tested, and there is no requirement for sample preparation. The ability to test smaller samples means that point load testing does not suffer the same test sampling bias which UCS testing does and that quantitative strength data may be obtained for most practical sample sizes (Brook, 1985).

To convert point load index values into uniaxial compressive strengths the following conversion equation will be used (Broch & Franklin, 1975):

Greywacke sandstone samples, on which point load testing was performed, consisted of 86 irregular lump samples of UW greywacke sandstone selected from 5 different locations within the quarry. Selecting samples from various locations allows for analysis for differences in intact rock strength throughout the quarry. Because, at this small scale, the sandstone appears to be isotropic, it was thought that testing either axially (load platens oriented perpendicular to bedding) or diametrally (load platens orientated parallel to bedding) was negligible.

Argillaceous mudstone samples also had point load testing undertaken. A total of 15 irregular lump samples were used. Due to the weak strength of the mudstone testing was

undertaken axially (perpendicular to bedding) on samples collected from one location within Pit 1.

All samples were collected in a dry state from the pit floor were they had fallen from adjacent walls. Moisture content tests were carried out to evaluate the moisture content of UW greywacke sandstone a SW-UW argillaceous mudstone. Moisture content testing was undertaken in accordance with the ISRM suggested methods (1985) and details of the test method and calculations are presented in Appendix C2.

b) Results

A summary of the point load test results is presented in Table 2-1. Point load testing results are as follows:

Sandstone:

- Average corrected point load index values ($I_{s(50)}$) for tests on the greywacke sandstone ranged from 7.3 MPa (very strong) to 10.5 MPa (extremely strong), with a mean average index strength of approximately 8.98 MPa (very strong).
- The ratio of valid to invalid tests was less than 9%; invalid tests were usually the result of fracturing along a pre-existing fracture or micro-fractures, containing mudstone content, or samples failing through the 'sides' of the sample.
- The moisture content test carried out on a sandstone sample indicated approximately 0.7% moisture within the rock indicating a dry rock sample. This is unlikely to be entirely indicative of subsurface conditions.

Mudstone:

- Results for the mudstone returned an average corrected ($I_{s(50)}$) point load index value of approximately 0.19 MPa, indicating a moderately weak rock that can be broken by hand only with difficulty, also small thin pieces can be broken by finger pressure.
- The ratio of valid to invalid tests was much greater for the mudstone at approximately 20%; invalid tests were mostly due to sandstone content masked within the core of the sample.

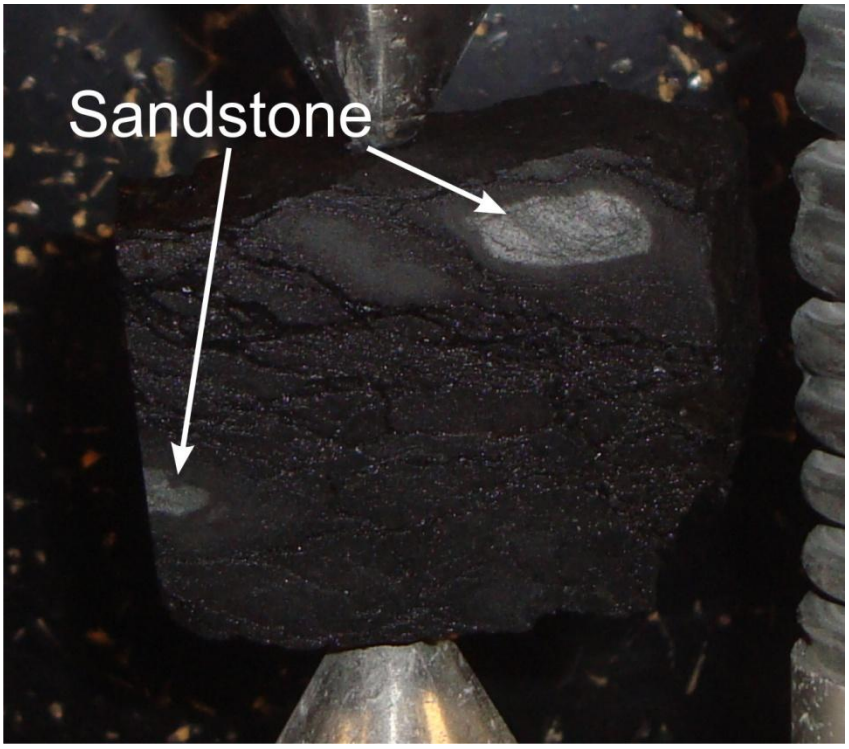

Figure 2-3: Invalid test, mudstone sample contains sandstone material.

- The moisture content test carried out on a mudstone sample indicated approximately 1.4% moisture within the rock indicating a dry rock sample. Again, this is unlikely to be entirely indicative of subsurface conditions.

Table 2-4: Summary of Point Load Testing Results.

Sample No.	Sample Description	No. Of Samples	Average Strength (MPa)		Strength Term[2]
			$I_{s(50)}$	UCS[1]	
WH1	Unweathered, grey, massive, coarse sandstone	20	10.5	252	Extremely Strong
WH2	Unweathered, grey, massive, coarse sandstone	22	8.8	211	Very Strong
WH3	Unweathered, grey, massive, coarse sandstone	12	7.3	175	Very Strong
WH4	Unweathered, grey, massive, coarse sandstone	15	9.4	226	Very Strong
WH5	Unweathered, grey, massive, coarse sandstone	17	8.9	214	Very Strong
WH ARG	Unweathered, greyish black, finely layered, argillaceous mudstone	15	0.2	5	Moderately Weak

[1] Assuming calculated correction factor of 24

[2] Terms after Bell and Pettinga (1983)

c) Discussion

Results from point load testing indicate some degree of homogeneity in intact rock strength within the quarry at similar elevations. The very strong to extremely strong characterisation of the sandstone was expected. This suggests that rock mass failure within sandstone is most likely to occur along pre-existing defects, such as joints and faults, rather than failure through fracturing rock.

The moderately weak classification of the mudstone is anticipated to be an anomalously high result due to the difficulty in sample selection. Samples in the field generally crumbled once extracted from the face. This introduces a considerable amount of bias in sample selection, as only competent samples are collected which are not representative of the mudstone strength throughout the quarry. The only competent sample was collected from Pit 1 with great care. If it were possible, more samples would have been collected for testing and thus producing more representative results although higher than expected.

Point load results can then be converted into UCS values. Various studies have been carried out to determine a suitable conversion factor for various rock types. These studies approximated conversion factors between 16 and 45. It is unreasonable to use the upper and lower limits in this conversion as this would result in extreme UCS results and a very large range of acceptable values. Applying the conversion factor of 16 is likely to produce conservatively low values for sedimentary rock strength, while an assumed conversion factor of 45 in contrast is likely to produce unrealistically high values for strength. Both Bieniawski (1975) and Broch and Franklin (1975) postulated a relatively accurate conversion factor of 24 for sedimentary rocks through various point load versus UCS experiment. The relationship is expressed in the following equation:

Using the above equation, results from point load tests are converted to UCS and shown in Table 2-4. Sandstone tests return a UCS range of 175 to 252 MPa, which relates to strong (100-200 MPa) to very strong rock (>200 MPa) (Hoek & Bray, 1981). This range of values are within the typical range (150 to 200+ MPa) for greywacke sandstones within New Zealand (D.H. Bell, personal communication, December 11, 2010).

This provides evidence suggesting stability of the rock mass relies on rock mass defects rather than failure through the formation of new rock fractures. Even when the rock mass is significantly loaded failure is still most likely to occur along defects such as bedding, joints and/or faults.

The corresponding UCS for the mudstone is approximated at 5 MPa characterised as very weak rock (1 to 25 MPa) by Hoek and Bray (1981). This characterisation suggests that the conversion factor was relatively accurate as the suggested rock type for this UCS range is chalk, rocksalt, and mudstone.

2.3.4 Shear Box Testing of Rock Discontinuities

a) Introduction

In analysing the stability of a rock slope, one of the most important factors to be considered is the shear strength of the potential failure surface. This potential failure may consist of a single discontinuity plane or a complex path following several discontinuities and involving some fracture of intact rock material (Hoek & Bray, 1981). Determination of reliable shear strength values is a critical part of a slope design because relatively small changes in shear strength can result in significant changes in the safe height or angle of a slope.

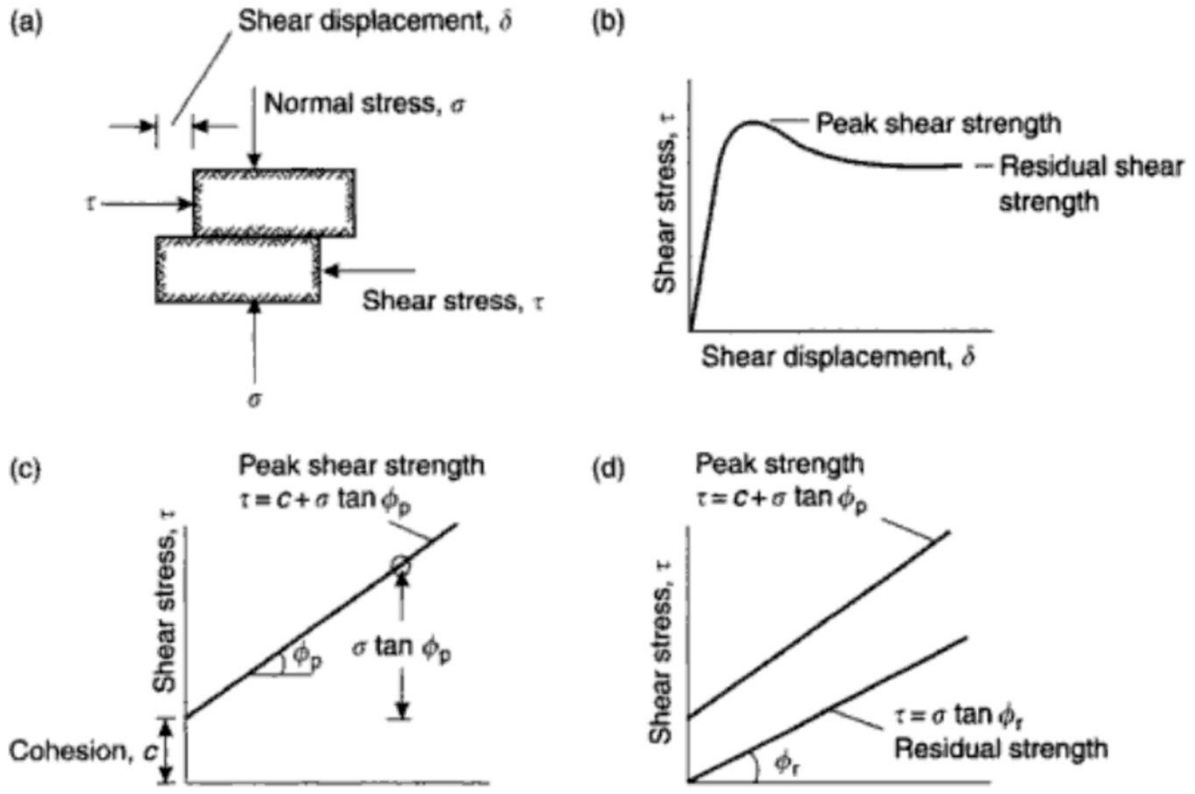

Figure 2-4: Definition of shear strength; (a) shear test of discontinuity; (b) plot of shear displacement vs. shear stress; (c) Mohr plot of peak strength; (d) Mohr plot of peak and residual strength (Wyllie & Mah, 2004).

Shear strength testing produces a value for cohesive strength (c, the strength of bonding between two surfaces) and an angle of internal friction (φ, the angle relating to the shear stress required for sliding to the normal stress on a plane). It is assumed that sliding will be initiated on joints and bedding planes at the residual shear strength rather than peak shear strength, thus residual shear testing was under taken on one argillaceous mudstone bedding plane and one smooth joint representative of a typical joint within the quarry.

Residual shear strength refers to the shearing resistance remaining after large displacements have occurred (Patton, 1966). Residual shear testing was carried out using the Robertson Geologging Ltd Shear Box apparatus housed within the Rock Mechanics Laboratory at the University of Canterbury. Two samples were tested:

- Mudstone Bedding Plane: A plane within a sample of SW-UW, very weak mudstone to evaluate the shear strength of the weakest material within the quarry.
- Sandstone Joint: A smooth joint (joint roughness coefficient (JRC) ~3) within UW, very strong sandstone to evaluate the shear strength of a typical joint within the quarry.

Testing of samples was carried out in accordance with the ISRM suggested methods (1974) and details of the test method, calculations and photographs are presented in Appendix C4. It must be noted that a key deviation from the suggested methods is the use of the same sample for each different normal force applied.

b) Results

Plots of residual shear stress versus normal stress and shear stress versus shear displacement for each sample are presented in Figure 2-5 to Figure 2-8.

The mudstone bedding plane shear box test returned a residual angle of internal friction of 31^{o} at a moisture content of 1.4%. The sandstone joint shear box test returned an angle of internal friction of 34^{o} at a moisture content of 0.7%. Being residual shear strength, cohesive shear strength was 0.0 kPa.

Issues were encountered in the shear box test of the sandstone joint sample when loaded to 15.0 kPa. At this normal force the plaster mould failed during the test at an approximate displacement of 3 mm, thus reducing the normal force and shear stress and is noticed in the 15.0 kPa line of Figure 2-8, but it appears that the resulting residual shear stress was relatively unaffected. Another issue was with the accuracy of the shear box apparatus, the read-out dial was in increments of 1.0 kN where fractions of a kilo-newton had to be estimated. This apparatus is generally used as a field test but will suffice for this type of testing.

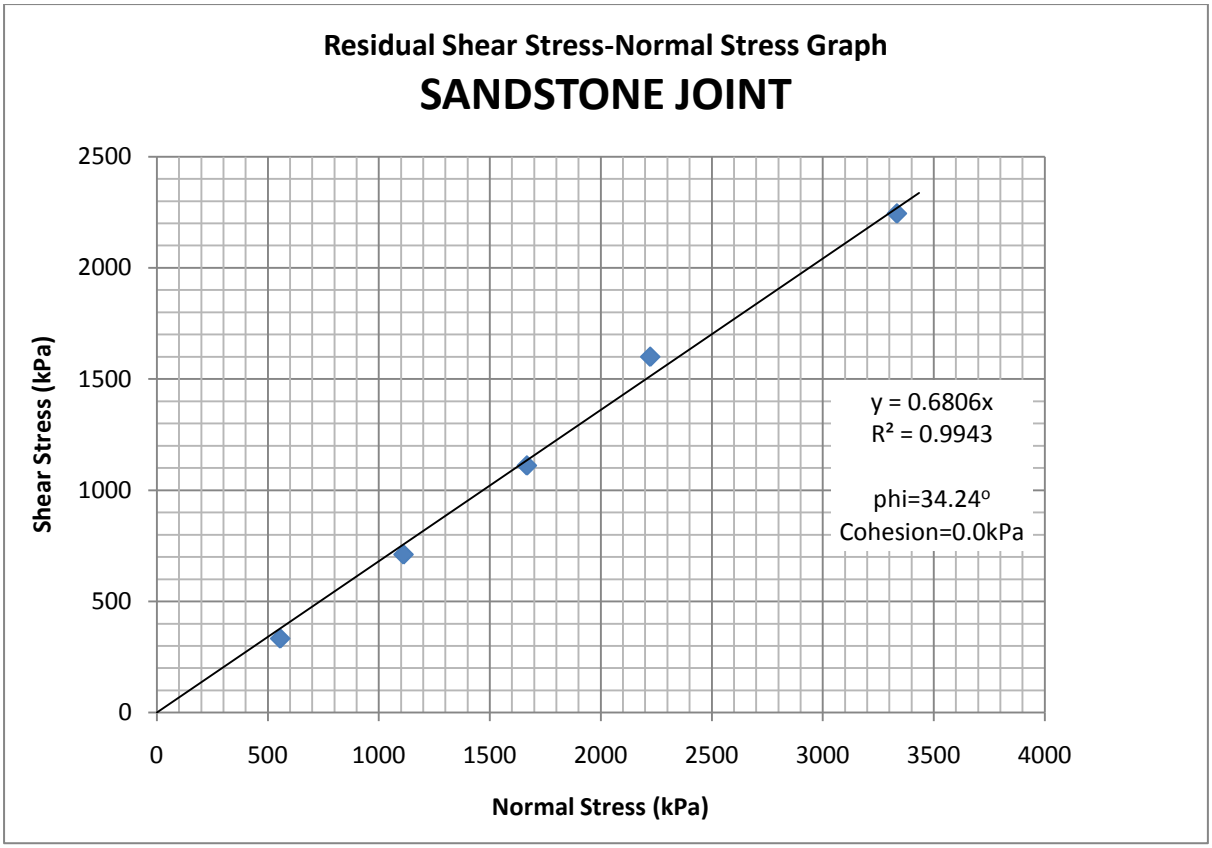

Figure 2-5: A plot of normal stress (σ_n) versus residual shear stress (τ_r) for a mudstone bedding plane.

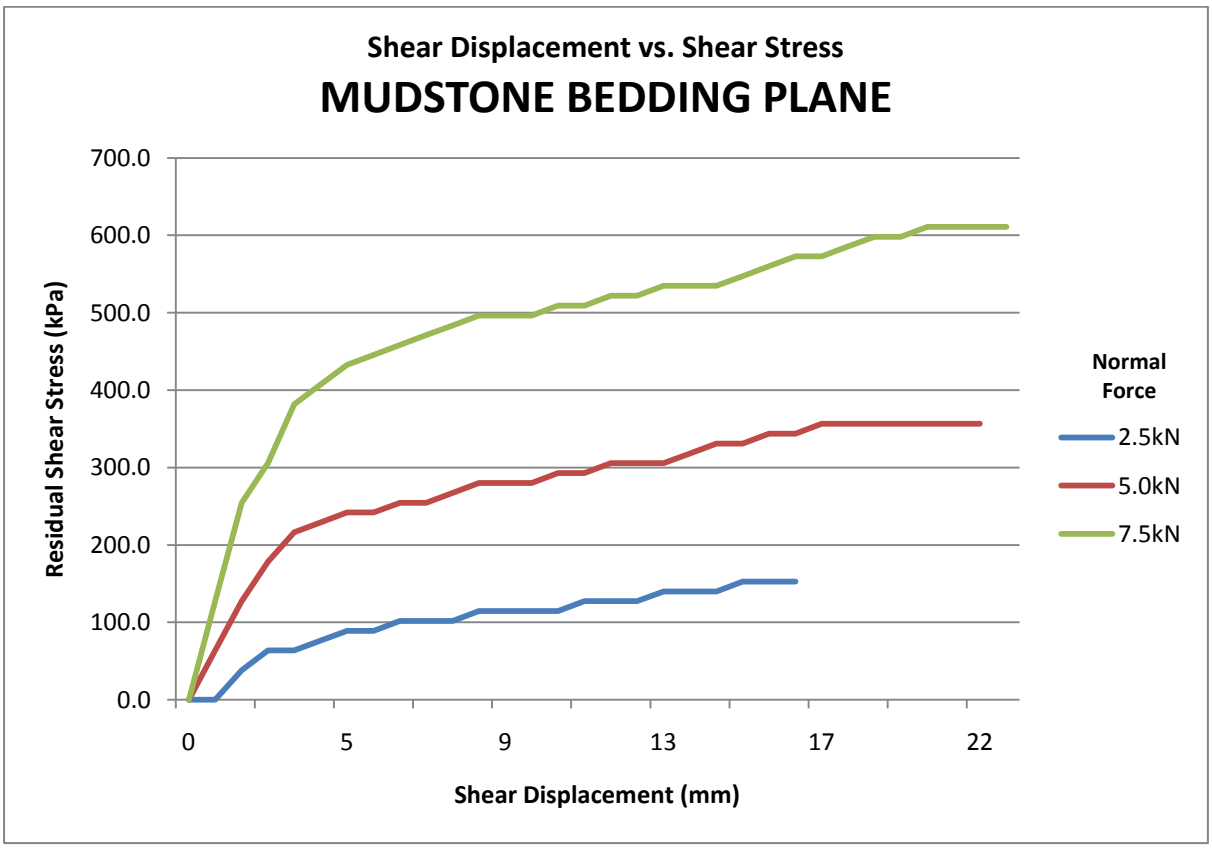

Figure 2-6: A plot of shear displacement versus residual shear stress (τ_r) for a mudstone bedding plane.

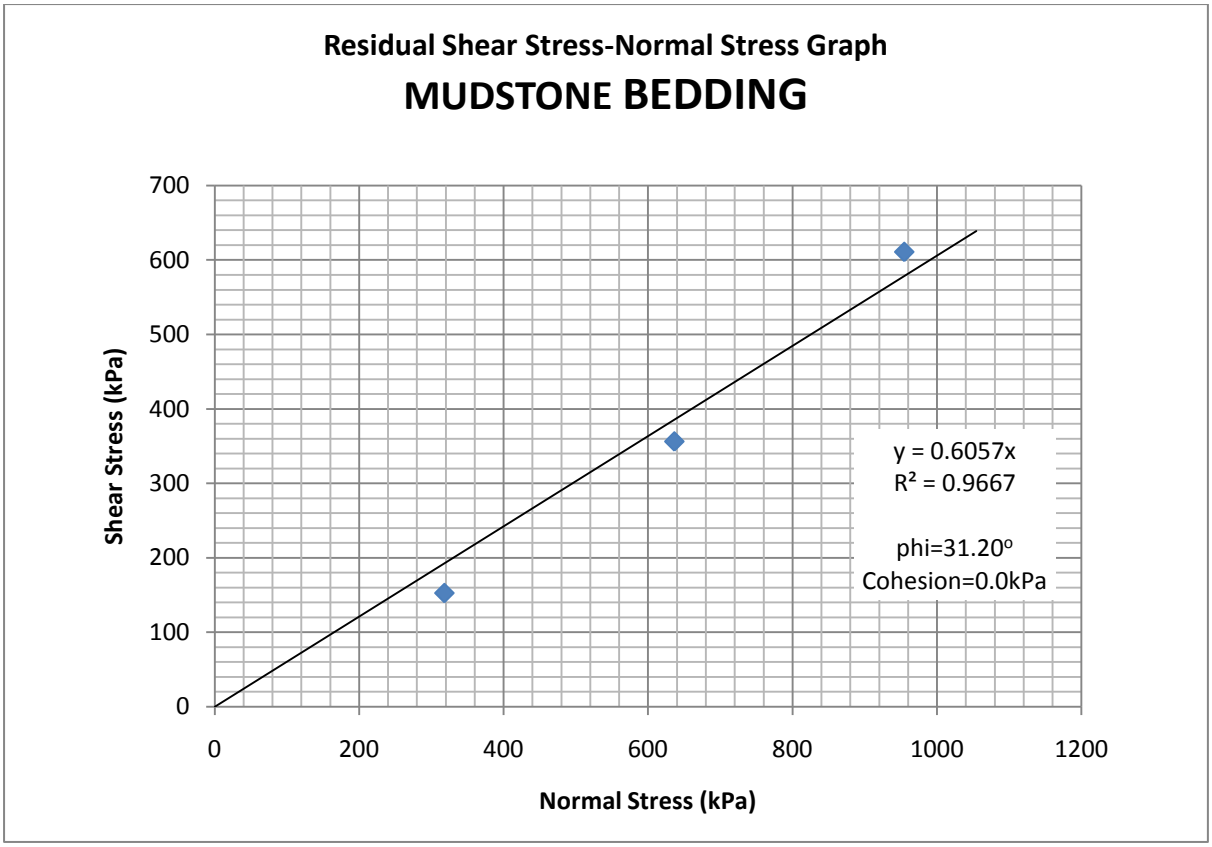

Figure 2-7: A plot of normal stress (σ_n) versus residual shear stress (τ_r) for a smooth sandstone joint.

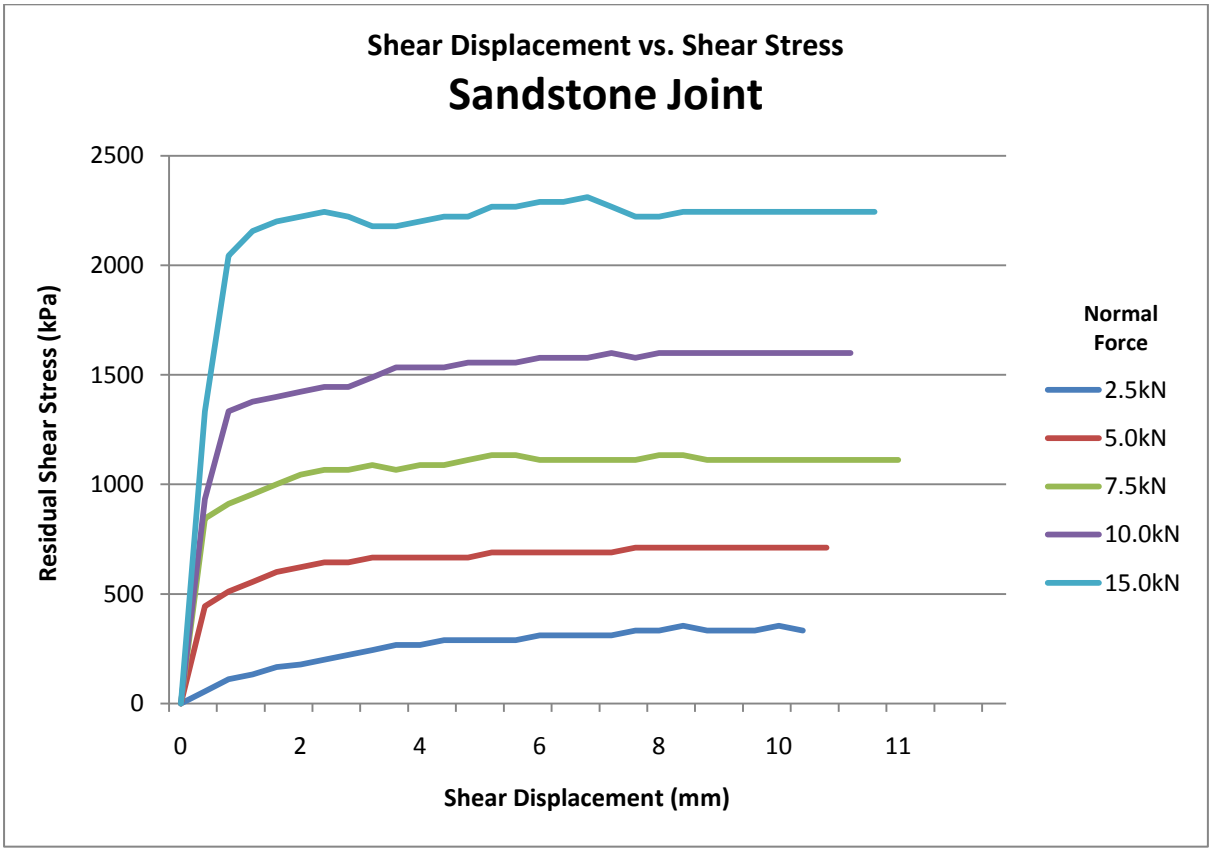

Figure 2-8: A plot of shear displacement versus residual shear stress (τ_r) for a smooth sandstone joint.

c) Discussion

The shear test of the mudstone bedding plane returned expected results (residual angle of internal friction, $\varphi_r = 31^o$). Barton (1973) suggested a range of φ_r values from 31^o to 33^o for mudstone which encompasses the residual angle of internal friction approximated in this study for a mudstone bedding plane. Testing of the sandstone joint also returned expected results ($\varphi_r = 34^o$) which lies within the range of 26^o to 35^o for sandstone (Barton, 1973). The ranges of values derived from Barton (1973) are derived from shear box tests carried out on sand-blasted, rough-sawn and residual surfaces for various rock types and moisture contents.

Shearing along the mudstone bedding plane caused the sample to fail via micro-fractures, thus causing the material to disintegrate. However the original JRC of 4 to 5 did not appear to decrease as asperities were sheared off. The final JRC was estimated at 3 to 4, a minor decrease. Shearing on the sandstone joint did not appear to reduce the original JRC of 3. However, shearing of asperities produced fine grained silt on the sheared surface.

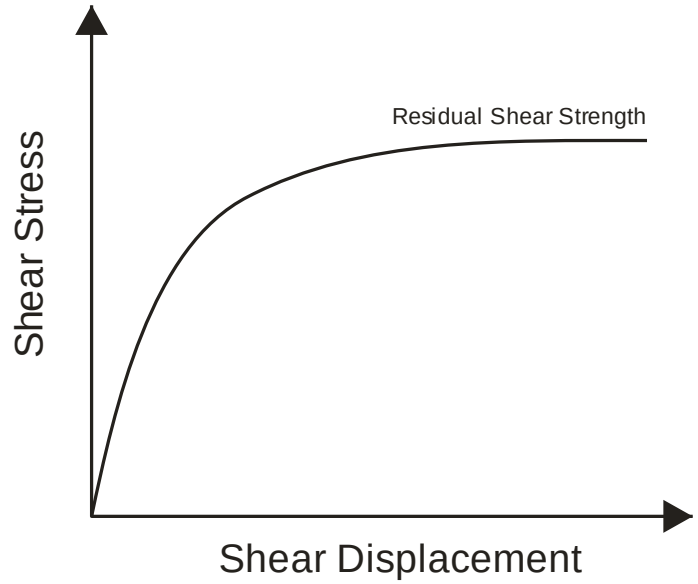

Figure 2-9: Typical plot for surfaces at residual shear strength, adapted from Wyllie and Mah (2004).

Laboratory values of cohesion for rock discontinuities are usually inapplicable to engineering analyses, since it is not possible to test joints with surface roughness features which are representative of field conditions. In the field, the cohesive shear strength between joints it usually non-existent. Therefore, it is best practice to estimate the cohesion as zero, consequently assessing the worst case scenario for rock slope engineering.

There was a degree of bias in the selection of the mudstone sample. As discussed in the point load results, the very weak rock is difficult to sample. Most of the mudstone samples collected from the pit wall or floor disintegrated on collection or transport. Therefore the sample that survived collection and transport exhibited a stronger strength than typical and was therefore tested. This is likely to indicate a higher than average shear strength for the mudstone bedding plane.

Both of these tests were undertaken in natural surface moisture contents and do not fairly replicate sub-surface water conditions. Moisture contents of the mudstone and sandstone were recorded as 0.7% and 1.4% respectively, indicating relatively dry conditions. This is not representative of sub-surface conditions where 100% saturation is likely. The presence of water in a rock discontinuity leads to several mechanical effects, the most of which is the reduction in effective stress (Barton, 1973). This has the subsequent effect of lowering the shear strength for the surface being tested. Barton (1973) carried out several shear strength tests to assess the effect moisture content has on rock shear strength. For mudstone he postulated very little to no change in shear strength in either dry or wet state.

The results for UW sandstone appear to correlate with estimated values from the 2004 study carried out by Tonkin & Taylor Ltd of rock material on the eastern slopes of the quarry, summarised in Table 2-5. The residual angle of internal friction for sandstone from this study plots within 3 degrees of the result on the sample material by Tonkin & Taylor Ltd in 2004, thus the results for MW-HW sandstone and overburden material may be used for later slope stability analysis. However, it must be noted that results obtained from this investigation and that of Tonkin & Taylor Ltd (2004) are estimates and should carry an uncertainty of plus or minus five degrees for smooth surfaces (Barton & Choubey, 1977).

Table 2-5: Summary of Tonkin & Taylor Ltd investigation only (2004).

	UW-SW (Blue Rock)	MW-HW (Brown Rock)	CW-RW (Overburden)
Phi (degrees)	37	32	23
Cohesion (kPa)	500	200	100

2.3.5 X-ray Diffraction (XRD) Analysis

a) Introduction

X-ray diffraction (XRD) analysis was used to identify the clay mineralogy of fault gouge samples collected from the Main Quarry Shear Zone and a sliding plane of the Northern Wedge Failure. The identification of clay minerals within fault gouge is important due to the different behaviours of different clay types. The clay minerals, if any, identified in this analysis should be considered in both pit slope stability (MQSZ) and the Northern Wedge Failure.

XRD analysis is a widely used technique for the identification of clay minerals which cannot be easily identified through more conventional methods such as petrology. In this study whole sample analysis is carried out on two samples of fault gouge material collected from Pit 1,northern wedge failure sliding plane (fault gouge sample 1, FG1) and Pit 2, the Main Quarry Shear Zone (FG2) during field investigations, was analysed for clay mineralogy. FG1 was taken from a representative sample of gouge material used in direct shear and Atterberg Limit testing. This allows for the correlation of residual shear strength with clay mineralogy. Percentages of each mineral were visually estimated as the proportion of the areas corresponding under each peak for each mineral to the total area encompassed under all peaks for all minerals. It must be noted that this whole sample analysis technique provides an indication of the clay minerals present within the sample only; due to larger particles present overprinting on smaller clay minerals occurs thus producing unreliable clay mineral content. The XRD test technique used in this study is presented in Appendix C8.

b) Results

The diffractograms for each of the two fault gouge samples tested are presented in Appendix C8, while Table 2-6 presents a summary of the constituent clay minerals identified in each of the samples tested. FG 1 was collected from the northern wedge fault zone and FG 2 was collected from the main shear zone trending east west within Pit 2 (Figure 2-2).

Table 2-6: Approximate visual percentage estimates of the mineral composition for the whole sample analysed using X-ray diffraction.

	FG1	FG2
Quartz	60%	40%
Calcite	-	40%
Albite	30%	10%
Kaolinite	5%	-
Montmorillonite	5%	10%
TOTAL	100%	100%

c) Discussion

Whole sample XRD analysis carried out on two different fault gouge samples returned expected results. Most of the fault gouge particles appear to be derived from the mechanical weathering of sandstone rich in quartz and feldspar. However, the high content of calcite in one sample suggests strong chemical weathering of calcareous minerals within the sandstone. Calcite, along with zeolite, is also present on joint surfaces and within some faults.

Both results estimate approximately 10% of the fault gouge material is clay minerals of either kaolinte or montmorillonite. Kaolinite was found to be present within one sample estimated at 5% and is likely to have been formed via weathering of feldspathic greywacke sandstone in acidic conditions (Grimm, 1968). Kaolinite has a one tetrahedral: one octahedral (1T:1O) structural arrangement bonded by hydrogen, this causes very little swelling or shrinking behaviour due to the little difference in charge (Meunier, 2005).

Montmorillonite was indicated to be present in both samples at 5% and 10%. This clay mineral belongs to the smectite group of clays. Smectite clays are significant in slope stability because of their ability to shrink and swell more than any other clay group (Grimm, 1968). They also have the characteristic of high plasticity, typical montmorillonite plasticity indices range from approximately 100 to 710. This combined with high shrink and swell ability reduces the angle of internal friction resulting in a range of 4 to 9 degrees. Therefore, smectite clays are greatly significant in any clay gouge material within engineered slopes.

However, XRD whole sample analysis only provides an indication of the clay minerals present as well as an unreliable content estimate. The clay mineralogy present within the sample is all that can be taken away from this analysis due to larger particles in the

sample overprinting smaller clay minerals. Therefore, it must be assumed that the contents indicated are unreliable. In this investigation clay mineral content can only be estimated via Atterberg limits with supporting shear strength data from ring shear testing.

2.3.6 Atterberg Limits

a) Introduction

As previously stated, understanding the behaviour of fault gouge material is imperative for slope stability assessment. Specifically, the plasticity of the material plays a significant role in the sliding of material on a plane, such as a fault. Atterberg Limits are the basic measure of the nature of a fine-grained soil, in this case fault gouge material. The limits are used to determine the gouge material's behaviour from which the boundary between silt and clay can be distinguished and the type of soil can be approximated (Figure 2-10). The Atterberg Limits are based on the soil's moisture content to evaluate its' plasticity.

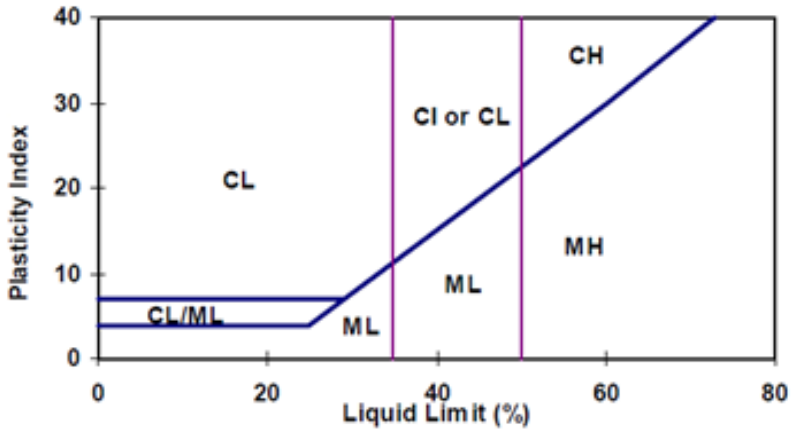

Figure 2-10: Classification based on plasticity properties of fine-grained soils (Golder Associates Ltd, 2002).

The Atterberg limits are defined by the Liquid Limit (LL), Plastic Limit (PL) and the Shrinkage Limit (SL) (note: Shrinkage limit was not tested in this investigation).

- The Plastic Limit (PL) is the water content where soil starts to exhibit plastic behaviour.
- The Liquid Limit (LL) is the water content where a soil changes from plastic to liquid behaviour.

Testing of Atterberg Limits was carried out in the Soil Mechanics laboratory at the University of Canterbury in accordance with NZS 4402:1986 Test 2.3 and NZS 4402:1986 Test 2.5. Details of the test method, calculations and photographs are presented in Appendix C7.

b) Results

A summary of the results obtained through Atterberg Limit testing are presented in Table 2-7.

Table 2-7: Summary of Atterberg Limits for fault gouge.

Soil Type	Plastic Limit	Liquid Limit	Plasticity Index
Fault Gouge	31	51	20

c) Discussion

The plastic limit is the division between semi-solid and plastic state for the gouge material. Therefore, the plastic limit of 31 is the water content at which the gouge begins to behave in a plastic manner. If the water content of the surrounding fault is reduced below 31% the fault gouge will act as a semi-solid material, thus increasing the resisting force on the fault.

The liquid limit is the division between plastic and liquid state for the gouge material. Therefore, a liquid limit of 51 is the moisture content at which the soil will flow at very low shear forces. If the water content below the surface increases above 51%, which is likely in this case, the gouge will begin to flow when subjected to high shear stresses, such as those applied at a fault.

The plasticity index indicates the range of water content through which the soil remains plastic. The plasticity of the fault gouge material is 20 indicating low plasticity (20 to 25% clay minerals present within sample). This value also indicates a Unified Soil Classification System (USCS) symbol of CL, indicating an inorganic clay of low to medium plasticity with none to very slow dilatancy (Bell & Pettinga, 1983). The clay mineral content estimated at 20 to 25% is supported by the low angle of internal friction (13^{o}) obtained from ring shear testing by Works Consulting Services Ltd, thus highlighting the inaccuracy in the whole sample XRD analysis (clay content of 10%).

2.3.7 Direct Shear Testing of Fault Gouge

a) Introduction

Residual shear strength is generally applied to soils that have been subjected to large strains so that the soil particles either side of the shearing surface will have rearranged to produce a more parallel orientation. As such the strength is lower than the peak strength, similar to rock. Shear strength for soils, in this case fault gouge, is approximated via direct shear testing.

Two samples were collected for residual direct shear testing from a major fault (south-western sliding plane of the northern wedge) in Pit 1 orientated at 60^{o}/035. The fault gouge material is approximately 50 mm thick and described as:

> *MW-UW, moist, soft to firm, light brownish grey, massive, low plasticity, silty CLAY with some fine gravel [CL].*

Gouge or infilling is the material between two faces of a structural discontinuity, in this case, a fault. This material will have an important influence upon the shear strength of the fault. If the thickness of the gouge is such that the faces of the fault do not come into contact, the shear strength will be equal to that of the gouge material (Hoek & Bray, 1981).

Atterberg Limits and XRD analyses were also undertaken on the same sample as explained in Section 2.3.5 and 2.3.6 respectively. Due to the significance of the fault as the sliding plane for a large wedge, it is important to carefully analyse gouge behaviour and interpret results accordingly.

Direct shear testing was carried out using the WF25300 Direct Shearbox apparatus housed in the Soil Mechanics Laboratory at the University of Canterbury. Testing was carried out in accordance with ASTM D3080-04 and details of the test method, calculations and photographs are presented in Appendix C5. It must be noted that samples were not sieved to leave only clay sized particles (less than 2 μm), but instead samples were tested without changing the particle size or sample saturation. Furthermore, there were two samples of the same fault gouge; each sample was loaded twice with different normal forces.

b) Results

A plot showing residual shear stress versus normal stress is presented in Figure 2-11. Direct shear testing returned an approximate residual angle of internal friction of 41.8^{o} for the sampled fault gouge. The residual cohesive shear strength for the fault gouge sample was approximated at 0.5 kPa.

Samples appeared to exhibit little to no volume changes while submerged in water during testing, suggesting the lack of swelling clays within the sample.

There was a small issue with the testing apparatus at the time of testing, where the strain and/or displacement was not recorded into the final spreadsheet. This leads to the lack of displacement versus residual shear stress and strain versus residual shear stress plots and data for the analysis of the behaviour of gouge material undergoing shear.

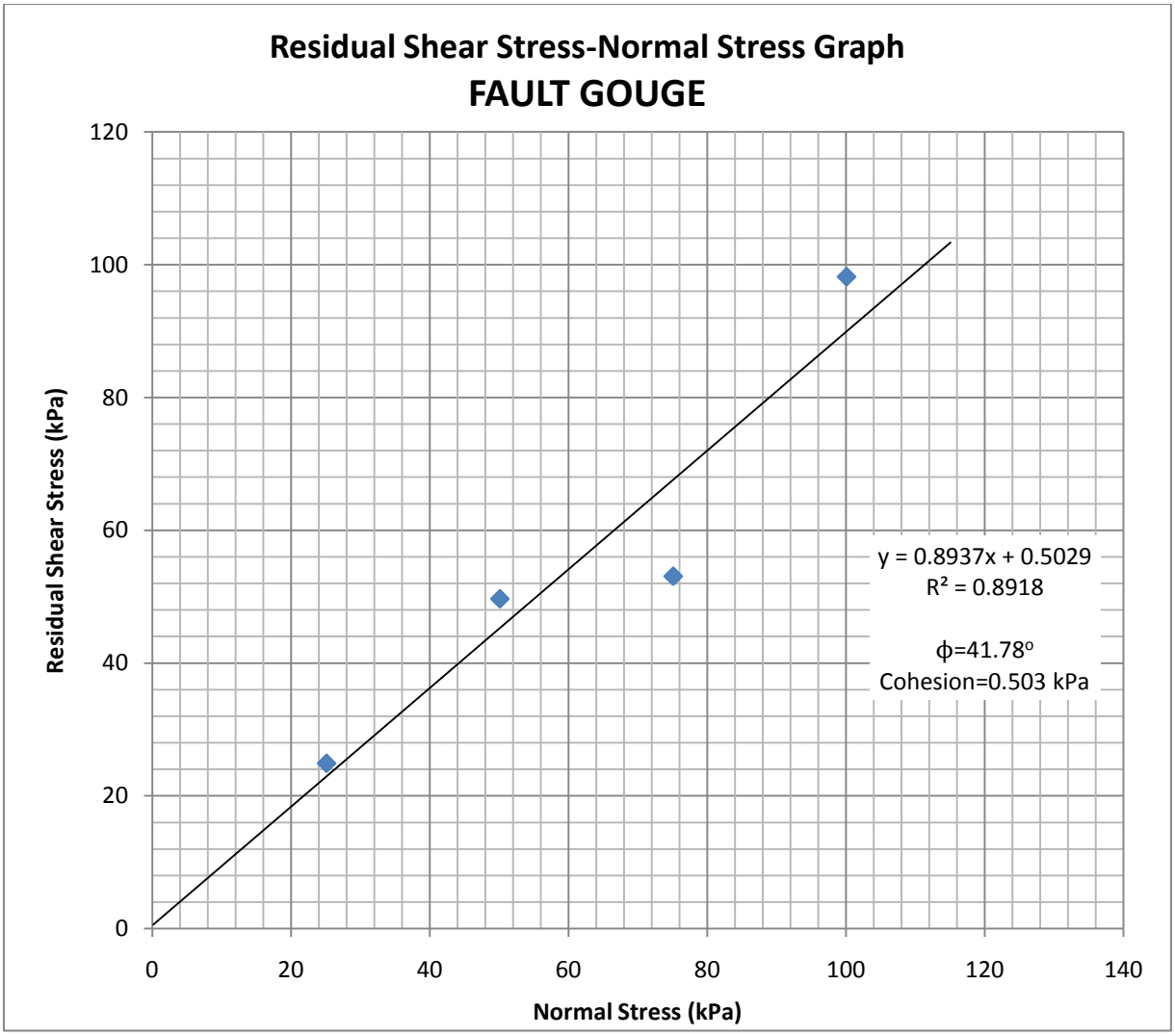

Figure 2-11: A plot of normal stress (σ_n) versus residual shear stress (τ_r) for fault gouge.

c) Discussion

Results of four set of data obtained from direct shear testing show an R^2 of 0.89 using the method of least squares. This indicates some spread in the data set with some relative confidence in the line of best fit. Results obtained show a linear relationship required for estimating angle of internal friction and cohesion for the fault gouge material.

However, the results obtained are unexpectedly high for typical fault gouge material. Previous studies into fault gouge and infilling material, as presented in Figure 2-12, show the result obtained in this study (42^o) falls significantly outside the typical range of 8 to 25 degrees for angle of internal friction (Barton, 1973).

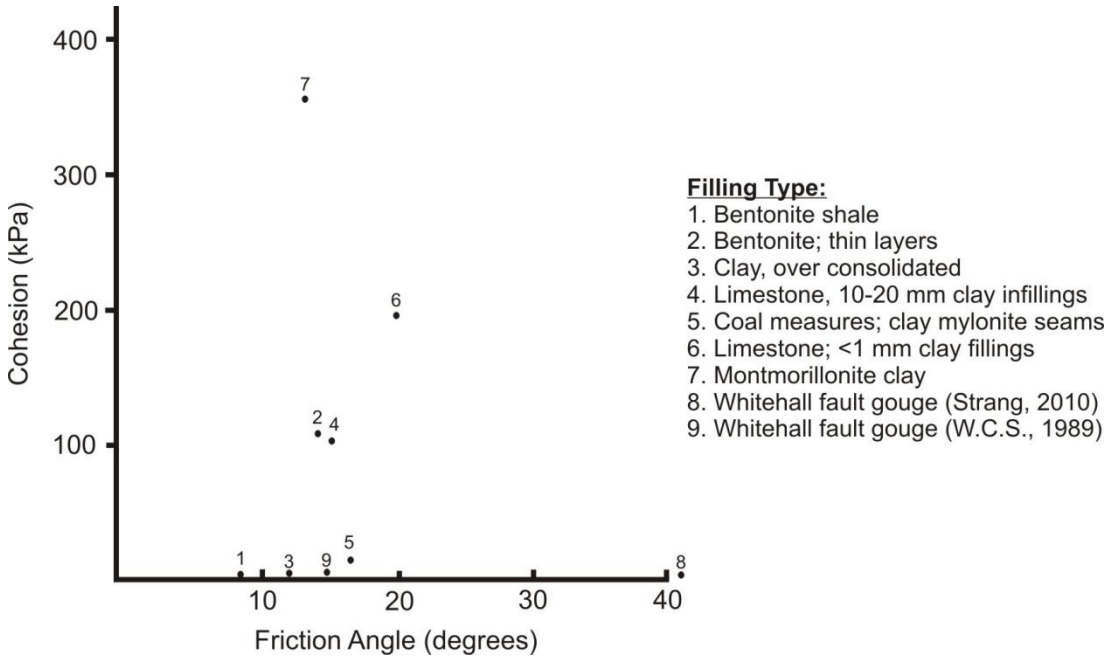

Figure 2-12: Shear strength of selected filled discontinuities (modified from Barton (1973)).

Works Consulting Services approximated that a similar fault gouge from the same fault had an approximated angle of internal friction of 13.1^{o} and cohesion of 4.0 kPa from ring shear testing carried out in 1989 (Figure 2-13). The difference in the two results is likely to be due to the different sample preparations. The 1989 ring shear test was carried out on a sieved material that represented only clay sized particles. This 2010 test result on a fault gouge sample with 5 to 10% fine gravel and sand present highlights the need for proper sample preparation for the determination of shear strengths for gouge material. If the sample in this 2010 test was sieved to less than 2 µm then it is possible than a resultant residual angle of internal friction would be much lower.

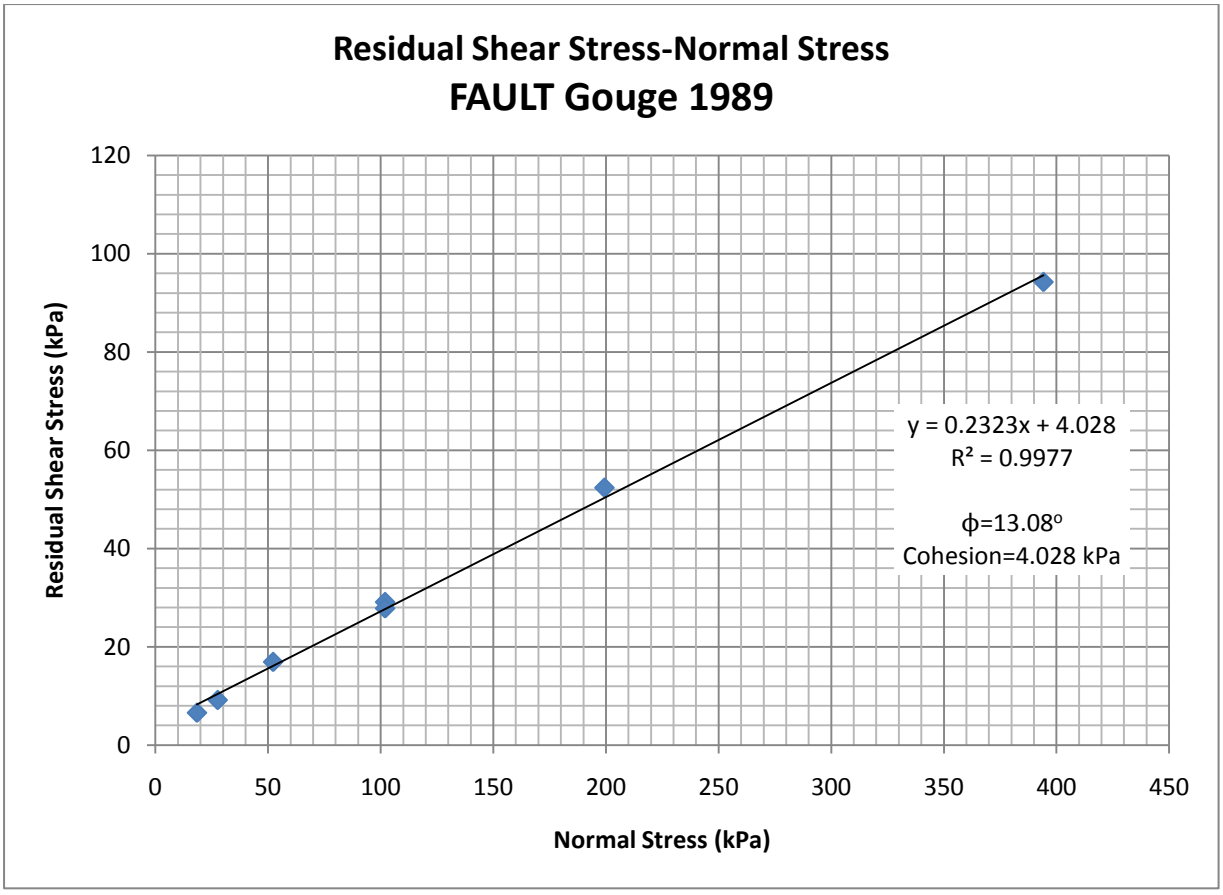

Figure 2-13: A plot of normal stress (σ_n) versus residual shear stress (τ_r) for fault gouge (Works Consultancy Services, 1989)

Due to the stringent sample preparation carried out in the 1989 ring shear test by Works Consultancy Services, the angle of internal friction of 13.1^o will be used in stability analysis. A cohesive strength of zero will also be used in stability assessment.

Moisture contents of both samples used in this test were approximated at 20% and 25%. Moisture content was tested in accordance with testing standard NZS 4402 (1986). Samples were collected from an excavated face therefore not likely to represent sub-surface water conditions.

2.4 Discussion and Synthesis

The principal aim of the engineering geological investigations undertaken during this thesis has been to provide geotechnical input data to assist in the long term performance, and provide data for the development of an engineering geological model of Whitehall Quarry. Investigations fall into the categories of field investigations, laboratory investigations and desktop investigations.

Field investigations provided adequate data on rock mass properties, such as defect data, rock mass quality, hydrogeological observations, and current pit slope performance. This data is combined with data gathered during laboratory investigations to be used in the development of an engineering geological model (Chapter 3).

Point load testing was carried out on various slightly weathered sandstone and mudstone samples as irregular lumps. Sandstone samples returned point load index values between 7.3 and 10.5 MPa indicating very strong rock (Bell & Pettinga, 1983). Mudstone testing experienced few issues particularly with interbedding with sandstone. Some samples appeared to be mudstone but on testing exhibited interbedded sandstone within the core of the sample. These samples were discarded for increased approximation of intact rock strengths for mudstone. The resulting point load index value for mudstone was approximately 0.2 MPa indicating a moderately weak rock (Bell & Pettinga, 1983). However, bias in sample selection is likely to have forced the indication of higher than typical intact rock strengths, this issue must be considered in the engineering geological model.

Resulting point load index values were converted to uniaxial compressive strengths (UCS) which can be compared to the computed UCS gathered from Schmidt hammer testing. The UCS for slightly weathered sandstone and mudstone were 175 to 255 MPa and 4.8 MPa respectively for point load testing. UCS values for Schmidt hammer testing of similar samples were estimated at 150 to 250 MPa for sandstone and 37 MPa for mudstone. The results for both testing methods are similar for sandstone samples with little weathering. Results for mudstone samples for both methods do not correlate. UCS for mudstone should be much less than the Schmidt estimation of 37 MPa. This highlights the impracticality of Schmidt hammer testing on weak rock or highly fractured rock masses as outlined by Bieniawski (1975).

Shear testing was carried out on a typical sandstone joint and mudstone bedding. These samples were selected due to being most likely of contributing to slope failure at Whitehall Quarry. Residual angles of internal friction for the sandstone joint and mudstone bedding were approximated at 34^{o} and 31^{o} respectively. Samples were tested as dry masses, this is likely to increase the shear strength of each sample in particular the mudstone bedding as outlined by Hawkins and McConnell (1992). These shear strength values will be used in Patton's equation (Patton, 1966) to evaluate the effective angle of internal friction to be used in slope stability assessment in Chapter 4.

Direct shear testing of a selected fault gouge material was undertaken to assess the residual shear strength of the gouge material. The residual angle of internal friction obtained during the laboratory investigation of this study was approximately 42^{o}. This result was unexpectedly high results for fault gouge and will not be used in slope stability analysis. This is likely to be attributed to the sample preparation. The sample tested was not sieved as suggested by the standard ASTM D3080-04 and exhibited fine gravel which appears to have increased the residual shear strength considerably. Ring shear testing was carried out on a similar sample from a similar location by Works Consulting Services in 1989 and obtained a residual angle of internal friction of approximately 13^{o}. This value seems more appropriate and consistent with the approximated plasticity index (20). This residual angle of internal friction of 13^{o} will be used in the analysis of pit slope stability in Chapter 4 and northern wedge stability in Chapter 5.

X-ray diffraction (XRD) analysis was carried out on two separate fault gouge samples of significance to both pit slope and northern wedge stability. The analysis was carried out on a whole sample rather than the 9φ fraction. This will only give an indication of minerals present within the gouge rather than accurate mineral content. This is due to large particles within the whole sample overprinting smaller particles resulting in unreliable mineral content estimates. XRD analysis indicated the presence typical gouge minerals, such as quartz, calcite and albite, as well as clay minerals kaolinite and montmorillonite. Clay minerals play significant roles in slope stability especially montmorillonite which exhibits high swelling and shrinking capabilities. These capabilities can have significant adverse affects on slope stability and must be considered carefully in the engineering geological model. It is difficult to quantitatively estimate the amount of instability attributed to clay mineral content.

Atterberg limits were also approximated during laboratory investigations. Plastic and liquid limits of a selected clay gouge material were approximated at 31 and 51 respectively with a resultant plasticity index of 20 indicating the gouge has a low plasticity. This low plasticity indicates a clay mineral composition of 20 to 25% within the fault gouge. This indication is also supported by the low angle of internal friction (13^{o}) approximated in ring shear tests.

3.0 Engineering Geology of Whitehall Quarry

3.1 Introduction

The engineering geology of the quarry must be understood in order to construct a reliable engineering geological model. The fundamental principles of an engineering geological model are:

- Geological units
- Wall strength (intact and rock mass)
- Weathering profile
- Groundwater table and hydrogeological features
- Discontinuity types
- Domain analysis for geometric discontinuities

The aim of this section is to develop an engineering geological model using the results obtained from laboratory and field investigations. The development of an engineering geological model for Whitehall Quarry serves two principal purposes. Firstly, the model will be utilised as the basis for slope stability analysis in Chapter 4. Secondly, the model will be aid quarry operators in future pit design.

3.2 Rock and Soil Characterisation

3.2.1 Introduction

The characteristics of the rock mass are an integral part of the engineering geological model. Rock mass properties and characteristics govern the masses ability to stand competently within the quarry face. An extremely strong rock with very few defects has the ability to stand at high slope angles. Weak rock with many defects has a much lower stability in a slope and must be designed at lower angles.

Whitehall Quarry exhibits two rock types of varying weathering grades, greywacke sandstone interbedded with argillaceous mudstone. Both units were analysed for residual shear strength, point load index and corresponding UCS in Chapter 2. A rhyolitic alluvium was also mapped as part of a paleo-channel within the quarry (Map Sheet 1). There was no laboratory testing carried out on this material due to the rarity of this material within the quarry. This section summarises the parameters of rock and soil types at the quarry.

This section ignores the Ongatiti ignimbrite and alluvial sandy silts surrounding the quarry because they have little effect on quarry slope stability.

3.2.2 Greywacke Sandstone

Field investigations revealed a monotonous greywacke sandstone sequence within the quarry. The rock mass exhibits predominantly well indurated, strong to very strong, moderately to thickly bedded sandstone. Bedding typically strikes east west and dips at approximately 60 to 80 degrees. Bedding spacing is approximated at 2 to 5 m. Although monotonous, the unit is locally interbedded with argillaceous mudstone (Section 3.2.3) and varies in weathering grade. A detailed map of the weathering profile and geological unit distribution is presented in Map Sheet 1.

The greywacke sandstone mass is subdivided into three main weathered rock types, divisions are based on quarrying terms derived from the degree of weathering, for slope design. The weathering profile within the quarry is relatively flat-lying on a north-south trend and gently follows topography to the east and west of the two main pits. This is illustrated in cross-sections presented in Map Sheets 2 and 3.

<u>HW-RW Greywacke Sandstone (Overburden)</u>

Highly weathered (HW) to residually weathered (RW) greywacke sandstone, referred as overburden for purpose of quarrying, was encountered in the surrounding upper slopes of the quarry. This unit typically appears at varying elevations due to topography, but is on average 20 to 30 m thick. Overburden typically comprises the sandy silts on the surface as well as the HW to RW sandstone. These units are generally characterised by yellowish brown clayey and silty sands with varying proportions of greywacke sandstone gravel and by very weak, highly fractured, residually to highly weathered sandstone and siltstone. Within the highly weathered rock core-stones of less weathered parent sandstone are common. Core-stones are where the weathering process has caused the disintegration of permeable material around a less permeable core-stone of parent material (Yang & Wu, 2006).

Schmidt hammer testing carried out during this investigation, indicated a maximum average rebound value of 15, with a correlated maximum mean UCS of 30 MPa (Section 2.2.3). This indicates that the greatest strength of the intact rock is moderately weak (25 to 50 MPa (Hoek & Bray, 1981)). In the field, this rock type is interpreted as a material that requires few firm blows with a geological hammer to break a specimen (Bell & Pettinga,

1983). From field observations, the lowest intact rock strength for this material is likely to be very weak where the material can be crushed by hand. When designing appropriate slopes within this material a conservative approach must be implemented due to the low intact rock strength.

A study carried out by Tonkin and Taylor in 2002 investigating slope stability of the eastern section of the quarry, estimated the angle of internal friction of 23^{o} and a cohesive strength of 100 kPa. These results were obtained from the shear box testing of multiple samples of the overburden material. A summary of this material is presented in Table 3-1. This data will be used in kinematic slope stability assessment in Chapter 4.

The overburden material may be weak and highly discoloured but it is still possible to distinguish structural features within the mass. The engineered slope above the Karapiro Stream to the east of the quarry, especially within the HW sequence, exhibits distinguishable joints, faults and the Main Quarry Shear Zone running through Pit 2, (Figure 3-1). Discontinuities are typically heavily stained with iron-rich limonite and some off-white veins of zeolite and calcite are evident.

Table 3-1: Generalised summary of HW-RW greywacke sandstone (overburden).

Engineering Geological Description:	*HW-RW, very weak to strong, light yellowish brown, massive, greywacke SANDSTONE.*
Average Angle of Internal Friction	~23^{o}
Estimated UCS	~30 MPa
Average Unit Thickness	20 m ± 10 m

Figure 3-1: Slopes within HW-RW greywacke sandstone (overburden).

MW-HW Greywacke Sandstone (Brown Rock)

Moderately weathered (MW) to highly weathered (HW) greywacke sandstone, also known as brown rock, was encountered in the surrounding slopes of the quarry below the overburden unit. This unit typically appears to follow topography and has an approximate thickness of 15 to 30 m throughout the quarry. The unit is mapped and presented in Map Sheet 1; cross-sections have also been prepared and are displayed in Map Sheets 2 and 3.

Brown rock comprises dark to light brown, moderately to highly weathered, highly fractured, weak to moderately weak greywacke sandstone. The typical rock structure is characterised by closely spaced, heavily iron stained defects with alteration of the joint wall surfaces. Soft clay is present on major defect surfaces where complete weathering of quartz and feldspar has occurred. The rock material between defects is discoloured and there is loss in material strength (weak to strong compared to very strong for SW rock). Argillite bands are often not clearly recognisable in drill-core and appear to weather out within the brown rock (Figure 3-2).

Schmidt hammer testing carried out during this investigation (Section 2.2.3) indicated a maximum average rebound value of 29 with a correlated maximum UCS of approximately 55 MPa. This indicates a moderately strong rock (50 to 100 MPa (Hoek & Bray, 1981)) type which requires several to few blows from a geological hammer to break a hand specimen (Bell & Pettinga, 1983). In an engineered rock slope, this material will stand much more competently than HW to RW greywacke sandstone (overburden).

A study carried out by Tonkin and Taylor in 2002 estimated the angle of internal friction of 32^{o} and a cohesive strength of 200 kPa. These results were obtained from the shear box testing of multiple samples of brown rock. A summary of this material is presented in Table 3-2. This data will be used in kinematic slope stability assessment in Chapter 4.

Structures within this unit are easily distinguishable. Joints, shear zones and faults exhibit deep iron-rich limonite staining. Calcite fibre-growths on fault surfaces are also becoming more evident in this material. Zeolite and some calcite covered joints are also distinguishable in the rock mass.

Table 3-2: Generalised summary of MW-HW greywacke sandstone (brown rock).

Engineering Geological Description:	*MW-HW, strong to very strong, light and dark brown, massive, greywacke SANDSTONE.*
Average Angle of Internal Friction	~32^{o}
Estimated UCS	~55 MPa
Average Unit Thickness	15-30 m

Figure 3-2: An example of MW-HW greywacke sandstone (brown rock).

UW-SW Greywacke Sandstone (Blue Rock)

Unweathered (UW) to slightly weathered (SW) greywacke sandstone, also known as blue rock, was encountered in the base of both pits of the quarry (Map Sheet 1). This unit occurs at maximum elevations of 110 m RL but typically below 60 m RL, and shown on Map Sheets 2 and 3.

The blue rock comprises bluish grey, slightly weathered to unweathered, strong to extremely strong sandstone with localised bands argillaceous mudstone. The rock mass is typically jointed (but less fractured than the overlying brown rock) with minor iron-rich

limonite staining on some defect surfaces and unaltered joint surfaces. Within major joint sets quartz and feldspar veins are evident. Some areas within the quarry exhibit prehnite-pumpellyite zones of metagreywacke facies.

Schmidt hammer testing carried out during this investigation (Section 2.2.3), indicated a maximum average rebound range of 54 to 62, with a correlated maximum UCS of approximately 150 to 230 MPa. This strength indicates a strong to very strong rock (100 to 200+ (Hoek & Bray, 1981)). In the field this is indicated as a rock that would require several blows, or could only be chipped with a geological hammer (Bell & Pettinga, 1983).

Results for shear strength obtained from this study estimate the residual angle of internal friction at 34^{o}. Tonkin & Taylor Ltd (2002) estimate the cohesive strength of this unit as 500 kPa. A summary of this material is presented in Table 3-2. This data will be used in kinematic slope stability assessment in Chapter 4.

Structures within this material are highly distinguishable. Joints, shear zones and faults exhibit minor limonite staining. Striations and fibre-growths on fault surfaces are also are evident in this material. Zeolite, calcite and prehnite-pumpellyite are also distinguishable in the rock mass as veins and defect infilling.

Table 3-3: Generalised summary of UW-SW greywacke sandstone (blue rock).

Engineering Geological Description:	*UW-SW, very strong to extremely strong, light and dark bluish grey, massive, greywacke SANDSTONE.*
Average Angle of Internal Friction	~34^{o}
Estimated UCS	~150-230 MPa

Figure 3-3: An example of UW-SW greywacke sandstone (blue rock).

3.2.3 Argillaceous Mudstone

Weathering grades vary throughout the quarry along with interbedded greywacke sandstone. Argillaceous mudstone has the quarrying term of argillite and is present throughout the quarry. However, there is a zone of high argillite content in the southern section of Pit 2 (Map Sheet 1).

Typical argillite comprises dark brown or dark blackish grey, extremely fractured, moderately strong to very weak argillaceous mudstone. The rock structure is characterised by thin beds (typically 5 to 25 mm thick) interbedded with greywacke sandstone. Quartz and feldspar veins are evident along with pyrite on some defect surfaces.

Schmidt hammer testing carried out during this investigation was relatively unsuccessful (Section 2.2.3), however it indicated a maximum average rebound value of 24 with a correlated maximum UCS of approximately 37 MPa, indicating a moderately weak rock type (25 to 50 MPa (Hoek & Bray, 1981)).

Results for shear strength obtained from this study estimate the residual angle of internal friction at 31^{o} for a slightly weathered to unweathered sample. A summary of this material is presented in Table 3-4. This data will be used in kinematic slope stability assessment in Chapter 4.

Table 3-4: Generalised summary of UW-RW argillaceous mudstone (argillite).

Engineering Geological Description:	*UW-RW, moderately strong to very weak, dark brown and dark blackish grey, thinly bedded (5-25 mm), argillaceous MUDSTONE.*
Average Angle of Internal Friction	31°
Estimated UCS	37 MPa (maximum)

Figure 3-4: An example of SW argillaceous mudstone interbedded with sandstone (argillite).

3.2.4 Rhyolitic Alluvium

The rhyolitic alluvium exists within a paleo-channel at the eastern margin of the quarry. This channel was the original path of the Karapiro Stream before it was diverted in 2004. The soil material is described as a light orangish brown with mottled brownish black lenses, pumaceous, coarse sandy gravel with some silt. The channel deposit is approximately 3 to 4 m thick and 3 to 4 m wide. Location of this material is shown on Map Sheet 1.

The estimated strength of the alluvium is hard to stiff (Bell & Pettinga, 1983) indicating a material that can only be removed from an exposure with an implement with some difficulty and indented by thumb pressure, but not moulded by fingers. The strength of this material was not tested due to its relative scarcity within the quarry; however it is important in slope stability. This material may not stand competently within a face designed

for sandstone parameters. It is likely that the rhyolitic alluvium will be removed from the face to increase slope stability and reduce the risk of contaminating lower high grade slopes with alluvial material.

Figure 3-5: An example of rhyolitic alluvium, coarse sandy gravel with bouldery coarse gravel fill on top.

3.2.5 Discussion

The geological materials described in this section are imperative in developing a reliable engineering geological model for the quarry to be used in slope stability assessment and future slope designs. The different weathering grades exhibited in material in and around the quarry affect the ultimate intact rock and residual shear strength.

Overburden and brown rock are expected to be the most important in slope design due to the low intact rock quality and vast abundance throughout the quarry. However, it must be noted that overburden material is generally stripped back and not stringently designed to stand the test of time while quarrying continues at greater depths.

Differing rock type distribution is shown on Map Sheet 1. Map Sheets 2 and 3 show the weathering profile of rock is relatively flat lying in the north-south trend and follows topography in the east-west trend. However, due to the lack of drill hole data, the depths of the weathering profile are only estimates and carry a degree of uncertainty. Greater sub-surface data would produce accurate weathering profiles within the quarry and it surroundings.

Field observations revealed the homogeneity of greywacke sandstone of all weathering grades. There exists very little variation within the same material. However, regarding stability, the variation the mudstone bed thickness and occurrence will affect the overall stability of a slope.

3.3 Structural Domain Analysis

3.3.1 Introduction

Structural domain analysis can be regarded as the investigation and delineation of structural characteristics within the rock mass at Whitehall Quarry, and besides orientation data includes important parameters such as defect persistence, spacing and waviness characteristics. In this section the aim of structural domain analysis has been to divide the rock mass at the quarry into a series of domains having essentially homogeneous geometric fracture characteristics.

Structural domain analysis serves two principal purposes in this thesis. Firstly, analysis into structural domains is required to gain more understanding of the engineering geological model for the quarry. Secondly, domain analysis was aimed at assessing the current and future slope stability, which is discussed in Chapter 4.

3.3.2 Methodology

Introduction

In a large scale domain analysis, such as this, it is likely that there is to be some degree of insufficient data collection and lack of good spatial coverage of data. Due to restricted access to most slopes within the quarry data is gathered from photogrammetric methods and some conventional scanline collected during this study. Therefore the methodology must take into account these issues.

Sampling Bias

Two principal sources of sampling bias arise from the method of structural data collection. Firstly, in the collection of structural data, a bias is likely to arise due to the selective mapping of features, referred to as ‘operator bias’. Operator bias may generally be attributed to subjectivities of the data collector. For example, it may be that those features with a greater length, aperture width, etc., are recorded more often as they are more easily

observed during data collection (Chapple, 1998), and this is common in photogrammetric data collection methods. The second source of bias is known as 'geometric bias' and has been recognised in the field of rock mechanics for some time. Geometric bias arises at the quarry because the number of features mapped on a particular slope will be dependent on the orientation of the features relative to the slope (Hoek & Diederichs, 1989). For example, two discontinuity sets with different orientations but the same spacing will be sampled differently since the apparent spacing, and consequently sampling distance at which observations are measured will be different, as shown in Figure 3-6.

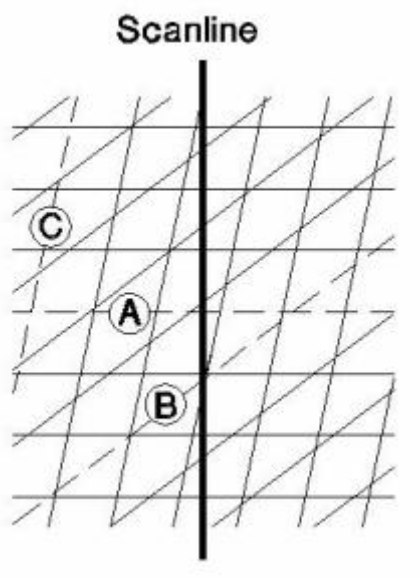

Figure 3-6: Plan view showing geometric sampling bias. Note how little defect C is sampled compared with A and B, but all have the same spacing (Hoek & Diederichs, 1989).

No simple quantitative method exists for correcting the effects of operator bias, but it must be considered when collecting structural data. As for geometric sampling bias, this can be corrected through the application of the Terzaghi weighting factor. The weighting factor uses the mean slope orientation and a series of calculations (Appendix D4) to reduce the effect of this sampling bias. The Terzaghi weighting factor is applied to all analyses in this investigation.

Interpretation Technique

A number of theories have been proposed in the literature for quantitative determination of structural domain boundaries (Piteau & Russell, 1971; Hume, 1983; Pointe & Hudson, 1985). A visual assessment of stereoplots and histograms was chosen as the basis for structural domain analysis in this study. As Hume (1983) points out, visual methods

are probably the most widely used technique for domain delineation because of their simplicity.

A number of advantages were recognised in using a visual method for structural domain analysis at Whitehall Quarry. Visual models are simple to interpret and require little knowledge of complex geostatistics, which many other methods of analysis rely upon. Geostatistical methods also generally require good data coverage and a large number of points to produce reasonable results (Swan & Sandilands, 1995). The statistical coverage of data at Whitehall is variable; therefore visual methods are best suited to this investigation.

There are significant variations in the amount of data coverage between different localities around the quarry, meaning the densities of poles on a stereoplot will vary at different localities. For a fixed counting circle of 1.0% the significance of any generated contours will depend on the pole densities on a stereoplot. By varying the size of the counting circle the significance of points falling within an area on the stereonet can be varied and the contours smoothed (Kamb, 1959). Figure 3-7 illustrates the effects of adjusting the size of the counting circle for a plot of 613 poles. As the counting circle is progressively increased the contours are smoothed and noised is reduced.

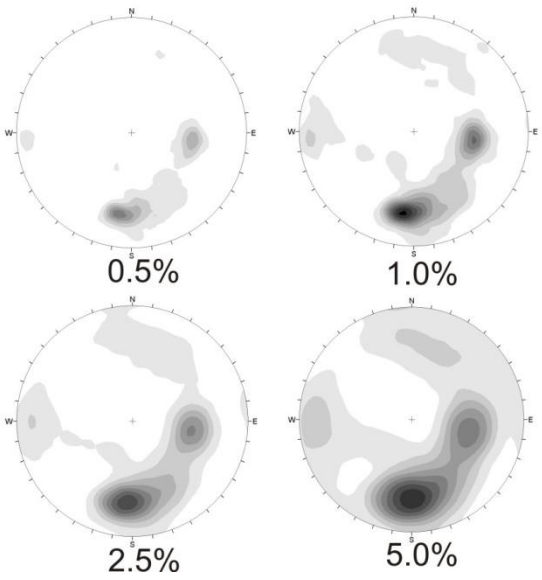

Figure 3-7: Effects of counting circle size on a generated contour plot for the same data set from Section A, Whitehall Quarry.

The counting circle size for the structural domain analysis in this investigation was 1.0%. This was chosen as the best size to represent the data clearly via reducing noise and increasing the likelihood of defining data sets. Another technique to be implemented in the

analysis of the data set was the exclusion of structural features with persistence less than one metre. Coupled with a counting circle of 1.0%, this reduces the number of smaller less predominant discontinuities within the data set.

3.3.3 Domain Identification

The most significant structural feature within Whitehall Quarry is the fault trending east-west within Pit 2, which is termed the Main Quarry Shear Zone (MQSZ). This feature is most likely to delineate the boundary between two recognisable domains within the quarry (Map Sheet 1).

The MQSZ has dip and dip direction of 45^{o}/190, and the associated shear zone is approximately 2 to 3 m wide. Fault gouge material collected from the shear zone was analysed for clay mineralogy, with both kaolinite and montmorillonite being present. The MQSZ structurally divides the quarry into the following domains:

- Northern Domain (ND), located immediately north of the MQSZ.
- Southern Domain (SD), located immediately south of the MQSZ.

The following sections explain the comparison of structural features such as bedding and joint sets within each domain.

3.3.4 Bedding

Northern Domain

The Northern Domain (ND) consists of greywacke sandstone interbedded with argillaceous mudstone to the immediate north of the MQSZ. Interpretation of bedding to the north of the MQSZ is presented in Figure 3-8, and is based on 18 poles.

Bedding planes are predominantly inclined sub-vertically towards the south west. The maximum concentration of bedding poles is approximated at 82^{o}/218, as shown in the stereoplot presented in Figure 3-8. The thickness of sandstone beds appear to be moderately to very thick (0.2 to >2 m thick), whereas mudstone bedding appears to be laminated to moderately thin (2 to 200 mm thick). Bedding discontinuities are closely to very widely spaced (60 mm to >2 m).

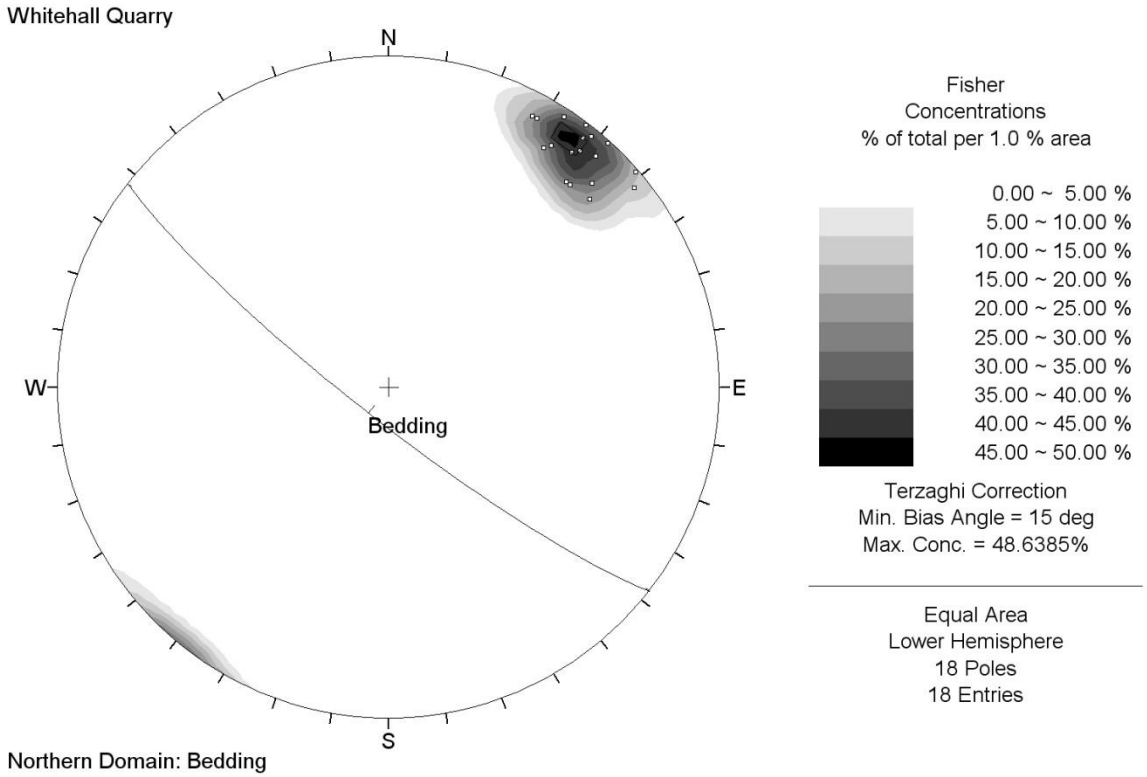

Figure 3-8: Stereoplot showing bedding plane poles and contours with resulting average bedding plane (82^{o}/218) for the Northern Domain.

Southern Domain

The Southern Domain (SD) comprises greywacke sandstone interbedded with argillaceous mudstone to the immediate south of the MQSZ. Interpretation of bedding to the south of the MQSZ is presented in Figure 3-9, and is based on 138 poles.

Bedding planes are predominantly steeply inclined towards the south west. The maximum concentration of bedding poles is approximated at 57^{o}/211, as shown on the stereoplot presented in Figure 3-9. Similarly to the ND thickness of sandstone beds appear to be moderately to very thick (0.2 to >2 m thick) whereas mudstone bedding appears to be laminated to moderately thin (2 to 200 mm thick). Bedding discontinuities are closely to very widely spaced (60 mm to >2 m).

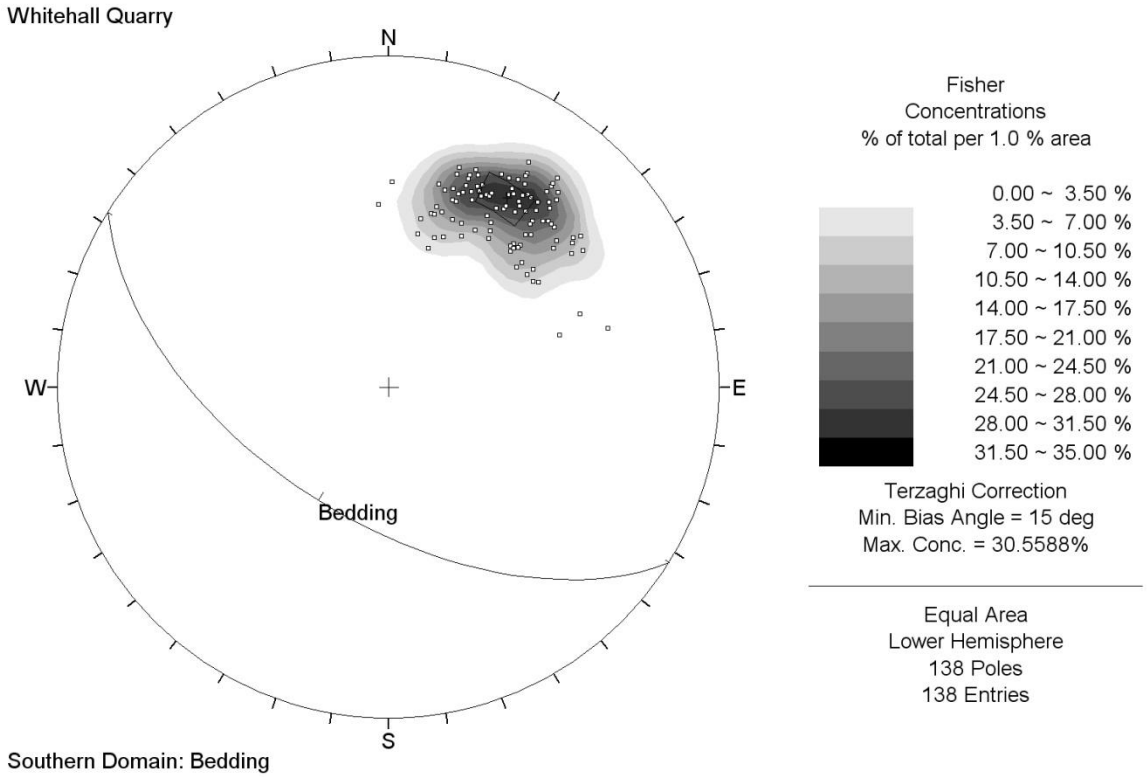

Figure 3-9: Stereoplot showing bedding plane poles and contours with resulting average bedding plane (57°/211) for the Southern Domain.

3.3.5 Jointing

Northern Domain

Stereonet analysis of joints is presented in Figure 3-10, and is based on 620 poles. Domain analyses of common joint properties, such as joint roughness coefficient (JRC), persistence, waviness, etc, are presented in Appendix E1.

Interpretation of joint poles for the ND identified three joint sets, all of which are steeply inclined towards the south west (Figure 3-10). Joint set 1 is the most common with the highest concentration of poles, while joint sets 2 and 3 have similar pole concentrations. The maximum concentrations of joint poles indicate average joint set orientations which are listed as follows:

- Joint set 1: 57°/107
- Joint set 2: 40°/139
- Joint set 3: 35°/173

Analysis of histogram plots indicated a mean JRC value of approximately 3 (48% of all JRC profiled joint surfaces), indicating a very smooth planar joint surface. Joints appear to have on average very to moderately narrow aperture with surfaces exhibiting a zeolite coating and limonite staining. Persistence of joints is in the order of 1 to 3 m termed low persistence. The spacing of joints is closely to moderately widely spaced (60 to 600 mm).

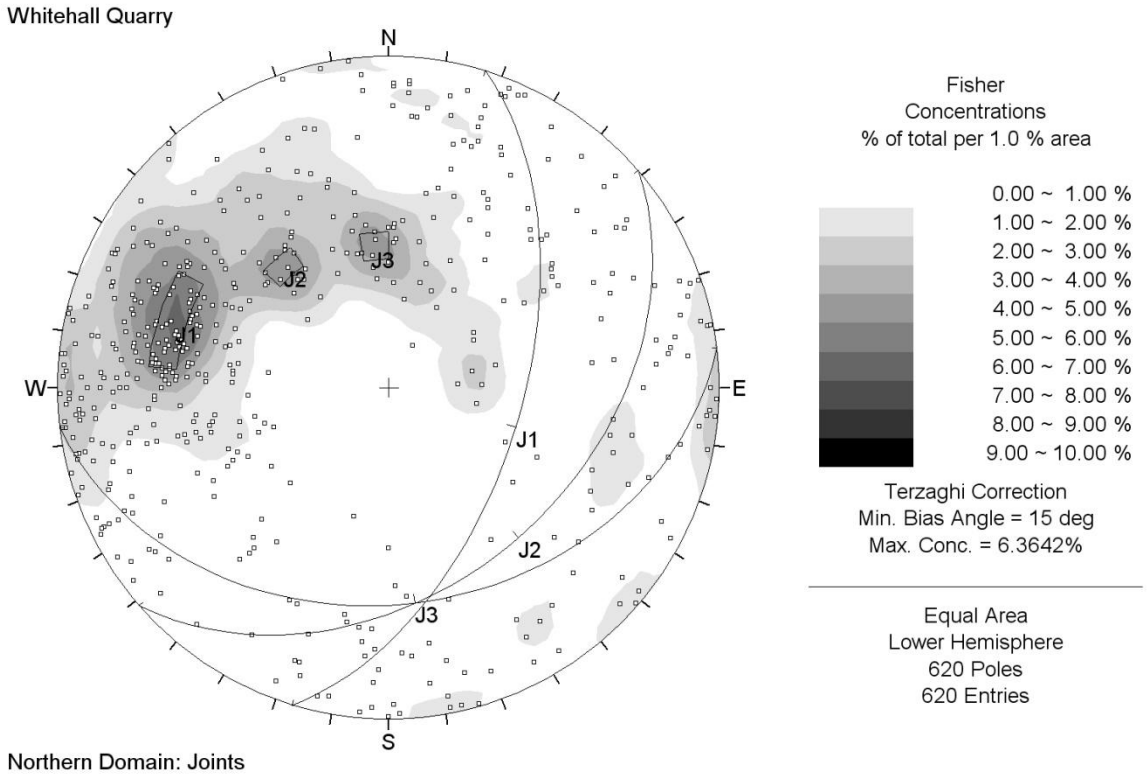

Figure 3-10: Stereoplot showing joint poles and contours with resulting average joint sets for the Northern Domain.

Southern Domain

Stereonet analysis of joints is presented in Figure 3-11, and is based on 1511 poles. Domain analyses of common joint properties, such as joint roughness coefficient (JRC), persistence, waviness, etc, are presented in Appendix E2.

Interpretation of joint poles for the SD identified four joint sets all with varying dip and dip direction (Figure 3-11). Joint set 1 is the most common, with the highest concentration of poles while joint set 2 and 3 have similar pole concentrations, Joint set 4 has the least number of poles within its pole concentration. The maximum concentrations of joint poles indicate approximate joint set orientations which are listed as follows:

- Joint set 1: 61^{o}/008
- Joint set 2: 65^{o}/333
- Joint set 3: 45^{o}/279
- Joint set 4: 82^{o}/084

Joint sets 4 and 3 could possibly be orthogonal conjugate pairs formed during the same tectonic event due to their opposing orientations.

Analysis of histogram plots gave a mean JRC value of approximately 3 (48% of all JRC profiled joint surfaces), indicating relatively smooth planar joint surfaces. Joints typically have an average of very to moderately narrow aperture with zeolite and limonite stained surfaces. Persistence of joints is in the order of 1 to 3 m termed low persistence. The spacing of joints is closely to moderately widely spaced (60 to 600 mm).

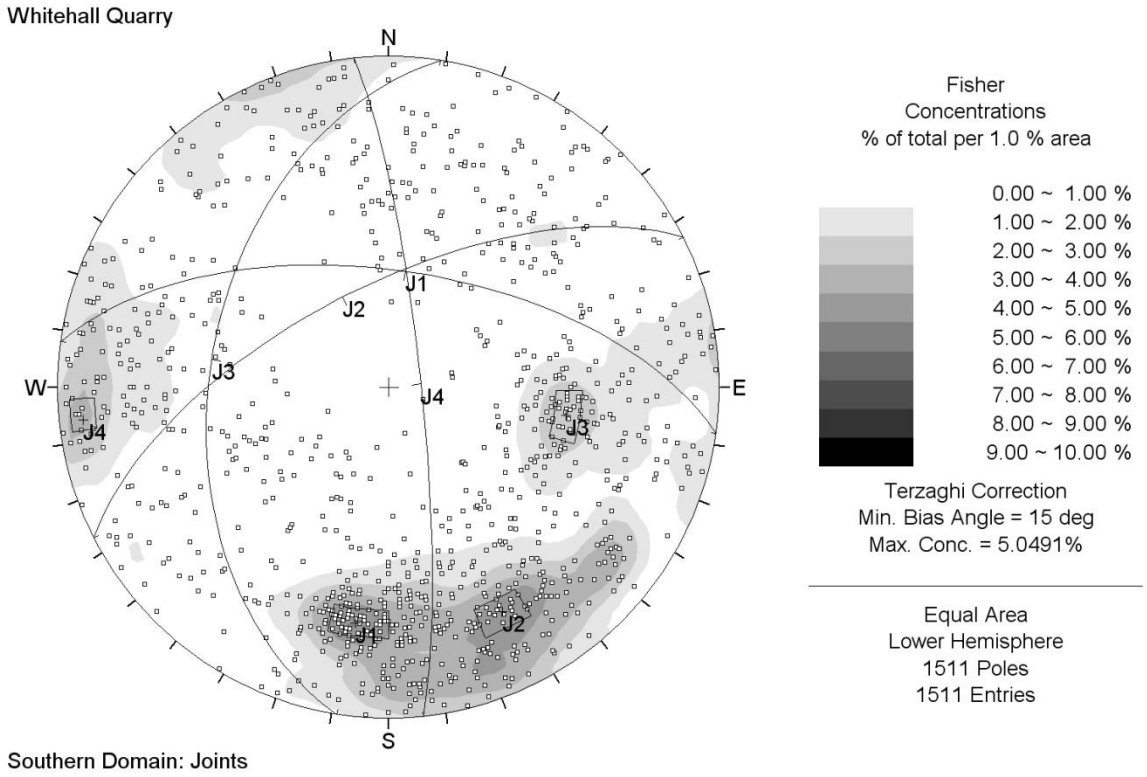

Figure 3-11: Stereoplot showing joint poles and contours with resulting average joint sets for the Northern Domain.

3.3.6 Discussion

The two domains identified have many similarities, and a few subtle differences. It is these differences that must be taken in to account when assessing slope stability and designing associated pit slopes. Both sets of data show very similar joint roughness coefficients, persistence and joint spacing. However joint sets are more variable within the southern domain, joints range from steeply inclined to sub-vertical in variable directions, while joint sets identified in the northern domain show little variation, and sets are predominantly steeply inclined towards the south west.

There exists a subtle difference in the bedding attitudes for both domains identified. Bedding in the north is predominantly orientated at 82^{o}/218, whereas in the south bedding is less steeply inclined at an orientation of 57^{o}/211. Dip directions only differ by 7 degrees which appears to be a relatively small difference.

The number of poles used for analysis of joints for each domain (620 and 1511) appears to be more than adequate. Joint data used in this analysis had the minimum persistence of approximately1 m. In doing so, this is likely to reduce the noise created from smaller less predominant joints.

The use of two different sampling techniques, conventional scanline and photogrammetry, does not appear to have had an adverse affect of the quality of data. If any affect it appears to have supplied more than expected orientation data. However, due to the inability of photogrammetry to sample JRC and defect waviness these properties were measured during fieldwork to supplement scanline data. Therefore sound conclusions could be drawn from the orientation and defect property data set. A comparison of the two data collection methods is discussed in Section 2.2.2.

3.4 Groundwater and Drainage

Introduction

Wyllie and Mah (2004) state that the presence of groundwater in a rock slope can have a detrimental effect upon stability for the following reasons:

- Water pressure reduces the stability of the slope by diminishing the shear strength of potential failure surfaces. Water pressure in tension cracks or similar near-vertical fissures reduces stability by increasing the forces that induce sliding.
- Changes in moisture content of some rock types can cause accelerated weathering and erosion, thus decreasing the shear strength and increasing the likelihood of isolated block or wedge failure.

Therefore, groundwater and associated drainage within the quarry and pit floor must be considered as a significant factor in slope stability analysis. This section analyses the hydrogeological features within Whitehall Quarry that were used in the engineering geological model.

Observations and Interpretations

Due to the absence of piezometric data within the quarry and the surrounding area, the groundwater table and associated hydrogeological model was estimated from observations within the pit. Pit slopes were inspected for seepages of water from defects within the pit walls during the summer and winter of 2010. An indication of seepage would suggest an elevation of groundwater above the pit floor.

During inspections, in both wet and dry seasons, no seepages were identified from pit walls. This indicates that the pit walls are situated above the level of water saturation and only exhibits surface water from recent rainfall. These interpretations have been extrapolated in cross-sections presented in Map Sheets 2 and 3. The groundwater table is estimated to be equal to the lowest point in Pit 2 due to the constant water level within the associated settlement pond. The phreatic surface is then interpreted as flowing from the Karapiro Stream in the east of the pit.

There remains a great deal of uncertainty in the western margin of the pit. There is no piezometric data, and no seepage was exhibited within the pit slopes. The minor stream flowing from the western valley into Pit 1 (Map Sheet 1) appears to only flow during or after periods of rainfall. This minor stream is interpreted as not being part of the overall phreatic surface. Therefore, the groundwater table is inferred as following topography on the western side of the quarry.

As presented in cross-sections (Map Sheets 2 and 3), the phreatic surface fluctuates from summer to winter by at least 2 m at the pit floor. This level of fluctuation was again estimated from observations of pit slopes and the surrounding area in summer and winter when the phreatic surface would have been at its highest and lowest elevations.

Fault planes and shear zones, where gouge material is present, are likely to alter the level of the groundwater table. Impermeable clay-rich fault gouge material will impede the flow of water from high to low head. Water levels are likely to appear at higher elevations on the side of a fault where water is flowing from higher head (Figure 3-12). The northern wedge failure is likely to exhibit higher pore water pressures due to impermeable fault gouge restricting the exit flow of water from the wedge mass. It is likely that water flows through the completely saturated toe of the mass due to the high level of the Pit 1 settling pond (Map Sheet 1).

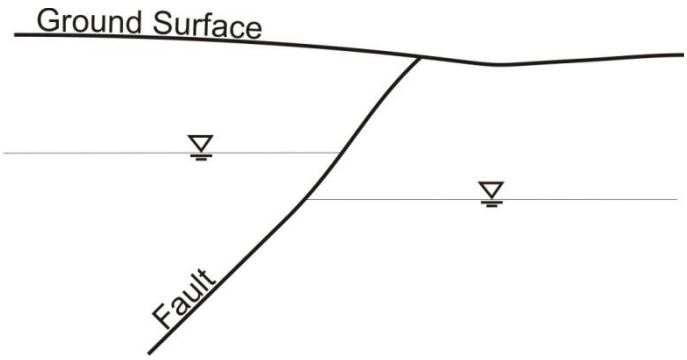

Figure 3-12: Diagram showing the effect a fault has on the ground water table (adapted from Wyllie & Mah (2004)).

The stream located within the south eastern side of Pit 2 is a flow of water discharged from the processing plant. This semi-constant flow of water passes through the pit floor and settles within the settlement pond of Pit 2, from where it is then pumped into Pit 1. Water settling in Pit 1 is then pumped to the processing plant for use.

Discussion

The hydrogeological model presented in this section is entirely based on observations within the pit. No piezometric data was available at the time of this investigation. Data presented in this section will lead to greater understanding of failure modes within the quarry. It will also shed light of the sub-surface pore pressures of the northern wedge. As illustrated in Map Sheet 1, the toe of the wedge failure mass is totally saturated due the settlement pond at the base of the wedge, and this is will have an adverse affect on the stability assessment of the wedge (Chapter 5).

As stated earlier, pore water pressure causes the decrease in rock mass shear strength and thus the stability of blocks and wedges within the pit slopes. However, the hydrogeological model suggests that the continual pumping of Pit 2 into Pit 1 leads to a phreatic surface just below the floor of Pit 2, indicating the pit walls are relatively dry apart from periods of rainfall.

To gain more understanding of the hydrogeological model for Whitehall Quarry more data must be acquired from piezometer measurements of the ground water table. Piezometers should be installed on the eastern and western flanks of the pit as well as singular piezometers at the north and south ends. The installation of piezometers immediately to the north south east and west of the quarry would provide adequate information on the phreatic surface on that side of the quarry. This data would be significant in planning of further development of the quarry to the west. Figure 3-13 shows suggested positions for piezometer installation.

Figure 3-13: Map showing the suggested positions for piezometer installation.

3.5 Rock Discontinuities

3.5.1 Introduction

The properties of rock discontinuities govern the overall behaviour of rock masses (Cripps, 1988). Discontinuities such as bedding planes, joints, and faults are all planes of

weakness where failure or sliding of the rock mass is likely to occur. It is imperative that the properties of these discontinuities are understood in the engineering geological model in order to understand potential failure modes and mechanisms.

Rock discontinuity properties are measured and assessed in field and laboratory investigations. Data is quantified and presented for typical discontinuities within the rock mass. Significant properties measured during the investigation of Whitehall Quarry were joint roughness coefficient (JRC), persistence, spacing, bedding thickness, and shear strength. Orientation of discontinuities is presented and discussed in Section 3.3.

3.5.2 Bedding planes

Introduction

Bedding planes within Whitehall Quarry play a significant role in slope stability due to the interbedding of very strong sandstone with weak mudstone. Significant bedding plane properties to be addressed for the quarry as a whole in this section are: persistence, bedding thickness, and effective shear strength.

Bedding Plane Properties

Properties of typical bedding planes within the quarry are approximated from data collected during field investigations undertaken during January 2010.

Bedding plane persistence is the real extent or observed length of the plane, and is crudely quantified by observing the trace lengths of bedding planes on exposed surfaces. The persistence of bedding planes often controls large scale sliding in engineered slopes. Bedding plane persistence is usually much larger than the persistence of joints. The typical persistence of bedding planes at the quarry is greater than 20 m, therefore the term very high persistence is applied. The classification and terms of persistence are based on those defined by the NZGS, as outlined in Appendix D5. The persistence is not affected by differing weathering profiles; the only affect is the reduced ability to visually define the length due to extreme discolouration of mudstone and sandstone beds in increasingly weathered material.

The thickness of bedding also affects rock mass behaviour in natural and engineered slopes. Rock masses with thick beds are likely to be more stable due to the reduced number of bedding planes or planes of weakness within the mass, and vice versa with thinly bedded masses. However, Whitehall Quarry exhibits interbedded mudstone and sandstone.

Sandstone beds have a much thicker bedding, typically moderately to very thick (0.2 to >2 m thick), while interbedded mudstone is typically laminated to moderately thin (2 to 200 mm thick). Disregarding joints, this shows that slope failures are likely to occur within thinly bedded mudstone than thickly bedded sandstone.

Effective shear strength is derived from the combination of laboratory shear strength data, discontinuity surface roughness and waviness. The approximation of effective stress was developed by Patton (1966) for discontinuity surfaces in slope stability assessment. The effective shear strength is the actual shear strength of the entire surface rather than the shear strength derived from laboratory test of a laboratory scale sample. The equation and parameters are shown below, and details are presented in Appendix C9.

(Patton, 1966)

Where:

$\varphi'_{effective}$ = the effective angle of internal friction over the surface.

φ'_{basic} = the angle of internal friction determined from shear strength testing.

i_r = roughness coefficient.

i_w = surface waviness.

ILA = inter-limb angle.

The estimated effective angle of internal friction for a mudstone bedding plane is 34^o, calculations and values are presented in Appendix C9. However, this is just an estimate, the acceptable range is plus or minus 5 degrees, and therefore the effective angle of internal friction is likely to be within 29^o and 39^o.

Table 3-5: Summary of bedding plane properties.

Bedding Plane Properties	Classification
Persistence	Very high persistence (>20m)
Bedding Thickness (Sandstone)	Moderately to very thick (0.2 to >2 m)
Bedding Thickness (Mudstone)	Laminated to moderately thin (2 to 200 mm)
Effective Angle of Internal Friction	34^o
Acceptable Range for Angle of Internal Friction	29^o to 39^o
Acceptable Cohesion	0.0 kPa

Bedding Plane Shear

Bedding plane shear is a defect type where failure or sliding occurs on a bedding plane thus shearing the weak rock material. This type of failure is exhibited within the quarry on rare bedding planes. It appears that bedding plane shear, generally striking east west is related to the regional extensional regime trending north south. This type of failure has predominantly developed within laminated to thinly bedded mudstone beds due to the low intact rock strength of the lithology.

3.5.3 Joints

Introduction

Joints within Whitehall Quarry play a significant role in slope stability. Significant joint properties to be addressed for the quarry as a whole in this section are: persistence, joint spacing, and effective shear strength.

Joint Surface Properties

Properties of typical joints within the quarry are approximated from data collected during field investigations undertaken during January 2010.

Joint surface persistence is the real extent or apparent length of the plane, and is quantified by observing the trace lengths of joints within exposed surfaces. The persistence of joints often controls large and small scale sliding in engineered slopes. The typical persistence of joints within the quarry is usually in the order of 1 to 3 m, therefore the term low persistence is applied.

The joint roughness coefficient (JRC) is the measured profile of a joint surface at a 10 cm scale. The JRC indicates how rough a joint surface is, 1 being very smooth showing slickensides, and 10 being extremely rough. This coefficient is significant in slope stability due to its varying affect on sliding, where low JRC values have less resistance to sliding than high JRC values. The typical JRC for joints within the quarry is 3 with a range of 1 to 5. This indicates a typical joint surface that is smooth but not slickenside smooth.

Surfaces of joints are typically stained with iron-rich limonite or coated with zeolite. Neither of these joint surface affects is likely to increase or decrease the angle of internal friction. Clay filling does not appear to be present of joints within slightly to unweathered

greywacke sandstone. However, clay infilling is present in some joints within more highly weathered material. Aperture, or width of joint surface separation, is typically narrow; therefore this thickness of clay filling will not exceed 6 to 8 mm unless the joint has been opened via local mass movement. Thicker clay infilling will significantly reduce the angle of internal friction. Clay infilling has been analysed as having an angle of internal friction of 13^{o}.

The estimated effective angle of internal friction for an unweathered sandstone joint is 37^{o} determined from this study. However, this is just an estimate, the associated acceptable range is plus or minus 5 degrees, and therefore the effective angle of internal friction is likely to be within 32^{o} and 42^{o}. This method of effective shear strength calculation has been applied to basic shear strength estimates made by Tonkin & Taylor Ltd (2004), as shown in Table 3-6.

Table 3-6: Summary of joint surface properties.

Joint Surface Properties	Classification
Persistence	Low persistence (1-3 m)
JRC	3
Effective Angle of Internal Friction (Blue Rock) Acceptable Range	37^{o} 32^{o} to 42^{o}
Effective Angle of Internal Friction (Brown Rock) Acceptable Range	35^{o} 30^{o} to 40^{o}
Effective Angle of Internal Friction (Overburden) Acceptable Range	26^{o} 21^{o} to 31^{o}
Acceptable Cohesion	0.0 kPa

3.5.4 Faults

Introduction

Major and minor faults play a significant role in slope stability at Whitehall Quarry (Map Sheet 1). Faults within any engineering geological model must be carefully analysed for persistence, fault gouge and distribution. This section generalises faults within the quarry which could affect slope stability.

Fault Properties

Properties of typical faults within the quarry are interpreted from data collected during field investigations undertaken during January 2010.

Many of the minor faults mapped (Map Sheet 1) exhibit low persistence (1 to 3 m) and do not exhibit fault gouge but have well developed striations and fibre growths. These identified minor faults do not pose as greater risk to stability as major faults do, therefore these will be treated similarly to joints.

Major faults are also mapped, as shown on Map Sheet 1, and pose a risk to overall stability of the quarry. These faults exhibit very high persistence (greater than 20 m) and exhibit fault gouge with typical thicknesses of 25 to 100 mm. Clay minerals kaolinite and montmorillonite have been identified within fault gouge. The clay content in fault gouge has been estimated as being between 20 and 25% determined from Atterberg Limit analysis discussed in Section 2.3.6. This clay content is likely to have an unquantifiable adverse affect on stability which is likely to be the reduction of the angle of internal friction.

Major faults appear to have approximated displacement in the order of 2 to 8 m causing displacement of weathering profiles (Map Sheets 1, 2 and 3). The distribution of these major faults is relatively sparse therefore these can be assessed as isolated features. Also mapped is the northern wedge within the north western corner of Pit 1. This is a complex fault bounded wedge and in depth analysis of this wedge will be carried out in Chapter 5.

The estimated angle of internal friction for typical fault gouge is 13^{o} determined from ring shear testing discussed in Section 2.3.7. The associated range of acceptable values is plus or minus 5 degrees resulting in a range of 8^{o} to 18^{o}. The approximated value and range will be used in slope stability analysis in Chapter 4 and in the analysis of wedge stability in Chapter 5.

3.5.5 Discussion

Patton's Law was applied to rock shear strength results to estimate the effective angle of internal friction for joints and bedding discontinuities. This effective shear strength result is more realistic to apply to large discontinuity surfaces rather than the basic shear strength obtained from laboratory testing of small samples.

The alternative to Patton's Law is the Barton-Bandis Criterion (1973). The Barton-Bandis approach is one of the most common applications for evaluating effective shear strength. However, this approach does not take into account the waviness of a discontinuity surface; it only includes the JRC which is typically measured from a 10 cm profile therefore excluding the overall shape or waviness of the discontinuity. Waviness must be taken into account; a surface that exhibits a high degree of waviness is likely to have a higher angle of internal friction, whereas a surface with no waviness exhibited is likely to have a much lower angle of internal friction.

Patton's Law was not only applied to shear strengths approximated during laboratory investigations undertaken in this study but the shear strengths approximated by Tonkin and Taylor Ltd for brown rock and overburden. The resulting shear strengths were expected and will be applied to slope stability analyses in Chapter 4.

3.6 Rock Mass Quality

3.6.1 Introduction

Assessing the rock mass quality involves the application of an appropriate classification system to a rock mass producing a term or value dependent on quality. This term or value enables quarry operators to gain a quick brief understanding of the rock mass and can treat it appropriately.

Bieniawski (1989) identifies the following properties as the aims of rock mass classifications:

- To identify the most significant parameters influencing the behaviour of a rock mass.
- To divide a rock mass formation into rock mass classes of varying quality.
- To provide a basis for understanding the characteristics of each rock mass class.
- To relate rock conditions at one site to the conditions and experience encountered at others.
- To derive quantitative data and guidelines for engineering design.
- To provide a common basis for communication between engineers and geologists.

Qualitative rock mass analysis of Whitehall Quarry used Bieniawski's 1989 Rock Mass Rating (RMR) system and the Geological Strength Index (GSI) developed by Marion and Hoek (2000).

3.6.2 Application of RMR and GSI

Bieniawski's 1989 Rock Mass Rating system utilises the following six parameters:

1. Uniaxial compressive strength of rock material.
2. Rock quality designation.
3. Spacing of discontinuities.
4. Condition of discontinuities.
5. Groundwater conditions.
6. Orientation of discontinuities.

RMR values are a result of the combination of these parameters. High values indicate a good quality rock mass while low values indicate poor rock quality (Appendix B5). However, while this process is acceptable for rock masses with RMR values of more than approximately 25, it does not work for very poor rock masses since the minimum value which RMR can assume is 18. In order to overcome this limitation the Geological Strength Index (GSI) is applied (Hoek, et al. 1997).

For RMR_{89}>23:

The RMR and GSI are applied to rock mass units at the quarry. Although it is possible to assess slope stability based on rock mass quality and favourability of discontinuities, it is not desirable in such a detailed stability assessment such as this. Therefore rock masses will be assessed under RMR and GSI with disregard to discontinuity orientation. Stability analysis based on discontinuity orientations is presented in Chapter 4. Table 3-7 summarises rock mass quality for the three main quarrying rock types.

Table 3-7: Summary of rock mass quality.

SW-UW Greywacke Sandstone (Blue Rock)	
RMR	82
GSI	77
Descriptive Class and Term	I. Very good rock
MW-HW Greywacke Sandstone (Brown Rock)	
Rock Mass Rating	65
GSI	60
Descriptive Class and Term	II. Good rock
CW-RW Greywacke Sandstone (Overburden)	
Rock Mass Rating	34
GSI	29
Descriptive Class and Term	IV. Poor rock

3.6.3 Discussion

Rock mass classification is a means for the evaluation of the performance of a rock mass based on the important inherent and structural parameters (Pantelidis, 2009). This investigation into rock mass parameters and the resulting rock mass rating (RMR) provides an insight into the rock mass characteristics and its ability to stand competently within an engineered rock slope. However, the application of RMR and GSI was only to gain a quick and brief assessment of rock mass similarities and differences around the quarry. The characteristics of the differing rock masses can now be conveyed to engineers and quarry operators easily based on the classification system used.

The rock mass classifications for each rock mass assessed in this investigation showed acceptable values when compared with values obtained from Tonkin & Taylor Ltd (2004). However, the slightly to unweathered greywacke sandstone mass showed slightly higher than expected results. This mass was expected to have a RMR of 60 to 80 reflecting an angle of internal friction of 35 to 45 degrees, as shown in laboratory testing carried out in this investigation. Instead, this mass returned an RMR of 82 indicating an angle of internal friction greater than 45 degrees. This raises questions relating to the application of the RMR and GSI systems, and the accuracy of laboratory testing undertaken during this investigation. Therefore, it must be assumed that results obtained via independent shear strength tests are more accurate than assumptions from rock mass classifications. This may indicate that a range of values for RMR and GSI should be applied rather than a singular number. Possibly

an uncertainty or range of values in the order of plus or minus 5 would result in acceptable values for classifying rock masses at the quarry.

Although critical to slope stability, argillaceous mudstone beds were excluded from rock mass classification due to the large variation in locality and the difficulty in assessing the reduction in rating due to its presence. Mudstone beds consist of highly fractured weak rock; this is likely to reduce the intact rock strength, rock quality designation (RQD) and spacing of discontinuities, thus resulting in a much lower rating for the rock mass. But due to the variability in mudstone locality an overall rating of a rock mass would be inconsistent throughout the quarry, therefore evaluation of mudstone rich rock masses should be carried out on a locality basis.

3.7 Discussion and Synthesis

The engineering geological model outlines the fundamental parameters required for slope stability analysis. Understanding these parameters is paramount in order to accurately assess rock mass stability and predict future performance. Key parameters analysed in the engineering geological model include:

- Rock and soil types.
- Major structural features.
- Groundwater and drainage.
- Discontinuities.
- Rock mass classification.

The rock and soil types identified were sandstone of differing weathering grades, argillaceous mudstone and rhyolitic alluvial sandy gravels. The last of the three, restricted to the paleo-channel identified within the eastern edge of the quarry, is unlikely to cause slope instability due to the relative scarcity of the material. However, the presence of mudstone beds within the quarry is likely to have an adverse affect on slope stability. It is likely that slope failures will occur along the bedding plane of this weak rock. As discussed in Section 3.6.3, it is difficult to apply the RMR or GSI to this rock type because it is variably interbedded with very strong sandstone. Therefore argillaceous mudstone beds must be considered as likely failure planes in the assessment of pit slope stability.

Patton's Law for effective shear strength was applied to joints and bedding planes. The resultant effective shear strength of these surfaces, as well as the associated range of values, will be applied to the overall pit slope stability assessment undertaken in Chapter 4. Due to issues associated with laboratory testing, such as sample selection bias, results are not exact; therefore a range of values will give the best estimate in stability analysis.

Bedding plane shears were identified within the Southern Domain of the quarry. These features appear to have an average dip and dip direction of 57^{o}/211, which is relatively similar to the Main Quarry Shear Zone (MQSZ), 46^{o}/190, identified as the domain boundary, these features could be related. As regional extension continues in the north south trend, weak argillaceous bedding planes undergo shearing to release stress from the MQSZ, identified as a normal fault. These bedding shear exhibit striations and fibre growths indicating movement began some time ago. It is likely that these features will be reactivated as quarrying operations continue. As the quarry expands into the western slope, more of the bedding shear surfaces will be exposed thus the likelihood of initiating failure of part of the slope down dip towards the south.

There appears to be no consistency in joint patterns between the northern and southern domains. Joints identified from 620 poles within the Northern Domain are typically steeply inclined towards the south east. Joints in the Southern Domain are more sporadic with four sets of steeply inclined to sub-vertical joints identified from 1511 poles. However, this remains the only significant difference in structural features as bedding planes have similar orientations. Bedding planes identified within the Northern Domain have an average orientation of 82^{o}/218 while in the south they average at 57^{o}/211. Dip directions are similar while dip angles differ by approximately 25 degrees. This small difference is likely to have been caused by regional tectonics influencing the different blocks either side of the MQSZ.

Although the engineering geological model presented in this chapter appears complete. It must be noted that the associated hydrogeological model is based on pit observations and interpretations only. No piezometric or drilling data was available at the time of this investigation. In order to increase the reliability of this engineering geological model more hydrogeological data must be input, more specifically groundwater elevation and pit drainage information. If the hydrogeological model is significantly inaccurate the assessment of slope stability will be compromised. Slopes will be assessed as dry, if this is not the case and the actual slope is almost completely saturated, the pore water pressures will

be elevated thus decreasing the shear strength of the rock slope resulting in slope failure (Hawkins & McConnell, 1992). The estimation of the hydrogeological model also affects the resultant rock mass classifications given significant quarrying rock types. An increased level of water will decrease the RMR and GSI of each rock mass affected.

The engineering geological model presented in this chapter is the best possible estimate for engineering geological and geotechnical parameters at Whitehall Quarry. To increase the quality and reliability of the model a greater amount of data is required. For one, accurate hydrogeological measurements are missing from this model resulting in the estimation of groundwater levels from pit observations. The weathering profile could also have been better estimated had there been drilling data available for the quarry at the time of this investigation.

4.0 Pit Slope Stability Assessment

4.1 Introduction

Hoek and Bray (1981) state that one of the most obvious economic issues involved with slope stability is that in order to reduce to amount of waste rock to be excavated in order to acquire high quality rock, the ultimate slopes of the quarry are generally cut to the steepest possible angle. Since the economic benefits gained in this way can be negated by a major slope failure, evaluating the stability of the ultimate pit slopes is an important part of open pit planning.

In civil engineering projects, where rock slope stability is assessed, it is typical to assess with a factor of safety in mind. This is a value at which the boundary of stability and instability lies. Below this value failure of one or more slopes is likely to occur. However this may be the case in civil projects it is not in open pit excavation. As stated earlier, it is the economics that typically govern the design of a slope. A steeper slope equates to greater earning potential, however a steeper slope also increases risk of failure. Applying a factor of safety to slope stability may significantly reduce the risk of failure, however if the factor of safety is set too high the earning potential of the slope is reduced; therefore equilibrium between the two must be reached.

The pit slope stability assessment undertaken in this chapter describes current pit slope performance, potential modes of failure identified in kinematic analysis and specific areas within the quarry that exhibit potentially significant instability.

4.2 Current Pit Slope Performance

A field based investigation into the current slope stability and performance of benches and batters was undertaken in January 2010. The aim of this was to identify features associated with slope instability, such as crest break back and rill accumulation. Typical features of instability also include tension cracks. These features were largely identified on the Northern Wedge Failure in Pit 1, and in depth analysis of this wedge is presented in Chapter 5.

Rill accumulation and crest break back are directly related. The crest or edge of a bench typically exhibits small failures along discontinuities that propagate through the bench

and batter. The material that falls from these small scale failures accumulates at the base of the batter as rill (Eggers, 2010), hence rill accumulation (Figure 4-1).

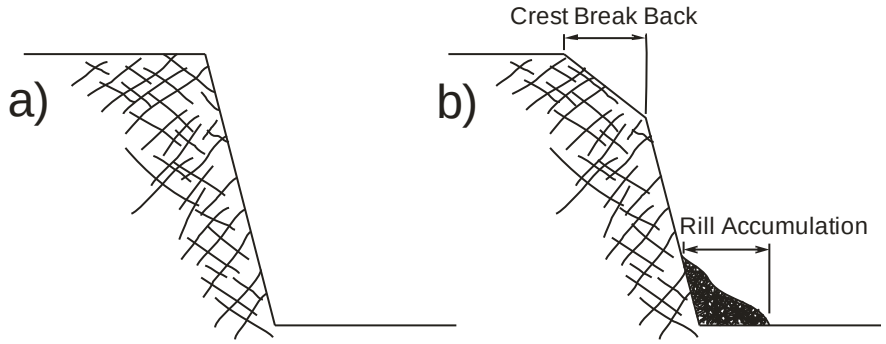

Figure 4-1: Diagram depicting the relationship between crest break back and rill accumulation, a) newly cut slope, b) slope after some time.

Areas within the quarry where there is a high degree of crest break back and rill accumulation may suggest that the slope is not performing to a satisfactory standard where over-steepened batter slopes allow blocks to failure from the closely jointed rock mass. Obviously it is difficult to design economic slopes that produce no crest break back or rill accumulation, so to a small degree it is acceptable. In this investigation crest break back and rill accumulation indicates not only an ageing slope, but areas with increased fracture frequency or, more importantly, areas with small low persistent discontinuities striking parallel with the slope.

Whitehall Quarry exhibits both crest break back and rill accumulation as shown in selected face maps (Map Sheets 4 to 8).

Pit 1 exhibits the largest amount of rill accumulation and crest break back; up to 5 m of rill accumulation from the slope base and up to 4 m of crest break back within slightly to unweathered sandstone. The average block size of rill accumulated at the base of slopes within Pit 1 is approximately 150 mm. Instability features within Pit 2 are easier to distinguish than Pit 1 due to the vastly reduced amount of vegetation. Pit 1 exhibited lower amount of crest break back, up to 2 m, and rill accumulation, up to 3 m, however the differently orientated slopes showed similar quantities of rill accumulation and crest break back, this was not expected due to the likely exposure of sub-parallel discontinuities within the rock slope.

The amount of rill accumulation and crest break back exhibited in Pit 2 is low and does not appear to interrupt quarry operations. Crests appear to be competent thus rill

accumulation is reduced. However, having two excavation pits of the same material but different age, offers a window into the future for Pit 2. It is expected that after 20 years Pit 2 will have slightly higher degrees of crest break back and rill accumulation.

Other instability features related to slope stability identified during fieldwork were small isolated wedge and block failures. The size of these failures typically ranges from 1 to 3 m^3. More wedge failures were identified than block type failures and these were typically exhibited within highly weathered material. Wedge failures are typically joint-joint wedges where two joint sets intersect forming a small wedge.

Directly related to current pit slope performance is the current pit slope inter-ramp angles. Throughout this study inter-ramp angles are measured from toe-to-toe to obtain an average of the engineered rock slope angle (Figure 4-2). Inter-ramp angles at the quarry range from 35 to 50 degrees. Overburden material is typically engineered at 30 to 40 degrees while more competent strong sandstone is designed at 40 to 50 degrees. Average slope orientations for selected slopes are presented in Map Sheets 4 to 8.

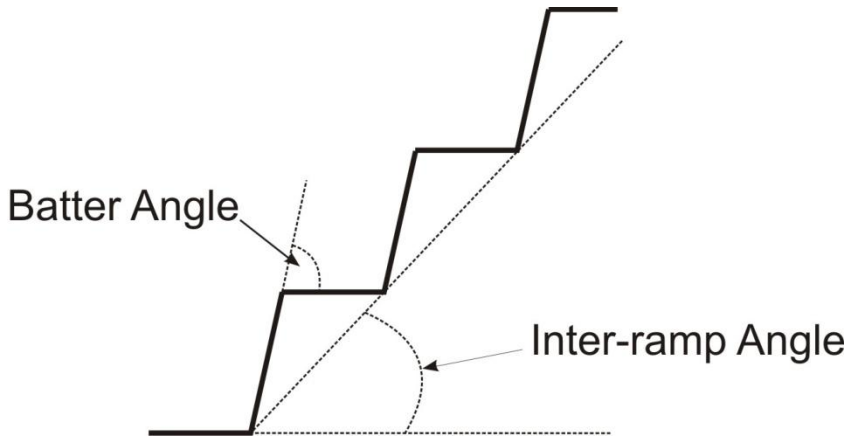

Figure 4-2: Slope angle measurement convention.

4.3 Slope Stability Analysis Methodology

Assessment of open pit slope stability and providing associated future design plans requires the understanding of possible slope failure modes and associated directions of failure and geometry. This type of assessment is carried out via kinematic slope stability analysis. Kinematic analysis is purely geometric in that it examines which modes of failure are possible in a rock mass with respect to an existing or proposed rock slope. In a kinematic

analysis, it is the orientation of the combination of discontinuities, the slope face, and any other slope surfaces of interest, together with friction, that is examined to determine if certain modes of failure can possibly occur (Kliche, 1999).

This analysis is normally conducted with aid of a stereographic representation of the planes and/or the lines of interest. The Markland test is an extremely valuable tool for identifying those discontinuities that could lead to planar, wedge, or toppling failure in the rock mass and for eliminating other discontinuities from consideration. Laboratory results gained from this study are used in the application of the Markland test to best identify potential instability (Table 4-1).

Table 4-1: Summary of friction angle derived from shear box testing.

Rock Type	Angle of Internal Friction
Overburden (HW-RW Sandstone)	26°
Brown Rock (MW-HW Sandstone)	35°
Blue Rock (UW-SW Sandstone)	37°

The Markland test stereographic analysis is conservative because it makes two very important assumptions:

1. All discontinuities are assumed to be continuous and through going, though in reality many of them are not. Even a small percentage of intact rock along a discontinuity can generate enough strength to make the rock safe against sliding.
2. The stereonet procedure assumes that the cohesion is equal to zero, meaning the effects of cohesion are ignored. When this assumption is made, the fundamental limiting equilibrium equation for the factor of safety reduces to:

Where: = angle of internal friction for the rock surface

β = dip of the discontinuity or plunge of the line of intersection.

4.3.1 Planar Failure

Planar failures, also known as a plane failure, in engineered rock slopes occur when a geological discontinuity strikes sub-parallel (within 15 degrees) to the slope face and dips at an angle greater than the angle of internal friction (Hoek & Bray, 1981). Once the frictional force is overcome, sliding begins (Figure 4-3).

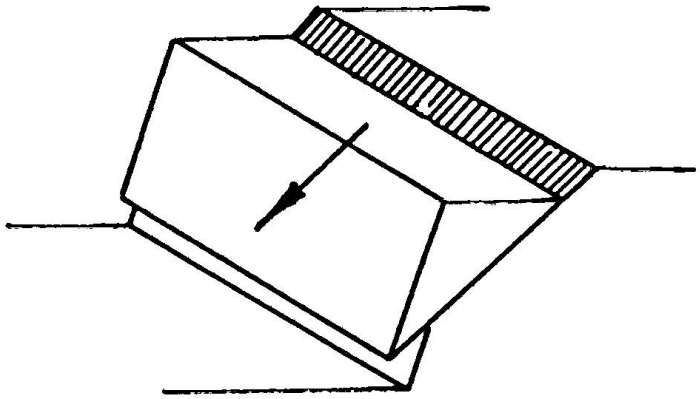

Figure 4-3: Planar failure (Wyllie & Mah, 2004).

The Markland test for planar failure utilises a stereographic projection of the great circle representing the slope face together with a circle representing the angle of internal friction of the discontinuity (Figure 4-4). The zone between the rock slope great circle and the friction circle represents the potential failure envelope within which planar failure is kinematically possible if the three additional criterions for failure are met (Kliche, 1999):

1. The dip of the discontinuity must exceed the angle of internal friction for the discontinuity surface.
2. The discontinuity must daylight in the slope face.
3. The dip of the discontinuity must be less than the dip of the rock slope face.
4. The discontinuity must strike within 15 degrees of the slope face (Hoek & Bray, 1981).

These conditions can be expressed by the following relationship:

Where:

ψ = dip of the slope face

β = dip of the discontinuity

= angle of internal friction for the discontinuity surface

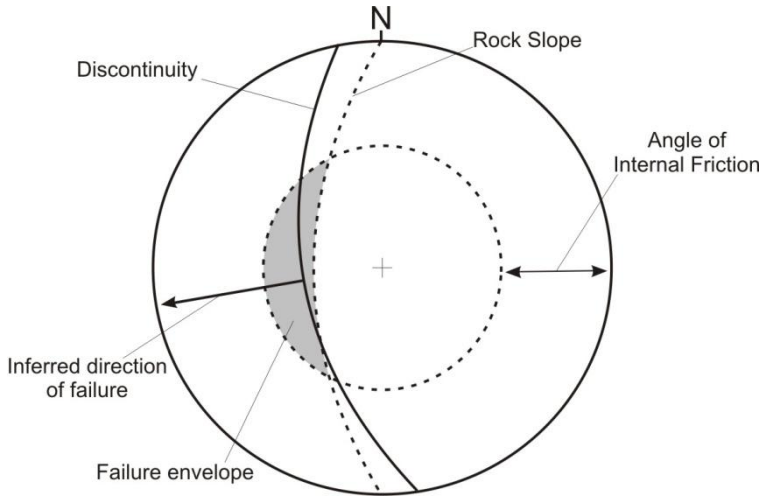

Figure 4-4: Stereographic representation of potential planar failure (adapted from Villeneuve 2010).

This method of analysis identifies and assesses the potential for planar failure and the likely direction of sliding.

4.3.2 Wedge Failure

Wedge failures result when rock masses slide along two intersecting discontinuities both of which dip out of the cut slope at an oblique angle to the cut face, forming a wedge-shaped block (Norrish & Wyllie, 1974) (Figure 4-5). Commonly, these rock wedges are exposed by excavations that daylight the line of intersection that forms the axis of sliding, precipitating movement of the rock mass either along both planes simultaneously or along the steeper of the two planes in the direction of maximum dip.

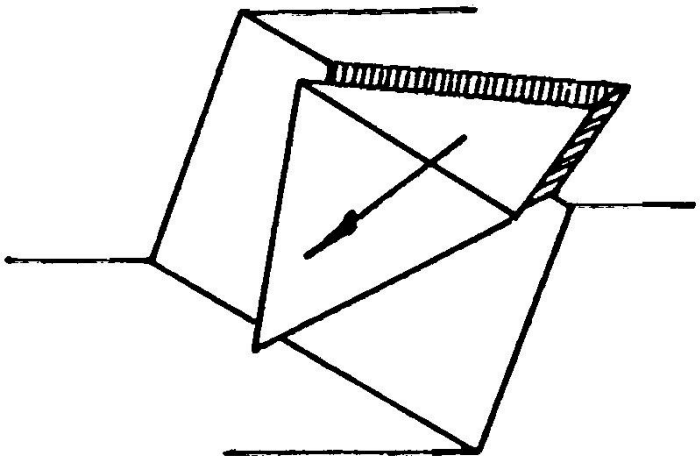

Figure 4-5: Wedge failure (Wyllie & Mah, 2004)

The Markland test identifies potential wedge failure if the intersection of the two discontinuities lies within the failure envelope (Figure 4-6), and the following three additional conditions for failure are met (Kliche, 1999):

1. The plunge of the line of intersection of two discontinuities must exceed the angle of internal friction for the discontinuity surface.
2. The line of intersection of two discontinuities must daylight in the slope face.
3. The plunge line of intersection of two discontinuities must be less than the dip of the rock slope face.

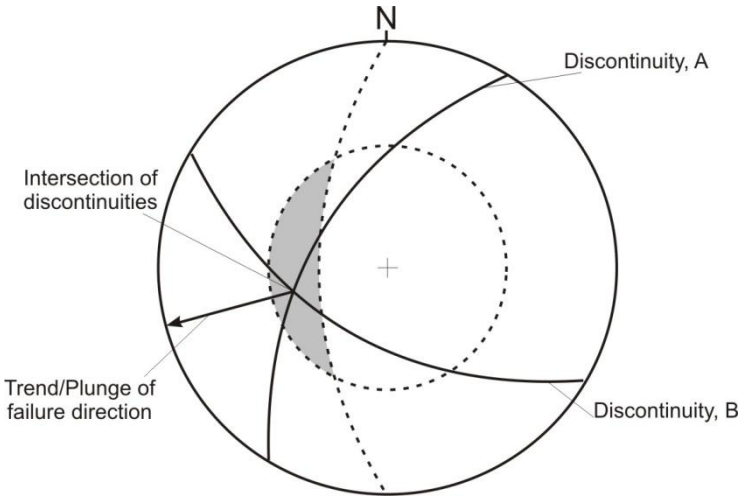

Figure 4-6: Stereographic representation of potential wedge failure (adapted from Villeneuve 2010).

This method of analysis identifies and assesses the potential for wedge failure and the likely direction of sliding.

4.3.3 Toppling Failure

Toppling failures most commonly occur in rock masses that exhibit a series of slabs or columns formed by a set of discontinuities that strike sub-parallel to the slope face and dip steeply back into the face. In a toppling failure the rock column or slab rotates about an essentially fixed point at or near the base of the slope at the same time that slippage occurs between the layers, (Norrish & Wyllie, 1974) (Figure 4-7).

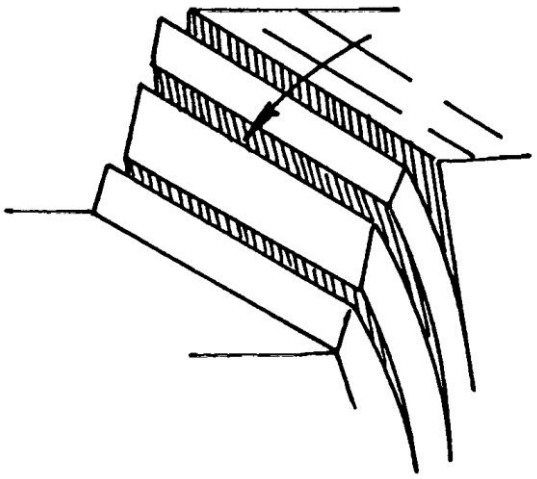

Figure 4-7: Toppling failure (Wyllie & Mah, 2004).

The stereographic projection of the slope face and the friction circle can also be utilised to determine a kinematic potential for the toppling failure mode (Figure 4-8). In order for toppling failure to be kinematically possible, the following conditions must exist:

1. The dip of the face is greater than the dip of the discontinuity which greater than the angle of internal friction.
2. The potential direction of topple plots within 10 degrees of the dip direction of the cut slope.

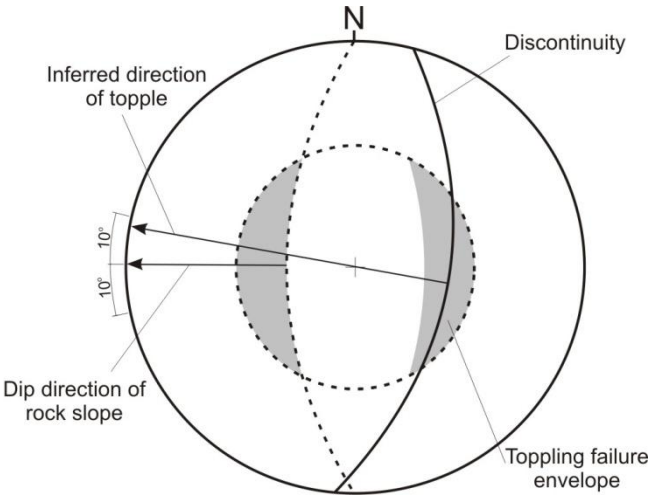

Figure 4-8: Stereographic representation of potential toppling failure (adapted from Villeneuve 2010).

This method of analysis identifies and assesses the potential for toppling failure and the likely direction of toppling.

4.4 Kinematic Analysis of Pit Slopes

Kinematic slope stability analysis was purely based on the engineering geological model for Whitehall Quarry, which was outlined in the preceding chapter. This involved the use of the Markland test in the assessment of engineered rock slopes for failure and instability modes described in Section 4.3. The kinematic slope stability assessment carried out during this investigation is presented in Map Sheet 9. The failure modes identified in this assessment are only potential failures not actual documented failures.

Selected sections of average batter and inter-ramp orientations show varying degrees of instability marked by the population of failure modes identified for the specific slope orientation. Slopes orientated towards the west within the Northern Domain were deemed to be stable, as they show no potential failure modes at inter-ramp or batter scales. However, this slope design orientation was the only to be given the stable status, all other rock slope within the quarry exhibited potential wedge, planar or toppling failure modes. The failure modes are presented with an associated factor of safety to illustrate the relative instability of a potential failure.

4.4.1 Wedge Failures

Devised from kinematic analysis presented in Map Sheet 9 the wedge failure mode is the most common type of potential instability. Of the 35 potential failures identified within

the quarry, 85% were wedge failures. Most wedge failures occur within weak overburden material at the batter scale (face dipping at 60 to 70 degrees). The typical range of plunge for the line of intersection, or sliding surface, is 25 to 35 degrees for joint bounded wedges resulting in factor of safety values in the order of 1.6 to 1.1 for blue rock, 1.5 to 0.9 for brown rock, and 1.0 to 0.6 for overburden. The typical size of these joint bound wedges ranges from approximately 2 to 9 m^3. But this analysis does not rule out the possibility of much larger wedge failures formed via stepped joints. This phenomena is formed where increased persistence is created from joint planes failing together to form a stepped failure plane. This is a complex failure type and will not be covered in this investigation.

It appears that greater instability lies within wedges semi-bound by major fault planes. Wedges that are formed via the intersection of a fault plane and another discontinuity tend to have a greater potential instability than joint bound wedges. The lines of intersection for wedges semi-bound by faults typically have a plunge of between 38 and 60 degrees, thus resulting in much lower factor of safety values. The factor of safety values estimated for wedges semi-bound by fault planes are upper limit estimates based on angles of internal friction for rock surfaces, therefore fault gouge material has been ignored. In reality, these wedge types will exhibit much lower friction angles and thus be much less stable than estimated in this assessment. The effective angle of internal friction for a fault-joint wedge is likely to range from 15 to 25 degrees resulting in a range for factor of safety of 0.60 and 0.15 indicating potentially very high instability. Wedges semi-bound by fault planes are typically only on a batter scale and are limited in size by the joint persistence. These wedges have an estimated maximum size of 9 m^3 if they are bound by a fault and a joint. If the wedge is bound by a major fault and a bedding plane, instability of the wedge is on a much grander scale due to the high persistence of both discontinuities; therefore it is difficult to estimate the potential size.

Due to the typically high fracture frequency for the quarry, wedge failures are anticipated to initially fail along the bounding discontinuities, as failure continues the wedge mass is more likely to disintegrate into small blocks. This failure type is likely to fail rapidly once initiated, possibly in the order of greater than 5 ms^{-1} (Chapple, 1998).

4.4.2 Planar Failures

Planar failures are not as common as wedge failures but they potentially exist with greater instability. Planar failures occur at batter and inter-ramp scale along joint sets, major

faults and bedding planes. Planar failures along joint sets are unstable and typically exhibit an estimated factor of safety of greater than 0.7 for shallowly dipping sets.

It is anticipated that planar failures within the quarry will not exceed 3 or 4 m^3 within the same failure event due to the high fracture frequency exhibited by the rock mass. Isolated blocks are likely to slide as a planar failure with smaller, less dominant and random joints making up the sub-perpendicular block edges. Similar to wedge type failures, planar failures are expected to rapidly accelerate once sliding is initiated by increased pore water pressure, blasting, excavation or seismic acceleration. Failure velocities are expected to exceed 5 ms^{-1}, therefore once initiated they will be near impossible to control.

4.4.3 Toppling Failures

One potential toppling failure was identified within slopes dipping towards the east with the Southern Domain of the quarry. Toppling failure is likely to occur on the least prevalent joint set 4. Blocks within this slope are expected to topple towards the east. The factor of safety range has been estimated at 0.75 to 0.49 (blue rock to overburden material) for this failure type. However, failure of this type is unlikely to be significant enough to disrupt quarrying operations due to the high fracture frequency of the rock mass, this may result in increased ravelling in this slope rather than large toppling slabs.

4.4.4 Quarry Sections

The following sections have been identified as exhibiting potentially critical failures at the batter or inter-ramp scale. The following sections are identified from the analysis presented in Map Sheet 9.

Section B

The average inter-ramp and batter dip direction for Section B is 180 with dips of 38 and 70 degrees respectively. Kinematic analysis identified two potentially critical failures within this section, a wedge and planar failure, both at the batter scale.

Wedge Failure

The potential wedge failure occurs via the intersection of three discontinuities:

- J1: 57^{o}/107
- Bedding: 82^{o}/218
- Major fault: 60^{o}/178, Plane B (sliding plane) of the Northern Wedge Failure

This failure is anticipated to occur within slopes orientated at approximately 180 (dip direction) and steeper than 52 degrees. Potential failure is likely to occur within all three material types with a range of factor of safety values of 0.4 to 0.6. The potential size of this failure is difficult to predict due to the persistence of both the bedding plane and major fault, but it is likely to be in the order of 50 to 200 m^3. A summary of the potential failure is presented in

Table 4-2.

Table 4-2: Summary of a potential wedge failure within Section B.

Failure Type	Wedge
Daylights at	Batter scale only
Rock Type	Blue rock, brown rock, overburden
Discontinuities	J1, bedding, major fault
Direction of Sliding	52^{o}/138
Factor of Safety	Overburden = 0.38 Brown Rock = 0.55 Blue Rock = 0.59

Planar Failure

The potential planar failure occurs along a major fault (60^{o}/178). This failure is anticipated to occur within slopes orientated at approximately 180 (dip direction) and steeper than 60 degrees. Potential failure is likely to occur within all three material types with a range of factor of safety values of 0.3 to 0.5. The potential size of this failure is difficult to predict due to the persistence the major fault, but it is likely to be in the order of 50 to 150 m3. A summary of the potential failure is presented in Table 4-3.

Table 4-3: Summary of a potential planar failure within Section B.

Failure Type	Planar
Daylights at	Batter scale only
Rock Type	Blue rock, brown rock, overburden
Discontinuities	Major Fault
Direction of Sliding	60^o/178
Factor of Safety	Overburden = 0.28 Brown Rock = 0.40 Blue Rock = 0.44

Section C

The average inter-ramp and batter dip direction for Section C is 130 with dips of 38 and 70 degrees respectively. Kinematic analysis identified one potentially critical failure within this section. A potentially critical wedge failure is anticipated with all materials at the batter scale. The wedge is formed via the intersection of three discontinuities:

- J1: 57^o/107
- Bedding: 82^o/218
- Major fault: 60^o/178, Plane B (sliding plane) of the Northern Wedge Failure

Failure is likely to occur within batters steeper than 52 degrees. The potential size of this failure is difficult to predict due to the persistence of both the bedding plane and major fault, but it is likely to be in the order of 50 to 200 m^3. A summary of the potential failure is presented in Table 4-4.

Table 4-4: Summary of a potential wedge failure within Section C.

Failure Type	Wedge
Daylights at	Batter scale only
Rock Type	Blue rock, brown rock, overburden
Discontinuities	J1, bedding, major fault
Direction of Sliding	52^o/138
Factor of Safety	Overburden = 0.38 Brown Rock = 0.55 Blue Rock = 0.59

Section G

The average inter-ramp and batter dip direction for Section G is 010 with dips of 38 and 65 degrees respectively. Kinematic analysis identified two potentially critical failures within this section, a wedge and planar failure, both at the batter scale.

Wedge Failure

The potential wedge failure occurs via the intersection of three discontinuities:

- J1: 57^{o}/107
- J2: 65^{o}/333
- J3: 82^{o}/084

This failure is anticipated to occur within slopes orientated at approximately 010 (dip direction) and steeper than 59 degrees. Potential failure is likely to occur within all three material types with a range of factor of safety values of 0.3 to 0.5. The potential size of this failure is likely to be in the order of 10 to 50 m^3 due to the low persistence of the joint surface. A summary of the potential failure is presented in Table 4-5.

Table 4-5: Summary of a potential wedge failure within Section G.

Failure Type	Wedge
Daylights at	Batter scale only
Rock Type	Blue rock, brown rock, overburden
Discontinuities	J1, J2, J3
Direction of Sliding	59^{o}/008
Factor of Safety	Overburden = 0.29 Brown Rock = 0.42 Blue Rock = 0.45

Planar Failure

The potential planar failure occurs along J1 (60^{o}/008). This failure is anticipated to occur within slopes orientated at approximately 010 (dip direction) and steeper than 60 degrees. Potential failure is likely to occur within all three material types with a range of factor of safety values of 0.3 to 0.5. The potential size of this failure is difficult to predict due to the persistence the major fault, but it is likely to be in the order of 50 to 150 m^3. A summary of the potential failure is presented in Table 4-6.

Table 4-6: Summary of a potential planar failure within Section G.

Failure Type	Planar
Daylights at	Batter scale only
Rock Type	Blue rock, brown rock, overburden
Discontinuities	J1
Direction of Sliding	60^{o}/008
Factor of Safety	Overburden = 0.28 Brown Rock = 0.40 Blue Rock = 0.44

4.5 Discussion and Synthesis

Slope stability assessment detailed in this section allows quarry planners and operators to design safer slopes resulting in greater productivity. As stated earlier, it is paramount equilibrium between the steepness of pit slopes and the acceptable degree of slope failure be reached via appropriate slope design considering the engineering geological model. At equilibrium the greatest potential productivity will be reached.

The application of kinematic slope stability assessment to the quarry via the Markland test was chosen over the limit equilibrium method because of its simplicity. The limit equilibrium method is numerically based and requires the use of accurate values for variable parameters. This method is not applicable in this case due to the uncertainty in each different parameter of the engineering geological model. Thus the Markland test was applied with success. The test of selected slopes of varying inter-ramp and batter orientation allowed analysis based on kinematics to assess slopes for potential failure modes in a geometrically simplistic manner. The Markland test highlights slopes with potentially critical failures at both inter-ramp and batter scale. The test also allows the fundamental analysis of effective friction angles for different rock mass types. Differently sized friction cones geometrically represent the failure or critical zone of a slope, effectively where a sliding surface daylights in the direction of slope dip.

An estimated factor of safety was equated from effective friction angles and the plunges of sliding surfaces. Although the factor of safety principle is not fully applicable to mining or quarrying practices, it does give operators an insight into which pit slope orientations are more susceptible to failure.

However, the Markland test only kinematically analyses purely gravitational failures with zero application of external or internal forces such as pore pressure. This is not an issue in the analysis of the quarry due to the earlier estimate of the hydrogeological model putting the groundwater table below the surface of pit slopes. Therefore pore pressure from groundwater is not considered to affect the pit slope stability of the quarry. However, water infiltration over a long period of time from rainfall will inevitably increase pore pressure resulting in increase slope instability, this affect has not been included in this assessment due to the difficulty in its mitigation.

The final issue with the Markland test is the assumption of infinitely continuous discontinuities. Although this eases simplistic assessment of stability it is not reality. The reality is that discontinuities vary in persistence thus resulting in variously sized failure masses. Joint set and discontinuity spacing's as well as random joints or fractures govern the size of blocks and wedges that fail from the slope. The quarry rock mass exhibits a high fracture frequency therefore reducing the maximum size of potential block or wedge size. The maximum potential block and wedge size estimated in this assessment is approximated at 200 m^3. Again, due to the large number of fracture present in the rock mass, as the block or wedge begins to slide it is likely to break up into much smaller blocks. If this type of failure occurs at batter scale, which is more likely, the cleanup will be simplistic and costs will be minimal thus resulting in an acceptable failure. However, if this same failure occurs on an inter-ramp scale where several benches failure simultaneously, the material below the failure could become contaminated with lower grade rock thus lowering productivity drastically while the cleanup is undertaken.

The largest failure identified within the quarry is the Northern Wedge Failure within Pit 1. Analysis of this failure is not included in this kinematic slope stability assessment of the quarry but discussed in detail in Chapter 5.

4.5.1 Recommendations

The following recommendations are derived from the analysis of the engineering geological model and pit slope analysis presented in this study. It is advised that these recommendations are implemented to increase stability, safety and possibly profitability of Whitehall Quarry.

- The lack of hydrogeological data is of concern in this study and will be a significant concern when quarry operations continue at greater depth. To gain more understanding of the fundamental groundwater table and the associated seasonal fluctuations, piezometers should be installed in locations surrounding the quarry. It is recommended that a piezometer is installed at least above the pit slopes to the south of Pit 2 and more importantly a piezometer should be installed on top of the hill to the immediate west of the quarry. Due to the probable expansion of the quarry to the west, hydrogeological data should be collected for analysis of possible lower than anticipated depths to the fundamental groundwater table.
- More defect data information from sections to the south west of the quarry where stripping is currently taking place. Data acquisition was restricted in this area so the stripping programme was not interrupted. Defect data in this area may show a continuation of the trends identified within the Southern Domain or there may exist a new domain. New data will provide greater understanding of the orientations of discontinuities to the west of the current operating pit and aid future pit designs in this area.
- The adverse affects blasting has on the pit slopes of Whitehall Quarry are unknown due to the lack of information regarding the blasting practices at the quarry. Analysis of this data may show that blasting causes greater instability to areas where critical instability exists. Blasting within the quarry may also cause greater instability to the Northern Wedge Failure.
- There are several unfavourable pit slopes within the quarry where the application of the Markland test has identified potentially large or unsafe wedge, planar or toppling failure modes (Map Sheet 9). The most notable pit slopes that could develop potentially large or critically unsafe failures are within the northern section of Pit 1, and the mid western and southern sections of Pit 2. These slopes experience potential instability due to over steepened inter-ramp and/or batter angles. If potentially critical instability has been identified for an average inter-ramp and/or batter, these slopes should be designed and engineered to a more suitable angle which is approximately 5 degrees less than the identified potential sliding plane plunge in Map Sheet 9. This should ensure the maximum possible stability of that slope within the designated material type.

5.0 Case Study: Northern Wedge Failure

5.1 Introduction

The Northern Wedge Failure (NWF) exists within the north western corner of Pit 1 within Whitehall Quarry, as shown on Map Sheet 1. Failure of the wedge was initiated during November of 1988 following a very wet period which occurred after a major overburden stripping programme in April-June 1988. The estimated volume of this wedge is in the order of 250,000 to 440,000 m^3 (Hancock Consultants Ltd, 1989). The wedge has not completely failed to date, however it is believed by Winstone Aggregates that the wedge mass has ceased sliding and thus regarded as relatively stable.

The stability of the wedge is paramount to the safety of employees, equipment, and quarry production. Should the wedge catastrophically fail the high grade rock below the failure will become contaminated with much lower grade rock. Cleaning up the wedge failure run-out will be time consuming thus significantly reducing productivity for the quarry. The failure will also cause ravelling of the over-steepened slope, and the failure could extend back into the slope thus affecting neighbouring properties. Failure of this wedge is anticipated as an economic disaster for Whitehall Quarry.

This chapter aims at identifying failure mechanisms, current stability, and potential mitigation measures for increasing wedge stability if necessary. The investigation will entail engineering geological mapping of structural and instability features while a laboratory investigation will evaluate the behaviour the materials affecting sliding of the wedge mass.

5.2 Previous Assessment

The NWF has been assessed for stability by two separate consultants. Hancock Consultants Ltd carried out an engineering geological assessment of the wedge failure, independent consultant Mr John Ashby then undertook failure date estimates and assessment of wire line monitoring. This work was completed in 1989 and 1991. This section outlines the findings of both Hancock Consultants Ltd and John Ashby particularly the failure geometry, initiation and rates of recorded movement.

5.2.1 Failure Geometry and Initiation

Hancock Consultants Ltd (1989) describe the failure as diamond shaped and approximately 230 m from the toe to the apex of the headscarp and 140 m across at the widest point. The height difference between the toe and head region is approximately 130 m. The lower two thirds of the failure is a very well defined wedge shape whilst the boundary of the upper third is less distinct and arcuate in shape (Figure 5-1).

The wedge geometry is defined by the following planes (Hancock Consultants Ltd, 1989):

- Fault 1 on the eastern limb orientated at 40^{o}-55^{o}/205-225 (dip/dip direction).
- Joint 1 on the western limb orientated at 30^{o}-45^{o}/100-120.

Within these bounding planes the failure mass can be subdivided into semi distinct zones defined by a parallel set of faults and joint sets (Figure 5-1). The north-eastern side of the failure is distinctively wedge shaped at the bottom and becomes less well defined in the middle and upper sections. The middle section is characterised by numerous tension cracks, scarps and graben features defining secondary debris flow failures within the failure mass. Most of these features appear to be structurally controlled.

Hancock Consultants Ltd (1989) describe the failure as being controlled almost entirely by rock discontinuities. With the lower section of the slide is a simple wedge and the head region of the southern secondary wedge is almost certainly one or several joints giving a simple wedge/tension crack geometry on the southern side of the failure (Figure 5-1).

The main area of uncertainty is the position of the basal failure surface in the upper section of the slide. It is most likely that the surface approximates a circular failure plane through highly weathered greywacke in this area. Based on the geometric limits given above, the volume of the slide is inferred to be some 350,000 m^3 but could be as low as 250,000 m^3 and as high as 440,000 m^3 (Hancock Consultants Ltd, 1989).

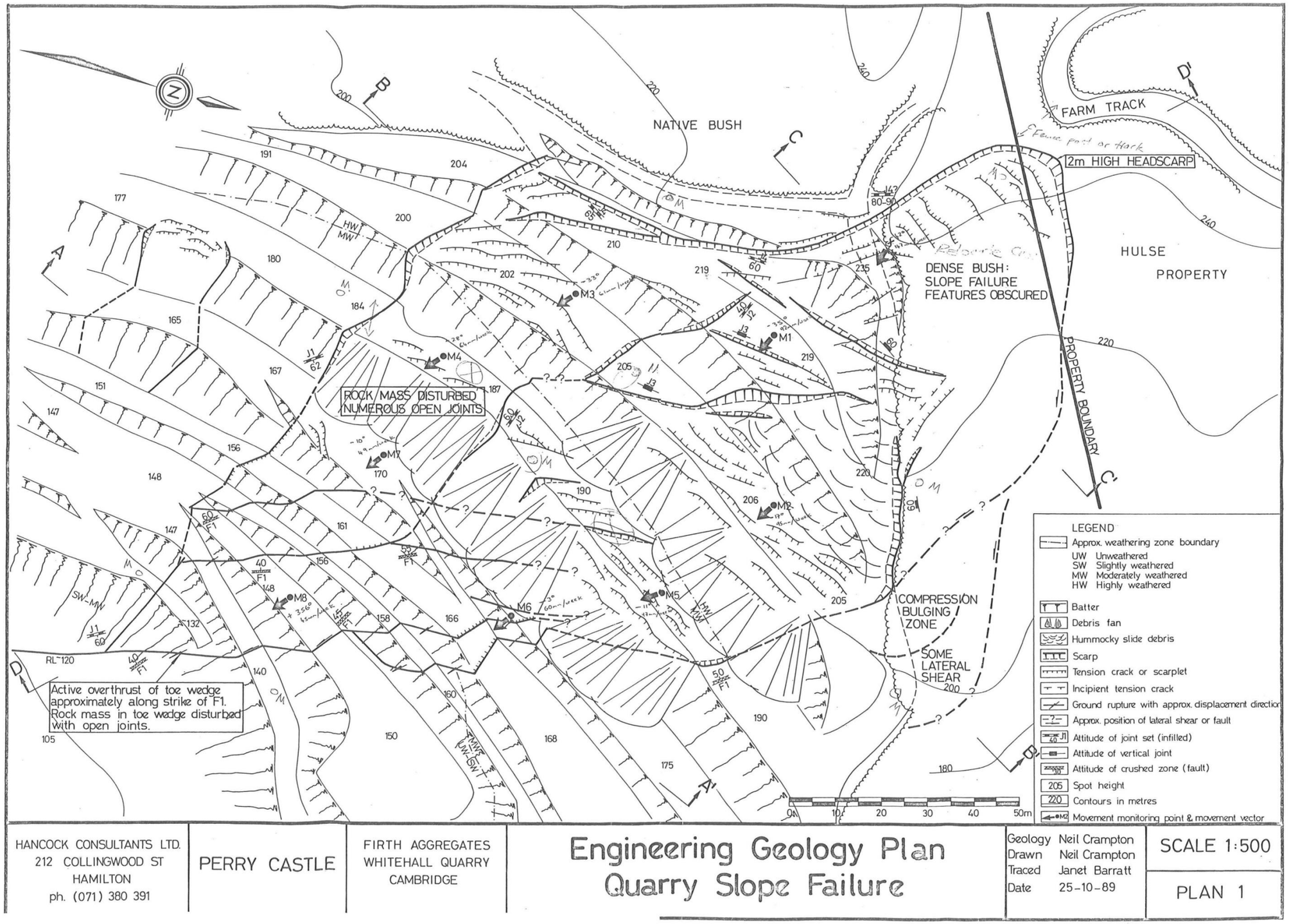

Figure 5-1: Engineering Geology Plan of the Northern Wedge Failure (Hancock Consultants Ltd, 1989).

Hancock Consultants Ltd (1989) describe the following factors as contributing to the general instability of the NWF:

1. The presence of unfavourably orientated structural discontinuities in the rock mass.
2. The face orientation and overall slope angle.
3. Groundwater conditions.
4. Removal of toe support by previous rock extraction in 1988.

As stated earlier, the major failure was initiated some time after the stripping programme carried out in April-June 1988. The initiation coincided with the end of a very wet period in approximately July-September 1988. The major factors contributing to the triggering of the major slope failure are considered by Hancock Consultants Ltd to be:

1. Quarrying operations exposing the daylighting toe of the wedge and removing support.
2. The stripping programme altering the critical load balance on the slope, changing the face orientation in relation to the structural defects and changing the overall slope angle.
3. The very wet period which occurred immediately following the stripping programme which would have increased pore pressures and increased slope loading by ground saturation.

Hancock Consultants Ltd were unable to quantify the relative contribution of each of the above factors to the failure initiation.

5.2.2 Electronic Survey Monitoring - Hancock Consultants Ltd

Hancock Consultants Ltd set up a monitoring programme during the winter of 1989 based on the displacement of eight ground movement points over a period of 2 months. These points were monitored biweekly from the date of installation.

Relatively constant movement occurred over the short monitoring period, with horizontal movement in the order of 45 to 100 mm per week (2.3 to 5.6 m per year) (Figure 5-2). Most movement occurred in the middle and upper sections of the failure on the northern side. According to Hancock Consultants Ltd higher movement rates on the northern

side probably relate to the quasi-circular failure mechanism and shallow soil failures causing maximum surface disturbance (Hancock Consultants Ltd, 1989).

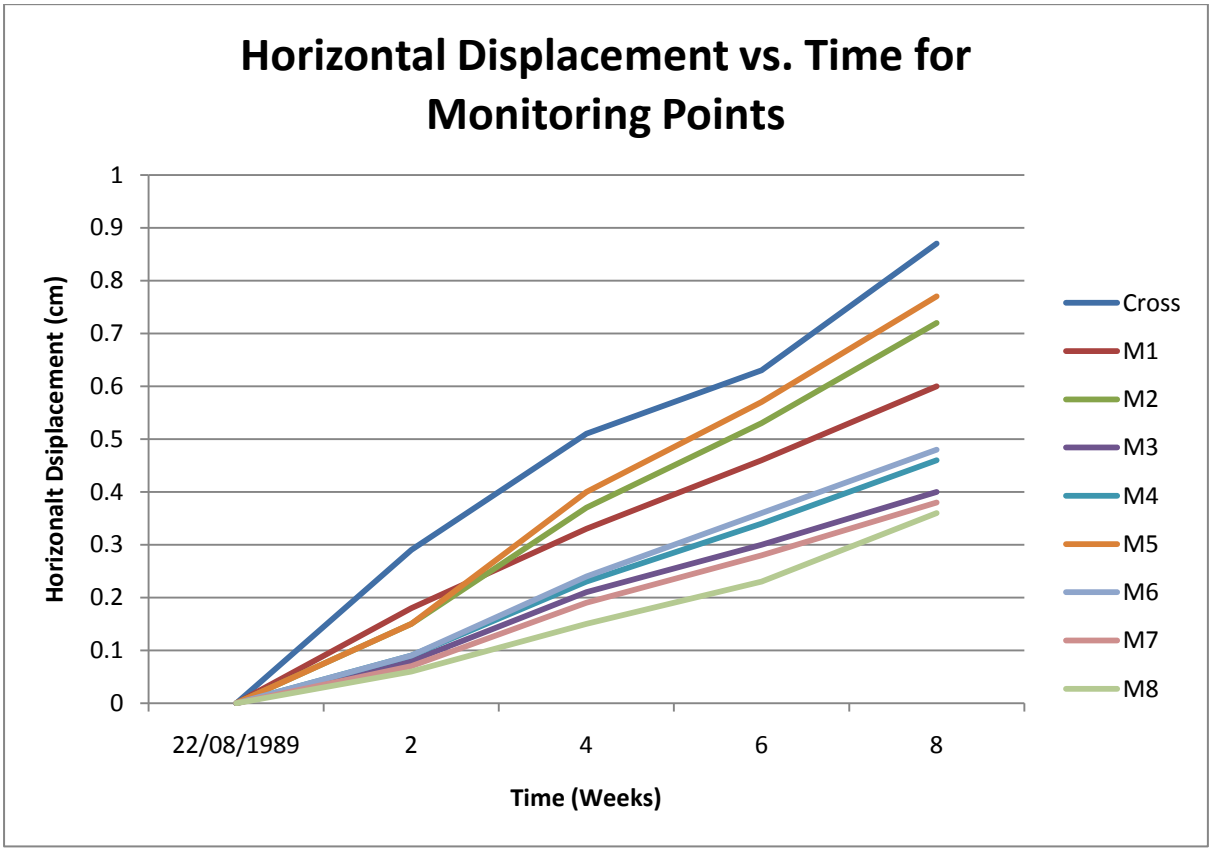

Figure 5-2: Horizontal displacement versus time graph for monitoring points on wedge mass (Hancock Consultants Ltd, 1989).

Less movement is occurring in the toe and southern sections where the material is more competent and movement occurs as a well defined wedge with little or no intrablock secondary failures (Hancock Consultants Ltd, 1989).

5.2.3 Wireline Monitoring - Ashby

To provide direct measurement of the failure and to maintain continuous surveillance while operating beneath the failure, quarry staff, under the guidance of Mr John Ashby, installed a wire gauge from a bench in the middle of the mass anchored behind the backscarp.

Once the wire was installed, daily reading was possible. Daily recordings provided surprising results, rather than a pattern of relatively continuous displacement with time over the winter months as suggested by Hancock Consultants Ltd's electronic survey monitoring, the displacement rate versus time graph of daily measurements of the wire show a series of spikes above the baseline of 2 to 5 mm per day (Figure 5-3).

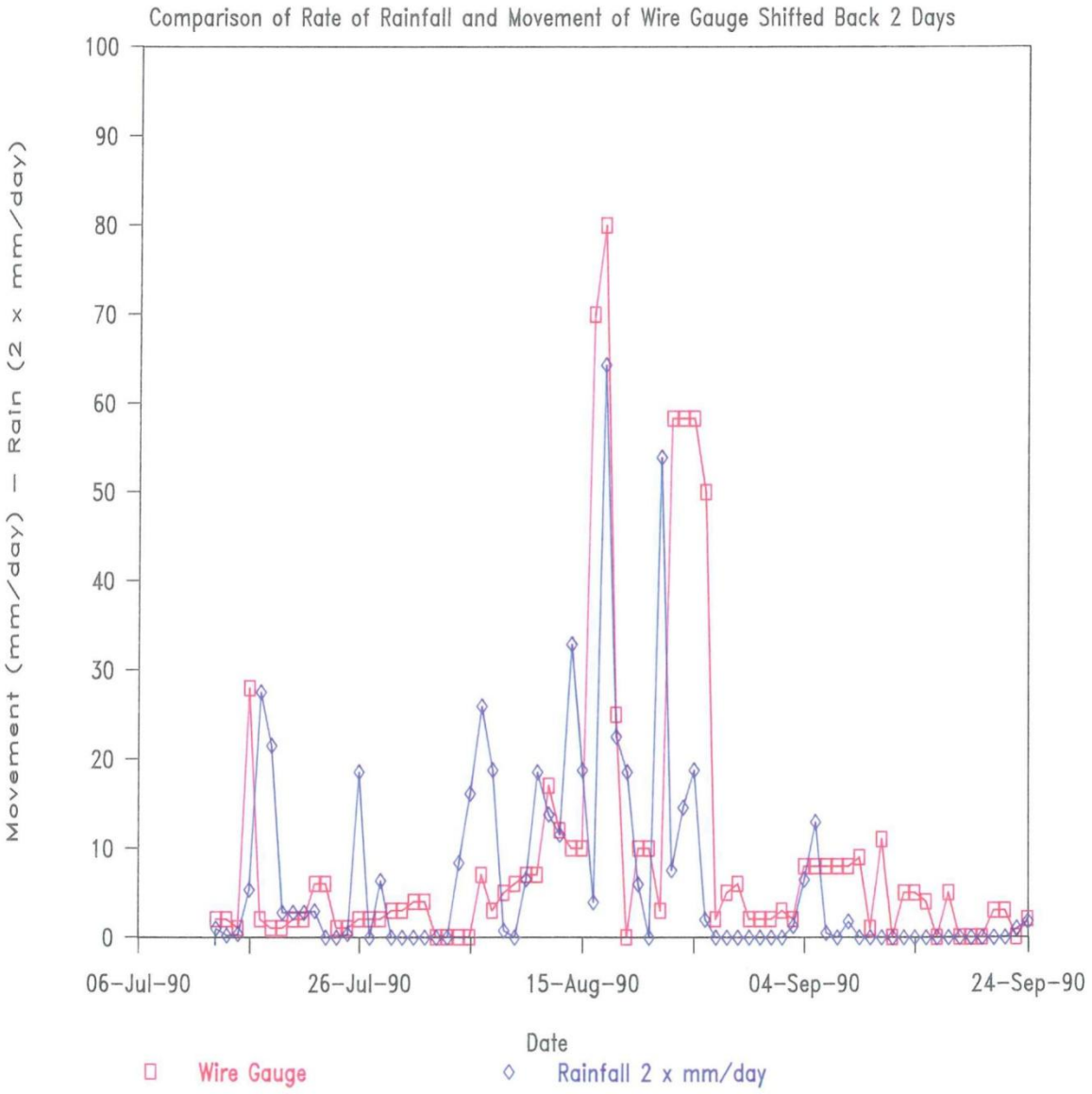

Figure 5-3: Comparison of rate of rainfall and movement of wire gauge shifted back two days (Ashby, 1991).

The spikes appear to occur in response to heavy rainfall (Figure 5-3). The severity of the movement spikes, some greater than 50 mm per day, albeit in response to heavy storm events during August 1990, is major cause for concern (Ashby, 1991). During winter the movement spikes appear to occur about two days after the rain, giving adequate time to respond to monitoring of the wire and pull out of the quarry (Ashby, 1991).

5.2.4 Future of the Failure

The future of the Northern Wedge Failure (NWF) was predicted by Mr John Ashby through failure strain comparison with other well documented wedge failures. Ashby stated, by comparing monitoring results from Whitehall with those of other failures (Appendix F1),

it was apparent that the NWF was entering a critical stage. Ashby (1991) calculates strain as the percentage of displacement over the total length of the sliding surface. He considered other documented wedge failures and determined that failure typically occurs at a strain of approximately 5%. Assuming the estimated total displacement (9.017 m) and the overall length of the failure surface (183 m) are correct the approximate strain exhibited by the core of the NWF mass is 4.9% (Ashby, 1991). A number of other documented failures, including that at Molycorp's Questa Mine, have triggered at an estimated strain as low as 5%.

Ashby noted that already wire gauge monitoring readings in excess of 0.01 %/day (25 mm/day) have been sustained at Whitehall, rates typical of the accelerating phase prior to total failure.

Ashby identifies two features of the NWF that complicate prediction of the ultimate behaviour as:

1. An almost linear cumulative displacement history if the seasonal steps are ignored.
2. The severity of storm induced movement spikes, i.e. rapid acceleration to at least 0.03% strain per day followed by rapid decay.

Ashby states, assuming that the total displacement estimated for the core of the mass is realistic, 5% strain would have been reached by autumn 1991, and therefore acceleration leading to total dislocation could start as early as winter 1991 with failure being most likely in 1992.

5.2.5 Current Situation

The NWF has not failed to date. Winstone Aggregates Senior Engineering Geologist Mr Mike Harris believes that the NWF is currently stable where wedge bounding discontinuities are in a state of stick-slip (Harris, 2010). The stick-slip phenomena is described as a failure-resisting mechanism, where the acting shear force during sliding becomes less than the static shear strength of the discontinuity leading to equilibrium, thus the 'sticking' of discontinuities causing the reduction in sliding and even stopping (Zou, et al. 1989).

The following sections discuss the investigations carried out in this study to develop an engineering geological model and assess the current stability of the NWF.

5.3 Engineering Geological Model – This Study

5.3.1 Investigations

The engineering geological model of the Northern Wedge Failure (NWF) is based entirely on field and laboratory investigations undertaken in this study. A site walkover, photogrammetric analysis, and detailed engineering geological mapping and sampling were carried out in January 2010. The laboratory component was largely undertaken during 2010. However, some laboratory results obtained from investigations carried out by Hancock Consultants Ltd are included in this study to aim in accurately characterising the failure.

The engineering geological model must be as accurate as possible in order to provide the best possible analysis of the NWF instability. This section aims at identifying significant and relevant aspects of the model to be used in further NWF analysis and assessment. A map showing the extent of lithological units and associated cross-sections are presented in Map Sheets 10 and 11.

5.3.2 Wedge Geometry

Understanding the wedge geometry is significant in the assessment of wedge stability. Planes of failure identified in the wedge geometry govern the failure mechanism and the stability of the mass. At first glance (Figure 5-4), the wedge geometry appears to be a straight-forward diamond shaped wedge, characteristic of a typical wedge. Therefore the basic mechanics of sliding should be simply identified.

The wedge geometry of the Northern Wedge Failure (NWF) is complex. The bounding sliding planes are difficult to gain an overall orientation due to debris covering most of the sliding planes on either side, more so the northern side. The mean orientations for the sliding planes are both faults depicted below as dip/dip direction (Figure 5-5):

- Plane A: 60^{o}/035
- Plane B: 65^{o}/190

Figure 5-4: Aerial view of the Northern Wedge Failure (Google Earth, 2010).

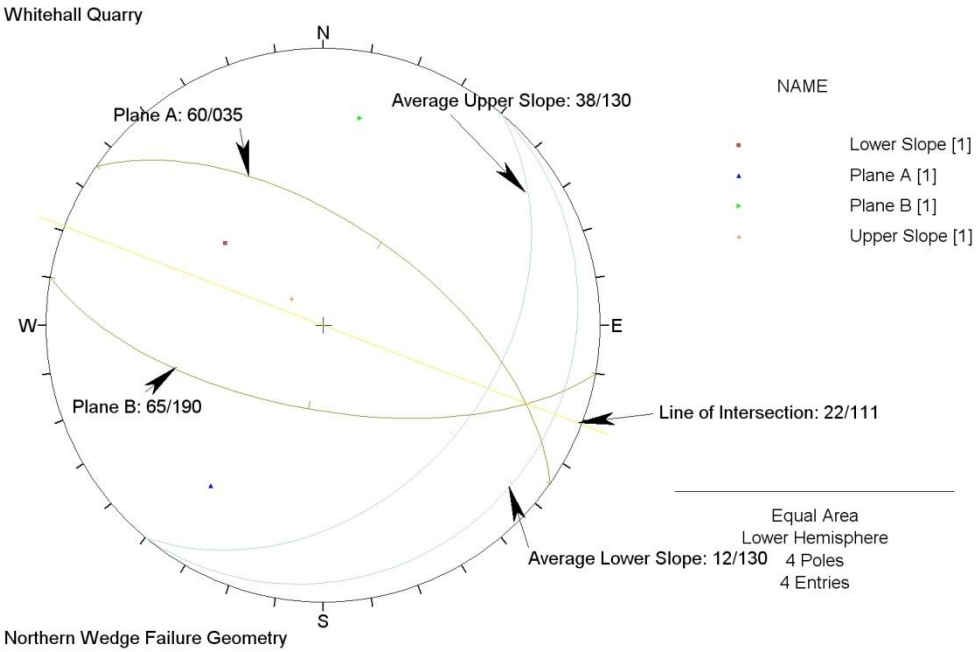

Figure 5-5: Stereographic representation of the Northern Wedge Failure geometry.

The wedge mass is subdivided into two semi-distinct sections (Map Sheet 10), the upper (at and above section line B) and lower (immediately below section line B). The lower section of the slide mass, approximately below the dense bush boundary (Map Sheet 10), is a simple wedge bound by two distinct planes, Planes A and B, with a line of intersection orientated at 23^{o}/111. The trend and plunge estimated from simplified wedge geometry indicates the most likely failure direction which is approximately 111 towards the east.

Lower Section (below section-line B)

The lower section (Figure 5-6, Map Sheet 10) exhibits large volumes of rockfall debris from upper bench failures and fault scarps. Debris cover on the north eastern side of the lower section restricts access to most benches as well as concealing the main sliding plane (Plane B). There appears to be little to no displacement at the toe of the wedge. This suggests that below the surface of the settlement pond at the base of the wedge the mass may exhibit overthrusting or compressional bulging. Within the midregion of the lower section tension cracks are dominant on the eastern side of the wedge. The tension cracks located within the top of the lower section closest to the north-eastern margin range from 0.5 to 2 m in depth and 0.1 to 0.9 m in width. These cracks indicate a tensional or pulling apart regime within the eastern flanks of the wedge mass. The cause of these cracks is likely to be attributed to the rock mass of the wedge rising above the lower opposing footwall thus significantly reducing the lateral stresses holding the mass together. These cracks appear to be consistent with J1 and J2 identified as the main joint sets of the Northern Domain.

Upper Section (above section-line B)

The upper section is more complex than the lower due to what appears to be quasi-circular mass movement to the east (Figure 5-6, Map Sheets 10 and 11). This trans-rotational displacement occurs within and including materials stratigraphically above the highly weathered greywacke sandstone. Cross-section A, presented in Map Sheet 11, shows an inferred circular failure plan within the weaker, highly to residually weathered sandstone and alluvial material. Evidence for the quasi-circular motion lies within the mass surface and scarps within the upper section. The western edge scarp exhibits 2 to 3 m of vertical displacement while the eastern edge exhibits a hummocky surface indicating subsurface thrusting via transrotational displacement to the immediate east. Therefore the failure style of the upper section differs from the lower, it is expected that the upper section is also moving at a more easterly direction than the lower.

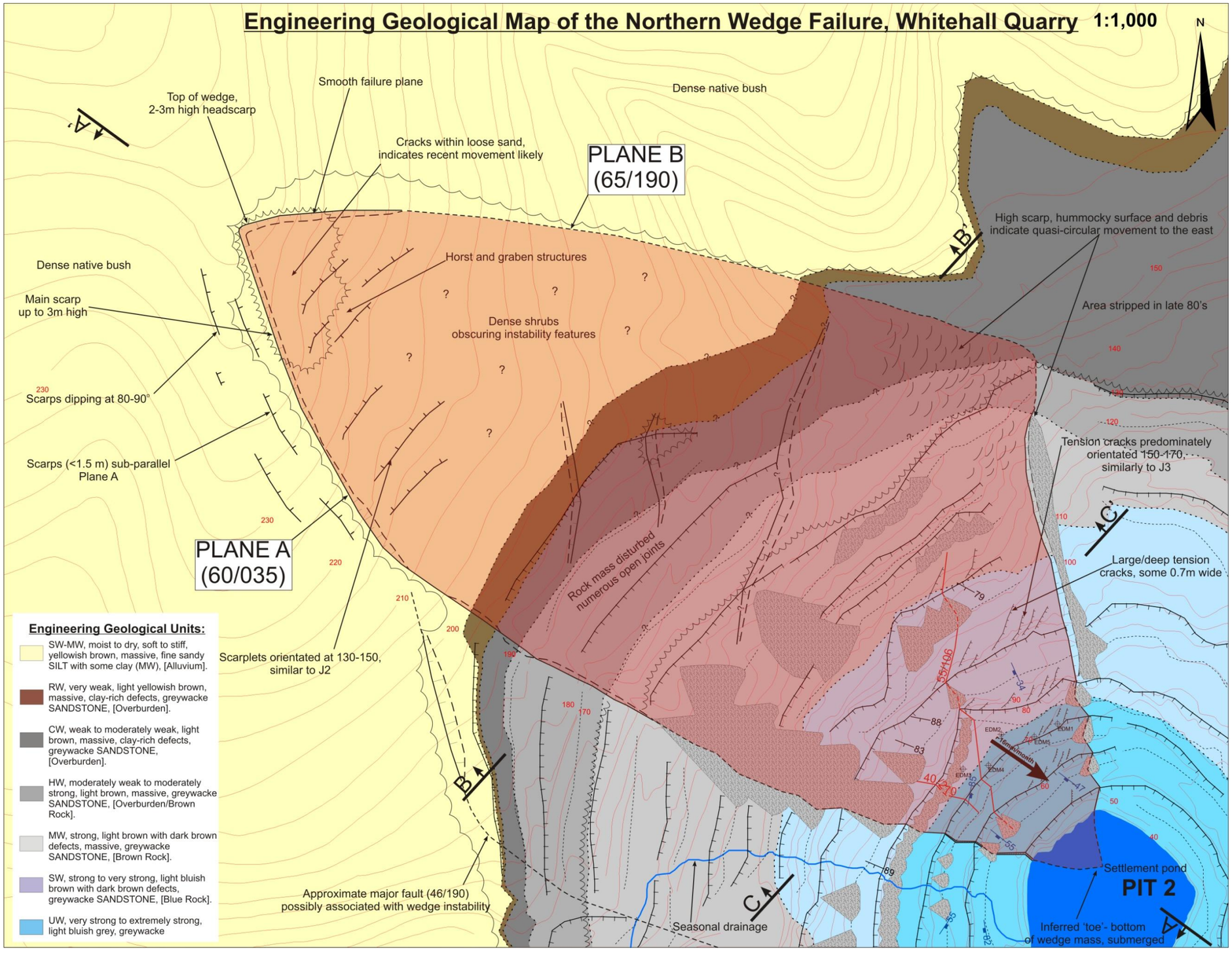

Figure 5-6: Simplified engineering geological map of the Northern Wedge Failure (adapted from Map Sheet 10).

5.3.3 Rock, Soil and Gouge Types

The main rock and soil types identified during the field investigation stage are the greywacke sandstone interbedded with argillaceous mudstone, and overlying alluvial sands and silts. The characterisation of these materials is important in assessing the stability of the NWF due to their affects on the wedge failure mechanism.

This section summarises the relevant parameters for the units identified. A detailed geological description and analysis is presented in Chapter 3.

a) Greywacke Sandstone

The greywacke sandstone is the economic resource excavated from Whitehall Quarry and naturally is the dominant lithological unit in the local area. However, quarry operators have divided this material into three sub-units dependent on weathering grade. These are overburden (highly to residually weathered), brown rock (moderately to highly weathered) and blue rock (slightly weathered to unweathered). All three units are exhibited within the NWF, (Figure 5-6, Map Sheet 10).

HW – RW Sandstone (Overburden)

Highly weathered (HW) to residually weathered (RW) greywacke sandstone, also known as overburden exists, within the upper section of the NWF, typically above elevation 150 to 180 m. The unit is generally characterised by yellowish brown clayey and silty sands with varying proportions (increasing with lower elevation) of greywacke sandstone angular gravel and by very weak, highly fractured, residually to highly weathered sandstone and siltstone. Within the highly weathered rock, core-stones of less weathered parent sandstone are common. A summary of significant material parameters is presented in Table 5-1.

Table 5-1: Summary of overburden material.

Description	*HW-RW, very weak to strong, light yellowish brown, massive, greywacke SANDSTONE.*
UCS	~30 MPa
Effective Angle of Internal Friction	$26^{o} \pm 5^{o}$
Dry Density (by ND)	1475 t/m^3
Wet Density (by ND)	1893 t/m^3
Average Water Content (by ND)	28.50%
Average Unit Thickness	20 ± 10 m

*ND = Nuclear Densometer method to 300 mm depth.

MW – HW Sandstone (Brown Rock)

Moderately weathered (MW) to highly weathered (HW) greywacke sandstone, also known as brown rock exists within the middle section of the NWF typically between elevation 110 to 180 m. Brown rock comprises dark to light brown, moderately to highly weathered, highly fractured, weak to moderately weak greywacke sandstone. The typical rock structure is characterised by closely spaced, heavily iron stained defects with alteration of the joint wall surfaces. Soft clay is present on major defect surfaces where complete weathering of quartz and feldspar has occurred. The rock material between defects is discoloured and there is loss in material strength (weak to strong compared to very strong for slightly weathered rock). Argillite bands are often not clearly recognisable in the core of the mass and appear to weather out within the brown rock. A summary of significant material parameters is presented in Table 5-2.

Table 5-2: Summary of brown rock.

Description	*MW-HW, strong to very strong, light and dark brown, massive, greywacke SANDSTONE.*
UCS	~55 MPa
Effective Angle of Internal Friction	$35^{o} \pm 5^{o}$
Dry Density (by ND)	1510 t/m^3
Wet Density (by ND)	1893 t/m^3
Average Water Content (by ND)	26.90%
Average Unit Thickness	60 ± 10 m

*ND = Nuclear Densometer method to 300 mm depth.

SW – UW Sandstone (Blue Rock)

Unweathered (UW) to slightly weathered (SW) greywacke sandstone, also known as blue rock, makes up the lower section of the wedge including the toe of the failure (Map Sheet 10). This unit occurs at maximum elevations of 110 to 140 m.

The blue rock comprises bluish grey, slightly weathered to unweathered, strong to extremely strong sandstone with localised bands of argillaceous mudstone. The rock mass is typically jointed (but less fractured than the overlying brown rock), with minor iron-rich limonite staining on some defect surfaces and unaltered joint surfaces. On the surfaces of major joint sets quartz and feldspar is evident. A summary of significant material parameters is presented in Table 5-3.

Table 5-3: Summary of blue rock.

Description	*UW-SW, very strong to extremely strong, light and dark bluish grey, massive, greywacke SANDSTONE.*
UCS	~150-230 MPa
Effective Angle of Internal Friction	$37^{o} \pm 5^{o}$
Dry Density (by ND)	1860 t/m^3
Wet Density (by ND)	2110 t/m^3
Average Water Content (by ND)	14.40%

*ND = Nuclear Densometer method to 300 mm depth.

b) Argillaceous Mudstone

Argillaceous mudstone is present within the NWF and has the quarrying term of argillite. Typical argillite comprises dark brown or dark blackish grey, varying weathering grade, extremely fractured, moderately strong to very weak argillaceous mudstone. The rock structure is characterised by thin beds (typically 5 to 25 mm thick) interbedded with greywacke sandstone. Bedding attitudes are typically $82^{o}/218$. Quartz and feldspar veins are evident, along with pyrite on some defect surfaces.

Table 5-4: Summary of argillaceous mudstone.

Description	Completely to unweathered, moderately weak to weak, dark brown to dark blackish grey, finely to coarsely layered, argillaceous MUDSTONE.
UCS	~37 MPa (Maximum)
Effective Angle of Internal Friction	$31^{o} \pm 5^{o}$

c) Alluvial Sandy Silts

The alluvial silty sand and sandy silts make up the cap overlying the greywacke sandstone bedrock at the top of the failure mass (Map Sheet 10). This material is only present on the upper reaches of the wedge including the head scarp. The alluvial material is typically 20 to 30 m thick.

Structural features, such as surface cracks, are distinguishable within the alluvium but are difficult to obtain orientation data from. This material is unlikely to affect the wedge failure mechanism and therefore properties were determined. The material is described as:

Slightly to moderately weathered, moist to dry, soft to stiff, light yellowish brown, massive, fine sandy SILT with some clay.

d) Gouge

The two major sliding planes identified as the bounding surfaces of the NWF (Map Sheet 10) are faults and exhibit fault gouge in varying thicknesses. The gouge identified in Plane A was analysed for clay mineralogy during this study while Plane B was analysed for angle of internal friction in studies carried out by Works Consultancy Services Ltd (1989). During this study fault gouge was not sampled from Plane B due to restricted access and limited fault exposure due to debris cover.

The fault gouge for both planes is reported as being typically 25 to 100 mm thick in places. Analysed clay mineralogy from fault gouge sampled from Plane A shows the presence of both kaolinite and montmorillonite. It is estimated that these clay minerals make up 20 to 25% of the fault gouge material.

In 1989, Works Consultancy Services Ltd carried out a series of ring shear tests on the fault gouge sampled from Plane B. The resulting angle of internal friction for the material was estimated at 13^{o} with an acceptable range estimated at 8 to 18 degrees. This result is appears typical for fault gouge with 20 to 25% clay mineral content. However, due to the presence of montmorillonite, it is possible for the angle of internal friction to be within the lower end of the acceptable range, and this must be considered in wedge stability analyses.

Due to the similarity of both Plane A and B, it is assumed to be acceptable to apply the same shear strength parameters for both i.e. angle of internal friction of 13^{o} for both sliding planes. Ultimately, sampling and shear strength determination of fault gouge collected from both sliding planes should have been done, but due to limited accessibility on Plane A was sampled.

5.3.4 Hydrogeology

The presence of groundwater is highly influential to the stability of any failure mass. Therefore it is imperative that the hydrogeological model is understood and the associated parameters applied appropriately to stability analyses. Groundwater is associated with increasing pore water pressure within planar and wedge failure masses. Increased pore pressures result in increased mass instability.

There is no piezometric data available for the NWF, therefore the mean groundwater table must be estimated from surface observations and interpretations. No springs or seepages were identified within the wedge mass therefore the main hydrological feature affecting the NWF is the settlement pond at the base of the wedge mass. The pond completely saturates the toe of the wedge (Figure 5-6, Map Sheet 10 and 11). This is interpreted as the ultimate base level for the groundwater table. Also to be considered is the fluctuation of the settlement pond level due to seasonal effects and quarrying operations. During the winter the pond is at its' highest at an RL of 44 m while in the summer the lowest at an RL of 42 m.

Seepage from joints or faults was not observed during field investigations. Therefore the groundwater table must be below the surface of the wedge upper and lower slopes. However, it is difficult to estimate the depth to the mean groundwater table with very little hydrogeological data. It must be assumed that the groundwater table loosely follows topography as shown within cross-sections presented in Map Sheet 11.

It is also assumed that the clay-rich fault gouge of both sliding planes will have an adverse affect of pore water pressure. It is likely that the less permeable fault gouge will impede groundwater flow through the rock mass. The inferred groundwater table is shown as exhibiting higher pore water pressures on the wedge side of both sliding planes. This is likely to decrease the stability of the wedge due to reducing the normal stress acting on the siding plane.

Atterberg Limits approximated for the fault gouge (Section 2.3.5), indicated a plastic limit of 31% and a liquid limit of 51%. This suggests that if the water content of the surrounding fault is reduced below the plastic limit of 31% the fault gouge will act as a semi-solid material, thus increasing the resisting force on the fault. If the water content increases above the liquid limit of 51%, the gouge will begin to flow thus reducing the resisting forces of the sliding plane.

However, due to the limiting hydrogeological data available for the NWF, Wyllie and Mah (2006) suggest that sensitivity analysis should be carried out on the mass to gain an understanding of the effect groundwater has on wedge stability. Sensitivity analyses are undertaken and presented in Section 5.5.

5.3.5 Electronic Distance Measurement

Electronic distance measurement, a mass movement monitoring technique, was implemented on the Northern Wedge Failure mass. This movement monitoring technique was utilised to indicate whether the failure mass with still moving and if so in what direction.

The initial understanding of the failure movement was that the mass had ceased failure due to the stick-slip joint phenomena (Harris, 2009). However, field investigations identified small cracks within the alluvial sandy silts at the head of the wedge mass (Figure 5-7), and these cracks were considered likely indicators for mass movement over a short period of time. The cracks, 10 to 20 mm wide, are within non-cohesive sandy silt which is highly likely to be washed over by heavy rainfall, therefore if the wedge mass has ceased movement, the small cracks in the sandy silt would have had to have been preserved for over 15 years of heavy seasonal rainfall which is unlikely.

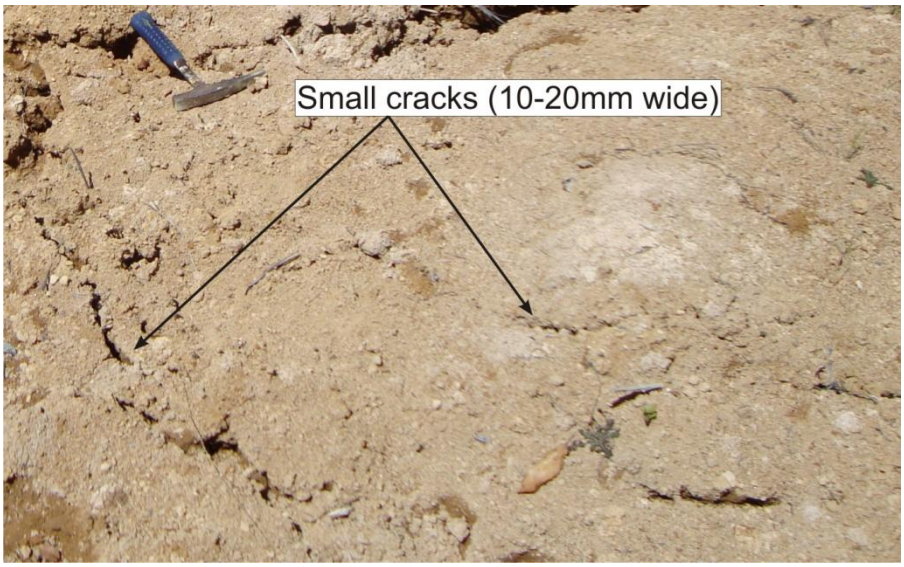

Figure 5-7: Small cracks identified within sandy silt material at the head of the wedge indicating recent movement.

Five monitoring pegs were installed on the only accessible bench within the wedge mass (Map Sheet 10). Over the period of January to November 2010 the pegs were surveyed a total of four times using the Trimble 5600 Total Station from the directly opposite side of the wedge. To ensure that the distances were true and not affected by errors relating to survey setup, a sixth peg was installed on the edge of the quarry where no movement associated with the wedge was to likely to occur. The survey coordinates for the 5 monitoring pegs were calibrated against the stationary peg to eliminate errors. The accuracy

of the Total Station over the survey distance was no greater than 10 mm in the x and y direction with a confidence of 97% (Trimble, 2010).

EDM surveys were carried out during the summer and winter of 2010. This enabled the analysis of seasonal rainfall versus rates of movement. Calculations, coordinates and comparison data are presented in Appendix F2, while summary data is presented in Table 5-5.

Table 5-5: Summary of NWF mass movement recorded via EDM.

Period	Average Daily Rainfall (mm/day)	Rate of Movement (mm/month)	Direction
11 January – 09 April	3.3	18.9	123
09 April – 01 September	4.5	20.8	124
01 September – 25 November	3.5	18.8	127

The average rate of movement recorded for the NWF during this study was 19.5 mm/month in the direction of 124 degrees from north over the total period of surveying. Table 5-5 presents summary data showing a distinct increase in the NWF mass velocity during the wetter months of the year (April to September), while in the drier months the wedge mass velocity reduces to below 19 mm/month. This supports Ashby's (1990) conclusion from wireline monitoring outlining that wedge rates of movement were influenced by seasonal rainfall. The cause of the 10% increase in velocity is likely to be attributed to water from rainfall percolating through the mass surface raising the groundwater table thus increasing pore water pressure reducing the total resisting forces.

The increase in velocity due to increased rainfall must be considered in any monitoring system implemented for the Northern Wedge Failure. It appears that the likely trigger for catastrophic failure of the wedge mass will be a prolonged period of heavy rainfall raising the groundwater table and lowering the failure resisting forces.

5.4 Stability Assessment

Assessing the stability of the Northern Wedge Failure (NWF) requires the application of the engineering geological model outlined in the preceding section. The materials that form the wedge, angles of internal friction for the sliding planes, and hydrogeological features, are the fundamental parameters required for estimating the stability of the NWF.

This section aims at assessing the stability of the NWF via the principle of factor of safety. It will also include the results and interpretation of electronic distance measurement (EDM) to determine whether the wedge is currently moving and at what velocity.

5.4.1 Kinematic Stability Analysis

Kinematic analysis is a very simplistic method for wedge analysis assuming that the wedge is defined by two simplistic sliding planes. It applies fundamental parameters defined by the engineering geological model. The kinematic wedge stability analysis for the NWF in this study is carried out using SWedge, a purpose designed wedge stability assessment programme developed by Rocscience Inc.

SWedge has the ability to carry out deterministic and probabilistic analysis. Deterministic analysis estimates a mean factor of safety for the wedge using the average parameter values. This type of analysis is simplistic but does not consider the variations in parameters. Probabilistic analysis analyses the stability resulting in a probability of failure. This method of analysis utilises the Monte Carlo sampling method to estimate the factor of safety and probability of failure from statistical input data entered to account for uncertainty in parameters (Rocscience Inc, 2002). This analysis will determine a mean factor of safety (deterministic) and an associated range of values (probabilistic).

The engineering geological parameters and the associated acceptable ranges of values outlined in Table 5-6 were entered into the SWedge model.

Table 5-6: Summary of parameter values entered into SWedge model for probabilistic analysis.

Parameter		Mean	Acceptable Range
Plane A Orientation	Dip Dip Direction	60° 35	55°-65° 030-040
Plane B Orientation	Dip Dip Direction	65° 190	60°-70° 185-195
Upper Slope Orientation	Dip Dip Direction	12° 130	7°-17° 125-135
Lower Slope Orientation	Dip Dip Direction	38° 130	33°-43° 125-135
Friction Angle (Plane A & B)**		13°	8°-18°

** defined via ring shear testing (Hancock Consultants Ltd, 1989).

SWedge does not allow the application of uncertainties for water pore pressure; therefore in this case the best estimate was approximated at 50%.

A three-dimensional model of the NWF is presented in Figure 5-8. The results obtained from the probabilistic analysis are presented in Table 5-7.

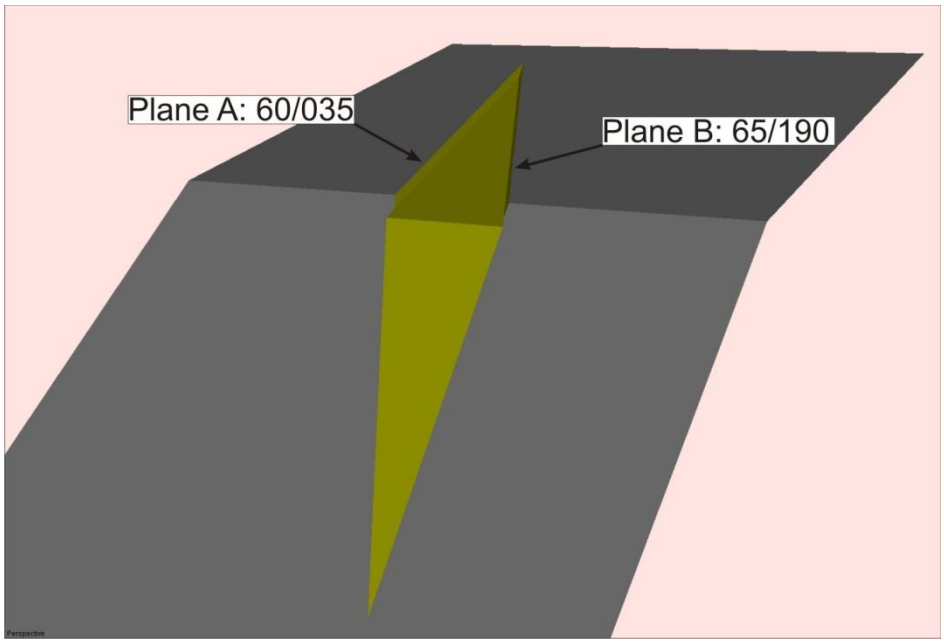

Figure 5-8: Perspective view of the 3D model generated by SWedge for the NWF.

Table 5-7: Summary of results from probabilistic analysis of the NWF.

Factor of Safety	0.97
Probability of Failure	59%

A list of SWedge analysis information is presented in Appendix F4. The mean wedge volume is approximately 520,000 m^3, while the corresponding mean factor of safety, 0.97, is estimated for the NWF is a realistic result. Factors below 1.0 are indicative of unstable wedge and planar masses where failure is likely. Masses that exhibit displacement, instability features and ongoing movement typically will have factors less than 1.0, as in this case. The factor of safety of 0.97 suggests that the mass is unstable and remedial or mitigation works are required to stabilise the mass, i.e. increase the factor of safety to above 1.0.

The probability of failure, 59%, is estimated via the Monte Carlo sampling methods using 100,000 random combinations of acceptable values. The value of 59% means that out of 100,000 randomly generated wedges with differing parameter values, but within the acceptable ranges, 59,000 of them had a factor of safety less than 1.0 indicating failure (Baecher & Christian, 2003). Therefore the NWF is highly likely to fail unless mitigated.

The probabilistic analysis produced a range of factor of safety values from the input acceptable range of values for each key parameter identified in the engineering geological model. The possible factor of safety range is between 0.0 and 1.6, with a mean factor of safety 0.97 (Appendix F3). This range of factor of safety values is vague, and more accurate data should reduce the range to values closer to the mean.

The main limitation of the SWedge kinematic analysis model is the inability to apply uncertainty to the pore water pressures exhibited within the failure mass. Although the probabilistic analysis undertaken here uses the best estimate for pore pressure it does not analyse the associated variability and uncertainty. However, as stated earlier, sensitivity analysis will be carried out to gain an understanding of the affect pore water pressure has on the stability of the slope.

Although a robust range of values for the NWF factor of safety has been produced from probabilistic analysis within this study, it must be noted that these values are only as good as the input engineering geological parameters. Due to significant uncertainty of the depth to the fundamental groundwater table the probabilistic analysis may have under or

over-estimated the probability of failure and the corresponding range of factor of safety values, however the mean factor of safety gained from this study should be used as a guideline for wedge instability. This model and method of analysis for the NWF is still applicable for analysis into possible remedial works, such as dewatering.

5.5 Sensitivity Analysis

Due to the inability for SWedge to carry out probabilistic analysis on pore water pressure variation and the significance it has on wedge instability, sensitivity analysis of pore water pressure is carried out in this section.

It appears that the Northern Wedge Failure (NWF) can experience both near-fully saturated and near dry hydrogeologic conditions, with an expected average fundamental groundwater table, depicted in Cross-Section A (Map Sheet 11), as 50% (SWedge terminology). Analysis has been carried out on the same model that was used in the probabilistic analysis, but with variations of pore water pressure between volumes of zero and 100% in 5% increments. The analysis compares the change in pore water pressure with the factor of safety thus the sensitivity of the slope to pore water pressure change. A plot showing factor of safety and versus pore water pressure is presented in Figure 5-9.

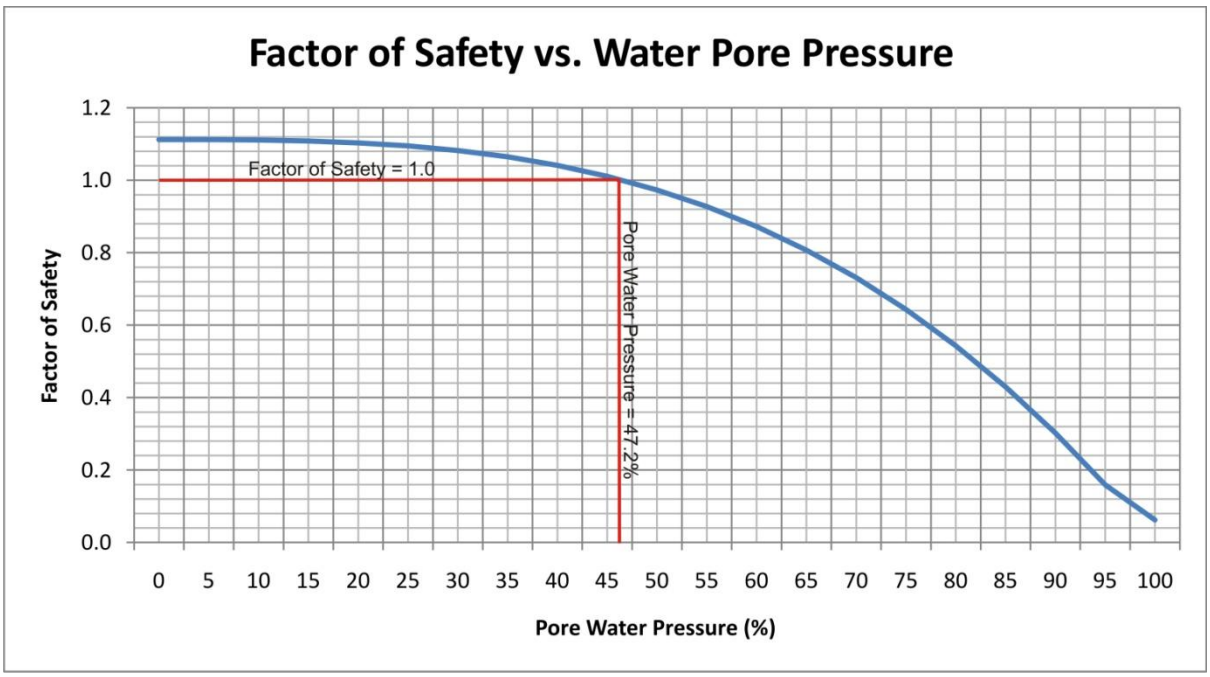

Figure 5-9: Sensitivity analysis of pore water pressure versus factor of safety.

Sensitivity analysis suggests the NWF is relatively sensitive to pore water pressure. As pore water pressure increases above 47% saturation of the wedge mass the corresponding

factor of safety begins to dramatically decrease below 1.0. This indicates that pore water pressure is a significant influence on the wedge stability, as indicated by increases in wedge mass velocities during wet periods. Although the sensitivity analysis indicates pore water pressures at which the wedge mass will be deemed stable, it does not indicate at what pore water pressure the wedge will begin to rapidly accelerate leading to ultimate failure.

For possible stabilising method is de-watering the wedge. Figure 5-9 shows that de-watering the wedge to below the estimated fundamental groundwater table the corresponding factor of safety is expected to increase above the 1.0 threshold.

5.6 Current Failure Model

Understanding the engineering geological model and the associated failure mechanism enables analysis of stability and long term performance of the Northern Wedge Failure (NWF). The NWF was extensively studied by two independent engineering geological consultancies, who devised a basic understanding of the engineering geological model, failure mechanism and predictions on future instability. Investigations carried out in this study support most of the findings from much earlier investigations.

The investigation into wedge instability and engineering geological features was difficult due to restricted access and dense bush cover around the perimeter and upper slopes of the wedge mass. Therefore some minor areas within the NWF mass were not investigated. An engineering geological map produced by Hancock Consultants Ltd (1989) is presented in Appendix F1, and shows the multiple instability features on the wedge mass, particularly the upper section. The relatively sparse features shown in the map produced during this study, Map Sheet 10, are due to the increase amount of bush and debris cover since 1989. Between the two investigation periods, late 1980's and early 2010, the wedge mass has left untouched therefore dense native bush began to regenerate. Between these two investigation periods there appears to be a greater amount of debris cover within the lower sections and edges of the wedge covering the fault planes. This caused much difficulty with sample and orientation data collection. The aim to collect gouge samples from both fault planes was abandoned when the northern plane (Plane B) was found to be buried beneath debris and inaccessible. Therefore data collected from laboratory testing on the southern plane (Plane A) was extrapolated to Plane B because it was assumed that the fault gouge material for both planes was likely to be similar.

The engineering geological model developed in this study characterises the rock and soil materials forming the wedge, wedge geometry and groundwater. The parameters outlined within the engineering geological model and the associated ranges of values were input to the SWedge failure model for probabilistic analysis.

The main issue for analysis via SWedge was the exclusion of uncertainties or a range of acceptable values for pore water pressure estimates. This is a concern due to the limiting data collected outlining the depth to groundwater within the wedge. To gain accurate groundwater information a piezometer should installed near the head of the scarp. Regular recordings will not only provide an insight into the hydrogeological model for the wedge mass but a greater understanding into the fluctuation between seasonally wet and dry periods.

The wedge geometry measured and identified during this investigation is similar to the geometry outlined by Hancock Consultants Ltd (1989), but with some subtle differences. Table 5-8 presents the geometries inferred by this study and the investigation carried out by Hancock Consultants Ltd in 1989.

Table 5-8: Summary of NWF geometry defined by the two different investigations (1989 Hancock Consultants Ltd, 2010 this study), orientations in dip/dip direction format.

	1989	2010
Plane A	50^{o}-60^{o}/045-060	55^{o}-65^{o}/030-040
Plane B	40^{o}-55^{o}/205-225	60^{o}-70^{o}/185-195
Mean Volume (m^3)	350,000	520,000

The two investigations appear to have similarities associated with Plane A, but orientation data presented for Plane B in this study falls outside the range values obtained from investigations carried out in 1989. The mean volume is very different for both investigations. The estimated wedge mass volume in this study is approximately 170,000 m^3 greater than the 1989 estimate. These differences are likely to have been generated from the following:

- Survey and orientation data collected by Hancock Consultants Ltd in 1989 is inaccurate.
- Survey and orientation data collected by the author in this investigation carried out in 2010 is inaccurate.

- Continual movement of the wedge has expanded the inferred size of the mass over the last 20 years.

It is difficult to determine whether the investigations carried out by Hancock Consultants Ltd are inaccurate, so it is more likely that displacement of the wedge over the last 20 years has exposed sliding planes surfaces where more accurate measurements can be obtained thus providing greater accuracy in the current model.

EDM surveying was aimed at estimating movement and failure direction of the wedge mass. The wedge mass velocity was determined to be 18 to 20 mm/month towards a bearing of 122 to 127. The direction of failure differs from the inferred failure direction of 111 computed using the wedge geometric limits. As stated earlier, this difference suggests that there is an error in the orientation measurements for the sliding planes or the strike of the northern sliding plane (Plane B) swings towards the east. The latter is more likely. As expected, the rate of displacement is much less than the 1989 and 1991 reported typical rates of 30 to 50 mm/week. However, to gain greater understanding of the current wedge mass velocity, EDM surveys should be carried out at regular intervals. The four intervals over 12 months in this study provide evidence of movement and a vague indication of the wedge velocity. Regular surveying is recommended.

The development of quasi-circular failure within weaker rock and soil of the upper section indicates greater complexity of the failure than initially anticipated. It appears as though there are two failure styles within the one failing mass, a quasi-circular failure in the upper section and pure wedge failure in the lower. This complexity was also identified by the two independent consultants during initial investigations. There also appears to be greater displacement on the northern sliding plane (Plane B) when compared with the southern sliding plane (Plane A). Plane B and the immediate inner edge of the failure exhibits large volumes of debris in the form of fans, and vertical uplift of the north eastern wedge mass edge. This is likely to be related to greater displacement or sliding along Plane B possibly suggesting the associated clay-rich fault gouge exhibits an angle of internal friction lower than the measured parameters of Plane A. If this is the case, the factor of safety estimated via SWedge is too high, therefore the wedge stability has been slightly over estimated.

5.6.1 Long-term Failure

Complete failure of the NWF is where the mass slides into the bottom of Pit 1, is likely due to evidence of current instability in the form of active displacement and a factor of safety marginally below 1.0. Complete failure is also likely to be retrogressive due to the closely spaced fracture spacing of the mass. This is where a rapid block failure near the base of the wedge mass occurs causing the remaining mass to readjust via another block failure (Cruden & Varnes, 1996).

Complete failure of the NWF is likely to be trigger by a period of heavy rainfall thus increasing the pore water pressure and decreasing the slide resisting forces. This trigger mechanism is most likely because of the responsiveness of the wedge to heavy rainfall as examined in this study and by Ashby (1991). However, as the mass continues to slide joints and surface fractures dilate increasing the free-drainage of the wedge mass. This may reduce the pore water pressure naturally causing the slide mass to increase stability and cease movement.

5.6.2 Failure Prevention by Drainage

Preventing complete failure of the NWF is possible by increasing the factor of safety above 1.0 thus ceasing wedge mass movement. This increase in the factor of safety can be done by installing two to five drainage holes into the mass from the base of the wedge. These drainage holes should be inclined at about 5 degrees in the upwards direction to allow for gravitational flow. The holes should also be drilled to an approximate length of 100 m to intersect the wedge sliding plane (Figure 5-10). The boreholes could either be left as is and open, or have a slotted PVC lining installed to maintain the integrity of the hole. Holes should be targeted at the inferred sliding plane and beyond to ensure the groundwater table is stepped back beyond the wedge sliding plane (Woodward, 2005).

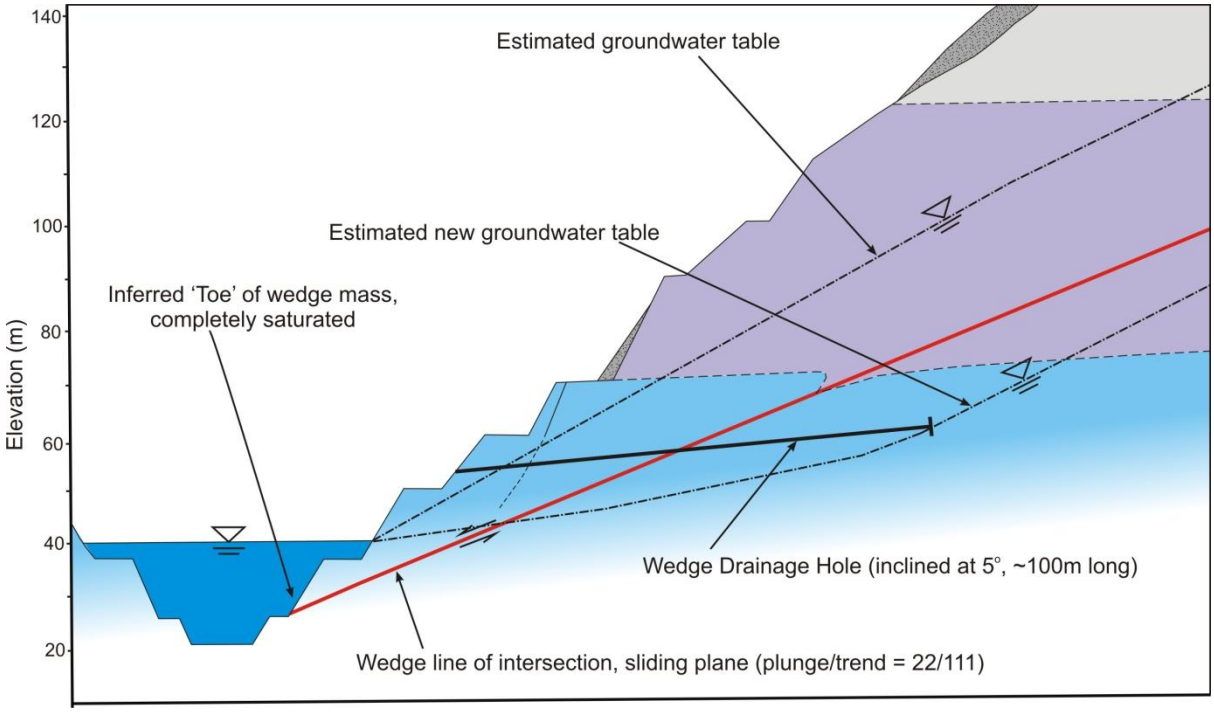

Figure 5-10: Cross-section showing inclination and length of wedge drainage holes.

Once the boreholes have been drilled, monitoring of flow rates should immediately follow. After the initial pore water pressure has been released via the drainage holes, monitoring of flow rates should continue on an initial weekly basis moving to monthly during the summer months. Flow rates should always be measured during and after periods of heavy rainfall to determine the delay in groundwater response to rainfall. In theory, the pore water pressure should be lowered by 10% resulting in an increase of the factor of safety by approximately 0.1 to 1.1. A factor of safety greater than 1.0 may allow quarrying operations to continue at depth below the toe of the wedge.

However, an increase in wedge stability by installing drainage holes is not guaranteed to be successful. Drilling the drainage holes may be difficult due to the closely spaced fracturing within the wedge mass.

5.6.3 Buttressing

The other possible stabilisation method for the NWF instability is the construction of an earth or rock fill buttress at the toe of the wedge. This method was extensively studied by Ashby (1991). The toe-buttress involves sidecasting overburden material from an upper bench down the slope of the wedge where it will gather to form a 10 m wide rockfill buttress. Ashby (1991) states that the problem with stabilisation by buttressing the failure is that the

inter-ramp slope angle of the wedge face is steeper than the anticipated angle of repose of granular fill, 37 degrees. Therefore, the sidecast material will fill up all lower benches before forming a buttress. To sidecast a 10 m wide buttress from an upper bench would require extending a haul road across the full face of the wedge and providing access and manoeuvring space for trucks. The required volume for the buttress is approximated at 200,000 m^3 of loose overburden material.

Ashby (1991) calculated an increase in the factor of safety of 0.08. This is a rather modest improvement given the large volume of material required. Another issue with the buttress method is the fact that it is final. Once the material is placed it will be near impossible to every continue quarrying in that pit again.

5.6.4 Mine and Monitor Option

Finally, there exists the mine and monitor option. This option is where the wedge failure mass remains untouched and quarrying continues with constant monitoring. This option is relatively inexpensive but requires constant analysis of data collected from piezometers, wireline gauges, rainfall gauges and crack-meters, all of which should be installed.

At least one piezometer should be installed at the head of the wedge. With regular recordings, this piezometer will provide the data missing from the engineering geological model outlined in this study. The location of the fundamental groundwater table and the associated fluctuation is vital information for the engineering geological model. This new data, combined with the data presented in this study, will allow future consultants and instability investigators to provide the best possible assessment of the wedge instability exhibited at Whitehall Quarry.

The installation of a basic wireline gauge trending at a bearing of approximately 124 as well as crack-meters will provide simplistic data indicating rates of movement a related ground deformation. Crack-meters, also termed crack gauges, should model the simplistic design implemented for the monitoring methods applied to the Clyde Power Project and the associated landslides. A simple measurement of the distance between two pins either side of an active tension crack at regular intervals will indicate movement. A simple wireline gauge installed with an alarm may be implemented to measure significant increases in wedge velocity typical of imminent catastrophic failure. This should give quarry operators adequate warning to initiate an evacuation of the pit.

5.7 Discussion and Synthesis

The study of the Northern Wedge Failure (NWF) presented in this thesis outline the previous investigations, the current engineering geological model, wedge stability, and future expectations. Findings from previous investigations carried out by Ashby (1991) and Hancock Consultants Ltd (1989) were compared to the parameters and associated findings identified within this study. There appears to be a difference in both the orientation of a sliding plane and the estimated wedge volume. As presented in Sections 5.2.1and 5.3.2 the variation in wedge geometry appears to be governed by the differences in the sliding plane orientation. However, the measurement of orientations in this study was carried out on several locations on each sliding plane, subject to accessibility. It is difficult to determine the accuracy of each different set of plane orientations, but measurements taken in this study were from sections of well defined sliding planes from which the mean orientation was estimated with a range of acceptable values.

Although there are slight differences in wedge geometry between separate wedge stability studies, there are similarities in the identification of the failure modes. All studies carried out on the NWF identified the well defined wedge within the lower section of the mass and in the upper a quasi-circular failure mode developed within weaker more weathered rock and soil.

The estimation of the angle of internal friction for the sliding planes is a crucial parameter in any large mass failure. The angle of internal friction was estimated as 13^{o} from ring shear testing on a fault gouge sampled from Plane A carried out by Hancock Consultants Ltd (1989). Fault was also identified by Hancock Consultants Ltd (1989) within Plane B but was not sampled or analysed for shear strength parameters. In 2010 Plane B in inaccessible where fault gouge exists due to unscalable slopes and debris cover. Therefore, the angle of internal friction of 13^{o} was estimated for both sliding planes. Although this friction angle returns an acceptable mean factor of safety more effort should have been made to sample fault gouge of Plane B.

The estimation of the fundamental groundwater table was approximated from observations from within the pit. There were no seepages identified within the upper of lower sections of the wedge, therefore the only control for the fundamental groundwater table was the settling pond just above the base of the wedge, encapsulating the toe of the slide.

The estimated groundwater table, shown in Map Sheet 11, is relatively similar to the approximation made by Hancock Consultants Ltd (1989). However, this is just an estimate, to gain more information regarding the depth to the groundwater table and the seasonal fluctuation; a piezometer should be installed near the head of the wedge failure.

The kinematic probabilistic analysis provided the best range of possible factors of safety values given the acceptable range of values for each parameter. The range of factors was 0.0 to 1.6 with a mean factor of safety of 0.97. This indicates that with the current estimated pore water pressure, the wedge geometrics and friction angles have enough uncertainty to indicate a critically low factor of safety as 0.0 and a stable wedge at 1.6. However, this range of values is likely to be affected by the variation and uncertainty in the pore water pressure. The input of recorded data from piezometric observations will enable a more accurately evaluated factor of safety.

The sensitivity analysis along with the EDM survey data showed that the wedge failure is highly responsive to periods of heavy rainfall. This theory is supported by Ashby (1991). The sensitivity of the wedge to increasing pore water pressure shows a distinctly sharp decrease in factor of safety after approximately 50%. This theory is supported by analysis of the Atterberg Limits; the fault gouge is anticipated to behave like a liquid at a water content of 51%, whereas it should behave as a semi-solid when the water content is less than 31%.

One factor that was not considered in this analysis was the affect the weight of the ponding water at the base of the slide had on the stabilisation of the wedge mass. The weight of the water at the wedge toe acts as a buttress and in theory should increase stability of the wedge mass. However, the ponding water also has an adverse effect of reducing stability by completely saturating the toe of the wedge thus increasing the pore water pressure to the maximum value. Analysis should be carried out on the pond to determine whether stability increases or decreases on de-watering the pit to a level below the wedge toe.

5.7.1 Recommendations

Recommendations for stabilising the Northern Wedge Failure at Whitehall Quarry will increase understanding of the failure mode and provide remedial works that increase the current wedge stability.

- Installation of a piezometer near the head of the wedge will give greater input data for modelling the failure and wedge failure prediction. This will identify the depth to the groundwater table and the associated pore water pressure. Regular recordings of the phreatic surface will also provide information on the seasonal fluctuation. A rain gauge should also be installed near the quarry office and regular recordings kept for correlation with piezometric and wedge movement data to provide further evidence to wedge failure triggered by heavy seasonal rainfall.
- The most effective method of wedge stabilisation is the de-watering of the mass. Lowering the pore water pressure below 50% will increase the factor of safety above 1.0. If the pore water pressure is lowered even further to less than 30%, the fault gouge is likely to begin acting as a semi-solid thus increasing the wedge stability dramatically. De-watering the wedge could be done by drilling at least two holes at the base of the wedge. These drainage holes should be drilled to at least 100 m in length to ensure the wedge sliding plane is intercepted. They should also be drilled at an inclination of 5 degrees to utilise the gravitational force drawing water from the slope.
- If the de-watering method is not implemented, the mine and monitor approach should be applied. This is where a series of instruments are installed to monitor the wedge stability. Instruments such as: wireline gauges, crack-meters and a rain gauge should be installed. A wireline gauge at the head and/or toe of the wedge should be installed with an electronic alarm which is rest regularly when movement rates are recorded. This should be setup to set off an alarm when the wedge begins to accelerate to movement rates of approximately 10 mm/day. This should give personnel within the quarry enough warning to evacuate. Crack-meters should be installed to monitor the dilation of tension cracks indicating movement in certain sections of the wedge mass. Finally, a rain gauge would provide adequate information relating to heavy periods of rainfall where it is anticipated the wedge rate of movement increases.

These recommendations are derived from observations and interpretations of the engineering geological model for the Northern Wedge Failure made in this study. They are not guaranteed to be successful. Greater research and input data, particularly relating to pore water pressure, is required to appropriately determine the ultimate stability of the wedge and the probability of failure in the near future. Finally, a risk assessment detailing the economic impacts of failure versus the implementation of the mine and monitor approach should be

undertaken. This will provide the best advice to quarry operators as to what the economics are surrounding the stability of the Northern Wedge Failure.

6.0 Summary and Conclusions

6.1 Project Objectives

Whitehall Quarry is located 4 km east of Karapiro, near Cambridge within the Waikato District. Current quarrying operations produce between 150,000 and 300,000 tonnes of aggregate for use as roading and construction material in the surrounding region. This thesis provides an engineering geological characterisation and pit slope stability assessment of the quarry, with recommendations for monitoring and future research.

The four principal objectives of this thesis were:

1. To determine and assess the structural domains within Whitehall Quarry, and calculate mean orientations for different structural features to kinematically predict failure types.
2. To carry out geotechnical testing to determine relevant geotechnical parameters for the Whitehall Quarry, including strength testing of rock and fault gouge samples to give quantitative data which could be used for stability analyses.
3. To analyse the complex wedge failure within the northern wall of Pit 1, and to provide geotechnical data input to assist in the design of possible remedial measures.
4. To provide recommendations for further quarrying practices and remedial work to assist with operation of the Whitehall Quarry.

6.2 Engineering Geological Investigations

6.2.1 Quarry Overview

The geological units identified within the quarry are greywacke sandstone interbedded with argillaceous mudstone. The local weathering profile follows topography where units are typically less weathered as depth increases. Three distinct classifications of material for quarrying are given to the variously weathered sandstone, they are:

- Highly (HW) to residually (RW) weathered sandstone (Overburden).
- Moderately (MW) to highly (HW) weathered sandstone (Brown Rock).
- Unweathered (UW) to slightly (SW) weathered sandstone (Blue Rock).

Overburden and mudstone are waste materials in quarrying operations; brown rock is used as a construction material while blue rock is the highest grade material used in roading and construction.

6.2.2 Structural Domains

Structural domains at Whitehall Quarry were assessed as part of this project from structural data collected via photogrammetric and conventional scanline analytical methods. A visual approach to stereographic structural domain interpretation was used in this thesis based on the interpretation of both stereoplots and histograms. Whitehall Quarry is divided into two separate domains by the Main Quarry Shear Zone (MQSZ), these being referred to as the Northern Domain (immediately north of the MQSZ) and the Southern Domain (immediately south of the MQSZ). Each different domain consists of similarly oriented bedding and joint discontinuities. Orientations are presented in dip/dip direction format.

Table 6-1: Discontinuity orientation data for the Northern Domain.

Northern Domain	Orientation
Bedding	82°/218
J1	57°/107
J2	40°/139
J3	35°/173

Table 6-2: Discontinuity orientation data for the Southern Domain.

Southern Domain	Orientation
Bedding	57°/211
J1	61°/008
J2	65°/333
J3	45°/279
J4	82°/084

6.2.3 Materials Testing

a) Intact Rock Properties

Greywacke Sandstone

Schmidt hammer and point load tests were carried out on various samples of sandstone with differing weathering grade. The results of these tests are summarised in Table 6-3.

Table 6-3: Summary table of intact rock strength for greywacke sandstone.

Unit	Schmidt Hammer		Point Load (MPa)	
	Average Rebound No.	UCS (MPa)	Index Value	UCS
HW-RW Sandstone (overburden)	15	30	-	-
MW-HW Sandstone (brown rock)	29	55	-	-
UW-SW Sandstone (blue rock)	54 - 62	150 - 230	7.3 - 10.5	175 - 252

Argillaceous Mudstone

UCS, estimated from Schmidt hammer testing, for argillaceous mudstone (argillite) was approximated at 37 MPa from a rebound number of 24. This approximation is likely to be a top end estimate due to testing difficulties.

Point load testing carried out on SW mudstone gave point load index value of 0.2 ± 0.05 MPa (correlated UCS of 4.8 ± 1.7 MPa).

b) Discontinuity Properties

Shear box testing was carried out on five times on a sandstone joint and four times on a mudstone bedding plane to evaluate the shear strength of these defect types. Samples selected for shear box testing were as representative as possible.

Sandstone Joint

Residual shear strength testing concluded that a smooth (JRC equals approximately 3) SW sandstone joint has an angle of internal friction of 34^{o}. On application of Patton's Law for effective shear strength of discontinuities, the effective angle of internal friction is 37^{o} for a typical joint within UW-SW sandstone (blue rock). Assumptions inferred the effective angle of internal friction for MW-HW sandstone (brown rock) is 35^{o}, and HW-RW sandstone

(overburden) is 26^{o}. However, it is also assumed that these approximations carry an uncertainty of 5^{o} to allow for variable pore water pressure and possible presence of clay infilling on joint surfaces.

Mudstone Bedding Plane

Residual shear strength testing found that bedding planes within SW mudstone has an angle of internal friction of approximately 31^{o}. On application of Patton's Law for effective shear strength, the effective angle of internal friction becomes 34^{o}.

c) Fault Gouge Properties

Whole sample x-ray diffraction (XRD) analysis of a sample collected from the Main Quarry Shear Zone identified quartz, albite, montmorillonite and kaolinite. XRD analysis on a sample collected from a sliding plane (Plane A) of the Northern Wedge Failure identified quartz, calcite, albite and montmorillonite.

The determination of Atterberg Limits was carried out on a fault gouge sample collected from the sliding plane of the Northern Wedge Failure, and gave a plastic limit of 31, a liquid limit of 51, and a resultant plasticity index of 20. The plasticity index value of 20 indicates the presence of 20 to 25% clay content within the sampled fault gouge.

6.2.4 Kinematic Stability

Kinematic pit slope stability analysis using the Markland test identified 35 potential failures (factor of safety less than 1.0) within Whitehall Quarry. Wedges failures are the most common potential failure mode comprising 85% of all potential failures identified. These failures occur predominantly at the batter scale but in some instances are predicted to occur at the larger inter-ramp scale. The typical plunge of the line of intersection, or dip of the sliding surface, is 25 to 35 degrees. The typical size of these wedge failures is anticipated to range between 2 and 10 m^{3}. Due to the likely small size of these wedge failures it is advisable to retain the current pit slope design and continue clearing catch-benches.

Potential planar failures were also identified during this analysis. Although not as prevalent as wedge failures they potential exist with greater instability especially within slopes dipping towards the south. These south dipping slopes are susceptible to bedding shear development forming potentially large planar failures. However, due to the high

fracture frequency exhibited by the quarry failures common planar failures are anticipated to be no larger than 5 m^3.

Potential failures identified within this analysis are generally no larger than 10 m^3, and are likely to ravel from the slope rather than fail as large masses. However, the existent of the Northern Wedge Failure, with an estimated volume between 300,000 and 500,000 m^3, larger failure such as this are possible within Whitehall Quarry.

6.3 Northern Wedge Failure

The Northern Wedge Failure (NWF) exists within the north-western corner of Pit 1 of Whitehall Quarry and is the largest failure mass identified within the quarry at between 300,000 and 500,000 m^3.

6.3.1 Engineering Geological Model

The Northern Wedge Failure is a complex failure consisting of a pure wedge failure mode in the lower half and a quasi-circular failure mode in the upper half of the wedge mass. Field investigations carried out on the Northern Wedge Failure identified the following planes as the primary sliding surfaces of the wedge.

- Plane A: 60^o/035
- Plane B: 65^o/190
- Line of intersection: 22^o/124

Fault gouge exists on the surface of these fault planes with varying thickness (50 to 120 mm). The fault gouge material is one of the key parameters in assessing the stability of the wedge and has been tested for shear strength.

The hydrogeology of the NWF was determined from field observations and interpretations. There were no seepages identified from the face in either the drier months of summer or wetter months in winter. Map Sheet 11 shows the inferred mean groundwater table within the NWF.

6.3.2 Geotechnical Investigations

Ring shear testing on a fault gouge sample collected from a sliding plane (Plane A) of the Northern Wedge Failure returned a residual angle of internal friction of 13^{o}. This test was carried out by Works Consultancy Services in 1989.

Other results obtained from tests, such as Atterberg Limit determination and XRD analysis are summarised in Section 6.2.3.

6.3.3 Stability Analysis

Electronic distance measurement (EDM) surveying of wedge mass velocities from the core of the wedge identified a mean velocity of 19.85 mm/month towards the bearing of 124. Summer months recorded slightly lower velocities (18.85 mm/month) while wetter winter months recorded higher velocities (20.8 mm/month). The velocities recorded from movement of the wedge show an increase of 2 mm/month (less than 10% variation) over the wetter months of the year. It appears that the wedge is responding to periods of seasonal heavy rainfall. This partially supports the wedge responsiveness to heavy rainfall theory postulated by Ashby (1991). Ashby recorded wedge velocities as high as 45 mm/week during the winter of 1990, while velocities in the winter of 2010 are only 5 mm/week. The wedge mass has significantly slowed over the past 20 years.

Probabilistic kinematic stability analysis was carried out using SWedge and the input data outlined in the engineering geological model of the wedge mass. A mean factor of safety for the Northern Wedge Failure was estimated at 0.97 with a range of 0.0 to 1.6. The mean factor of safety is consistent with current recorded velocities from the core of the wedge mass. This analysis was carried out using an estimated pore water pressure of 50% and an angle of internal friction of 13^{o}. It is anticipated that the factor of safety for the wedge could be approximated more accurately if the depth to the fundamental groundwater table was measured. However, this is the best estimate for the parameters provided.

6.3.4 Future Movement

The future movement or displacement of the NWF is difficult to predict. However, the investigations carried out in this thesis indicate that the wedge is marginally unstable and continues sliding at approximately 19 mm/month. Although this rate of movement is much

lower than the 45 mm/week recorded by Ashby in the winter of 1991, complete failure in the future is still possible.

Complete failure where the wedge mass slides in to the bottom of Pit 1 is likely to be retrogressive due to the closely spaced fracture spacing of the mass. This is where a rapid block failure near the base of the wedge mass occurs causing the remaining mass to readjust via another block failure (Cruden & Varnes, 1996). Complete failure of the NWF is likely to be trigger by a period of heavy rainfall thus increasing the pore water pressure and decreasing the slide resisting forces. This trigger mechanism is most likely because of the responsiveness of the wedge to heavy rainfall as examined in this study and by Ashby (1991). However, as the mass continues to slide joints and surface fractures dilate increasing the free-drainage of the wedge mass. This may reduce the pore water pressure naturally causing the slide mass to increase stability and cease movement.

6.4 Long-Term Quarry Management

Assessment of pit slope stability within the quarry determined that the potential failures are likely to be no larger than 10 m^3. These failures are relatively small and should be contained within catch-benches, where the failed mass falls out of the face and is caught on the lower bench rather than falling to the pit floor. Long-term quarry management should focus on the Northern Wedge Failure.

6.4.1 Recommendations for Wedge Monitoring

Monitoring of the Northern Wedge Failure should be undertaken before any stabilisation methods are implemented for a period of 2 years. In doing so this will allow greater understanding of the wedge movement and identify whether the mass is progressively decreasing or increasing in velocity.

The following monitoring systems should be implemented:

- At least one wireline gauge should be installed. A wireline gauge is where the movement of the wedge is recorded via the change in length of a wireline, one end of the wire is anchored to the wedge while the other is suspended from a pulley and free to move, thus indicating relative motion. This wire should be orientated at about 124 degrees from north.

- Regular inspections of the wedge should be conducted quarterly by a professional to identify any new instability features, such as tension crack widening, increased debris accumulation, etc.

6.4.2 Wedge Stabilisation Options

Methods to stabilise the wedge should only be implemented once the rate of movement for the NWF is fully understood. If the wedge velocities appear to be slowing it is advised that monitoring continue as well as a stability analysis to determine the current wedge stability. If wedge velocities appear to increase one of the following wedge stabilisation options should be applied.

- By wedge de-watering. This is where the pore water pressure within the wedge is significantly reduced to increase stability. This can be achieved by drilling at least two drainage holes at an inclination of 5^{o} targeting the wedge sliding plane in to the failure mass from the wedge toe. The length of these drainage holes should be approximately 100 m.
- By buttressing. This is where a buttress is constructed at the base of the wedge mass to apply an external resisting force to the wedge. This could be constructed by side-casting at least 200,000 m^3 of waste material from a higher bench down to the base of the wedge. Although this method is likely to increase the stability of the wedge mass, it is final and quarrying cannot continue in Pit 1.

6.5 Further Research

It is recommended that the following further work be carried out at Whitehall Quarry to gain more engineering geological and geotechnical data to increase the accuracy of pit slope stability and Northern Wedge Failure (NWF) stability analysis:

6.5.1 Fault Gouge Characteristics

Shear strength approximation via ring shear or direct shear testing of fault gouge sampled from the northern sliding plane (Plane B) of the NWF. The input of this data into the stability model for the Plane B angle of internal friction will increase the accuracy of the output estimation of wedge mass stability.

The identification of clay mineral content within fault gouge via 9φ analysis should be carried out on fault gouge samples for both NWF sliding planes. The identification of montmorillonite content should provide greater understanding to the possibility of shear strength fluctuation due to shrinking and swelling of the clay gouge.

6.5.2 Rainfall-Movement Response

More research needs to be carried out on the response of the wedge mass to periods of heavy rainfall. Similar research was carried out by Ashby in 1991 using a basic wireline and rain gauge. This simplistic instrumentation could be implemented again to give greater understanding of the increased wedge velocity relative to periods of heavy rainfall. The study should be carried out over a period of at least 18 months. In conjunction, a piezometer should be installed near the head of the wedge to provide information regarding the groundwater table location and fluctuation within the wedge mass. Finally, laboratory testing could also be carried out to determine the permeability of the materials making up the wedge mass.

This research could be carried out by a professional, or a student studying geology or geotechnical engineering at a tertiary institution.

Acknowledgements

I would like to gratefully acknowledge the assistance of the following organisations and people, given to me during this thesis:

My Senior Supervisor David Bell for timely thoughts and criticisms, reading draft copies of this thesis, and for passing on vast industry knowledge over the past 3 years. It has truly been a pleasure to learn from the master himself.

Winstone Aggregates, Mike Harris in particular, for providing this project. The project has kept me interested right the way through and provided me with vital skills applicable to the industry.

Funding was provided by scholarships from The Australasian Institute of Mining and Metallurgy (AusIMM), the University of Canterbury, and the Mason Trust Fund. Without this funding this experience could not have been possible.

Kevin Ha, Andrew Greenhill and the ADAM Technology team who provided me with the educational license for 3DM Analyst and 3DM CalibCam. This photogrammetric software is truly extraordinary, without it I would still be in the pit with chain and compass.

Staff at the Department of Geological Sciences, particularly Cathy Knight, Vanessa Tappenden, Sacha Baldwin-Cunningham, Stephen Brown, Rob Spiers, Anekant Wandres and John Southward, without your knowledge and willingness to help with my project would have taken so much longer.

Input from John Kennedy, Mark Eggers and Jocelyn Campbell has been invaluable and steered me in the right direction. I feel very grateful to have been able to tap into their industry and expert knowledge.

My family for their support. Mum and Dad, it is the work ethic and self motivation instilled in me from a young age that has enabled me to achieve my goals with a high standard. My sister, Kathryn, for putting her hand up when I needed a surveying assistant, thank you for putting up with me barking orders over the RT.

My friends and classmates over the past few years have made the university experience a blast. My flatmates Josh, Ken and Joe; you have always provided a good laugh, even if it was at my expense during fits of rage.

The Warlocks of Firetop Mountain. A social rugby team with whom I have been involved with since conception. A truly great bunch of loyal guys who always emphasize the social part of social rugby. Good luck for the future, hopefully the team can stand the test of time.

Finally, my best friend Alice. Your love and support has been the true driving force behind my success. Your ability to get me out of bed to do work and willingness to discuss engineering geological concepts, even though you don't understand what I'm talking about, has helped me complete this thesis and the final chapter of my university career.

References

Aydin, A. & Basu, A., 2005. The Schmidt hammer in rock material characterization. Engineering Geology, 81, pp.1-14.

Barton, N., 1974. A review of the shear strength of filled discontinuities in rock, Norwegian Geotechnical Institute.

Barton, N., 1973. Review of a new shear-strength criterion for rock joints. Engineering Geology, 7(4), pp.287-332.

Barton, N. & Choubey, V., 1977. The shear strength of rock joints in theory and practice. Rock Mechanics and Rock Engineering, 10, pp.1-54.

Bell, D.H. & Pettinga, J.R., 1983. Presentation of geologic data. Proceedings of the Symposium Engineering for Dams and Canals, IPENZ 9(4(G)), p.4.1-4.35.

Bell, F.G., 1987. Open excavation. In Bell, eds. London: Butterworths, p. 39/1-39/18.

Berkman, D.A., 2001. Field geologists' manual. , Monograph.

Bieniawski, Z., 1989. Engineering rock mass classifications: a complete manual for engineers and geologists in mining, civil and petroleum engineering, New York: Wiley.

Bieniawski, Z., 1975. The point-load test in geotechnical practice. Engineering Geology, 9(1), pp.1-11.

Black, P., 1996. Omahuta, Bay of Islands and Manaia Hill terranes: Waipapa composite terrane, North Island, New Zealand. Geological Society of New Zealand Miscellaneous Publications, 91A(29).

Broch, E. & Franklin, J., 1975. The point load strength test. International Journal of Rock Mechanics and Mining Sciences, 9, pp.669-697.

Brook, N., 1985. The equivalent core diameter method of size and shape correction, in point load testing. International Journal of Rock Mechanics and Mining Sciences, pp.61-70.

Chapple, A.P., 1998. An engineering geological investigation into pit slope stability at Macraes Gold Mine, Macraes Flat, Otago, New Zealand, Christchurch: University of Canterbury.

Collis, L., 1993. Aggregates: Sand, gravel and crushed rock aggregates for construction purposes.

Cripps, J.C., 1988. Rock mass discontinuities in theory, practice and reality. Quarterly Journal of Engineering Geology and Hydrogeology, 21, pp.101-105.

Davies, N.D., 1996. The effect weathering has on the strength of central North Island greywacke. , MSc.

Giani, G.P., 1988. Rock slope stability analysis, Brookfield: A.A Balkema Publishers.

Golder Associates, 2002. Technical Procedure: Soil Description and Classification TP3.

Grimm, R.E., 1968. Clay mineralogy 2nd ed., New York: McGraw-Hill.

Hanberg, W.C., Norrish, N.I. & Findley, D.P., 2006. Digital outcrop characterization for 3-D structural mapping and rock slope design along Interstate 90 near Snoqualmie Pass, Washington. In Breckenridge, Colorado.

Hancock Consultants Ltd, 1989. Engineering Geology assessment of a major slope failure at Firth Aggregates' Whitehall Quarry, Cambridge.

Hawkins, A.B. & McConnell, B.J., 1992. Sensitivity of sandstone strength and deformability to changes in moisture content. Quarterly Journal of Engineering Geology, 25(2), pp.115-130.

Healy, J., Schofield, C. & Thompson, B.N., 1964. Geological map of New Zealand: Sheet 5, Rotorua N. Z. G. Survey, ed. , p.Geological Map.

Heatherington, J.R., 1989. A quantitative study of the weathering of the Manaia Hill greywacke at Whitehall Quarry. , MSc.

Hoek, E. & Bray, J.W., 1981. Rock slope engineering revised., London: Institution of Mining and Metallurgy.

Hoek, E. & Diederichs, M., 1989. DIPS - A program for plotting, analysis and presentation of structural geology data using spherical projection techniques R. E. Group, ed., University of Toronto.

Hoek, E., Kaiser, P.K. & Bawden, W.F., 1997. Support of underground excavations in hard rock 1st ed., Balkema.

Hume, H.R., 1983. Geotechnical slope stability analysis, B & G sector, Bingham Canyon Open Pit, Utah, with a consequent investigation of methods for delineating rock mass fracture domains. , PhD, p.391.

Kamb, W.B., 1959. Ice petrofabric observations. Journal of Geophysical Research, 64(11), pp.1891-1909.

Kear, D., 1970. Basement rock facies northern North Island. N.Z.J. Geol. and Geophy., 14(2), pp.275-283.

Kliche, C.A., 1999. Rock slope stability, Littleton: Society for Mining, Metallurgy, and Exploration, Inc.

MacFarlane, D.F. et al., 1996. Monitoring stratergy and performance of instrumentation in the Clyde Power Project Landslides, New Zealand. In K. Senneset, ed. Rotterdam: A.A Balkema Publishers, pp. 1557-1564.

McKenzie, M.J., 1993. An evaluation of the rock mass rating (RMR) system and its potential applicability in the prediction of the stability of natural slopes. , M.Sc, p.341.

Meunier, A., 2005. Clays, New York: Springer Berlin Heidelberg.

Miller, D.S. & Kaiser, K., 1990. Numerical study of violent rock failure by stick-slip on joints Zou D.; Miller H.D.S.; Kaiser P.K. Min Sci Technol V9, N3, Nov 1989, P241. International Journal of Rock Mechanics and Mining Science, 27(3), p.A140.

Pantelidis, L., 2009. Rock slope stability assessment through rock mass classification systems. International Journal of Rock Mechanics and Mining Sciences, 46(2), pp.315-325.

Patton, F.D., 1966. Multiple modes of shear failure in rock and related materials. , Ph.D., p.293.

Piteau, P.R. & Russell, L., 1971. Cumulative sums technique: A new approach to analysing joints in rock.

Pointe, P.R. & Hudson, J.A., 1985. Characterisation and interpretation of rock mass joint patterns. Geological Society of America, (199), p.39.

Precision Aerial Surveys, 2007. Orthophoto of Whitehall Quarry.

Saeed, A., 2000. Petrographic and geochemical study of Morrinsville facies, North Island, New Zealand. , PhD.

Stanley, R.D., 1994. Geology of Matamata, Matamata: Matamata [N.Z.]: R.D. and J.C. Stanley.

Swan, A.R.H. & Sandilands, M., 1995. Introduction to geological data analysis, Oxford: Blackwell Science.

Tonkin & Taylor Ltd, 2008. Interim Stability Review - Whitehall Quarry Overburden Cut.

Tonkin & Taylor Ltd, 2004. Whitehall Quarry - Karapiro Stream Diversion Geotechnical Assessment.

Wandres, A.M.C., 2002. Provenance study of the Torlesse terranes - Implications for the origin of the continental crust of eastern New Zealand. , PhD.

Winstone Aggregates, Winstone Aggregates Homepage. , 2010(17/05/10), Website.

Woodward, J., 2005. An introduction to Geotechnical Processes 1st ed., Spon Press.

Wyllie, D.C. & Mah, C.W., 2004. Rock slope engineering: civil and mining 4th ed., London and New York: Taylor & Francis Group.

Yang, Z.Y. & Wu, T.J., 2006. An index for describing the core-stone shape in weathered columnar joints. Geotechnical and Geological Engineering, 24, pp.1349-1363.

Zou, D., Miller, D.S. & Kaiser, K., 1989. Rock slope stability analysis. Mining Science and Technology, 9, pp.241-251.

Appendices

Appendix A: Rock and Soil Classification

A1 Terminology

Intact Rock	a continuum or polycrystalline solid consisting of an aggregate of minerals or grains (Bell, 1987)
Discontinuity	any significant mechanical break or fracture of negligible tensile strength in a rock (Priest, 1993)
Rock Structure	the complex three-dimensional structure of discontinuities in a rock
Rock Mass	intact rock plus rock structure
Joint	a break of geological origin along which there has been no visible displacement (Bell, 1987)
Fault	a fracture in rock along which displacement has taken place (Bell, 1987)
Joint Set	a group of parallel joints
Fault Set	a group of parallel faults

A2 Field Descriptions for Rock Material

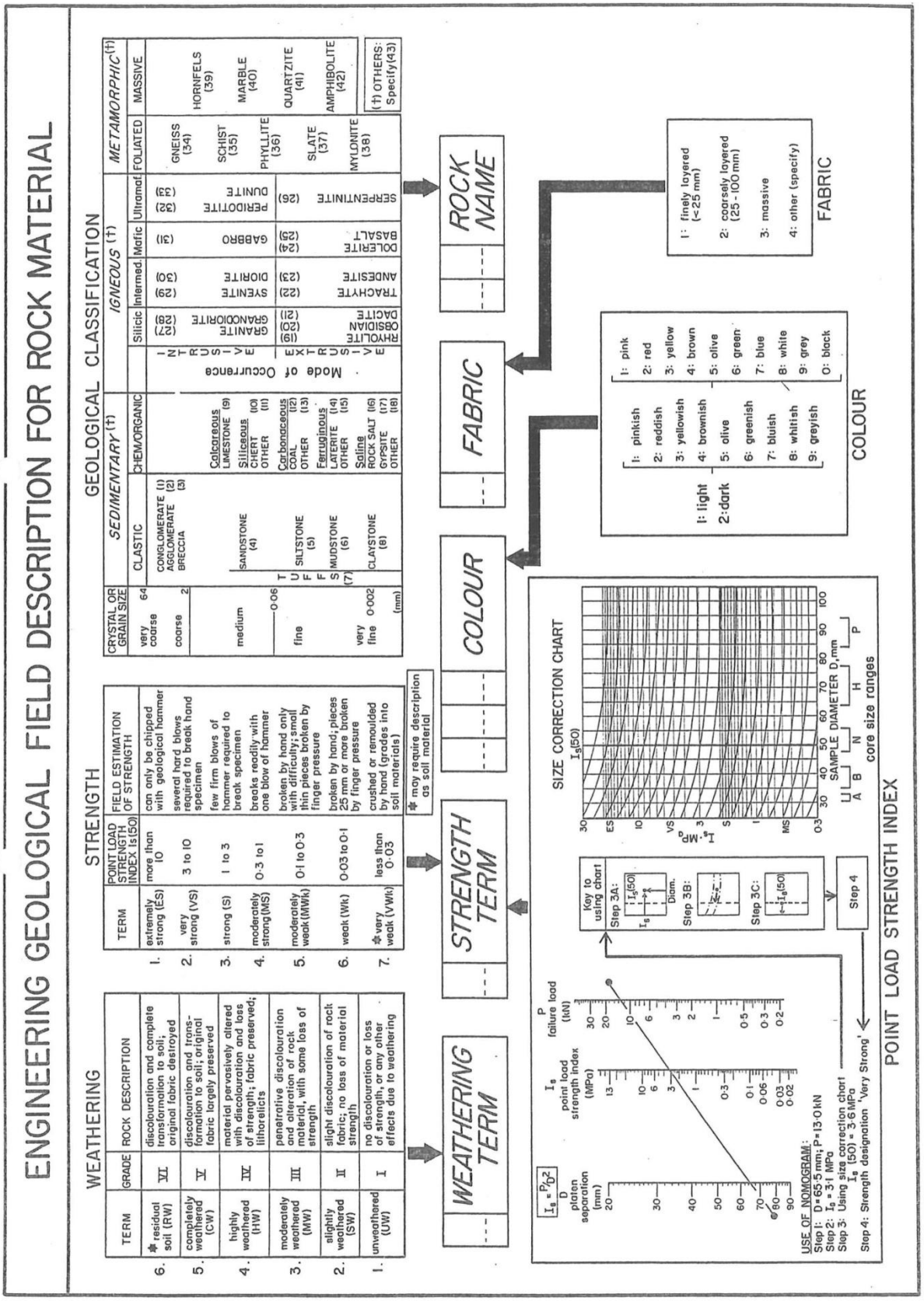

A3 Field Descriptions for Soil Material

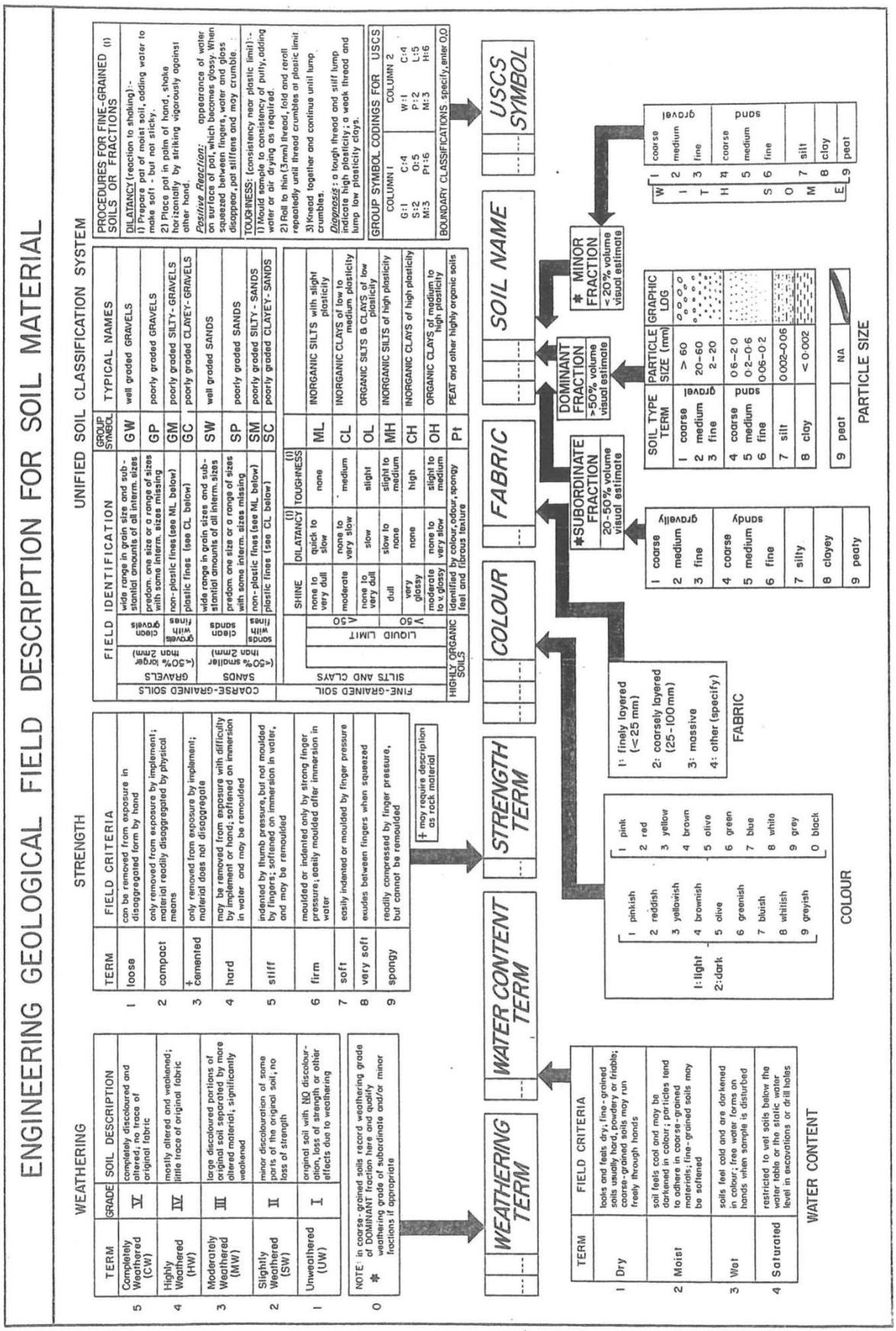

Appendix B: Field Data

B1 Rainfall Records

Whitehall Rainfall Statistics

Days	January	February	March	April	May	June	July	August	September	October	November	TOTAL
1	0.0	3.8	0.0	0.0	4.8	5.5	0.0	23.9	5.1	0.7	0.0	43.8
2	0.0	0.0	0.9	0.0	0.0	0.0	0.0	1.6	13.1	0.0	0.0	15.6
3	1.0	0.0	0.0	0.0	0.0	30.8	0.3	4.8	6.3	0.0	0.0	43.2
4	0.6	0.0	0.0	0.0	0.0	3.1	0.4	0.3	0.0	0.0	0.0	4.4
5	0.0	0.0	0.0	0.0	0.0	22.6	3.2	0.3	0.0	0.0	0.0	26.1
6	0.0	0.0	0.0	3.8	0.0	14.9	0.6	0.0	28.4	0.0	1.5	49.2
7	0.0	0.0	0.0	43.2	0.0	4.5	0.0	23.3	0.0	0.0	10.2	81.2
8	0.3	5.1	0.0	0.0	0.0	3.7	0.0	6.0	2.2	5.1	0.0	22.4
9	0.0	0.0	0.0	0.0	0.0	7.3	0.0	0.0	7.7	0.9	0.0	15.9
10	3.1	0.0	0.0	0.0	0.0	0.0	0.0	0.0	0.6	6.7	0.0	10.4
11	0.0	0.0	0.0	0.0	0.3	6.7	0.0	0.0	25.8	0.4	0.0	33.2
12	4.1	26.7	0.0	0.0	15.1	1.4	0.0	0.0	7.2	0.0	0.0	54.5
13	0.0	3.5	0.3	0.0	7.7	50.6	0.0	20.0	2.9	1.9	0.0	86.9
14	0.0	4.4	0.0	5.5	1.0	3.1	0.0	12.0	8.0	24.1	4.5	62.6
15	0.0	3.1	0.0	0.3	10.5	21.9	26.2	0.0	4.4	0.0	12.8	79.2
16	2.1	0.0	0.0	0.0	2.5	14.9	6.4	0.0	14.7	0.0	10.2	50.8
17	0.7	0.0	0.0	0.0	0.0	2.3	0.3	0.0	9.0	8.6	0.0	20.9
18	0.6	0.6	0.0	0.0	0.3	0.0	0.7	17.9	5.0	0.0	0.0	25.1
19	0.0	0.0	0.4	0.0	0.3	7.3	10.1	1.3	26.5	0.0	0.0	45.9
20	30.3	0.0	0.0	0.0	9.9	0.0	23.9	14.7	44.4	0.0	0.0	123.2
21	12.0	0.0	0.0	0.0	5.4	5.4	5.5	0.0	17.3	1.9	4.6	52.1
22	5.9	0.0	0.6	0.0	0.0	0.0	0.0	3.5	6.4	0.0	10.6	27.0
23	0.0	0.0	6.1	0.0	29.7	29.7	0.0	8.7	0.6	0.0	2.8	77.6
24	0.0	0.0	21.1	4.4	3.1	3.1	1.5	0.0	2.5	0.0	0.0	35.7
25	3.7	5.1	0.3	0.0	21.9	21.9	0.3	15.7	4.2	0.0	0.0	73.1
26	13.9	0.0	0.0	0.0	14.9	10.9	0.0	6.7	0.0	0.0	0.0	46.4
27	4.8	0.0	0.0	0.0	2.3	2.3	0.0	8.7	0.0	0.0	0.0	18.1
28	0.6	-	0.0	5.5	0.0	0.0	0.3	6.1	0.0	0.0	0.0	12.5
29	0.0	-	0.0	0.0	7.3	7.3	0.0	6.5	0.0	0.0	0.0	21.1
30	3.2	-	0.0	-	0.0	0.0	0.0	2.1	-	0.0	0.0	5.3
31	-	-	-	-	-	-	-	-	-	-	0.0	0.0

Total	86.9	52.3	29.7	62.7	137.0	281.2	79.7	184.1	242.3	50.3	57.2
Rain Days	16	8	7	6	17	23	14	20	22	9	8
Wettest Day	30.3	26.7	21.1	43.2	29.7	50.6	26.2	23.9	44.4	24.1	12.8
Average	76.7	74.2	75.6	78.8	117.6	140.4	137.0	92.2	91.0	119.4	82.9

Total for year (Jan-Nov), mm **1263.4**

Average for year (Jan-Nov), mm **1085.8**

Source: http://www.cambridge.net.nz/weather/raindetail2.html

B2 Photogrammetry

SECTION A

Camera and Lens Details										
Camera Name	Camera		Lens		Sensor Size		Pixel Size		Image Size	
	Type	Serial Number	Type	Serial Number	Width	Height	Width	Height	Width	Height
Canon EOS 5D Mark II 100mm	Canon EOS 5D Mark II		100mm		36.00	24.00	0.01	0.01	5616	3744

Image Residuals				
Image Names	RMS Error (Pixel)			Active Points
	X	Y	Total	
AL10conv.JPG	0.82	1.39	1.62	985
AL11conv.JPG	0.39	0.64	0.75	705
AL12conv.JPG	0.87	1.18	1.46	1053
AL13conv.JPG	0.95	1.39	1.68	1037
AL14conv.JPG	0.52	1.14	1.25	1052
AL15conv.JPG	0.40	1.27	1.33	683
AL1conv.JPG	1.65	1.70	2.37	942
AL2conv.JPG	1.80	1.68	2.46	1222
AL3conv.JPG	2.18	0.95	2.38	1120
AL4conv.JPG	1.90	1.54	2.44	1097
AL5conv.JPG	1.23	0.90	1.52	1038
AL6conv.JPG	2.00	1.26	2.36	1283
AL7conv.JPG	0.45	0.92	1.03	1339
AL8conv.JPG	1.55	1.37	2.07	1335
AL9conv.JPG	1.40	1.64	2.16	1305
AR16conv.JPG	1.30	1.48	1.97	885
AR17conv.JPG	2.24	1.46	2.68	1195
AR18conv.JPG	0.64	0.69	0.94	1145
AR19conv.JPG	0.60	1.01	1.17	1079
AR20conv.JPG	2.69	0.76	2.79	702
AR21conv.JPG	0.46	0.64	0.79	879
AR22conv.JPG	1.99	1.30	2.38	1234
AR23conv.JPG	1.25	0.94	1.56	1305
AR24conv.JPG	1.50	1.66	2.24	1346
AR25conv.JPG	0.95	1.43	1.72	1066
AR26conv.JPG	0.58	1.02	1.17	852
AR27conv.JPG	0.52	0.67	0.85	1069
AR28conv.JPG	0.47	0.97	1.08	1049
AR29conv.JPG	0.77	1.02	1.28	1023
AR30conv.JPG	0.57	0.99	1.14	733

Control Point Residuals									
Control Point Names	Image Point Residuals			Control Point Residuals			Adjusted Data		
	Num of Observations	X	Y	X	Y	Z	X	Y	Z
1	2	0.03	0.06	-0.02	0.19	0.13	2735770.68	6365484.17	50.73
2	2	0.12	0.35	-0.05	-0.17	-0.02	2735729.85	6365446.43	87.44
3	2	0.02	0.10	0.07	-0.03	-0.11	2735765.91	6365558.76	95.93
Control Point RMS				0.06	0.18	0.12			
Total				0.23					

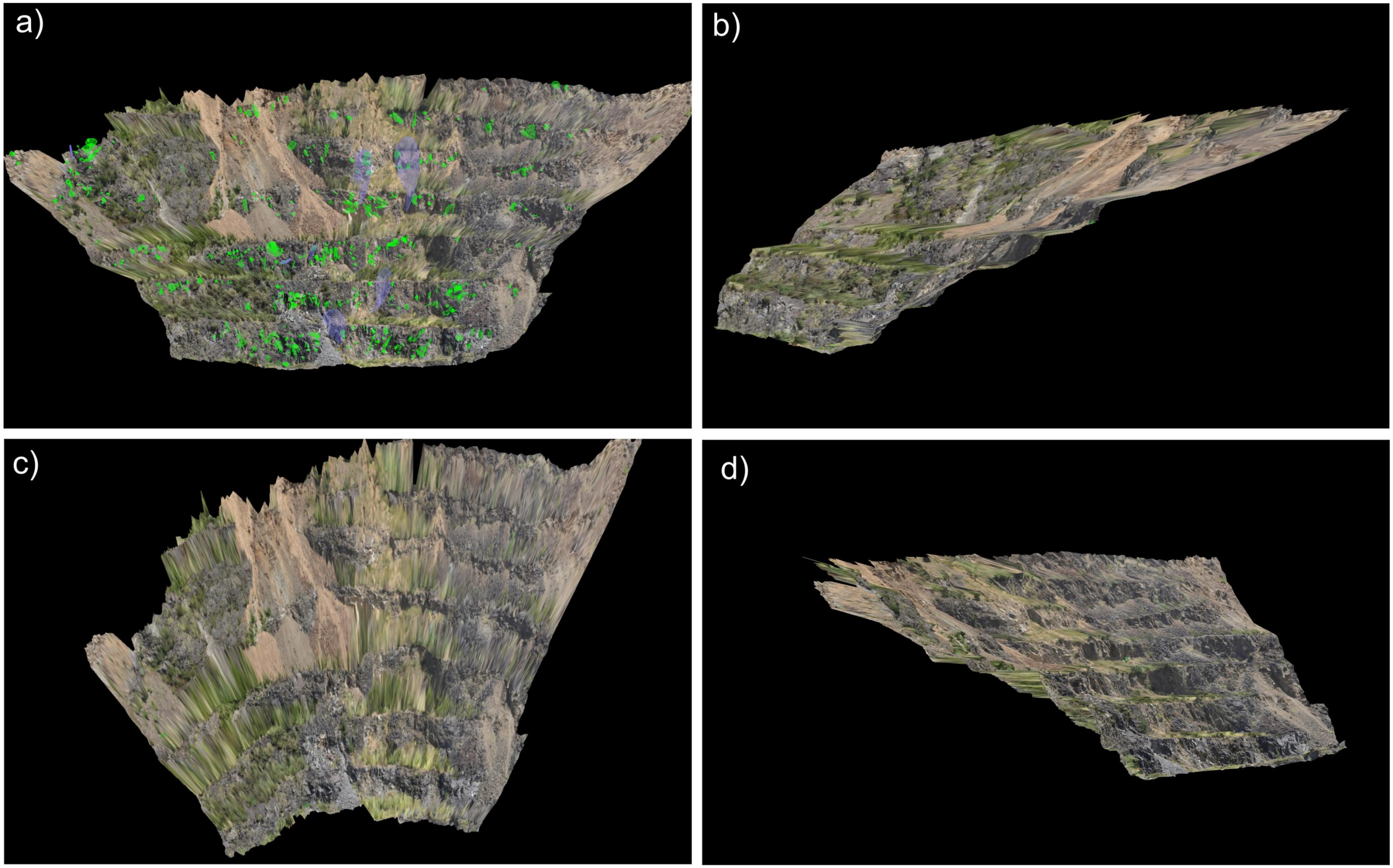

Figure B-1: 3D model of Section A; a) front view showing structural features (bedding-black, joints-yellow, and faults-blue), b) side view looking towards the south, c) plan view, d) side view looking towards the north.

SECTION B

Camera and Lens Details										
Camera Name	Camera		Lens		Sensor Size		Pixel Size		Image Size	
	Type	Serial Number	Type	Serial Number	Width	Height	Width	Height	Width	Height
Canon EOS 5D Mark II 100mm					36.00	24.00	0.01	0.01	5616	3744

Image Residuals				
Image Names	RMS Error (Pixel)			Active Points
	X	Y	Total	
BL1conv.JPG	0.58	0.44	0.73	558
BL2conv.JPG	1.56	1.07	1.89	672
BL3conv.JPG	1.03	1.19	1.57	487
BL4conv.JPG	1.24	0.44	1.31	746
BL5conv.JPG	1.85	0.64	1.96	937
BL6conv.JPG	1.50	0.51	1.59	830
BL7conv.JPG	1.20	1.19	1.69	717
BL8conv.JPG	1.11	0.97	1.47	788
BL9conv.JPG	0.34	0.41	0.54	564
BR1conv.JPG	0.56	0.51	0.76	537
BR2conv.JPG	0.42	0.51	0.66	784
BR3conv.JPG	0.32	0.69	0.76	636
BR4conv.JPG	0.40	0.39	0.56	848
BR5conv.JPG	0.26	0.36	0.44	970
BR6conv.JPG	0.23	0.34	0.41	735
BR7conv.JPG	0.36	0.86	0.94	633
BR8conv.JPG	0.19	0.37	0.41	786
BR9conv.JPG	0.16	0.61	0.63	654

Control Point Residuals									
Control Point Names	Image Point Residuals			Control Point Residuals			Adjusted Data		
	Num of Observations	X	Y	X	Y	Z	X	Y	Z
13	2	0.02	0.15	-0.00	-0.03	0.04	2735747.72	6365322.92	34.14
14	2	0.03	0.46	-0.07	-0.04	-0.06	2735707.72	6365317.25	42.61
15	2	0.00	0.10	-0.04	0.05	0.01	2735722.29	6365358.67	46.97
19	2	0.02	0.11	0.11	0.02	0.01	2735694.84	6365325.73	58.27
Control Point RMS				0.08	0.04	0.04			
Total				0.10					

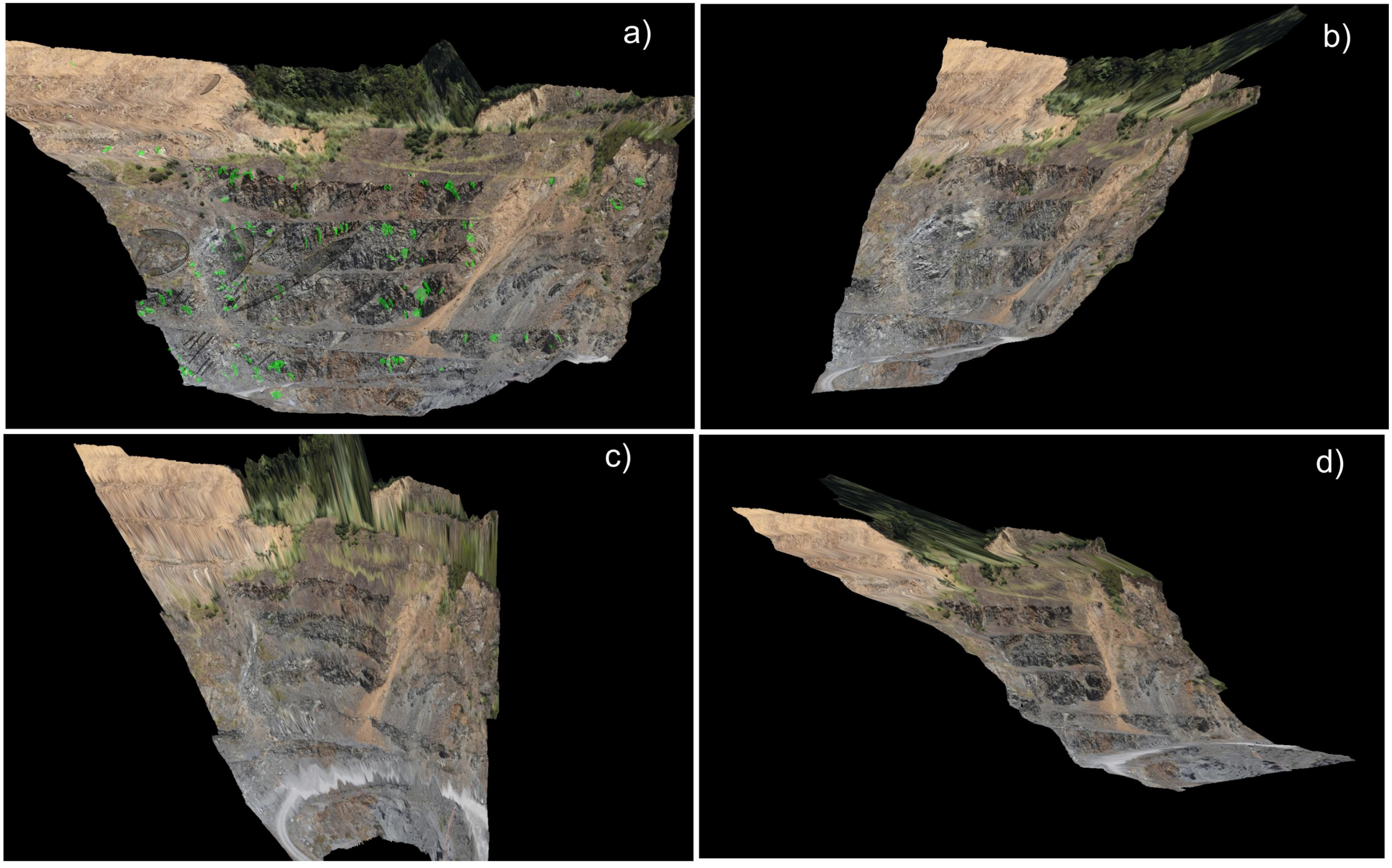

Figure B-2: 3D model of Section B; a) front view showing structural features (bedding-black, joints-yellow, and faults-blue), b) side view looking towards the south, c) plan view, d) side view looking towards the north

SECTION C

Camera and Lens Details										
Camera Name	Camera		Lens		Sensor Size		Pixel Size		Image Size	
	Type	Serial Number	Type	Serial Number	Width	Height	Width	Height	Width	Height
Canon EOS 5D Mark II 100mm					36.00	24.00	0.01	0.01	5616	3744

Image Residuals				
Image Names	RMS Error (Pixel)			Active Points
	X	Y	Total	
CL1conv.JPG	0.29	0.22	0.36	652
CL2conv.JPG	0.69	0.52	0.86	729
CL3conv.JPG	0.17	0.44	0.47	560
CL4conv.JPG	0.18	0.40	0.43	610
CL5conv.JPG	0.27	0.27	0.38	765
CL6conv.JPG	0.27	0.39	0.48	724
CR1conv.JPG	0.18	0.26	0.32	652
CR2conv.JPG	0.18	0.55	0.58	724
CR3conv.JPG	0.17	0.64	0.66	578
CR4conv.JPG	0.17	0.18	0.25	614
CR5conv.JPG	0.18	0.23	0.29	791
CR6conv.JPG	0.17	0.29	0.34	720

Control Point Residuals									
Control Point Names	Image Point Residuals			Control Point Residuals			Adjusted Data		
	Num of Observations	X	Y	X	Y	Z	X	Y	Z
7	2	0.01	0.07	0.07	-0.12	0.05	2735799.33	6365270.32	43.09
8	2	0.00	0.04	-0.08	0.00	-0.00	2735843.06	6365276.88	42.68
12	2	0.01	0.18	0.01	0.12	-0.04	2735796.36	6365296.92	33.80
Control Point RMS				0.07	0.12	0.04			
Total				0.15					

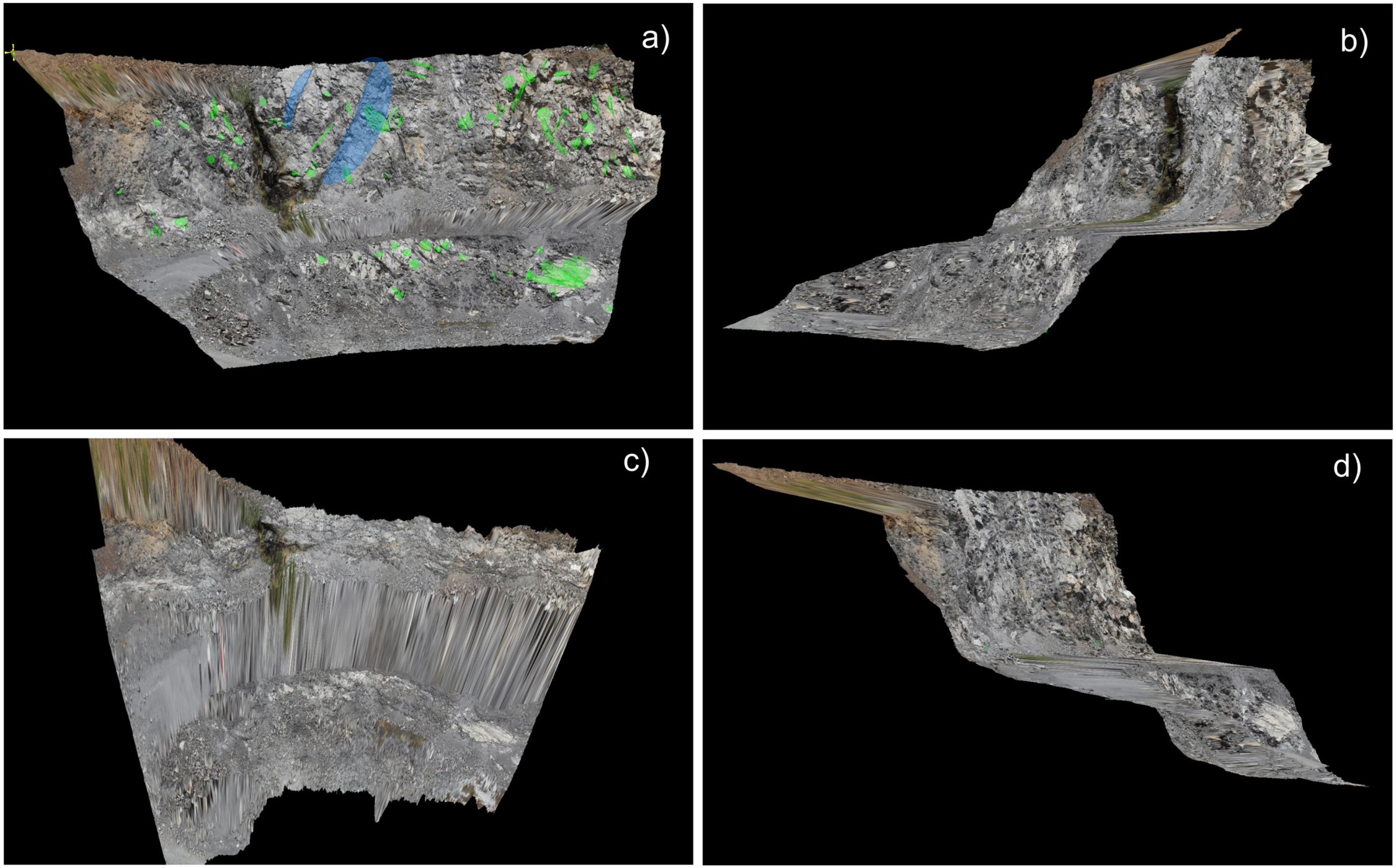

Figure B-3: 3D model of Section C; a) front view showing structural features (bedding-black, joints-yellow, and faults-blue), b) side view looking towards the east, c) plan view, d) side view looking towards the west.

SECTION D

Camera and Lens Details										
Camera Name	Camera		Lens		Sensor Size		Pixel Size		Image Size	
	Type	Serial Number	Type	Serial Number	Width	Height	Width	Height	Width	Height
Canon EOS 5D Mark II 100mm	Canon EOS 5D Mark II		100mm		36.00	24.00	0.01	0.01	5616	3744

Image Residuals				
Image Names	RMS Error (Pixel)			Active Points
	X	Y	Total	
DL10conv.JPG	0.53	0.61	0.81	579
DL11conv.JPG	0.92	0.53	1.06	768
DL12conv.JPG	2.16	1.54	2.65	940
DL13conv.JPG	3.92	1.41	4.17	951
DL14conv.JPG	3.67	1.30	3.89	772
DL15conv.JPG	3.05	0.89	3.18	310
DL1conv.JPG	0.79	0.31	0.85	401
DL2conv.JPG	0.89	0.74	1.16	694
DL3conv.JPG	13.28	6.75	14.90	780
DL4conv.JPG	2.45	0.84	2.59	796
DL5conv.JPG	2.63	1.06	2.84	698
DL6conv.JPG	2.63	1.22	2.90	1043
DL7conv.JPG	2.27	0.98	2.48	1122
DL8conv.JPG	0.90	0.85	1.23	1075
DL9conv.JPG	0.59	0.52	0.79	844
DR10conv.JPG	0.71	0.40	0.82	733
DR11conv.JPG	0.61	0.38	0.71	786
DR12conv.JPG	1.37	1.31	1.89	959
DR13conv.JPG	0.95	1.05	1.41	965
DR14conv.JPG	0.74	0.94	1.20	899
DR15conv.JPG	0.76	0.88	1.17	712
DR1conv.JPG	0.31	0.62	0.70	639
DR2conv.JPG	0.34	0.41	0.53	737
DR3conv.JPG	0.62	0.72	0.95	757
DR4conv.JPG	0.78	0.79	1.10	629
DR5conv.JPG	0.27	0.38	0.47	382
DR6conv.JPG	0.37	0.42	0.57	729
DR7conv.JPG	0.58	0.64	0.87	969
DR8conv.JPG	0.73	0.85	1.12	1074
DR9conv.JPG	0.61	0.62	0.87	1011

Control Point Residuals									
Control Point Names	Image Point Residuals			Control Point Residuals			Adjusted Data		
	Num of Observations	X	Y	X	Y	Z	X	Y	Z
4	2	0.02	0.23	0.12	0.02	0.09	2735778.03	6365247.51	42.88
5	2	0.04	0.25	-0.08	-0.16	0.02	2735747.60	6365198.53	43.47
17	2	0.06	0.51	-0.03	0.14	-0.11	2735783.85	6365200.29	74.65
Control Point RMS				0.10	0.15	0.10			
Total				0.21					

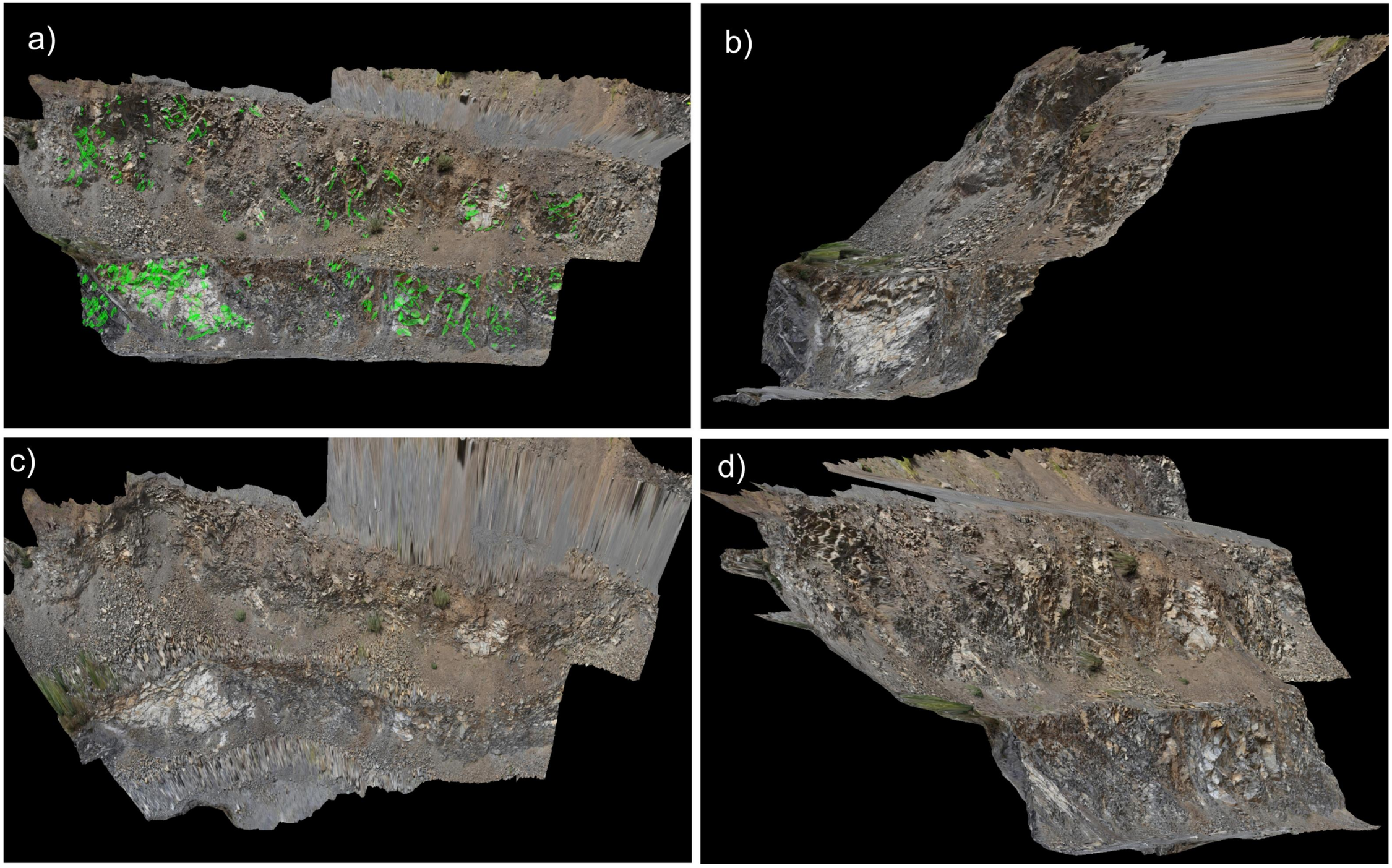

Figure B-4: 3D model of Section D; a) front view showing structural features (bedding-black, joints-yellow, and faults-blue), b) side view looking towards the north, c) plan view, d) side view looking towards the south

SECTION E

Camera and Lens Details										
Camera Name	Camera		Lens		Sensor Size		Pixel Size		Image Size	
	Type	Serial Number	Type	Serial Number	Width	Height	Width	Height	Width	Height
Canon EOS 5D Mark II 100mm	Canon EOS 5D Mark II		100mm		36.00	24.00	0.01	0.01	5616	3744

Image Residuals				
Image Names	RMS Error (Pixel)			Active Points
	X	Y	Total	
EL1convICC.JPG	0.15	0.16	0.23	490
EL2convICC.JPG	0.15	0.18	0.23	586
EL3convICC.JPG	0.14	0.17	0.22	351
ER1convICC.JPG	0.17	0.20	0.26	416
ER2convICC.JPG	0.16	0.20	0.26	578
ER3convICC.JPG	0.17	0.17	0.24	452

Control Point Residuals									
Control Point Names	Image Point Residuals			Control Point Residuals			Adjusted Data		
	Num of Observations	X	Y	X	Y	Z	X	Y	Z
9	2	0.02	0.06	0.11	0.10	0.01	2735855.02	6365286.22	41.80
10	2	0.00	0.02	0.06	-0.12	0.03	2735856.85	6365333.12	37.18
11	2	0.01	0.13	-0.17	0.02	-0.04	2735826.32	6365308.88	33.68
Control Point RMS				0.15	0.11	0.03			
Total				0.19					

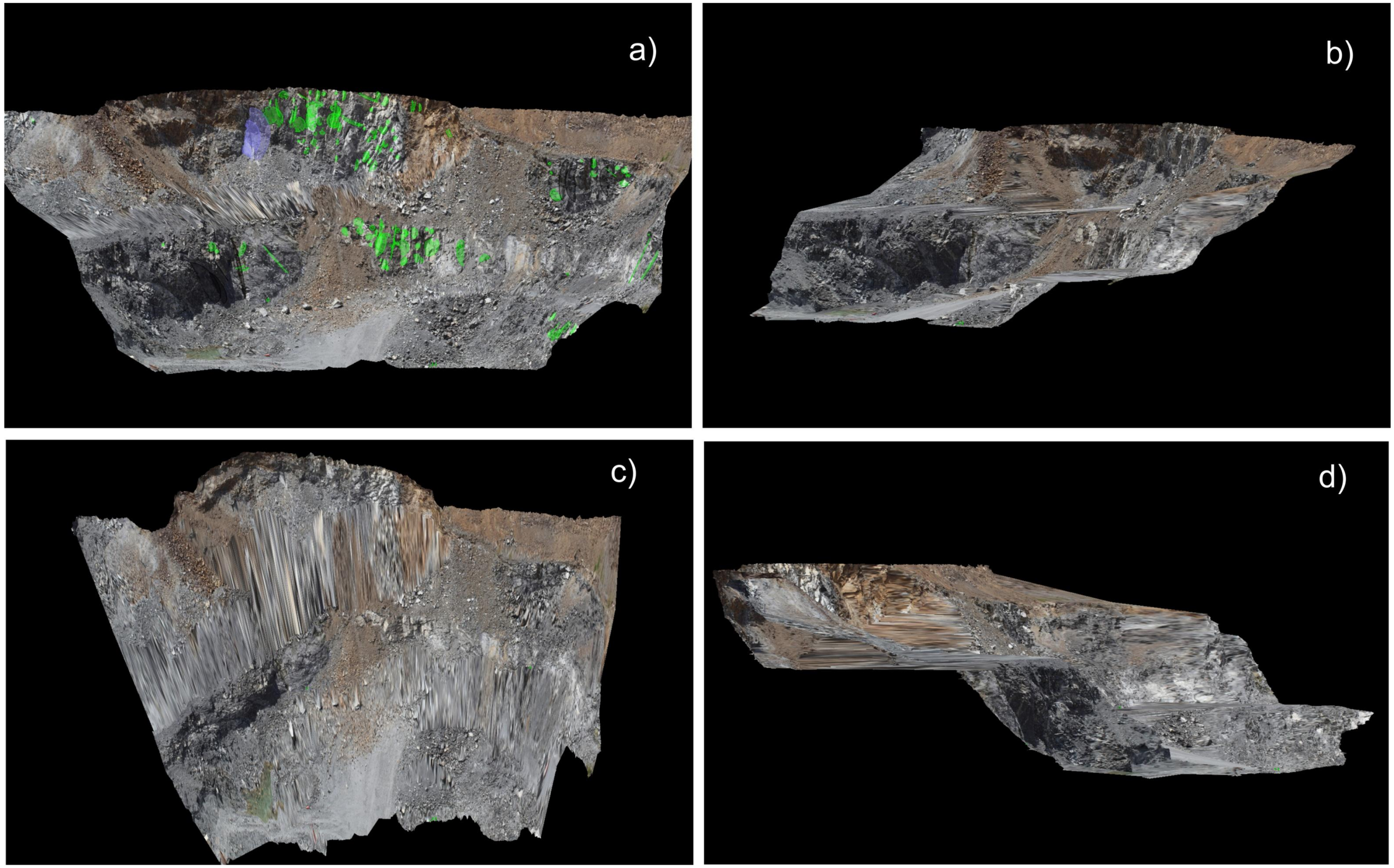

Figure B-5: 3D model of Section E; a) front view showing structural features (bedding-black, joints-yellow, and faults-blue), b) side view looking towards the east, c) plan view, d) side view looking towards the west

B3 Scanline Analysis

Type

0. Fault zone
1. Fault
2. Joint
3. Cleavage
4. Schistosity
5. Shear
6. Fissure
7. Tension Crack
8. Foliation
9. Bedding

Persistence

1. Very low persistence	<1 m
2. Low persistence	1–3 m
3. Medium persistence	3–10 m
4. High persistence	10–20 m
5. Very high persistence	>20 m

Aperture/width

1. Very tight (<0.1 mm)
2. Tight (0.1–0.25 mm)
3. Partly open (0.25–0.5 mm)
4. Open (0.5–2.5 mm)
5. Moderately wide (2.5–10 mm)
6. Wide (>10 mm)
7. Very wide (1–10 cm)
8. Extremely wide (10–100 cm)
9. Cavernous (>1 m)

Nature of filling

1. Clean
2. Surface staining
3. Non-cohesive
4. Inactive clay or clay matrix
5. Swelling clay or clay matrix
6. Cemented
7. Chlorite, talc or gypsum
8. Other — specify

Termination

0. Neither end visible
1. One end visible
2. Both ends visible

Surface shape

1. Stepped
2. Undulating
3. Planar

Surface roughness

1. Rough
2. Smooth
3. Polished
4. Slickensided

Compressive strength of infilling

	MPa
S1 Very soft clay	<0.025
S2 Soft clay	0.025–0.05
S3 Firm clay	0.05–0.10
S4 Stiff clay	0.10–0.25
S5 Very stiff clay	0.25–0.50
S6 Hard clay	>0.50
R0 Extremely weak rock	0.25–1.0
R1 Very weak rock	1.0–5.0
R2 Weak rock	5.0–25
R3 Medium strong rock	25–50
R4 Strong rock	50–100
R5 Very strong rock	100–250
R6 Extremely strong rock	>250

Spacing

1. Extremely close spacing	<20 mm
2. Very close spacing	20–60 mm
3. Close spacing	60–200 mm
4. Moderate spacing	200–600 mm
5. Wide spacing	600–2000 mm
6. Very wide spacing	2000–6000 mm
7. Extremely wide spacing	

Water flow (open)

0. Discontinuity is very light and dry, water flow along it does not appear possible.
1. The discontinuity is dry with no evidence of water flow.
2. The discontinuity is dry but shows evidence of water flow. i.e. rust staining, etc.
3. The discontinuity is damp but no free water is present.
4. The discontinuity shows seepage, occasional drops of water, but no continuous flow.
5. The discontinuity shows a continuous flow of water (Estimate 1/mm and describe pressure, i.e. low medium, high).

Water flow (filled)

6. The filling materials are heavily consolidated and dry; significant flow appears unlikely due to very low permeability.
7. The filling materials are damp, but no free water is present.
8. The filling materials are wet; occasional drops of water.
9. The filling materials show signs of outwash, continuos flow of water (estimate litres/minute).
10. The filling materials are washed out locally; considerable water flow along out-wash channels (estimate litres/minute and describe pressure, i.e. low, medium, high).

Figure B-6: Structural mapping codes.

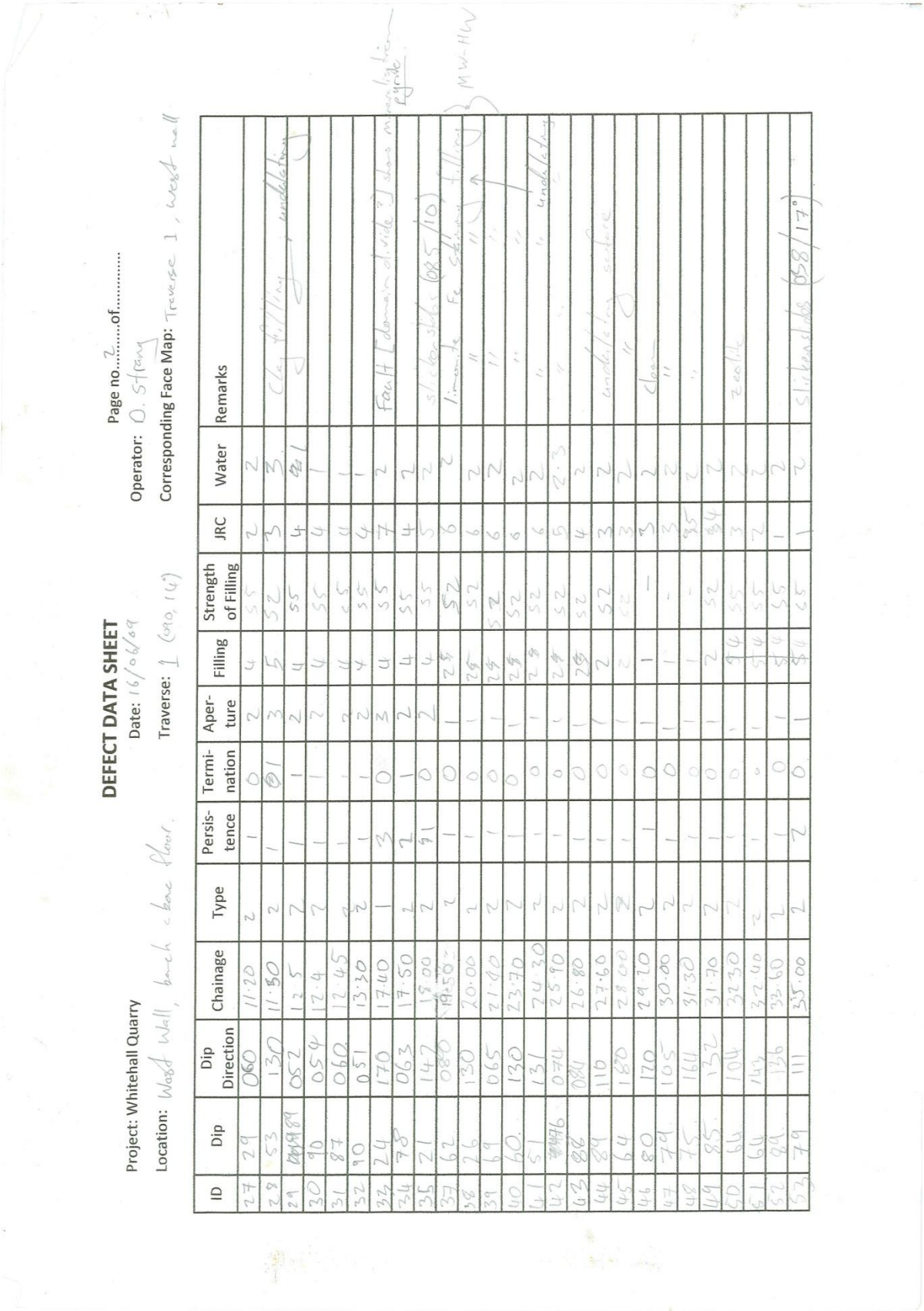

DEFECT DATA SHEET

Page no. 2 of.....

Project: Whitehall Quarry

Date: 16/06/09

Operator: O. Sloane

Location: West Wall, back of bench floor.

Traverse: 1 (090, 14°)

Corresponding Face Map: Traverse 1, west wall

ID	Dip	Dip Direction	Chainage	Type	Persis-tence	Termi-nation	Aper-ture	Filling	Strength of Filling	JRC	Water	Remarks
27	29	060	11.20	2	1	0	2	4	55	2	2	
28	53	130	11.50	2	1	01	3	5	52	3	3	
29	[illegible]	052	12.5	7	1	1	2	4	55	4	4? 1	
30	90	054	12.4	7	1	1	2	4	55	4	1	
31	87	060	12.45	7	1	1	2	4	55	4	1	
32	90	051	13.30	2	1	1	2	4	55	4	1	
33	24	170	17.40	1	3	0	3	4	55	7	2	
34	78	063	17.50	2	2	1	2	4	55	4	2	
35	71	147	18.00	2	41	0	2	4	55	5	2	
37	62	080	19.50	2	1	0	1	28	52	6	2	
38	26	130	20.00	2	1	0	1	28	52	6	2	
39	69	065	21.00	2	1	0	1	28	52	6	2	
40	60	130	23.70	2	1	0	1	28	52	6	2	
41	51	131	24.30	2	1	0	1	28	52	6	2	
42	[illegible]	074	25.90	2	1	0	1	28	52	6	2.3	
43	86	081	26.80	2	1	0	1	28	52	4	2	
44	89	110	27.60	2	1	0	1	2	52	3	2	
45	64	180	28.00	2	1	0	1	2	52	3	2	
46	80	170	29.10	2	1	0	1	1	—	3	2	
47	79	105	30.00	2	1	0	1	1	—	3	2	
48	75	161	31.30	2	1	0	1	1	—	3.5	2	
49	85	132	31.70	2	1	0	1	2	52	3.4	2	
50	64	104	32.30	2	1	0	1	4	55	3	2	
51	64	142	32.40	2	1	0	1	5/4	55	2	2	
52	24	126	33.60	2	1	0	1	5/4	55	1	2	
53	79	111	35.00	2	2	0	1	5/4	55	1	2	

Figure B-7: Example of scanline data collected during field investigations.

B4 Schmidt Hammer Testing

Schmidt hammer testing was carried out at Whitehall Quarry during December 2009 in accordance with the ISRM suggested methods (Aydin 2008). The L-9 type hammer was applied to six different rock types within the quarry, they were:

- Unweathered (UW) sandstone
- Slightly weathered (SW) sandstone
- Moderately weathered (MW) sandstone
- Highly weathered (HW) sandstone
- Slightly weathered (SW) mudstone

Samples were also collected of similar type to determine the average rock mass density required for uniaxial compressive strength approximation.

Table B-1: Schmidt hammer results for UW Sandstone.

Location: Whitehall Quarry									
Lithology: **UW Greywacke Sandstone**									
Date: 10/12/2009			Equipment: Schmidt Hammer (L-9)						
Correction: +45									
Rebound Values:	40	44	48	49	50	52	52	54	54
	55	56	56	56	57	58	58	58	59
	59	59	59	60	60	60	60	61	61
	61	61	61	62	62	62	62	63	64
	67	67	67						
Max:	64								
Min:	40								
Average:	62								
* average of upper 50% of rebound values									
Approximated UCS	**230 MPa**								

Table B-2: Schmidt hammer results for SW Sandstone.

Location: Whitehall Quarry									
Lithology: **SW Greywacke Sandstone**									
Date: 08/12/2009			Equipment: Schmidt Hammer (L-9)						
Correction: +45									
Rebound Values:	26	29	30	32	34	35	36	39	40
	40	42	42	43	45	45	46	48	48
	49	49	50	50	50	51	51	51	52
	52	54	54	55	59	60	60	60	63
Max:	63								
Min:	26								
Average:	54								
* average of upper 50% of rebound values									
Approximated UCS	**150 MPa**								

Table B-3: Schmidt hammer results for MW Sandstone.

Location: Whitehall Quarry									
Lithology: **MW Greywacke Sandstone**									
Date: 14/12/2009			Equipment: Schmidt Hammer (L-9)						
Correction: +45									
Rebound Values:	16	16	16	18	20	20	20	21	21
	21	22	22	23	24	24	25	25	26
	26	26	26	26	28	28	28	28	29
	30	30	30	32	32	32	33	35	
Max:	35								
Min:	16								
Average:	29								
* average of upper 50% of rebound values									
Approximated UCS	**55 MPa**								

Table B-4: Schmidt hammer results for HW Sandstone.

Location: Whitehall Quarry									
Lithology: **HW Greywacke Sandstone**									
Date: 14/12/2009			Equipment: Schmidt Hammer (L-9)						
Correction: +45									
Rebound Values:	9	10	10	10	10	10	11	11	11
	11	11	11	11	12	13	13	13	14
	14	14	14	15	15	15	15	15	15
	15	17	17	18	18				
Max:	18								
Min:	9								
Average:	15								
* average of upper 50% of rebound values									
Approximated UCS	**30 MPa**								

Table B-5: Schmidt hammer results for SW Mudstone.

Location: Whitehall Quarry										
Lithology: **SW Argillite**										
Date: 14/12/2009				Equipment: Schmidt Hammer (L-9)						
Correction: +45										
Rebound Values:	10	11	12	12	12	13	14	16	16	18
	18	19	21	22	23	26	26	28	28	30
Max:	30									
Min:	10									
Average:	24									
* average of upper 50% of rebound values										
Approximated UCS	**37 MPa**									

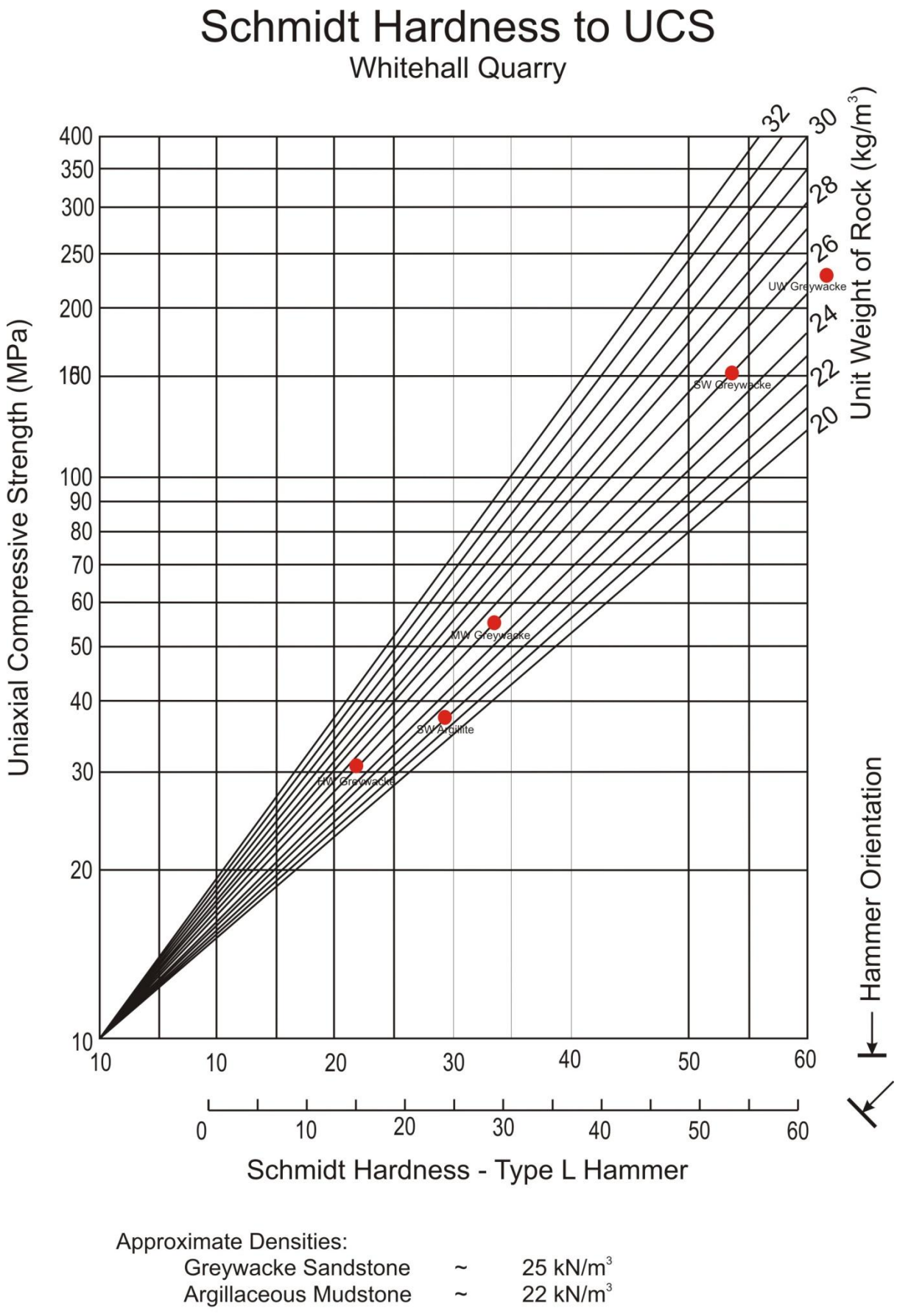

Figure B-8: Schmidt hammer rebound number to uniaxial compressive strength (UCS) conversion chart.

B5 Rock Mass Rating (RMR) Classification System

A. CLASSIFICATION PARAMETERS AND THEIR RATINGS									
Parameter			Range of values						
1	Strength of intact rock	Point-load strength Index	>10 MPa	4-10 MPa	2-4 MPa	1-2 MPa	For this low range UCS is preferred		
		Uniaxial comp strength	>250 MPa	100-250 MPa	50-100 MPa	25-50 MPa	2-25 MPa	1-5 MPa	<1 MPa
	Rating		15	12	7	4	2	1	0
2	Drill core quality		90-100%	75-90%	50-75%	25-50%	<25%		
	Rating		20	17	13	8	3		
3	Spacing of discontinuities		>2m	0.6-2m	200-600mm	60-200mm	<60mm		
	Rating		20	15	10	8	5		
4	Condition of discontinuities		Very rough surfaces, not continuous, no seperation, unweathered wall rock	Slightly rough surfaces, separation <1mm, highly weathered wall rock	Slightly rough surfaces, separation <1mm, highly weathered walls	Slickenslide surfaces or gouge <5mm thick or separation 1-5mm, continuous	Soft gouge >5mm thick or separation >5mm, continuous		
	Rating		30	25	20	10	0		
5	Ground-water	Inflow per 10m tunnel length	None	<10	Oct-25	25-125	>125		
		General conditions	Completely dry	Damp	Wet	Dripping	Flowing		
	Rating		15	10	7	4	0		
B. ROCK MASS CLASSES DETERMINED FROM TOTAL RATINGS									
Rating			100-81	80-61	60-41	40-21	<20		
Class Number			I	II	III	IV	V		
Description			Very good rock	Good rock	Fair rock	Poor rock	Very poor rock		
C. MEANING OF ROCK CLASSES									
Class number			I	II	III	IV	V		
Cohesion of rock mass (kPa)			>400	300-400	200-300	100-200	<100		
Friction angle of rock mass (deg)			>45	35-45	25-35	15-25	<15		

Appendix C: Laboratory Data

C1 Sample Location Map

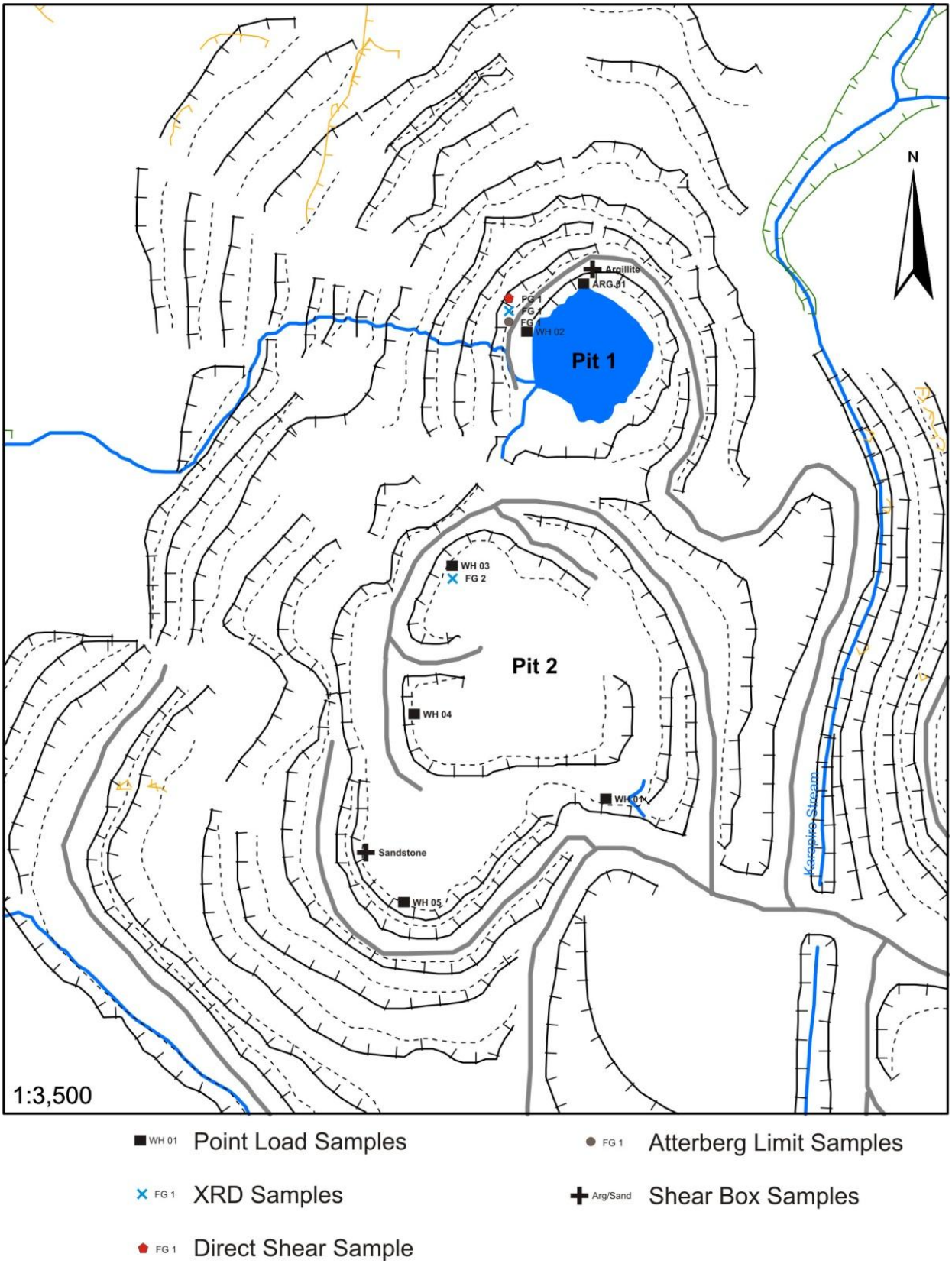

C2 Point Load Testing

Point load testing was carried out in accordance with the ISRM "Suggested method for determining point load strength" (1995).

Specimens were tested as irregular lump samples ranging in size from 25 to 70 mm. Testing was conducted in the Rock Mechanics Laboratory at the University of Canterbury during March 2010.

Calculations

The uncorrected point load strength index (I_s) is calculated as:

$$\frac{P}{D_e^2}$$

Where P= the force at which the sample fails and D_e is the "equivalent core diameter" and is given by:

and

A= the minimum cross-sectional area of a plane through the platen contact points.

The size-corrected point load strength $I_{s(50)}$ is calculated by applying a "size correction factor (F)" where:

Point load photographs and results are presented in the tables on the following pages.

Figure C-1: Point Load Tester, Rock Mechanics Laboratory, University of Canterbury.

Figure C-2: Sample WH01 (UW sandstone) before point load testing.

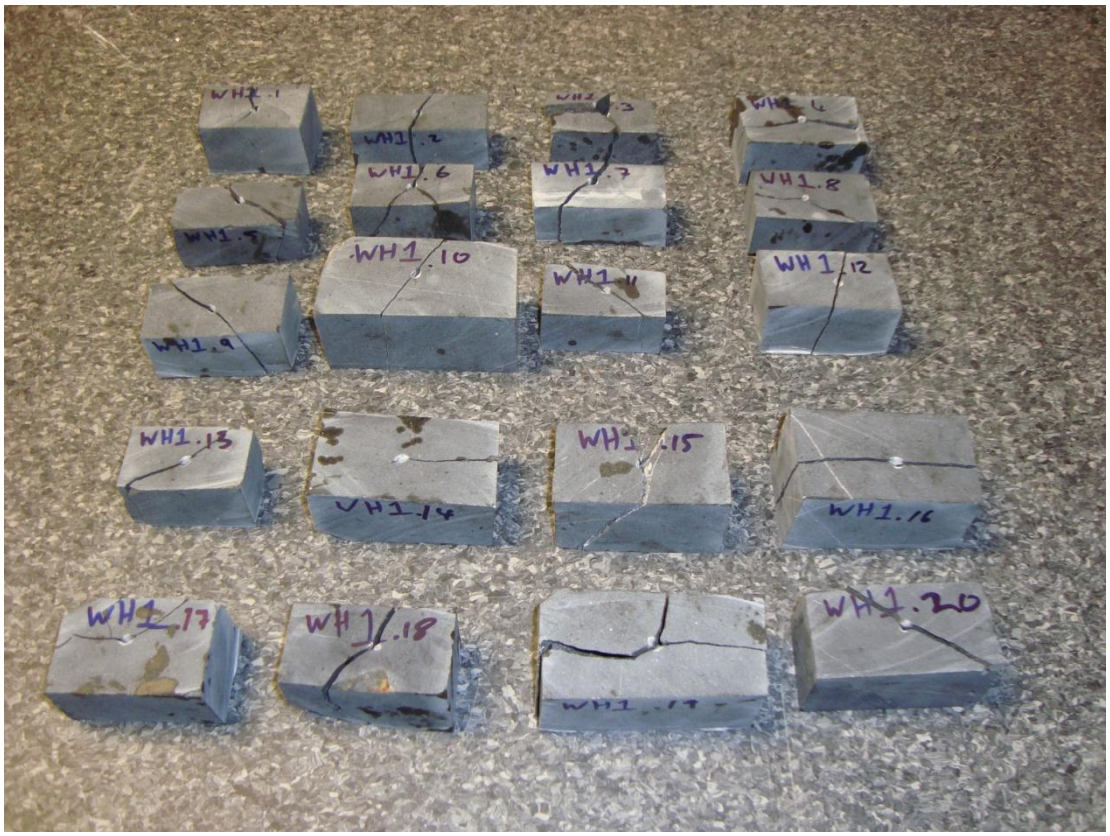

Figure C-3: Sample WH01 (UW sandstone) after point load testing.

Table C-1: Point load test results for sample: WH01 UW sandstone.

PROJECT: Whitehall Quarry				SAMPLE: WH01				LOCATION: (Sample Location Map)		
LITHOLOGY: UW Greywacke Sandstone				DATE: 10/03/2010						
Test No.	**Type**	**P (kN)**	**D (mm)**	**W (mm)**	**A = WD (mm^2)**	**D_e^2**	**D_e**	**I_s**	**F**	**$I_{s(50)}$ (MPa)**
1	parallel	16.00	34.2	35.54	1214	1546	39.3	10.35	0.897	9.29
2		16.00	30.3	30.33	918	1169	34.2	13.69	0.843	11.54
3		12.50	25.5	30.23	771	981	31.3	12.74	0.810	10.32
4		19.00	31.5	39.4	1241	1581	39.8	12.02	0.902	10.84
5		17.00	28.8	30.42	876	1115	33.4	15.25	0.834	12.71
6		20.50	33.6	34.59	1164	1482	38.5	13.84	0.889	12.30
7		15.00	28.4	30.54	866	1103	33.2	13.60	0.832	11.31
8		14.50	29.3	35.57	1042	1327	36.4	10.93	0.867	9.48
9		18.00	32.0	34.9	1117	1423	37.7	12.65	0.881	11.14
10		7.00	42.6	46.08	1962	2498	50.0	2.80	1.000	2.80
11		16.00	27.9	30.7	857	1091	33.0	14.66	0.830	12.17
12		15.50	32.7	37.85	1237	1575	39.7	9.84	0.901	8.87
13		18.00	29.5	32.34	955	1216	34.9	14.80	0.850	12.59
14		18.00	32.0	41.83	1336	1702	41.3	10.58	0.917	9.70
15		17.00	37.7	39.46	1486	1893	43.5	8.98	0.939	8.44
16		20.00	42.3	42.81	1810	2305	48.0	8.68	0.982	8.52
17		19.00	33.2	39.39	1307	1665	40.8	11.41	0.913	10.42
18		3.00	30.9	37.91	1170	1490	38.6	2.01	0.890	1.79
19		21.00	39.9	40.49	1616	2058	45.4	10.20	0.957	9.77
20		17.00	30.3	39.42	1196	1523	39.0	11.16	0.894	9.99
			Denotes excluded samples							
		Rejecting lowest and highest results, the **mean $I_{s(50)}$ =**					10.51			

Table C-2: Point load test results for sample: WH02 UW sandstone.

PROJECT: Whitehall Quarry				SAMPLE: WH02			LOCATION: (Sample Location Map)			
LITHOLOGY: UW Greywacke Sandstone				DATE: 05/03/2010						
Test No.	**Type**	**P (kN)**	**D (mm)**	**W (mm)**	**A = WD (mm^2)**	**D_e^2**	**D_e**	**I_s**	**F**	**$I_{s(50)}$ (MPa)**
1	parallel	14.71	33.6	35.59	1196	1523	39.0	9.66	0.894	8.64
2		19.67	38.2	38.03	1454	1851	43.0	10.63	0.935	9.93
3		20.73	32.9	38.38	1263	1608	40.1	12.89	0.906	11.67
4		8.34	26.6	29.35	780	994	31.5	8.39	0.813	6.82
5		13.97	33.3	34.46	1149	1462	38.2	9.55	0.886	8.47
6		12.63	35.4	38.06	1348	1716	41.4	7.36	0.919	6.76
7		20.18	34.9	36.26	1264	1609	40.1	12.54	0.906	11.36
8		8.50	29.9	32.2	963	1226	35.0	6.93	0.852	5.91
9		7.00	31.2	31.36	977	1244	35.3	5.63	0.855	4.81
10		16.00	31.5	34.37	1082	1378	37.1	11.61	0.875	10.15
11		9.00	31.1	32.94	1025	1305	36.1	6.90	0.864	5.96
12		18.00	35.2	36	1269	1615	40.2	11.14	0.906	10.10
13		17.75	35.2	37.57	1322	1683	41.0	10.54	0.915	9.65
14		17.00	35.4	38.7	1368	1742	41.7	9.76	0.922	9.00
15		8.00	35.1	37.55	1318	1678	41.0	4.77	0.914	4.36
16		16	32.71	33.25	1088	1385	37.2	11.55	0.876	10.12
17		14	38.06	35.97	1369	1743	41.8	8.03	0.922	7.41
18		18	35.47	39.28	1393	1774	42.1	10.15	0.926	9.39
19		18.5	35.64	40.11	1430	1820	42.7	10.16	0.931	9.46
20		18	35.2	36.95	1301	1656	40.7	10.87	0.911	9.91
21		17	29.35	33.39	980	1248	35.3	13.62	0.855	11.65
22		15	30.46	30.84	939	1196	34.6	12.54	0.847	10.62
			Denotes excluded samples							
		Rejecting lowest and highest results, the **mean $I_{s(50)}$ =**					8.75			

Table C-3: Point load test results for sample: WH03 UW sandstone.

PROJECT: Whitehall Quarry					SAMPLE: WH03			LOCATION: (Sample Location Map)		
LITHOLOGY: UW Greywacke Sandstone					DATE: 05/03/2010					
Test No.	**Type**	**P (kN)**	**D (mm)**	**W (mm)**	**A = WD (mm^2)**	**D_e^2**	**D_e**	**I_s**	**F**	**$I_{s(50)}$ (MPa)**
1	parallel	14.79	32.6	40.26	1314	1673	40.9	8.84	0.914	8.08
2		15.26	39.3	40.2	1581	2013	44.9	7.58	0.952	7.22
3		14.81	33.5	41.76	1398	1780	42.2	8.32	0.926	7.71
4		10.10	37.7	38.61	1456	1853	43.1	5.45	0.935	5.09
5		18.93	38.0	42.6	1618	2061	45.4	9.19	0.957	8.80
6		13.05	35.4	35.55	1258	1602	40.0	8.14	0.905	7.37
7		12.71	36.0	42.55	1530	1948	44.1	6.53	0.945	6.17
8		12.36	32.5	37.04	1202	1531	39.1	8.07	0.896	7.23
9		16.51	33.2	40.95	1358	1729	41.6	9.55	0.920	8.79
10		11.87	31.7	35.4	1123	1430	37.8	8.30	0.882	7.32
11		9.34	32.5	36.41	1184	1507	38.8	6.20	0.892	5.53
12		16.43	39.7	40.68	1615	2056	45.3	7.99	0.957	7.65
			Denotes excluded samples							
		Rejecting lowest and highest results, the **mean $I_{s(50)}$**					7.3			

Table C-4: Point load test results for sample: WH04 UW sandstone.

PROJECT: Whitehall Quarry				SAMPLE: WH04			LOCATION: (Sample Location Map)			
LITHOLOGY: UW Greywacke Sandstone				DATE: 10/03/2010						
Test No.	**Type**	**P (kN)**	**D (mm)**	**W (mm)**	**A = WD (mm^2)**	**D_e^2**	**D_e**	**I_s**	**F**	**$I_{s(50)}$ (MPa)**
1	parallel	18.00	42.5	42.94	1826	2325	48.2	7.74	0.984	7.62
2		15.00	36.5	37.92	1383	1760	42.0	8.52	0.924	7.87
3		16.50	33.9	34.64	1176	1497	38.7	11.02	0.891	9.82
4		18.00	42.1	45.37	1910	2431	49.3	7.40	0.994	7.36
5		22.00	35.2	43.28	1522	1938	44.0	11.35	0.944	10.72
6		16.00	33.0	38.52	1272	1619	40.2	9.88	0.907	8.96
7		16.00	30.9	33.66	1040	1324	36.4	12.09	0.867	10.48
8		16.25	30.2	30.72	927	1180	34.4	13.77	0.845	11.63
9		18.00	33.5	41.89	1404	1787	42.3	10.07	0.927	9.34
10		13.00	35.9	37.77	1356	1726	41.5	7.53	0.920	6.93
11		17.00	35.6	36.01	1282	1633	40.4	10.41	0.909	9.46
12		17.00	37.0	40.6	1502	1913	43.7	8.89	0.942	8.37
13		17.00	31.7	37.77	1198	1525	39.1	11.15	0.895	9.97
14		16.00	30.6	38.93	1192	1518	39.0	10.54	0.894	9.42
15		16.00	35.6	36.15	1288	1640	40.5	9.76	0.909	8.88
			Denotes excluded samples							
		Rejecting lowest and highest results, the **mean $I_{s(50)}$ =**					9.4			

Table C-5: Point load test results for sample: WH05 UW sandstone.

PROJECT: Whitehall Quarry				SAMPLE: WH05			LOCATION: (Sample Location Map)			
LITHOLOGY: UW Greywacke Sandstone				DATE: 05/03/2010						
Test No.	**Type**	**P (kN)**	**D (mm)**	**W (mm)**	**A = WD (mm^2)**	**D_e^2**	**D_e**	**I_s**	**F**	**$I_{s(50)}$ (MPa)**
1	parallel	14.16	36.6	39.04	1430	1821	42.7	7.78	0.931	7.24
2		6.16	33.1	38.32	1269	1615	40.2	3.81	0.906	3.46
3		14.56	26.3	35.23	928	1182	34.4	12.32	0.845	10.41
4		14.97	29.0	33.63	975	1242	35.2	12.06	0.854	10.30
5		15.89	30.6	31.82	974	1240	35.2	12.82	0.854	10.95
6		14.73	27.5	29.97	824	1049	32.4	14.05	0.822	11.55
7		15.40	32.9	35.55	1170	1490	38.6	10.34	0.890	9.20
8		12.63	31.0	33.43	1035	1317	36.3	9.59	0.866	8.30
9		13.56	27.1	34.66	941	1198	34.6	11.32	0.847	9.59
10		17.12	36.5	43.09	1573	2003	44.7	8.55	0.951	8.13
11		17.42	41.1	41.91	1723	2194	46.8	7.94	0.971	7.71
12		9.73	29.6	29.91	884	1126	33.6	8.64	0.836	7.22
13		18.69	34.5	35.04	1207	1537	39.2	12.16	0.896	10.90
14		8.08	34.4	40.73	1401	1783	42.2	4.53	0.927	4.20
15		13.26	35.3	37.37	1317	1677	41.0	7.91	0.914	7.23
16		13.77	36.9	39.32	1449	1845	43.0	7.46	0.934	6.97
17		8.47	31.3	38.09	1191	1516	38.9	5.59	0.894	4.99
			Denotes excluded samples							
		Rejecting lowest and highest results, the **mean $I_{s(50)}$**					8.93			

Table C-6: Point load test results for sample: ARG01 SW mudstone.

PROJECT: Whitehall Quarry				SAMPLE: WH ARG		LOCATION: Pit 1 (See Sample Location Map)				
LITHOLOGY: Argillaceous Mudstone				DATE: 01/09/2010						
Test No.	**Type**	**P (kN)**	**D (mm)**	**W (mm)**	**A = WD (mm^2)**	**D_e^2**	**D_e**	**I_s**	**F**	**$I_{s(50)}$ (MPa)**
1	perpendicular	4.50	26.10	46.66	1218	1551	39.4	2.90	0.898	2.61
2	perpendicular	0.39	49.00	54.41	2666	3395	58.3	0.11	1.071	0.12
3	perpendicular	1.97	43.02	61.69	2654	3379	58.1	0.58	1.070	0.62
4	perpendicular	0.51	47.89	46.98	2250	2865	53.5	0.18	1.031	0.18
5	perpendicular	0.30	20.39	49.28	1005	1279	35.8	0.23	0.860	0.20
6	perpendicular	0.61	59.97	73.93	4434	5645	75.1	0.11	1.201	0.13
7	perpendicular	0.57	30.95	58.45	1809	2303	48.0	0.25	0.982	0.24
8	perpendicular	1.58	49.37	51.68	2551	3249	57.0	0.49	1.061	0.52
9	perpendicular	0.59	47.56	49.99	2378	3027	55.0	0.19	1.044	0.20
10	perpendicular	0.55	64.28	45.34	2914	3711	60.9	0.15	1.093	0.16
11	perpendicular	0.75	38.34	45.23	1734	2208	47.0	0.34	0.972	0.33
12	perpendicular	0.39	51.06	46.47	2373	3021	55.0	0.13	1.044	0.13
13	perpendicular	0.53	58.10	48.48	2817	3586	59.9	0.15	1.085	0.16
14	perpendicular	0.67	51.58	51.73	2668	3397	58.3	0.20	1.071	0.21
15	perpendicular	0.55	34.07	44.61	1520	1935	44.0	0.28	0.944	0.27
			Denotes excluded result							
		Rejecting lowest and highest results, the **mean $I_{s(50)}$ =**					0.19	MPa		

Figure C-4: Example of argillaceous mudstone.

C3 Moisture Content and Porosity-Density Approximation

Porosity-density testing was carried out on greywacke sandstone samples collected from the pit floor at Whitehall Quarry. Moisture or water content approximations were carried out on argillaceous mudstone samples. These samples are tested in accordance with the ISRM-suggested method for determining water content, porosity, density, absorption and related properties and swelling and slake-durability index properties, 1977.

Table C-7: Moisture content approximation for argillaceous mudstone.

Moisture Content					
Job: MSc Project			Sample: Argillaceous Mudstone		
Location: Whitehall Quarry			Tested By: D. Strang		
Date: 15/03/10					
Test no.		1	2	3	4
Container No.		74	2	49	25
Mass of container an	M_2 (g)	37.6	39.7	50.8	40.6
Mass of container an	M_3 (g)	37.3	39.3	50.3	40.2
Mass of container	M_1 (g)	13.3	13.4	13.5	13.5
Mass of water	$M_2 - M_3$ (g)	0.3	0.4	0.5	0.4
Mass of dried rock	$M_3 - M_1$ (g)	24.0	25.9	36.8	26.7
Water Content	(%)	1.25	1.54	1.36	1.50
Average Moisture Content (%)		1.41			

Table C-8: Porosity-density approximation for samples of UW sandstone.

Porosity Density Approximation

Date: 15/03/2010 Project: Whitehall Quarry

Sample ID	1	2	3	4	5	6
Lithology	Greywacke	Greywacke	Greywacke	Greywacke	Greywacke	Greywacke
Weathering	UW	UW	UW	UW	UW	UW
M_S = Oven Dried Mass (g)	22.2	20.4	20.4	21.2	15.2	13.7
Length 1 (mm)	36.35	35.94	35.28	35.49	29.5	23.19
Length 2 (mm)	36.31	36.11	35.33	35.36	29.72	23.25
Length 3 (mm)	36.05	35.97	35.31	35.36	29.75	23.17
Mean Length (mm)	36.23666667	36.00666667	35.30666667	35.40333333	29.65666667	23.20333333
Width 1 (mm)	17.94	16.17	17.01	17.73	15.39	17.2
Width 2 (mm)	17.91	16.07	17.12	17.74	15.4	17.38
Width 3 (mm)	17.35	16.04	17.04	17.75	15.37	17.22
Mean Width (mm)	17.73333333	16.09333333	17.05666667	17.74	15.38666667	17.26666667
Height 1 (mm)	13.49	13.74	13.42	13.08	12.8	13.02
Height 2 (mm)	13.45	13.69	13.36	13.07	12.82	13.08
Height 3 (mm)	13.44	13.68	13.22	13.23	12.93	13.01
Mean Height (mm)	13.46	13.70333333	13.33333333	13.12666667	12.85	13.03666667
V = Total Volume (m^3)	8649.354124	7940.633415	8029.520593	8244.270384	5863.676591	5223.065177
M_{sat} = Saturated Surface	22.3	20.5	20.5	21.5	15.3	13.8
V_V = Pore Volume (m^3)	0.000100	0.000100	0.000100	0.000300	0.000100	0.000100
n = Porosity (%)	0.0000012	0.0000013	0.0000012	0.0000036	0.0000017	0.0000019
Dry Mass Density (kg/m^3)	0.002566666	0.002569065	0.002540625	0.002571483	0.00259223	0.002622981

	Average	**UW Greywacke**
	Pore Volume (m^3)	0.00013
	Porosity (%)	1.82E-06
	Dry Mass Density (kg/m^3)	0.0026

Table C-9: Porosity-density approximation for samples of SW sandstone.

Porosity Density Approximation				
Date: 15/03/2010		Project: Whitehall Quarry		
Sample ID	1	2	3	4
Lithology	Greywacke	Greywacke	Greywacke	Greywacke
Weathering	SW	SW	SW	SW
M_S = Oven Dried	12.7	10.9	23.8	14.8
Length 1 (mm)	29.44	24.82	27.81	28.45
Length 2 (mm)	29.8	24.41	27.78	27.76
Length 3 (mm)	29.63	24.81	27.81	27.39
Mean Length (mm)	29.62333333	24.68	27.8	27.86666667
Width 1 (mm)	13.77	14.5	19.77	14.42
Width 2 (mm)	13.85	14.53	19.78	15.13
Width 3 (mm)	13.76	14.93	19.3	14.78
Mean Width (mm)	13.79333333	14.65333333	19.61666667	14.77666667
Height 1 (mm)	12.47	11.99	17.04	15.19
Height 2 (mm)	12.36	12.14	17.24	14.56
Height 3 (mm)	12.75	12.15	16.89	14.21
Mean Height (mm)	12.52666667	12.09333333	17.05666667	14.65333333
V = Total Volume	5118.452509	4373.484665	9301.739456	6033.897499
M_{sat} = Saturated	13	11.1	23.9	14.8
V_V = Pore Volume	0.000300	0.000200	0.000100	0.000000
n = Porosity (%)	0.0000059	0.0000046	0.0000011	0.0000000
Dry Mass Density	0.002481219	0.002492292	0.002558661	0.002452809
	Average		**SW Greywacke**	
	Pore Volume (m^3)		0.00015	
	Porosity (%)		2.88E-06	
	Dry Mass Density (kg/m^3)		0.0025	

C4 Shear Box Testing

Shear box testing was carried out on two different samples: a smooth (JRC of 3) joint within unweathered sandstone, and a mudstone bedding plane. Testing was carried out using the Robertson Geologging Ltd Portable Rock Shear Box housed in the Rock Mechanics Laboratory at the University of Canterbury. Testing was carried out in accordance with ISRM 1974.

The key variation between the ISRM and the procedure in this test is the use of one singular sample for all variations in normal force, i.e. one sample was used for all tests on that rock type.

Photographs and test results are shown on the following pages.

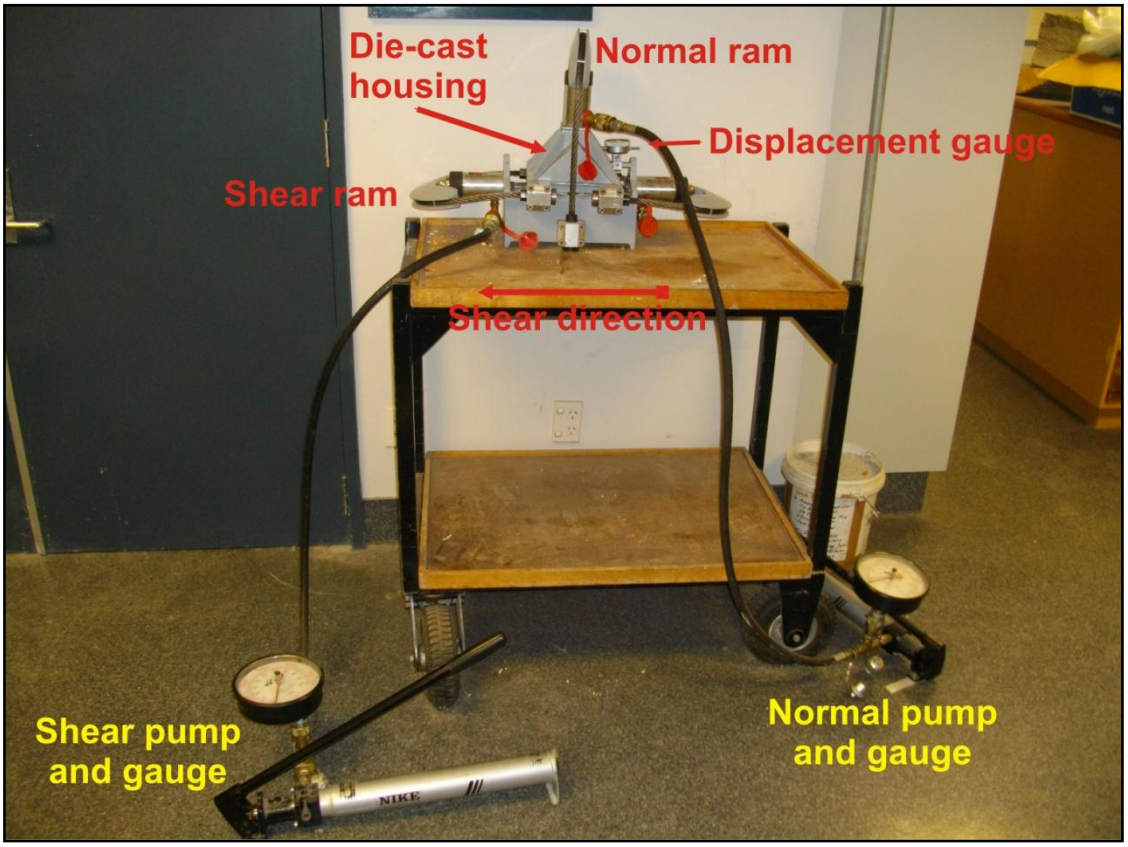

Figure C-5: The Robertson Geologging Ltd Portable Rock Shear Box (Photo: G. Kennedy).

Figure C-6: Argillaceous mudstone sample post shear box testing.

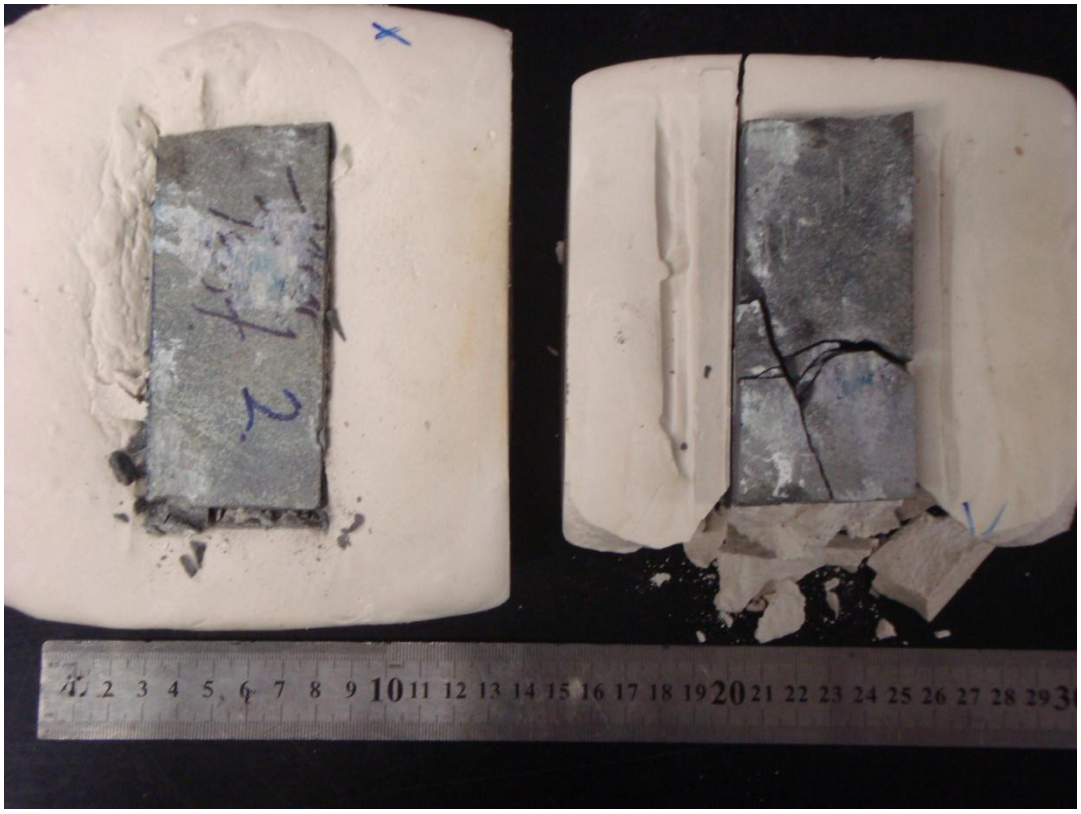

Figure C-7: Sandstone joint post shear box testing.

Table C-10: Shear box testing: Sandstone joint, normal force=2.5 kN.

Shear Box Testing		
Project: MSc Research		Carried Out By: D. Strang
Location: Whitehall Quarry		Date: 05/10/2010
Apparatus: Robertson Geologging Ltd Portable Rock Shear Box		Testing Standard: ISRM 1974
Lithology: UW, very strong, grey, massive, *Greywacke SANDSTONE*.		
Normal Force: 2.5 kN		Consolidation Time: 15min
Time (Minutes)	**Displacement (mm)**	**Shear Force(kN)**
0	0.00	0.0
1	0.30	0.3
2	0.83	0.5
3	1.32	0.6
4	1.95	0.8
5	2.32	0.8
6	2.75	0.9
7	3.08	1.0
8	3.51	1.1
9	3.95	1.2
10	4.29	1.2
11	4.75	1.3
12	5.10	1.3
13	5.55	1.3
14	5.89	1.3
15	6.50	1.4
16	6.95	1.4
17	7.35	1.4
18	7.71	1.4
19	8.07	1.5
20	8.46	1.5
21	8.97	1.6
22	9.40	1.5
23	9.92	1.5
24	8.42	1.5
25	10.89	1.6
26	11.10	1.5
27		
28		
29		
30		
Rate of Displacement (mm/minute)		0.43
Sample Area (m^2)=		0.0045
Residual Normal Stress (kPa) =		**555.6**
Residual Shear Stress (kPa) =		**333.3**

Table C-11: Shear box testing: Sandstone joint, normal force=5.0 kN.

Shear Box Testing		
Project: MSc Research		Carried Out By: D. Strang
Location: Whitehall Quarry		Date: 05/10/2010
Apparatus: Robertson Geologging Ltd Portable Rock Shear Box		Testing Standard: ISRM 1974
Lithology: UW, very strong, grey, massive, *Greywacke SANDSTONE* .		
Normal Force: 5.0 kN		Consolidation Time: 20min
Time (Minutes)	**Displacement (mm)**	**Shear Force(kN)**
0	0.00	0.0
1	0.21	2.0
2	0.44	2.3
3	0.72	2.5
4	1.02	2.7
5	1.35	2.8
6	1.77	2.9
7	2.22	2.9
8	2.65	3.0
9	3.08	3.0
10	3.48	3.0
11	3.85	3.0
12	4.28	3.0
13	4.71	3.1
14	5.12	3.1
15	5.60	3.1
16	6.07	3.1
17	6.55	3.1
18	6.97	3.1
19	7.46	3.2
20	7.82	3.2
21	8.80	3.2
22	9.20	3.2
23	9.80	3.2
24	10.15	3.2
25	10.49	3.2
26	10.85	3.2
27	11.25	3.2
28		
29		
30		
Rate of Displacement (mm/minute)		0.42
Sample Area (m^2)=		0.0045
Residual Normal Stress (kPa) =		**1111.1**
Residual Shear Stress (kPa) =		**711.1**

Table C-12: Shear box testing: Sandstone joint, normal force=7.5 kN.

Shear Box Testing		
Project: MSc Research		Carried Out By: D. Strang
Location: Whitehall Quarry		Date: 05/10/2010
Apparatus: Robertson Geologging Ltd Portable Rock Shear Box		Testing Standard: ISRM 1974
Lithology: UW, very strong, grey, massive, *Greywacke SANDSTONE* .		
Normal Force: 7.5 kN		Consolidation Time: 15min
Time (Minutes)	**Displacement (mm)**	**Shear Force(kN)**
0	0.00	0.0
1	0.25	3.8
2	0.65	4.1
3	0.95	4.3
4	1.37	4.5
5	1.78	4.7
6	2.18	4.8
7	2.54	4.8
8	2.95	4.9
9	3.39	4.8
10	3.83	4.9
11	4.24	4.9
12	4.62	5.0
13	5.02	5.1
14	5.41	5.1
15	5.87	5.0
16	6.25	5.0
17	6.58	5.0
18	6.92	5.0
19	7.29	5.0
20	7.63	5.1
21	7.99	5.1
22	8.30	5.0
23	8.69	5.0
24	9.12	5.0
25	9.53	5.0
26	9.87	5.0
27	10.29	5.0
28	10.70	5.0
29	11.12	5.0
30	11.49	5.0
Rate of Displacement (mm/minute)		0.38
Sample Area (m^2)=		0.0045
Residual Normal Stress (kPa) =		**1666.7**
Residual Shear Stress (kPa) =		**1111.1**

Table C-13: Shear box testing: Sandstone joint, normal force=10.0 kN.

Shear Box Testing		
Project: MSc Research		Carried Out By: D. Strang
Location: Whitehall Quarry		Date: 05/10/2010
Lithology: UW, very strong, grey, massive, *Greywacke SANDSTONE* .		
Normal Force: 10.0 kN		Consolidation Time: 20min
Time (Minutes)	**Displacement (mm)**	**Shear Force(kN)**
0	0.00	0.0
1	0.12	4.2
2	0.38	6.0
3	0.69	6.2
4	1.05	6.3
5	1.42	6.4
6	1.85	6.5
7	2.35	6.5
8	2.80	6.7
9	3.19	6.9
10	3.52	6.9
11	4.05	6.9
12	4.32	7.0
13	4.65	7.0
14	4.95	7.0
15	5.41	7.1
16	5.89	7.1
17	6.10	7.1
18	6.52	7.2
19	7.08	7.1
20	7.48	7.2
21	8.00	7.2
22	8.30	7.2
23	8.81	7.2
24	9.12	7.2
25	9.82	7.2
26	10.33	7.2
27	10.79	7.2
28	11.41	7.2
29		
30		
Rate of Displacement (mm/minute)		0.41
Sample Area (m^2)=		0.0045
Residual Normal Stress (kPa) =		**2222.2**
Residual Shear Stress (kPa) =		**1600.0**

Table C-14: Shear box testing: Sandstone joint, normal force=15.0 kN.

Shear Box Testing		
Project: MSc Research		Carried Out By: D. Strang
Location: Whitehall Quarry		Date: 05/10/2010
Apparatus: Robertson Geologging Ltd Portable Rock Shear Box		Testing Standard: ISRM 1974
Lithology: UW, very strong, grey, massive, *Greywacke SANDSTONE* .		
Normal Force: 15.0 kN		Consolidation Time: 20min
Time (Minutes)	**Displacement (mm)**	**Shear Force(kN)**
0	0.00	0.0
1	0.12	6.0
2	0.31	9.2
3	0.67	9.7
4	1.05	9.9
5	1.43	10.0
6	1.92	10.1
7	2.39	10.0
8	3.05	9.8
9	3.35	9.8
10	3.74	9.9
11	4.19	10.0
12	4.55	10.0
13	4.97	10.2
14	5.48	10.2
15	5.85	10.3
16	6.23	10.3
17	6.63	10.4
18	7.05	10.2
19	7.49	10.0
20	7.88	10.0
21	8.15	10.1
22	8.66	10.1
23	9.02	10.1
24	9.38	10.1
25	9.75	10.1
26	10.10	10.1
27	10.44	10.1
28	10.98	10.1
29	11.25	10.1
30		
Rate of Displacement (mm/minute)		0.39
Sample Area (m^2)=		0.0045
Residual Normal Stress (kPa) =		**3333.3**
Residual Shear Stress (kPa) =		**2244.4**
Comments: Appears plaster mould and sample broke at 7 minutes, a sharp decrease in normal force and cracking has noticed.		

Table C-15: Shear box testing: Mudstone bedding plane, normal force=2.5 kN.

Shear Box Testing		
Project: MSc Research		Carried Out By: D. Strang
Location: Whitehall Quarry		Date: 03/04/2010
Apparatus: Roberston Geologging Ltd Portable Rock Shear Box		Testing Standard: ISRM 1974
Lithology: SW-MW, moderately strong, dark greyish black, finely layered, *MUDSTONE*.		
Normal Force: 2.5 kN		
Time (Minutes)	**Displacement (mm)**	**Shear (kN)**
0	0.00	0.0
1	0.74	0.0
2	1.60	0.3
3	2.64	0.5
4	3.84	0.5
5	5.29	0.6
6	6.49	0.7
7	7.64	0.7
8	8.79	0.8
9	9.71	0.8
10	10.69	0.8
11	11.39	0.9
12	12.19	0.9
13	12.99	0.9
14	13.84	0.9
15	15.04	1.0
16	15.94	1.0
17	17.04	1.0
18	17.89	1.1
19	18.84	1.1
20	19.64	1.1
21	21.04	1.2
22	21.89	1.2
23	22.84	1.2
Rate of Displacement (mm/minute)		0.99
Moisture Content (%) =		1.4
Sample Area (m^2)=		0.007855
Residual Normal Stress (kPa) =		**318.2**
Residual Shear Stress (kPa) =		**152.8**

Table C-16: Shear box testing: Mudstone bedding plane, normal force=5.0 kN.

Shear Box Testing		
Project: MSc Research		Carried Out By: D. Strang
Location: Whitehall Quarry		Date: 03/04/2010
Apparatus: Roberston Geologging Ltd Portable Rock Shear Box		Testing Standard: ISRM 1974
Lithology: SW-MW, moderately strong, dark greyish black, finely layered, *MUDSTONE.*		
Normal Force: 5.0 kN		
Time (Minutes)	**Displacement (mm)**	**Shear (kN)**
0	0.00	0.0
1	1.35	0.5
2	3.10	1.0
3	3.55	1.4
4	4.90	1.7
5	5.30	1.8
6	5.65	1.9
7	5.90	1.9
8	6.30	2.0
9	6.75	2.0
10	7.15	2.1
11	7.55	2.2
12	8.00	2.2
13	8.45	2.2
14	9.20	2.3
15	9.75	2.3
16	10.45	2.4
17	10.95	2.4
18	11.45	2.4
19	12.35	2.5
20	13.10	2.6
21	13.90	2.6
22	14.55	2.7
23	15.00	2.7
24	15.90	2.8
25	16.65	2.8
26	17.35	2.8
27	18.30	2.8
28	19.15	2.8
29	19.90	2.8
30	20.45	2.8
Rate of Displacement (mm/minute) =		0.68
Moisture Content (%) =		1.4
Sample Area (m^2)=		0.007855
Residual Normal Stress (kPa) =		**636.5**
Residual Shear Stress (kPa) =		**356.4**

Table C-17: Shear box testing: Mudstone bedding plane, normal force=7.5 kN.

Shear Box Testing		
Project: MSc Research		Carried Out By: D. Strang
Location: Whitehall Quarry		Date: 03/04/2010
Apparatus: Roberston Geologging Ltd Portable Rock Shear Box		Testing Standard: ISRM 1974
Lithology: SW-MW, moderately strong, dark greyish black, finely layered, *MUDSTONE*.		
Normal Force: 7.5 kN		
Time (Minutes)	**Displacement (mm)**	**Shear (kN)**
0	0.00	0.0
1	1.00	1.0
2	1.55	2.0
3	2.15	2.4
4	2.95	3.0
5	3.80	3.2
6	4.50	3.4
7	5.05	3.5
8	5.85	3.6
9	6.50	3.7
10	7.05	3.8
11	7.70	3.9
12	8.75	3.9
13	9.75	3.9
14	10.50	4.0
15	11.05	4.0
16	11.75	4.1
17	12.40	4.1
18	12.85	4.2
19	13.30	4.2
20	14.00	4.2
21	14.80	4.3
22	15.45	4.4
23	15.95	4.5
24	16.75	4.5
25	17.55	4.6
26	18.30	4.7
27	19.00	4.7
28	20.80	4.8
29	21.90	4.8
30	22.35	4.8
31	23.20	4.8
Rate of Displacement (mm/minute) =		0.77
Moisture Content (%) =		1.4
Sample Area (m^2)=		0.007855
Residual Normal Stress (kPa) =		**954.7**
Residual Shear Stress (kPa) =		**611.0**

C5 Direct Shear Testing

Direct shear testing was conducted on a sample of fault gouge (FG1) to determine the shear strength parameters of the material. This test was carried out using the Direct Shearbox Apparatus WF25300 housed in the Soil Mechanics Laboratory at the University of Canterbury.

Testing was carried out in accordance with the ASTM D2080-04. With key differences, such as, samples were not sieved to leave only clay sized particles (less than 2 µm) but instead samples were tested without changing the particle size or sample saturation. Leading to an extraordinarily high shear strength. Furthermore, there were two samples of the same fault gouge; each sample was loaded twice with different normal forces.

Calculations

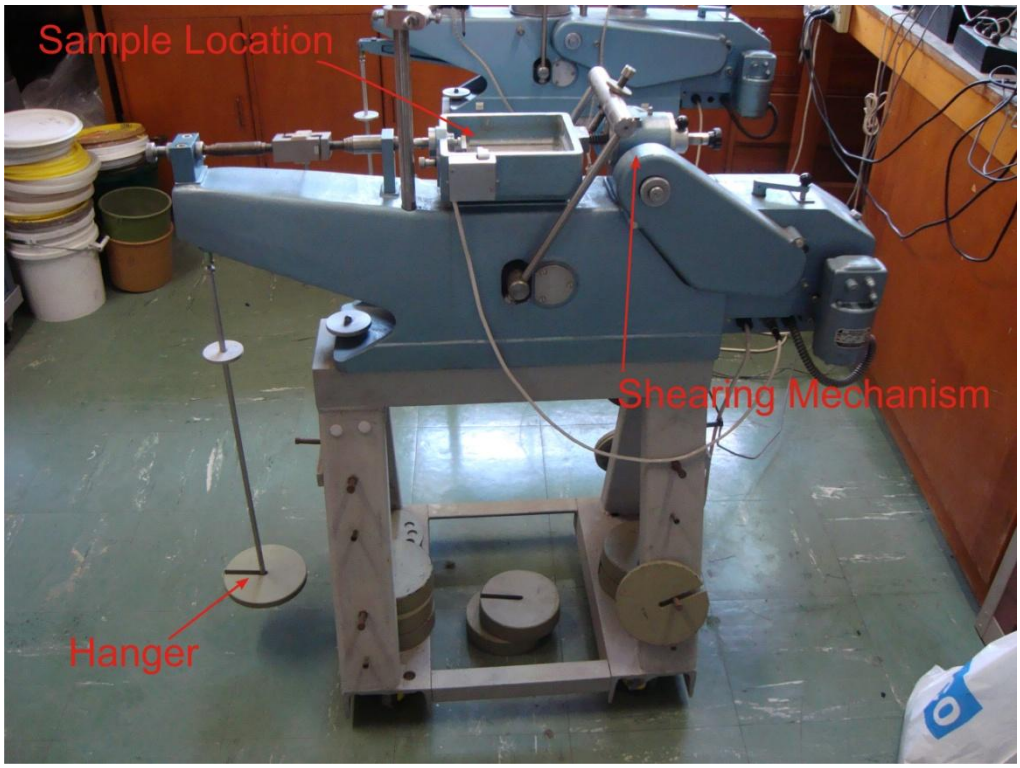

Figure C-8: Direct shear apparatus.

Table C-18: Results for direct shear testing of fault gouge.

Direct Shear Test

Project: MSc Project			Carried out by: D. Strang		
Location: Whitehall Quarry			Date: 23/03/2010		
Equipment: Direct Shearbox Apparatus WF25300					
Lithology: Fault Gouge					
Sample Area	m^2	0.00785398			
Mass on Hanger	(kg)	2	4	6	8
Peak Force	kN	0.1956	0.3902	0.4169	0.7712
Shear Stress	kPa	24.9046	49.6818	53.0814	98.1923
Normal Stress	kPa	25.1448	50.1258	75.1068	100.0877
Cohesion (kPa)	**0.503**				
Angle of Internal Frictic	**41.78°**				
Moisture Content	**Sample 1**				
Container No.		2	25	61	74
Mass of container and	M_2 (g)	31.411	30.435	22.578	25.565
Mass of container and	M_3 (g)	28.344	25.443	21.057	23.9
Mass of container	M_1 (g)	13.51	13.45	13.401	13.314
Mass of water	$M_2 - M_3$ (g)	3.067	4.992	1.521	1.665
Mass of dried soil	$M_3 - M_1$ (g)	14.834	11.993	7.656	10.586
Water Content	(%)	20.7	41.6	19.9	15.7
Water Content (Sample 1), %			2.8		
Note: Sample 1 contained ~5% gravel sized particles.					
Moisture Content	**Sample 2**				
Container No.		25	2	74	10
Mass of container and	M_2 (g)	29.732	22.192	26.455	25.49
Mass of container and	M_3 (g)	27.303	20.878	23.944	23.397
Mass of container	M_1 (g)	13.462	13.512	13.313	13.638
Mass of water	$M_2 - M_3$ (g)	2.429	1.314	2.511	2.093
Mass of dried soil	$M_3 - M_1$ (g)	13.841	7.366	10.631	9.759
Water Content	(%)	17.5	17.8	23.6	21.4
Water Content (Sample 2), %			2.1		

C6 Ring Shear Testing

Ring shear testing was carried out on a fault gouge sampled from a main fault within the quarry (sliding plane of the northern wedge failure). This test was carried out by Works Services Consultancy in 1989.

A summary of results is presented below.

Table C-19: Summary of ring shear result by WSC (1989), fault gouge sample.

Ring Shear				
Project: MSc Project		Carried out by: Works Consultancy Services		
Location: Whitehall Quarry		Date: 06/10/1989		
Equipment: Bromhead Ring Shear Apparatus				
Lithology: Fault Gouge				
Shear Rate: 0.024 deg/min (0.017808 mm/min)				
Normal Stress (kPa)		**Shear Stress (kPa)**		
18.38		6.58		
27.59		9.17		
52.2		16.92		
101.92		29.11		
199.31		52.38		
394.27		94.24		
101.92		27.82		
Cohesion (kPa)	**8.54**			
Angle of Internal I	**15.54**			

C7 Atterberg Limits

The approximation of Atterberg Limits was done in accordance to the NZS 4402:1986 Test 2.1, 2.3, and 2.4. These tests were carried out in the Soil Mechanics Laboratory at the University of Canterbury.

Calculations

Table C-20: Plastic limit for sampled fault gouge.

Determination of the Plastic Limit							
Test 2.3							
Job: MSc Project				Sample: Fault Gouge			
Location: Whitehall Quarry				Tested By: D. Strang			
Date: 17/03/10							
Test no.		1	2	3	4	5	6
Container No.		74	47	10	82	49	2
Mass of container and wet soil	M_2 (g)	15.237	15.642	15.789	15.906	16.008	16.030
Mass of container and dried soil	M_3 (g)	14.771	15.193	15.275	15.357	15.440	15.447
Mass of container	M_1 (g)	13.317	13.786	13.639	13.648	13.571	13.514
Mass of water	$M_2 - M_3$ (g)	0.466	0.449	0.514	0.549	0.568	0.583
Mass of dried soil	$M_3 - M_1$ (g)	1.454	1.407	1.636	1.709	1.869	1.933
Water Content	(%)	32.0	31.9	31.4	32.1	30.4	30.2
Plastic Limit		31					

Table C-21: Liquid limit for sampled fault gouge.

Determination of the Liquid Limit													
Test 2.5													
Job: MSc Project					Sample: Fault Gouge								
Location: Whitehall Quarry					Tested By: D. Strang								
Date: 17/03/10													
Test no.		1			2			3			4		
Initial dial gauge reading	R_1 (mm)	4.97	4.72		5.08	4.85		1.2	1.56		1.35	0.97	1.36
Final dial gauge reading	R_2 (mm)	24.83	24.51		20.24	20.46		23.61	23.74		23	21.81	22.66
Cone Penetration	P (mm)	19.86	19.79		15.16	15.61		22.41	22.18		21.65	20.84	21.3
Average cone penetration	(mm)	19.83			15.39			22.30			21.26		
Container No.		82			49			2			74		
Mass of container and wet soil	M_2 (g)	32.54			30.144			33.04			32.253		
Mass of container and dried soil	M_3 (g)	26.156			24.54			26.403			25.847		
Mass of container	M_1 (g)	13.636			13.561			13.513			13.313		
Mass of water	$M_2 - M_3$ (g)	6.384			5.604			6.637			6.406		
Mass of dried soil	$M_3 - M_1$ (g)	12.520			10.979			12.890			12.534		
Water Content	(%)	50.99			51.04			51.49			51.11		
Liquid Limit		51											

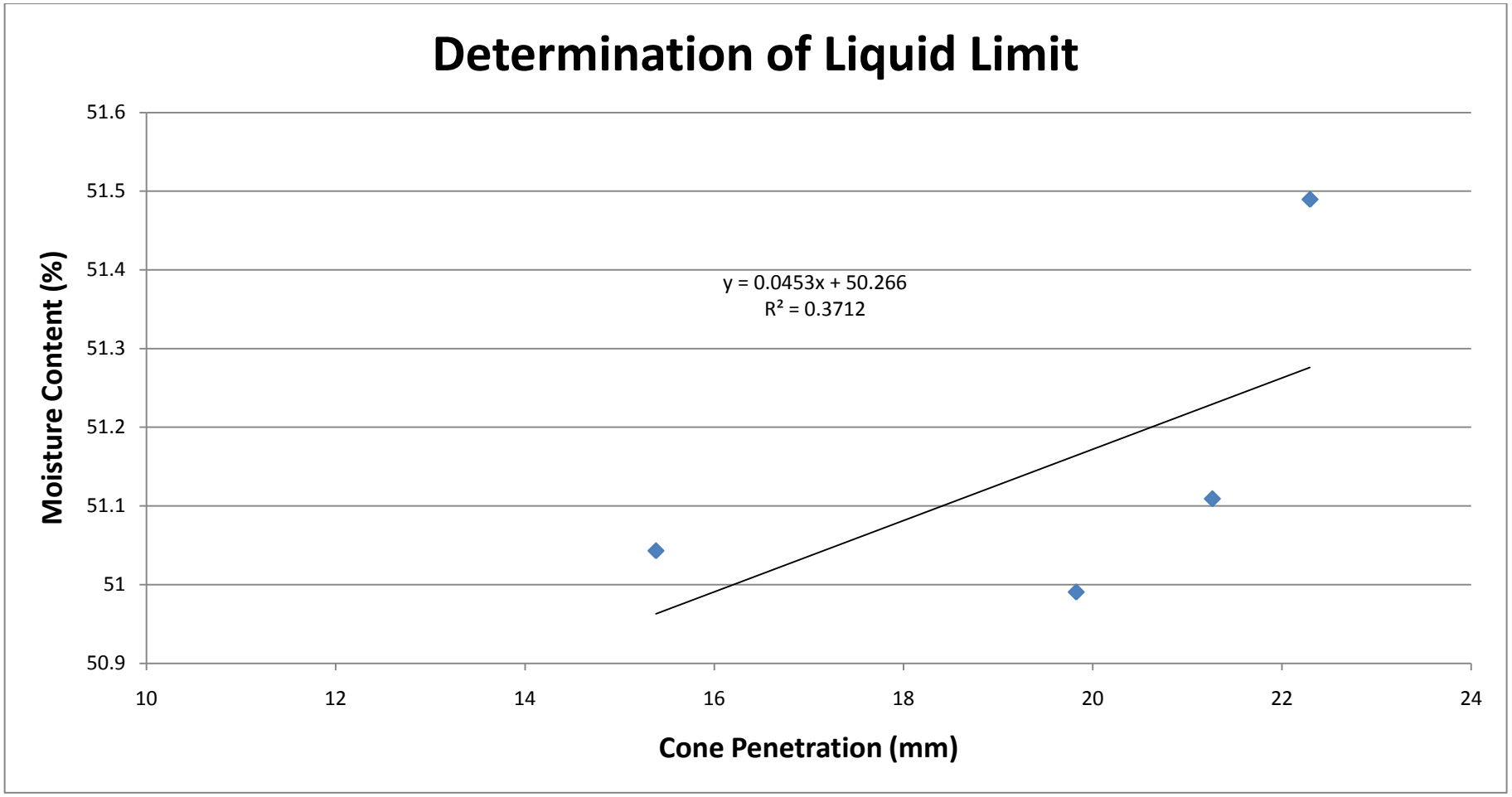

Figure C-9: Plot showing cone penetration vs moisture content.

C8 X-ray Diffraction Analysis

X-ray diffraction (XRD) analysis was carried out using the Phillips PW1729/PW1717 x-ray diffractometer. XRD analysis was carried out on whole samples to determine the mineralogy of fault gouge contents.

XRD diffractograms are presented on the following pages.

Figure C-10: Fault gouge sample, dry conditions.

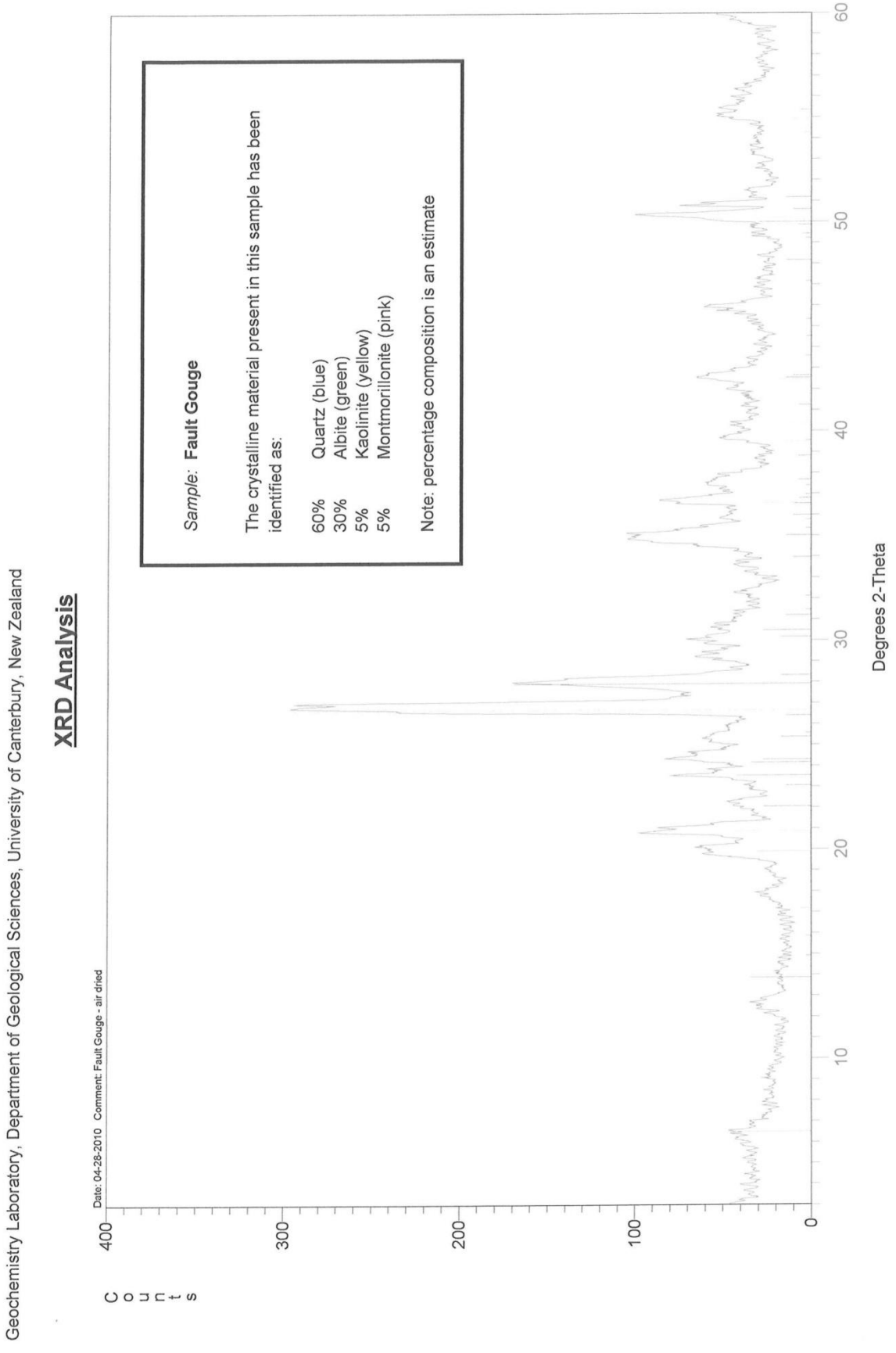

Figure C-11: XRD diffractogram, FG1 (Plane A, Northern Wedge Failure).

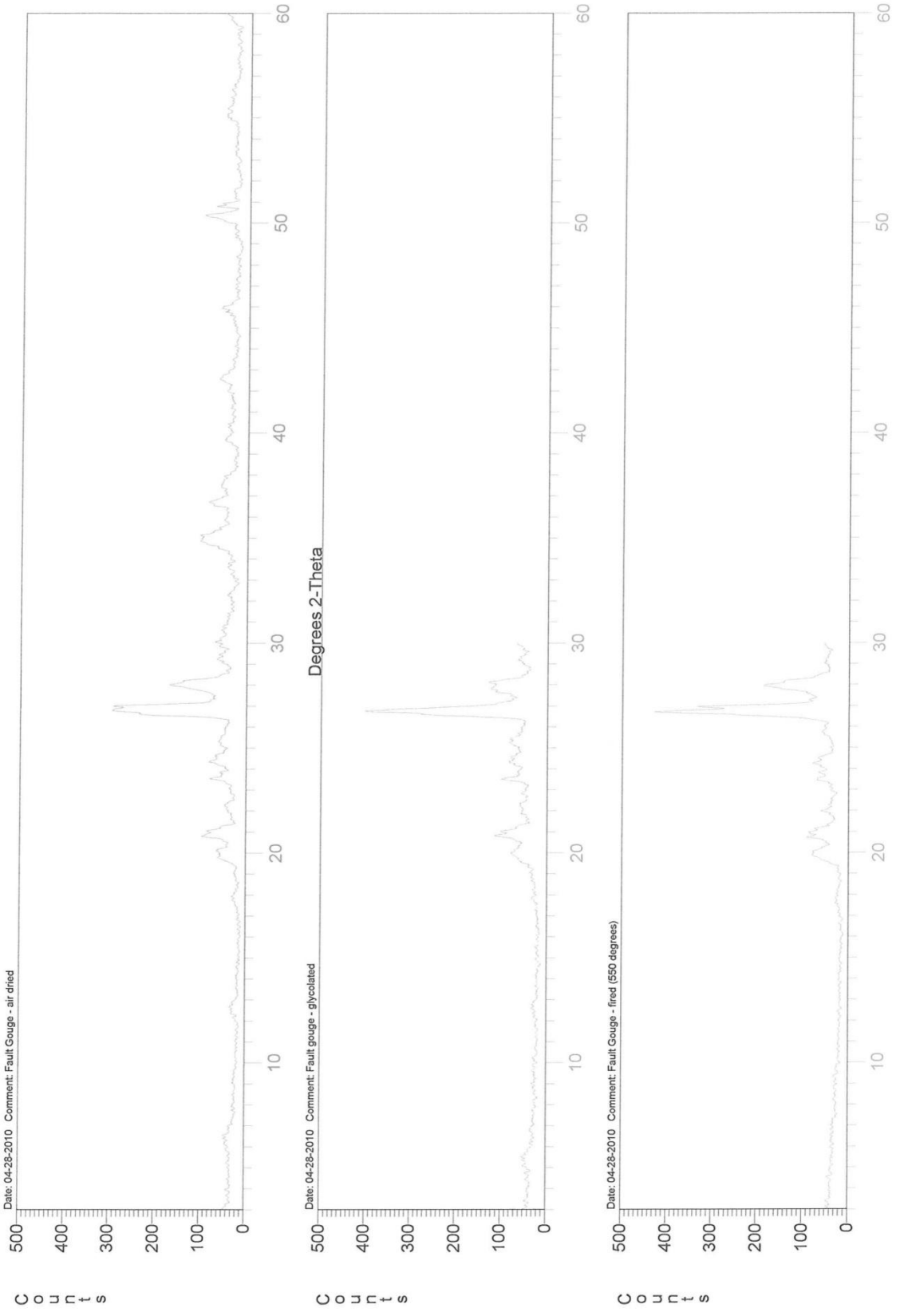

Figure C-12: XRD diffractogram, FG1 (Plane A, Northern Wedge Failure).

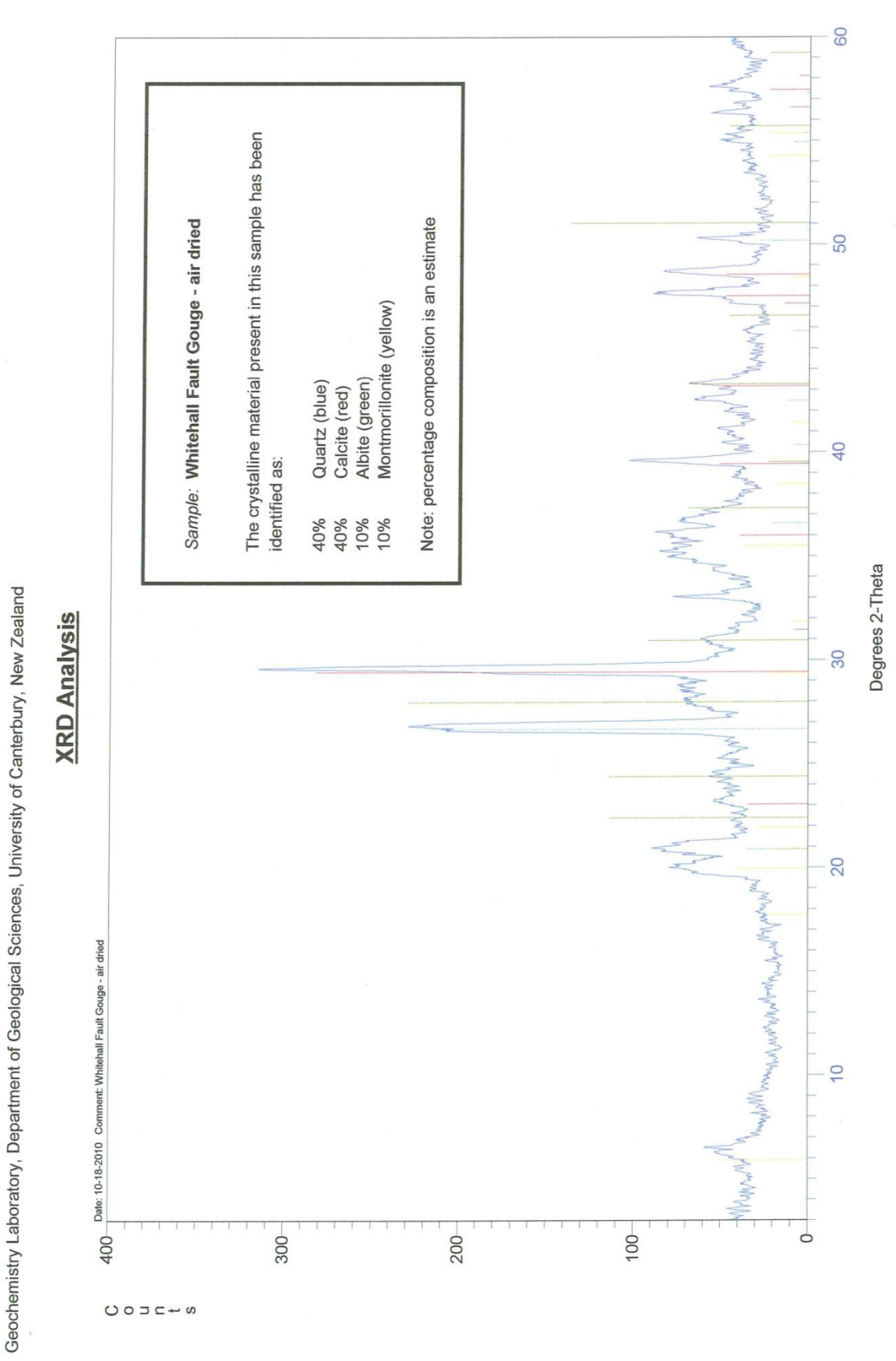

Figure C-13: XRD diffractogram, FG2 (Main Quarry Shear Zone, MQSZ).

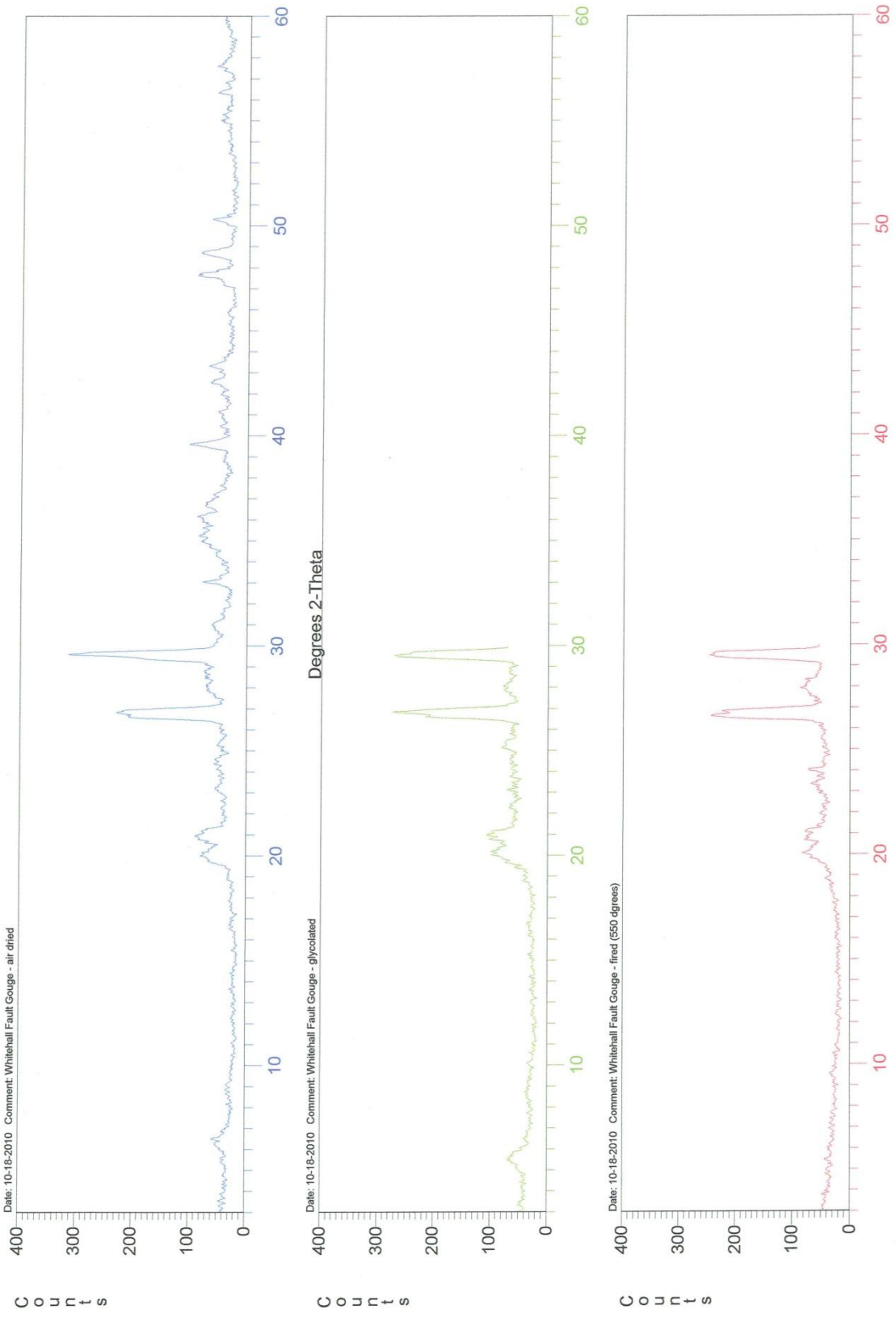

Figure C-14: XRD diffractogram, FG2 (Main Quarry Shear Zone, MQSZ).

C9 Patton's Law

Patton's Law is applied to raw shear strength data obtained from laboratory testing. The following calculations were carried out to approximate the effective angle of internal friction for the two discontinuities below:

BEDDING PLANE:

- Basic friction angle, 31^{o}
- Roughness, smooth (Basic friction angle + 2)
- Interlimb angle, 178^{o}

SANDSTONE JOINT:

- Basic friction angle, 34^{o}
- Roughness, smooth (Basic friction angle + 2)
- Interlimb angle, 178^{o}

Appendix D: Stereographic Projection Techniques and Failure Modes

D1 Pit slope failure terminology

NAME	DEFINITION
Crown	Practically undisplaced material adjacent to the highest parts of the main scarp.
Main Scarp	Steep surface on undisturbed ground at upper edge of landslide caused by movement of displaced material away from undisturbed ground; it is visable part of surface of rupture.
Top	Highest point of contact between displaced material and main scarp.
Head	Upper parts of landslide along contact between displaced and head scarp.
Minor Scarp	Steep surface on displaced material of landslide produced by differential movements within displaced material.
Main Body	Part of displaced material of landslide that overlies surface of rutpture between main scarp and toe of surface rupture.
Foot	Portion of landslide that has moved beyond toe of surface of rupture and overlies original ground surface.
Tip	Point on toe farthest from top of landslide.
Toe	Lower, usually curved margin of displaced material of a landslide, most distant from main scarp.
Surface of Rupture	Surface that forms (or has formed) lower boundary of displaced material below original ground surface; mechanical idealization of surface is called slip surface.
Toe of surface of Rupture	Intersection (usually buried) between lower part of surface of rupture of a landslide and original ground surface.
Surface of Seperation	Part of original ground surface now overlain by foot of landslide.
Displced Material	Material displaced from its original position on slope by movement in landslide; forms both depleted mass and accumulation.
Original Ground Surface	Surface of slope that existed before landslide took place.

D2 The Fisher distribution

The Fisher method for contouring was used throughout this thesis as opposed to the generally accepted Schmidt method. Under the Fisher method each pole is assigned a normal influence (or Fisher Distribution), rather than a point value as in the Schmidt method. The real advantage of the Fisher method over the Schmidt method is that it smooths density plots for sparse data sets (Hoek & Diederichs, 1989).

For a more detailed description on the mathematics behind the Fisher distribution the reader is referred to Cheeney (1982).

D3 Determination of the counting circle

The size of the counting circle used in contour plots was calculated in accordance with the method outlined by Kamb (1959) where:

For a given area A, expressed as its fraction of the area of the hemisphere, the distribution of *n* values for random samples of size *N* is binomial, and for the population without preferred orientation we find:

$$\sigma = \sqrt{\frac{E}{N}}$$

Where E=NA

Setting σ/E=1/3, we compute for a given fabric with *N* points the appropriate area *A* of the computer to be used in preparing the density diagram.

D4 Calculation of Terzaghi Weighting Function

The geometric weighting function in Dips is calculated as follows (Hoek & Diederichs, 1989):

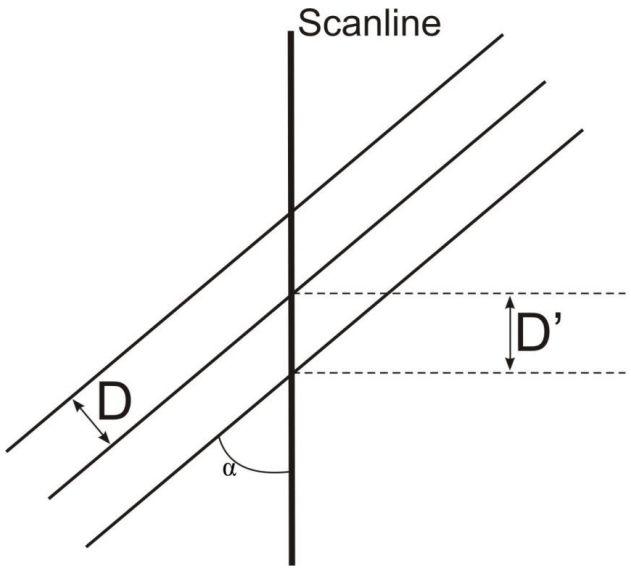

α	Minimum angle between plane and traverse
D’	Apparent spacing along traverse
D = D’sin α = D’ 1/W	True spacing of discontinuity set
R’ = 1/D’	Apparent density of joint population
R = 1/D = 1/D’ sin α = D’ cosec α	True density of joint population
W = (1) cosec α	Weighting applied to individual pole before density calculation

Since the weighting function tends to infinity as α approaches 0^o, a maximum weighting must be set to prevent unreasonable results. This maximum limit corresponds to a minimum angle, before the weighting function is applied. For the interpretation of structural domains the minimum α angle before the weighting function was applied was set to 15^o.

D5 Bedding Terminology

BEDDING INCLINATION TERMS

Term	Inclination (from horizontal)
Sub-horizontal	0° – 5°
Gently inclined	6° – 15°
Moderately inclined	16° – 30°
Steeply inclined	31° – 60°
Very steeply inclined	61° – 80°
Sub-vertical	81° – 90°

Appendix E: Structural Domain Data

E1 Northern Domain

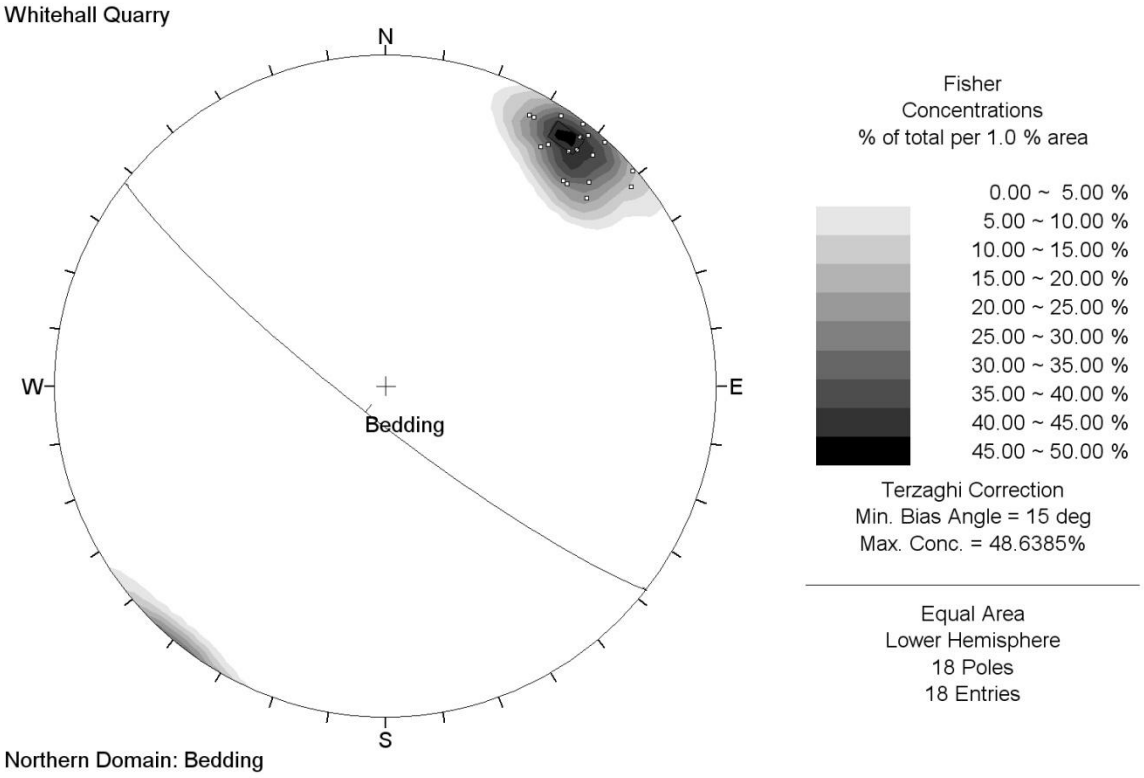

Figure E-1: Stereoplot showing bedding of the Northern Domain.

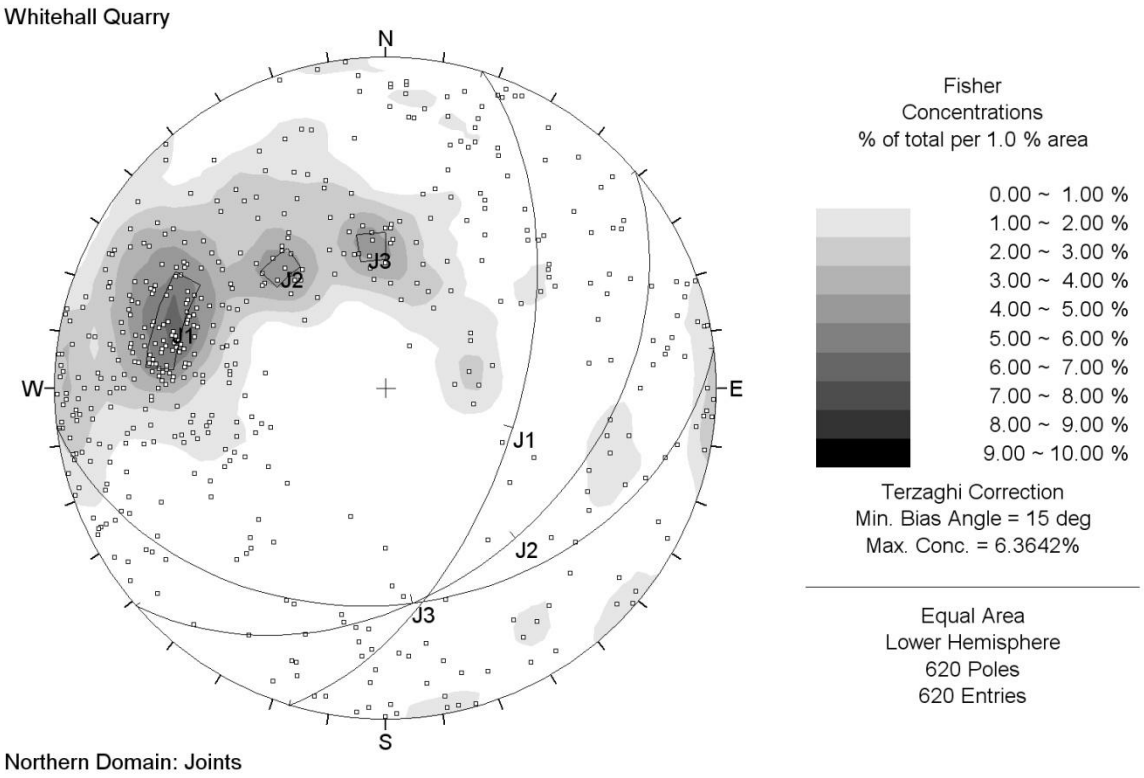

Figure E-2: Stereoplot showing joint sets of the Northern Domain.

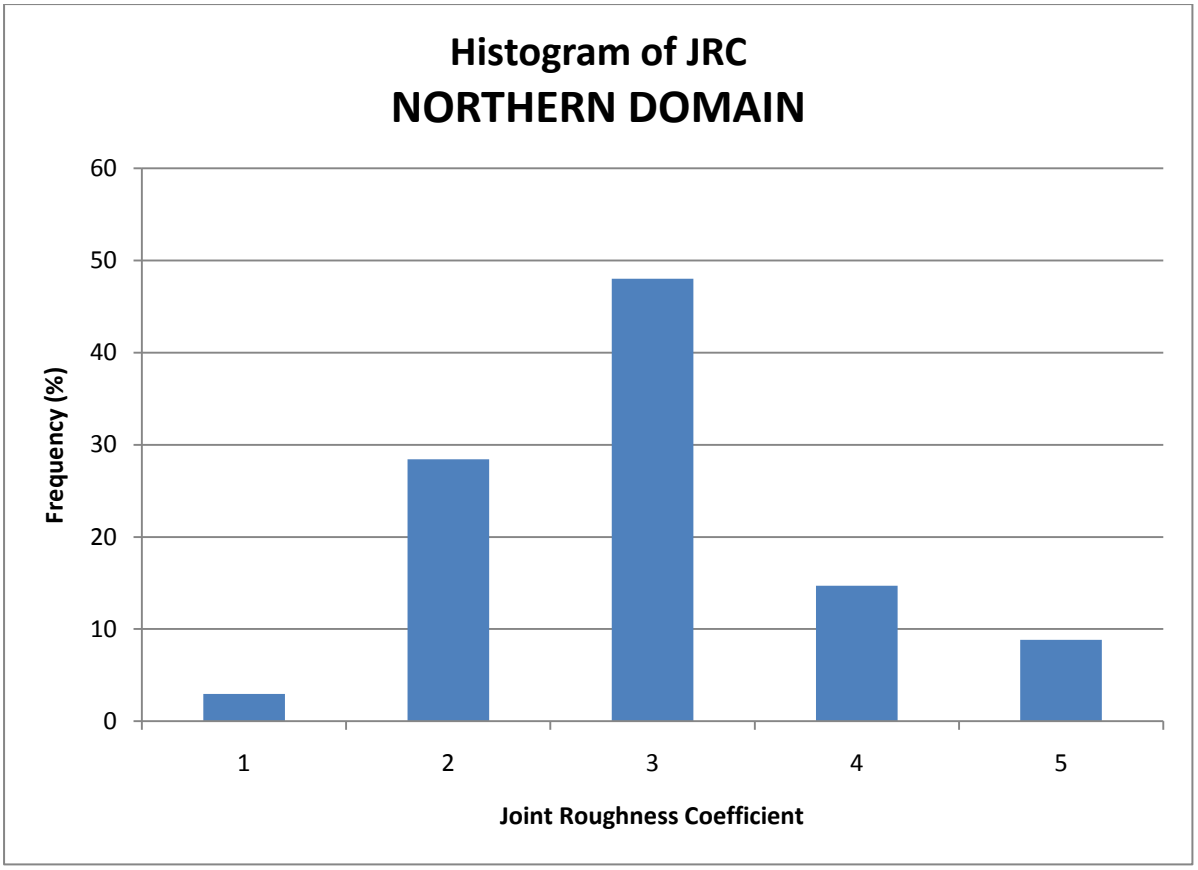

Figure E-3: Histogram showing the distribution of joint roughness coefficient (JRC) for the Northern Domain.

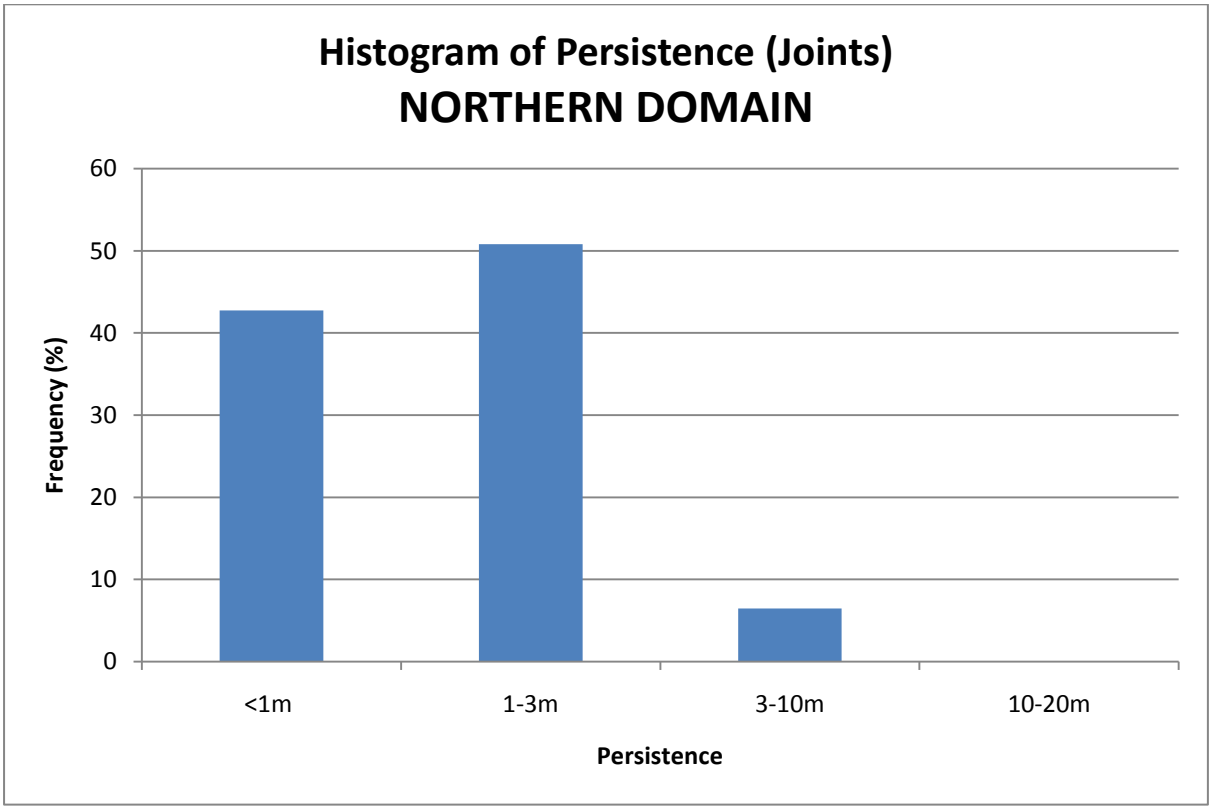

Figure E-4: Histogram showing the distribution of joint persistence for the Northern Domain.

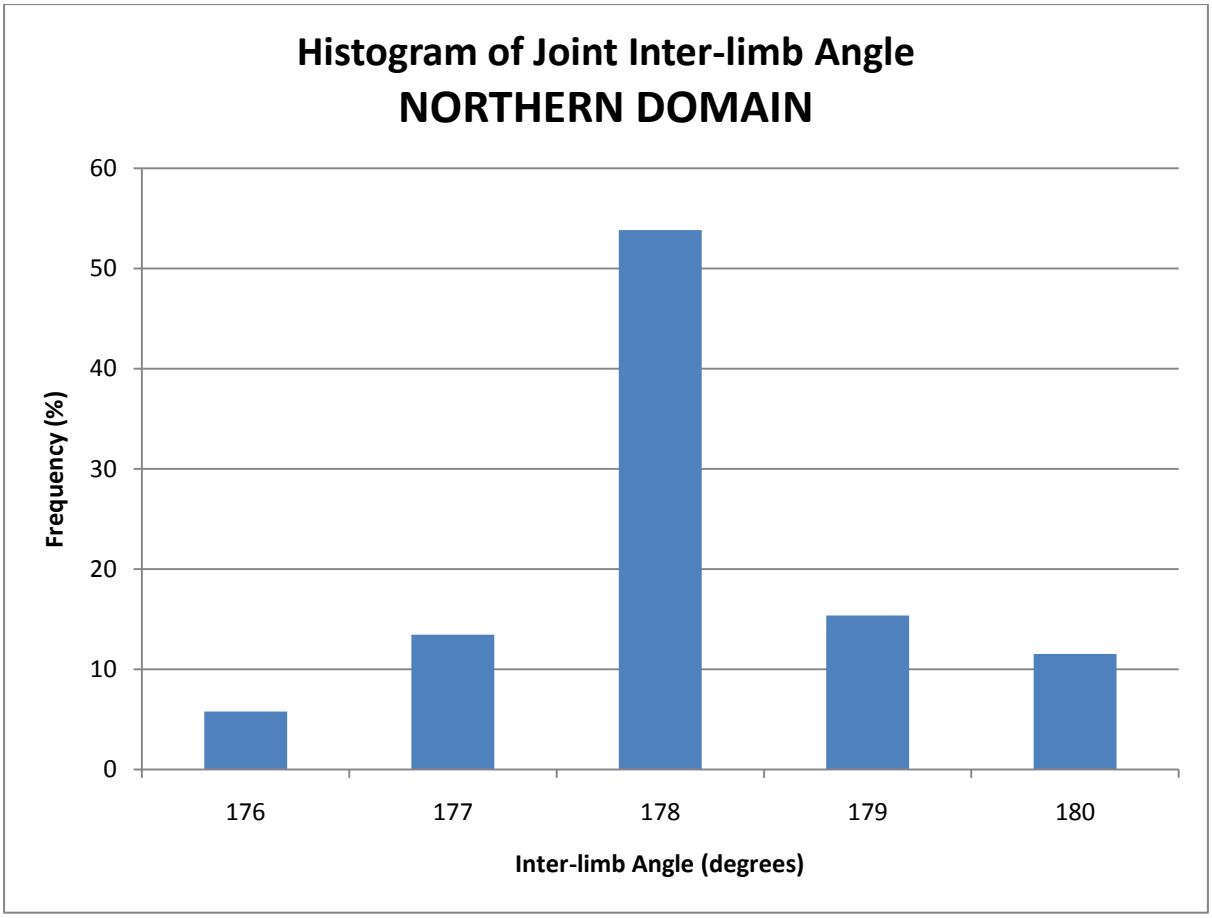

Figure E-5: Histogram showing the distribution of joint inter-limb angle for the Northern Domain.

E2 Southern Domain

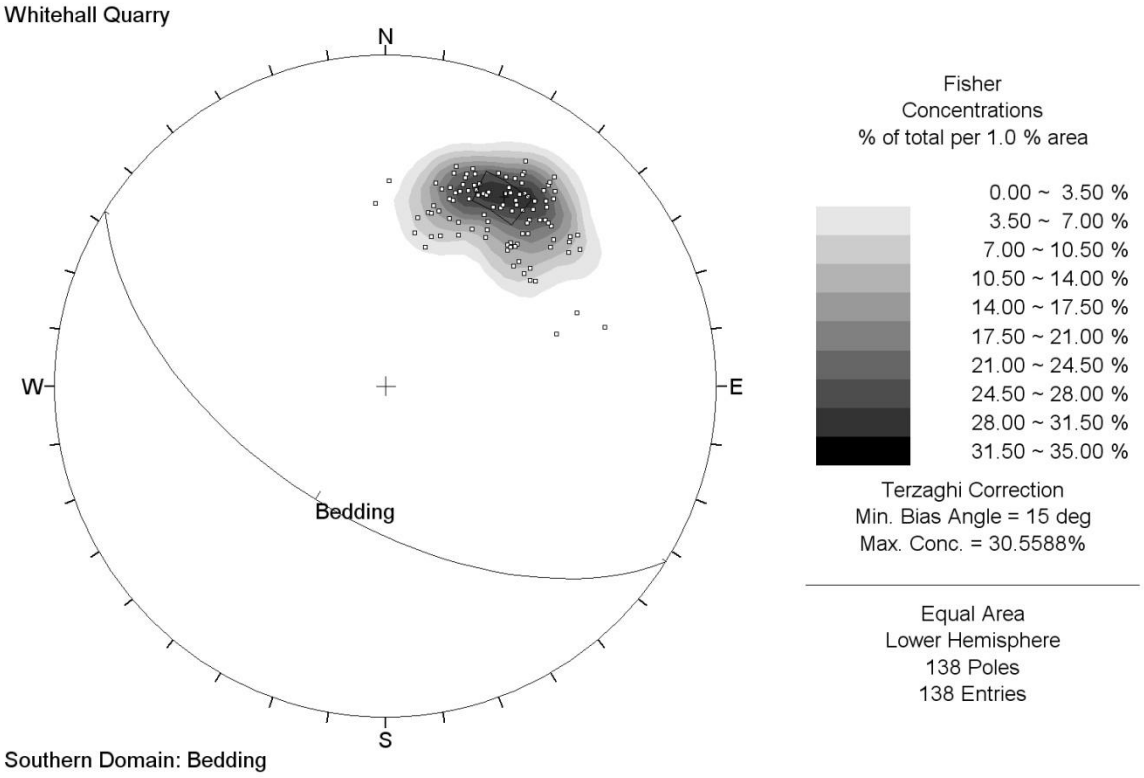

Figure E-6: Stereoplot showing bedding of the Southern Domain.

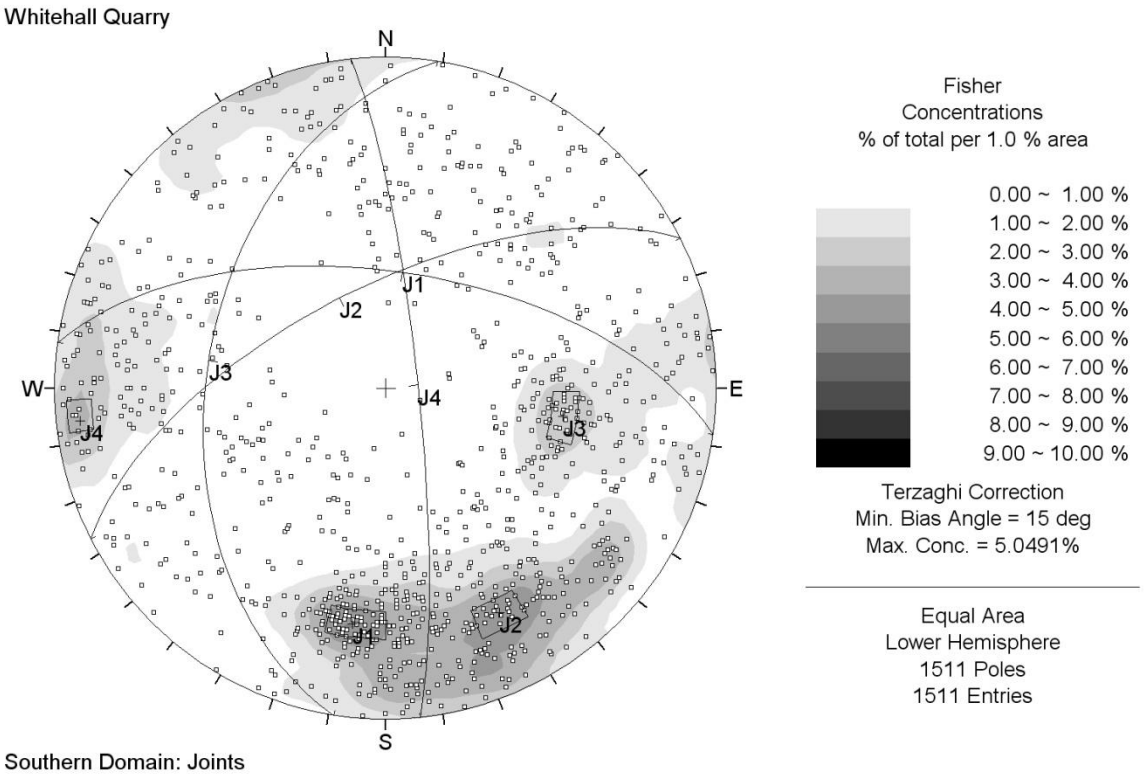

Figure E-7: Stereoplot showing joint sets of the Southern Domain.

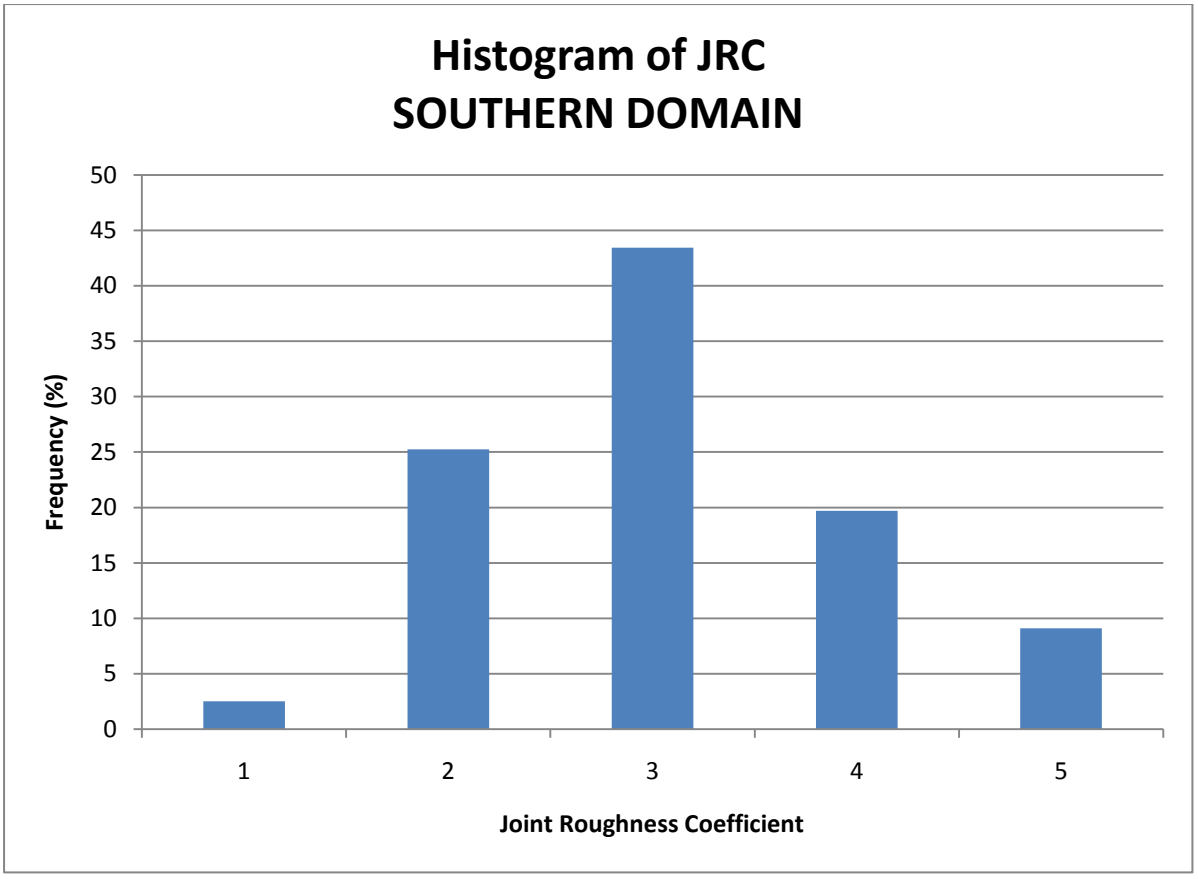

Figure E-8: Histogram showing the distribution of joint roughness coefficient (JRC) for the Southern Domain.

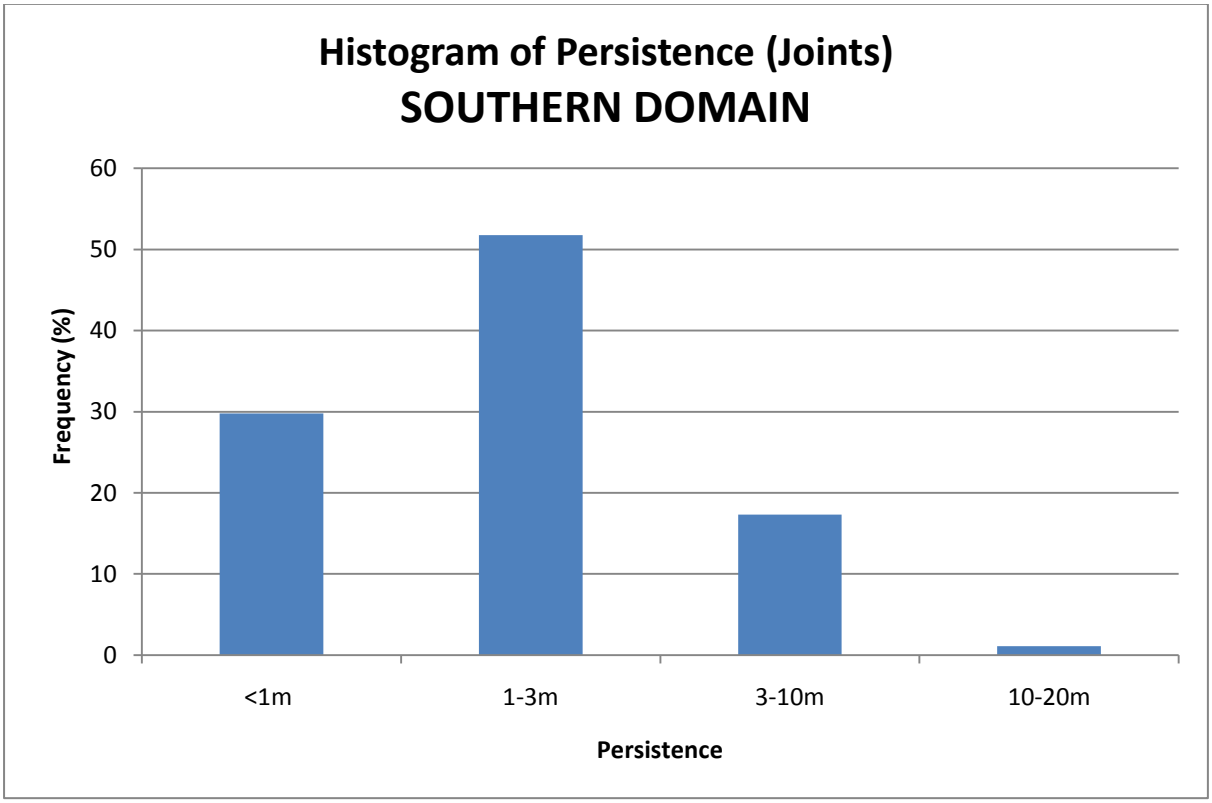

Figure E-9: Histogram showing the distribution of joint persistence for the Southern Domain.

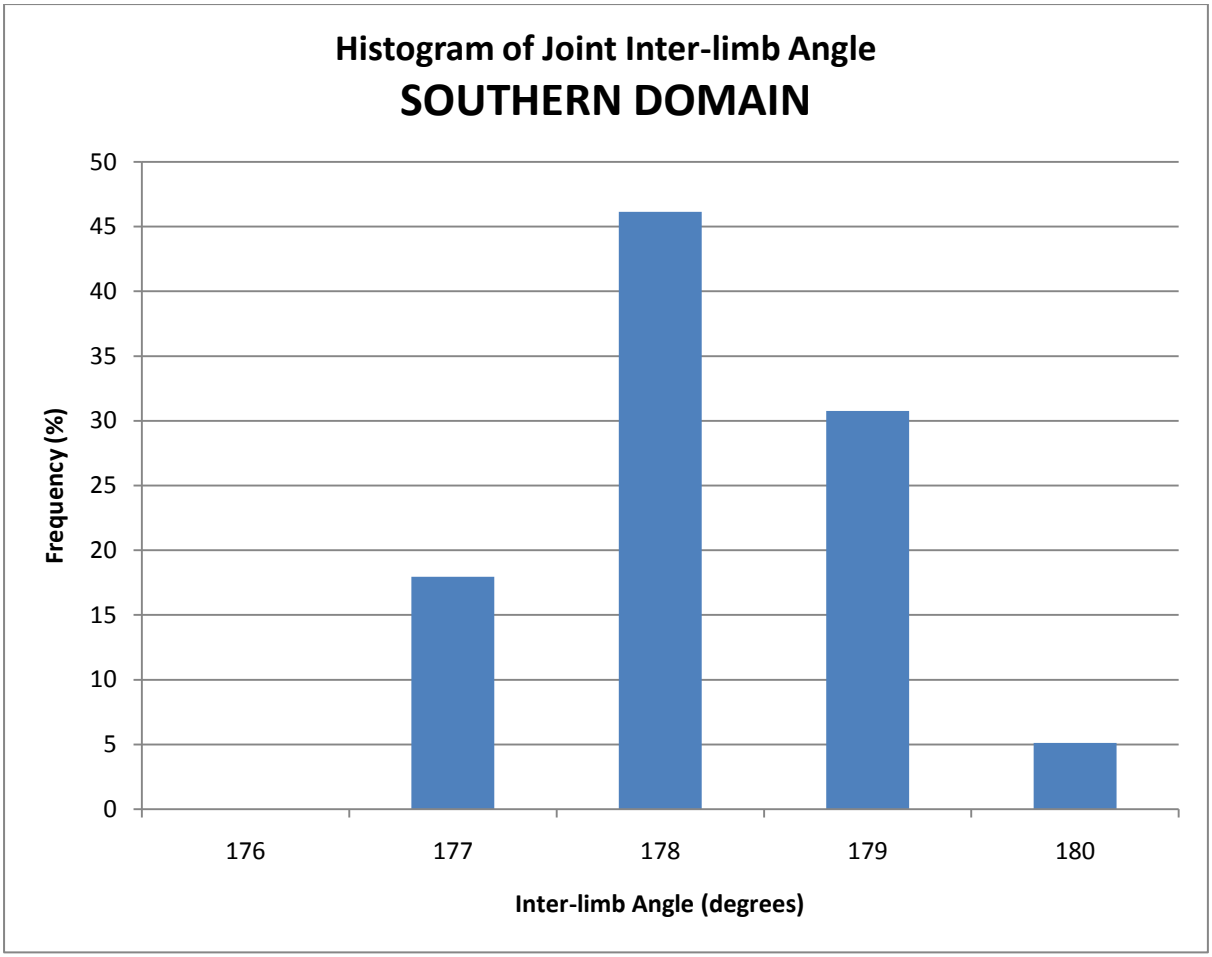

Figure E-10: Histogram showing the distribution of joint inter-limb angle for the Southern Domain.

Appendix F: Northern Wedge Failure Data

F1 Previous Data

The following pages present maps and figures obtained from previous investigations into the stability of the Northern Wedge Failure. These investigations were carried out by John Ashby (1991) and Hancock Consultants Ltd (1989).

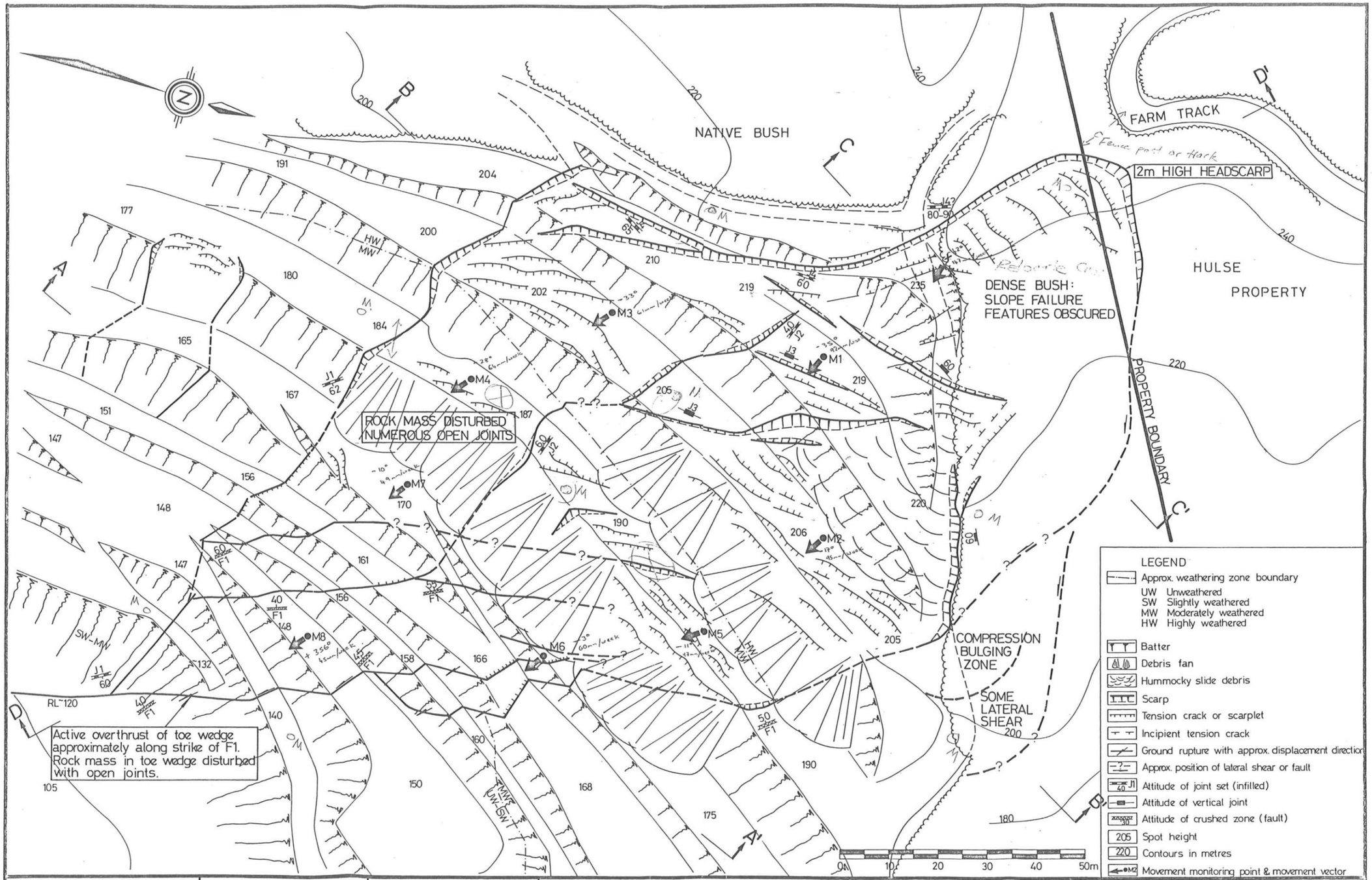

HANCOCK CONSULTANTS LTD. 212 COLLINGWOOD ST HAMILTON ph. (071) 380 391	PERRY CASTLE	FIRTH AGGREGATES WHITEHALL QUARRY CAMBRIDGE	**Engineering Geology Plan** **Quarry Slope Failure**	Geology Neil Crampton Drawn Neil Crampton Traced Janet Barratt Date 25-10-89	SCALE 1:500 PLAN 1

SECTION D-D'

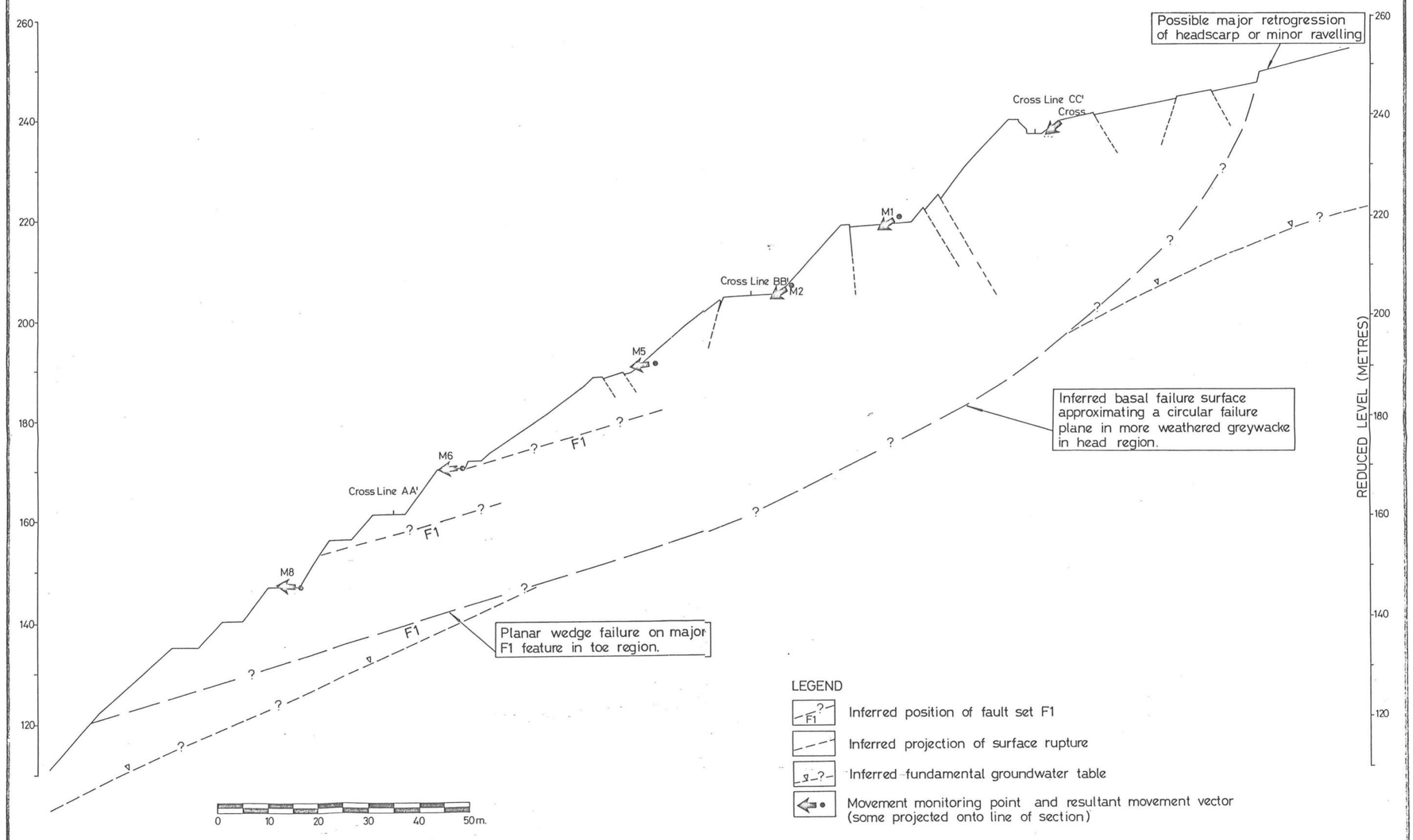

HANCOCK CONSULTANTS LTD. 212 COLLINGWOOD ST HAMILTON ph. (071) 380 391	PERRY CASTLE	FIRTH AGGREGATES WHITEHALL QUARRY CAMBRIDGE	LONG SECTION D-D' QUARRY SLOPE FAILURE	Geology Neil Crampton Drawn Neil Crampton Traced Janet Barratt Date 25-10-89	SCALE 1:500 H=V PLAN 3

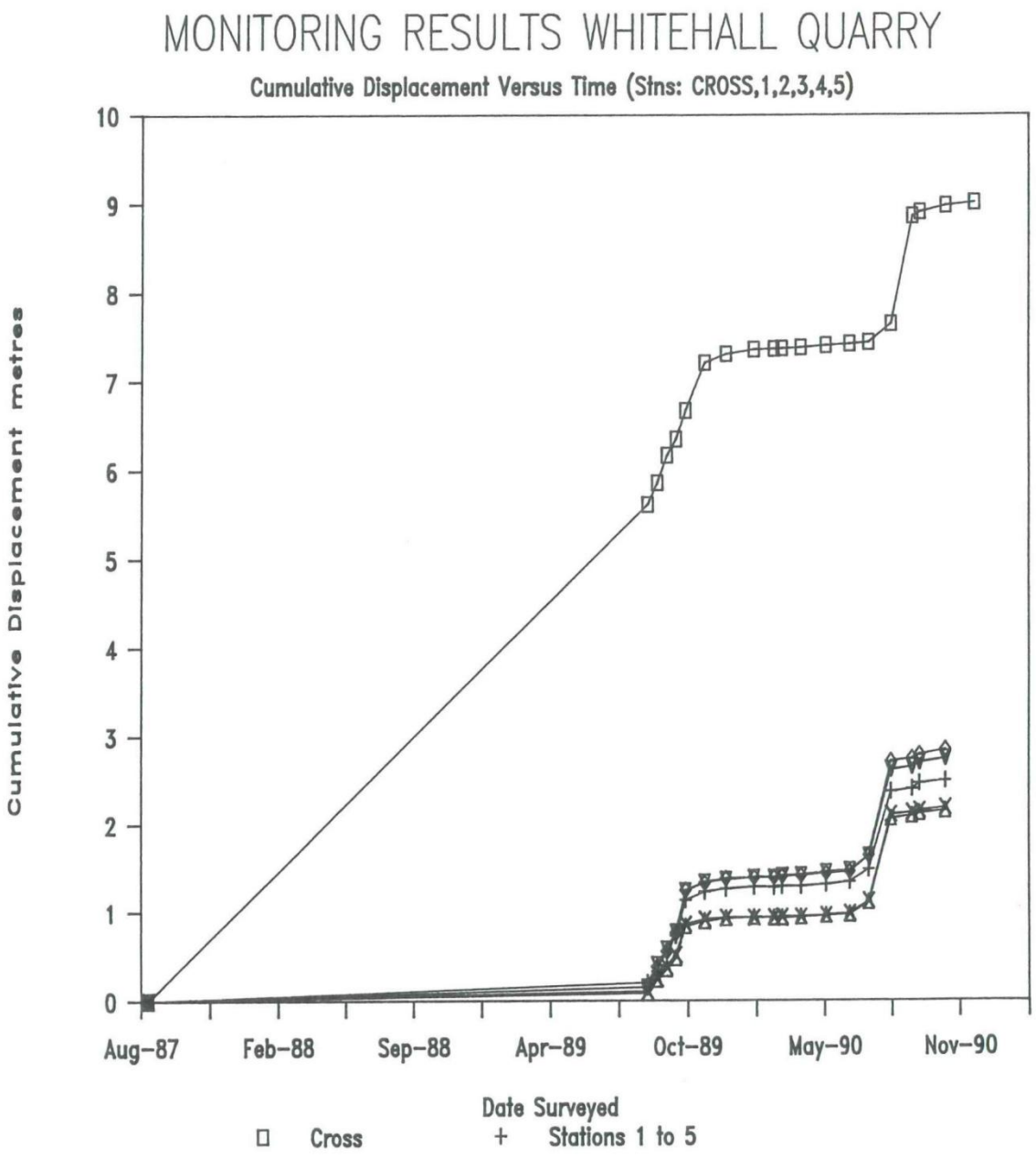

Figure F-1: Plot showing cumulative displacement versus time for the Northern Wedge Failure (Ashby, 1991).

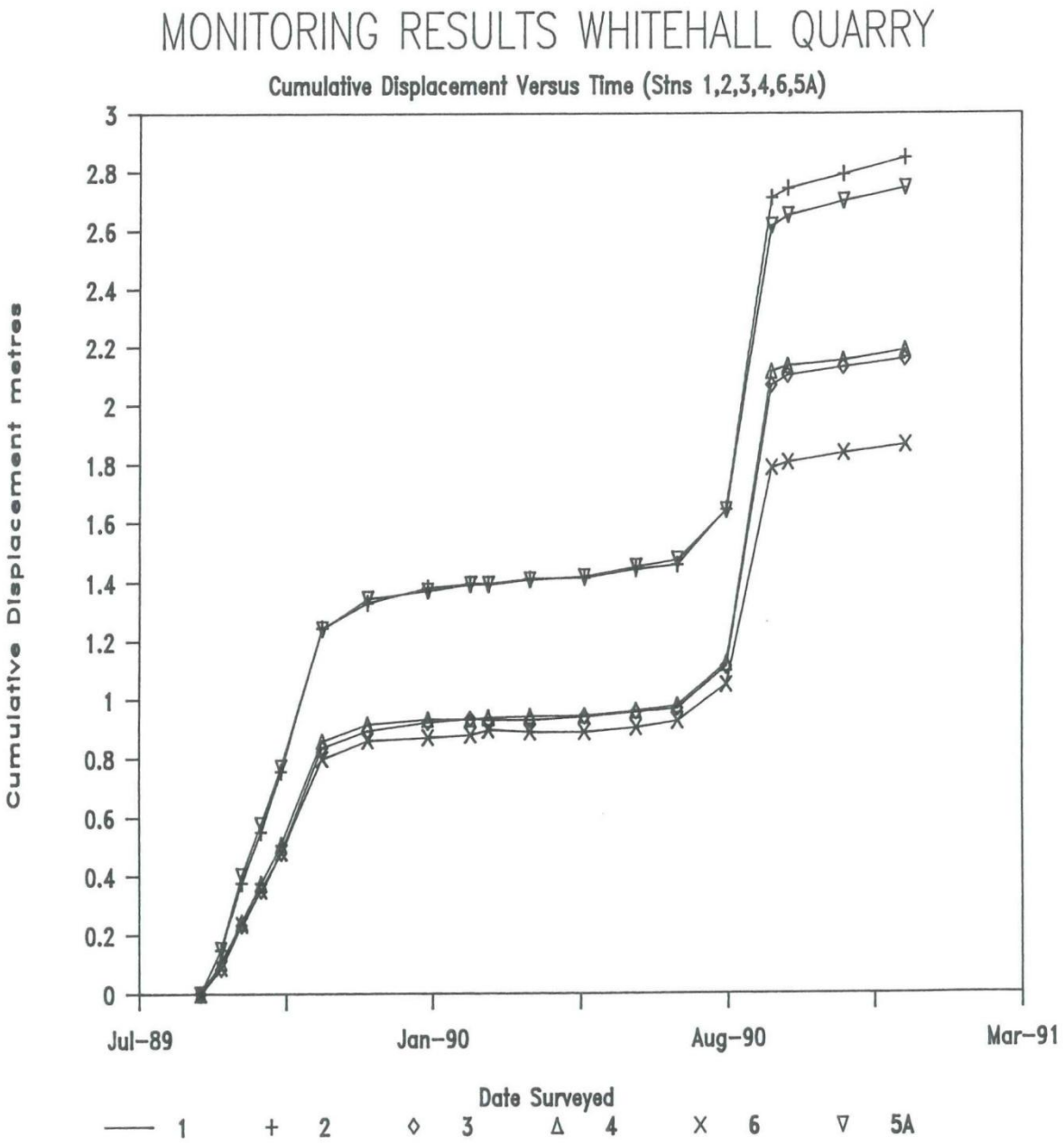

Figure F-2: Plot showing cumulative displacement versus time for the Northern Wedge Failure (Ashby, 1991).

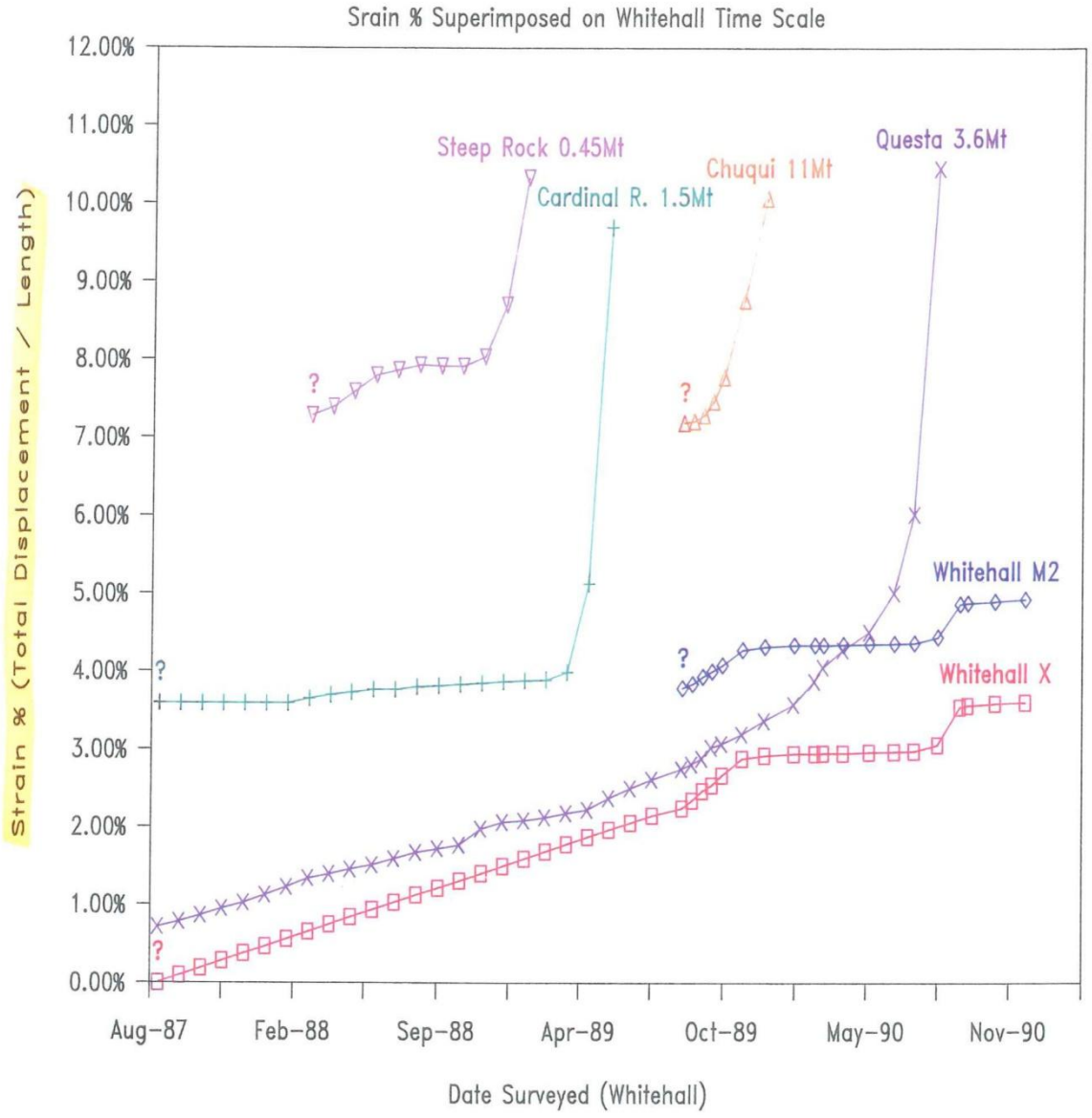

Figure F-3: Plot of recorded strain versus time for other similar wedge failures.

F2 Electronic Distance Measurement (EDM) Data

Electronic Distance Measurement Survey

Survey 1		Date: 11/01/2010						
	Easting	Northing	Elevation (m)					
1	2735767.601	6365552.775	90.27831					
2	2735754.852	6365540.46	92.49516					
3	2735762.824	6365541.271	92.00335					
4	2735779.814	6365551.896	90.59146					
5	2735788.46	6365556.658	90.42611					
6	2735911.934	6365445.524	85.86318					
Survey 2		Date: 09/04/2010			**Comparison of Survey 1 & 2**			
	Easting	Northing	Elevation (m)		Easting Difference	Northing Difference	Average m/88 days	
1	2735767.668	6365552.752	90.27346		0.06727	-0.022799999	East	North
2	2735754.893	6365540.418	92.48637		0.04047	-0.04214	0.05015	-0.03205
3	2735762.871	6365541.236	91.78797		0.04763	-0.034829999		
4	2735779.856	6365551.873	90.58356		0.04202	-0.0228	Average mm/month	
5	2735788.514	6365556.621	90.42432		0.05338	-0.03767	15.95809165	-10.19709132
6	2735911.934	6365445.524	85.86182		0	0		
Survey 3		Date: 01/09/2010			**Comparison of Survey 2 & 3**			
	Easting	Northing	Elevation (m)		Easting Difference	Northing Difference	Average m/145 days	
1	2735767.764	6365552.718	92.50309		0.09544	-0.033860001	East	North
2	2735754.989	6365540.328	92.00337		0.09672	-0.08982	0.08927	-0.06014
3	2735762.956	6365541.175	90.59615		0.08436	-0.061650001		
4	2735779.934	6365551.814	90.43054		0.07731	-0.05911	Average mm/month	
5	2735788.606	6365556.564	90.28515		0.09252	-0.05628	17.23834625	-11.61401481
6	2735911.934	6365445.524	85.87794		0	0		
Survey 4		Date:25/11/2010			**Comparison of Survey 3 & 4**			
	Easting	Northing	Elevation (m)		Easting Difference	Northing Difference	Average m/85 days	
1	2735767.796	6365552.687	92.50213		0.03230	-0.03170	East	North
2	2735755.039	6365540.295	92.00235		0.04923	-0.03279	0.04541	-0.03430
3	2735762.987	6365541.144	90.59327		0.03130	-0.03035		
4	2735779.986	6365551.773	90.43123		0.05193	-0.04079	Average mm/month	
5	2735788.669	6365556.528	90.28519		0.06230	-0.03589	14.95924846	-11.30014214
6	2735911.934	6365445.524	85.87794		0.00000	0.00000		
Total Displacement (mm)								
	Easting	Northing						
1	195.01000	-88.36000			Mean Rate Of Displacement (mm/month)			
2	186.42000	-164.75000			Easting	Northing		
3	163.29000	-126.83000			13.56239096	-9.281677838		
4	171.26000	-122.70000						
5	208.20000	-129.84000			**Resultant Displacement = 16.43 mm/month**			
6	0.00000	0.00000			**Resultant Direction = 124.4**			
Mean	154.03000	-105.41333						

F3 SWedge Models

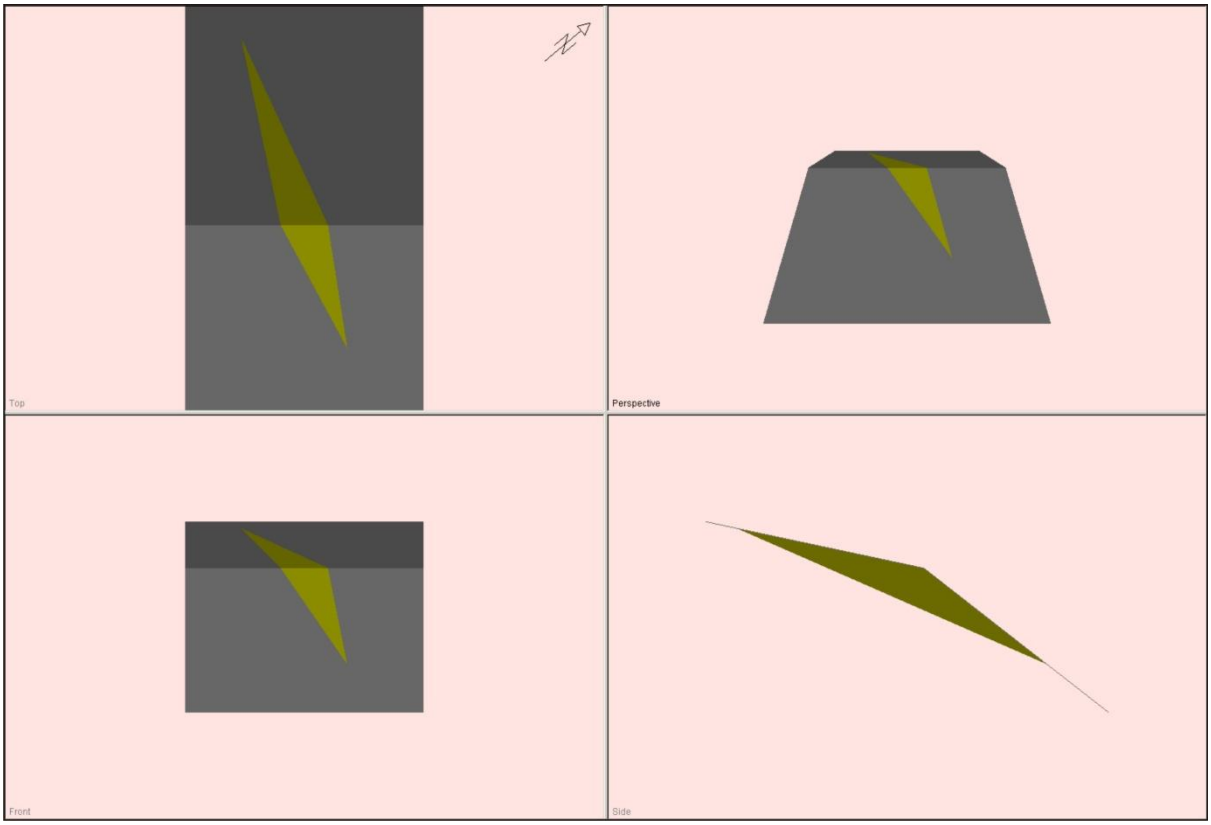

Figure F-4: SWedge generated mean 3D model of the Northern Wedge Failure.

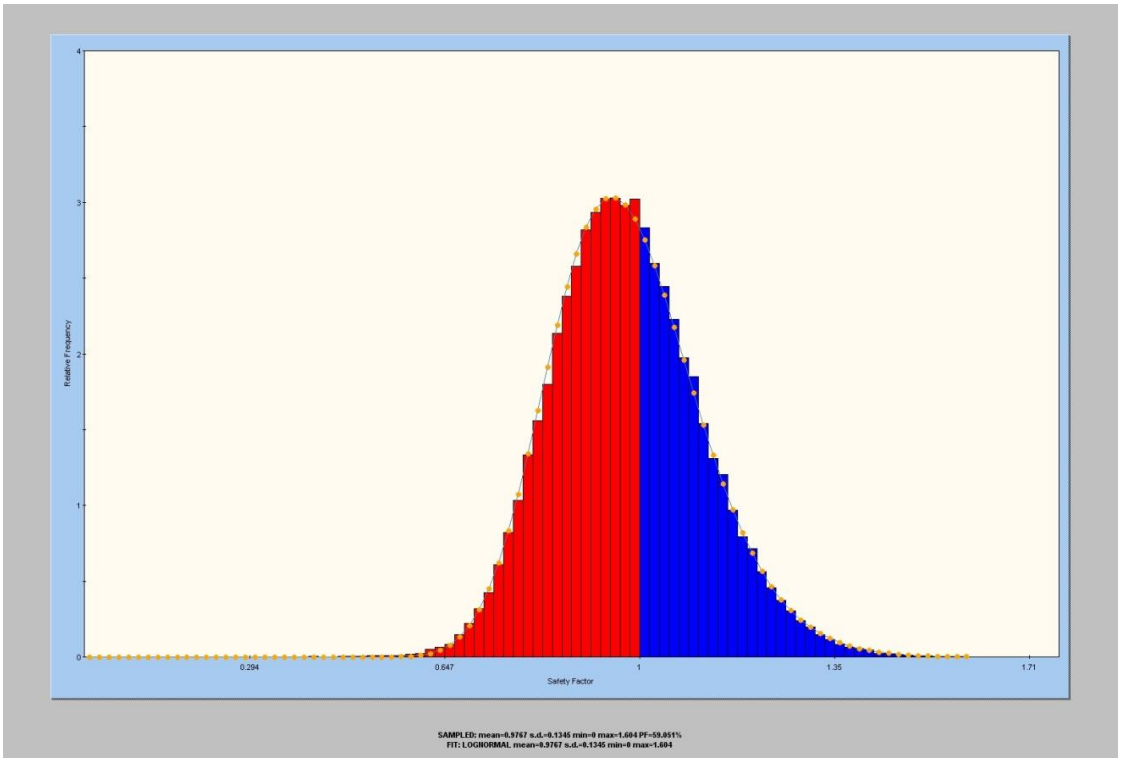

Figure F-5: Probability of failure plot showing the distribution of generated wedges from input variables and the associated probability of failure. Mean Probability of Failure: 59%, range of Factor of Safety: 0.0 to 1.6.

F4 SWedge Printouts

SWedge Model: BEST ESTIMATE OF PORE WATER PRESSURE =50%.

Swedge Analysis Information

Document Name:
WedgeAnalysis.swd

Job Title:
Northern Wedge Stability Assessment

Analysis Results:

Analysis type=Probabilistic
Sampling method=Monte Carlo
Pseudo-random sampling=NO
Probability of failure=0.592892
Number of samples=100000
Number of valid wedges=99993
Number of failed wedges=59285
Number of safe wedges=40708

Current Wedge Data - Mean Wedge:
Safety factor=0.973374
Wedge height(on slope)=165 m
Wedge width(on upper face)=328.384 m
Wedge volume=520939 m3
Wedge weight=989784 tonnes
Wedge area (joint1)=24577.1 m2
Wedge area (joint2)=22359.5 m2
Wedge area (slope)=10856.3 m2
Wedge area (upper face)=13302.2 m2
Normal force (joint1)=768292 tonnes
Normal force (joint2)=830129 tonnes
Driving force=379119 tonnes
Resisting force=369025 tonnes

Water Pressures/Forces:
Average pressure on fissures=4.85989 tonnes/m2
Water force on joint1=119442 tonnes
Water force on joint2=108665 tonnes

Failure Mode:
Sliding on intersection line (joints 1&2)

Joint Sets 1&2 line of Intersection:
plunge=22.5216 deg, trend=111.149 deg

Trace Lengths:
Joint1 on slope face=270.039 m
Joint2 on slope face=291.283 m
Joint1 on upper face=360.478 m
Joint2 on upper face = 335.284 m

Maximum Persistence:
Joint1=609.022 m
Joint2=609.022 m

Intersection Angles:
J1&J2 on slope face = 16.024 deg
J1&Crest on slope face = 97.038 deg
J1&Crest on upper face = 65.6397 deg
J2&Crest on slope face = 66.938 deg
J2&Crest on upper face = 101.644 deg
J1&2 on upper face = 12.7162 deg

Joint Set 1 Data:

Dip (degrees):
dist=NORMAL,mean=65 ,sd=2
minimum=60,maximum=70
Dip Direction (degrees):
dist=NORMAL,mean=190 ,sd=2
minimum=185,maximum=195
Cohesion (tonnes/m2):
dist=NONE,cohesion=0
Friction Angle (degrees):
dist=NORMAL,mean=13 ,sd=0
minimum=5,maximum=31

Joint Set 2 Data:

Dip (degrees):
dist=NORMAL,mean=60 ,sd=2
minimum=55,maximum=65
Dip Direction (degrees):
dist=NORMAL,mean=35 ,sd=2
minimum=30,maximum=40
Cohesion (tonnes/m2):
dist=NONE,cohesion=0
Friction Angle (degrees):
dist=NORMAL,mean=13 ,sd=0
minimum=5,maximum=31

Slope Data:

Dip (degrees):
dist=NORMAL,mean=38 ,sd=2
minimum=33,maximum=43
Dip Direction (degrees):
dist=NORMAL,mean=130 ,sd=2
minimum=125,maximum=135
Other Data:
Slope height=165 meters
Rock unit weight=1.9 tonnes/m3
Water pressures in the slope=YES
Overhanging slope face=NO
Externally applied force=NO
Tension crack=NO

Upper Face Data:

Dip (degrees):
dist=NORMAL,mean=12 ,sd=2
minimum=7,maximum=17
Dip Direction (degrees):
dist=NORMAL,mean=130 ,sd=2
minimum=125,maximum=135

Water Pressure Data:

Water unit weight=1 tonnes/m3
Pressure definition method=Percent Filled Fissures
Percent Filled=50 %

Wedge Vertices - Mean Wedge:

Coordinates in Easting,Northing,Up Format
1=Joint1, 2=Joint2, 3=Upper Face, 4=Slope
Point 124: 0, 0, 0
Point 134: -183, 110, 165
Point 234: -235, 48.3, 165
Point 123: -525, 203, 233

SWedge Model:
PORE WATER PRESSURE =0%.

Swedge Analysis Information

Document Name:
WedgeAnalysis.swd

Job Title:
Northern Wedge Stability Assessment

Analysis Results:

Analysis type=Probabilistic
Sampling method=Monte Carlo
Pseudo-random sampling=NO
Probability of failure=0.188784
Number of samples=100000
Number of valid wedges=99998
Number of failed wedges=18878
Number of safe wedges=81120

Current Wedge Data - Mean Wedge:
Safety factor=1.11228
Wedge height(on slope)=165 m
Wedge width(on upper face)=328.384 m
Wedge volume=520939 m3
Wedge weight=989784 tonnes
Wedge area (joint1)=24577.1 m2
Wedge area (joint2)=22359.5 m2
Wedge area (slope)=10856.3 m2
Wedge area (upper face)=13302.2 m2
Normal force (joint1)=887734 tonnes
Normal force (joint2)=938793 tonnes
Driving force=379119 tonnes
Resisting force=421687 tonnes

Water Pressures/Forces:
Average pressure on fissures=0 tonnes/m2
Water force on joint1=0 tonnes
Water force on joint2=0 tonnes

Failure Mode:
Sliding on intersection line (joints 1&2)

Joint Sets 1&2 line of Intersection:
plunge=22.5216 deg, trend=111.149 deg

Trace Lengths:
Joint1 on slope face=270.039 m
Joint2 on slope face=291.283 m
Joint1 on upper face=360.478 m
Joint2 on upper face = 335.284 m

Maximum Persistence:
Joint1=609.022 m
Joint2=609.022 m

Intersection Angles:
J1&J2 on slope face = 16.024 deg
J1&Crest on slope face = 97.038 deg
J1&Crest on upper face = 65.6397 deg
J2&Crest on slope face = 66.938 deg
J2&Crest on upper face = 101.644 deg
J1&2 on upper face = 12.7162 deg

Joint Set 1 Data:

Dip (degrees):
dist=NORMAL,mean=65 ,sd=2
minimum=60,maximum=70
Dip Direction (degrees):
dist=NORMAL,mean=190 ,sd=2
minimum=185,maximum=195
Cohesion (tonnes/m2):
dist=NONE,cohesion=0
Friction Angle (degrees):
dist=NORMAL,mean=13 ,sd=0
minimum=5,maximum=31

Joint Set 2 Data:

Dip (degrees):
dist=NORMAL,mean=60 ,sd=2
minimum=55,maximum=65
Dip Direction (degrees):
dist=NORMAL,mean=35 ,sd=2
minimum=30,maximum=40
Cohesion (tonnes/m2):
dist=NONE,cohesion=0
Friction Angle (degrees):
dist=NORMAL,mean=13 ,sd=0
minimum=5,maximum=31

Slope Data:

Dip (degrees):
dist=NORMAL,mean=38 ,sd=2
minimum=33,maximum=43
Dip Direction (degrees):
dist=NORMAL,mean=130 ,sd=2
minimum=125,maximum=135
Other Data:
Slope height=165 meters
Rock unit weight=1.9 tonnes/m3
Water pressures in the slope=YES
Overhanging slope face=NO
Externally applied force=NO
Tension crack=NO

Upper Face Data:

Dip (degrees):
dist=NORMAL,mean=12 ,sd=2
minimum=7,maximum=17
Dip Direction (degrees):
dist=NORMAL,mean=130 ,sd=2
minimum=125,maximum=135

Water Pressure Data:

Water unit weight=1 tonnes/m3
Pressure definition method=Percent Filled Fissures
Percent Filled=0 %

Wedge Vertices - Mean Wedge:

Coordinates in Easting,Northing,Up Format
1=Joint1, 2=Joint2, 3=Upper Face, 4=Slope
Point 124: 0, 0, 0
Point 134: -183, 110, 165
Point 234: -235, 48.3, 165
Point 123: -525, 203, 233

SWedge Model:
PORE WATER PRESSURE =100%.

Swedge Analysis Information

Document Name:
WedgeAnalysis.swd

Job Title:
Northern Wedge Stability Assessment

Analysis Results:

Analysis type=Probabilistic
Sampling method=Monte Carlo
Pseudo-random sampling=NO
Probability of failure=1
Number of samples=100000
Number of valid wedges=99998
Number of failed wedges=99998
Number of safe wedges=0

Current Wedge Data - Mean Wedge:
Safety factor=0.0622122
Wedge height(on slope)=165 m
Wedge width(on upper face)=328.384 m
Wedge volume=520939 m3
Wedge weight=989784 tonnes
Wedge area (joint1)=24577.1 m2
Wedge area (joint2)=22359.5 m2
Wedge area (slope)=10856.3 m2
Wedge area (upper face)=13302.2 m2
Normal force (joint1)=-67801.8 tonnes
Normal force (joint2)=69476 tonnes
Driving force=383639 tonnes
Resisting force=23867 tonnes

Water Pressures/Forces:
Average pressure on fissures=38.8792 tonnes/m2
Water force on joint1=955536 tonnes
Water force on joint2=869317 tonnes

Failure Mode:
Sliding on joint2

Joint Sets 1&2 line of Intersection:
plunge=22.5216 deg, trend=111.149 deg

Trace Lengths:
Joint1 on slope face=270.039 m
Joint2 on slope face=291.283 m
Joint1 on upper face=360.478 m
Joint2 on upper face = 335.284 m

Maximum Persistence:
Joint1=609.022 m
Joint2=609.022 m

Intersection Angles:
J1&J2 on slope face = 16.024 deg
J1&Crest on slope face = 97.038 deg
J1&Crest on upper face = 65.6397 deg
J2&Crest on slope face = 66.938 deg
J2&Crest on upper face = 101.644 deg
J1&2 on upper face = 12.7162 deg

Joint Set 1 Data:

Dip (degrees):
dist=NORMAL,mean=65 ,sd=2
minimum=60,maximum=70
Dip Direction (degrees):
dist=NORMAL,mean=190 ,sd=2
minimum=185,maximum=195
Cohesion (tonnes/m2):
dist=NONE,cohesion=0
Friction Angle (degrees):
dist=NORMAL,mean=13 ,sd=0
minimum=5,maximum=31

Joint Set 2 Data:

Dip (degrees):
dist=NORMAL,mean=60 ,sd=2
minimum=55,maximum=65
Dip Direction (degrees):
dist=NORMAL,mean=35 ,sd=2
minimum=30,maximum=40
Cohesion (tonnes/m2):
dist=NONE,cohesion=0
Friction Angle (degrees):
dist=NORMAL,mean=13 ,sd=0
minimum=5,maximum=31

Slope Data:

Dip (degrees):
dist=NORMAL,mean=38 ,sd=2
minimum=33,maximum=43
Dip Direction (degrees):
dist=NORMAL,mean=130 ,sd=2
minimum=125,maximum=135
Other Data:
Slope height=165 meters
Rock unit weight=1.9 tonnes/m3
Water pressures in the slope=YES
Overhanging slope face=NO
Externally applied force=NO
Tension crack=NO

Upper Face Data:

Dip (degrees):
dist=NORMAL,mean=12 ,sd=2
minimum=7,maximum=17
Dip Direction (degrees):
dist=NORMAL,mean=130 ,sd=2
minimum=125,maximum=135

Water Pressure Data:

Water unit weight=1 tonnes/m3
Pressure definition method=Percent Filled Fissures
Percent Filled=100 %

Wedge Vertices - Mean Wedge:

Coordinates in Easting,Northing,Up Format
1=Joint1, 2=Joint2, 3=Upper Face, 4=Slope
Point 124: 0, 0, 0
Point 134: -183, 110, 165
Point 234: -235, 48.3, 165
Point 123: -525, 203, 233

F5 Relevant Photographs

Figure F-6: Tensions cracks soon after wedge failure initiation (Hancock Consultants Ltd, 1989).

Figure F-7: Initial wedge shape soon after failure initiation (Hancock Consultants Ltd, 1989).

Figure F-8: Fault gouge on Plane B of Northern Wedge Failure (Hancock Consultants Ltd, 1989).

Figure F-9: Northern Wedge Failure, September 2010.

Figure F-10: Minor scarps sub-parallel to main scarp.

Figure F-11: Main scarp, looking towards apex (head scarp).

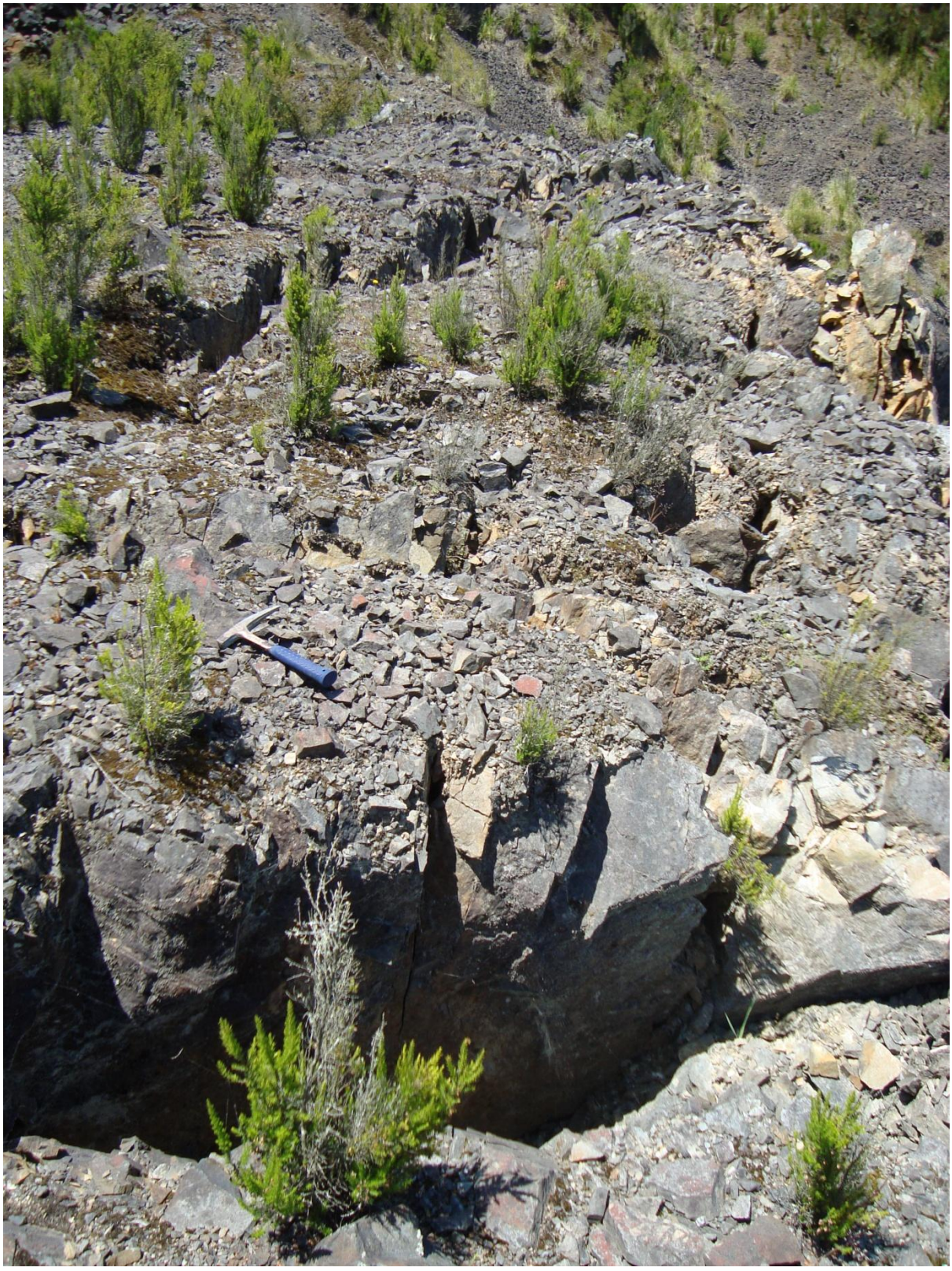

Figure F-12: Major tension cracks within wedge mass on the north-eastern edge.